ISBN NO : 978-81-983356-6-1

PROCEEDINGS

International conference on Smart Material, Manufacturing and Characterization Techniques (ICSMMCT-2024)

Date : November 23 & 24, 2024

Planting Future

ORGANIZED BY

IPS COLLEGE OF TECHNOLOGY & MANAGEMENT, GWALIOR, INDIA

IN ASSOCIATION WITH

GWALIOR LOCAL CHAPTER THE INSTITUTION OF ENGINEERS (INDIA)

Edited By

Dr. Manoj Narwariya
Dr. Snehika Shrivastava
Dr. Vijay Verma
Mr. Vineet Raj Singh Kushwah

Disclaimer

Conference Proceedings of International Conference on Smart Material, Manufacturing and Characterization Techniques (ICSMMCT 2024)

Editor: Dr. MANOJ NARWARIYA

Associate Editors: Dr. Snehika Shrivastava

Dr. Vijay Verma

Mr. Vineet Raj Singh Kushwah

ISBN No. 978-81-983356-6-1

Published by **IPS College of Technology and Management**, Shivpuri Link Road, Gwalior, M.P. India

Tel: +91-9285052400

Website - https://ipsgwalior.org/icsmmct2024/

About the Host Institute

IPS College of Technology and Management *was established in the year 2007, aiming to become the most preferred engineering college in central India for students and to obtain a world-class engineering education, thus developing into the leaders of tomorrow. IPS CTM endeavours to make the students technologically superior and ethically strong, who in turn, shall contribute to the advancement of society and humankind. The committed faculty advances the boundaries of knowledge through interdisciplinary research. The Institute, on its part, pursues continuous development of infrastructure and enhancement of state-of-the art equipment to provide our students a technologically up-to-date and intellectually inspiring environment of learning, research, creativity, innovation, and professional activity.*

Research and Development Cell *of the institute facilitates faculty members and students to shaper their skills through various projects and activities. Research and Development Cell was established to encourage faculty members to engage themselves in research work. The R & D Cell also promotes and inspires students to have research oriented approach by creating a research environment in the institute. The objective of the R & D Cell is to guide the students to focus their research skills to create the best form of technology needed for human excellence. The performance of any R&D Cell is measured in terms of publications, patents, hosting conferences /seminars, funding received and industrial consultancy. We have taken solid steps to achieve these targets and are continually moving towards further success in these areas. We have been doing this by organizing workshop, short term training program and international conference, producing technical magazines, undertaking several research projects, inviting industrial experts and collaborating industrial visit to ignite confidence among the technocrats.*

About Conference

With era of industry 4.0, new technologies are introducing every day to drastically transform the future of Industry. The economic growth of a nation largely depends upon the development of new technologies and products that suit to ever changing demands of consumer.

International Conference on Smart Material, Manufacturing and Characterization Techniques aims to provide an international forum to scientists, engineers, researchers, academicians, industry professionals and research students from all over the world to interact and discuss the latest challenges and trends in material science focusing "Industry 4.0". This conference covers the area of material science, manufacturing and characterization techniques.

The conference focuses on the role of engineers/scientists in development of affordable technologies and concepts to fulfil the consumer requirements. It is important for the engineers to look out for research and development opportunities.

MESSAGE FROM

SHRI ANOOP MISHRA

With The advent of new technologies, new avenues are opening up. Emergence of new Technology is also throwing up new challenges. In the context of the new Challenges educational Institutions need to constantly review, update knowledge and adopt technology driven skills. This is possible through mutual exchange of thoughts and sharing of knowledge and skills.

I am quite sure that this International Conference on "Smart Material, Manufacturing and Characterization Techniques" will provide a unique opportunity of sharing and equipping trend the professionals on the current and latest research work.

It is my heartfelt wish that this event becomes a successful forum of exchange of ideas and knowledge for one and all.

Shri Anoop Mishra

Hon'ble Former Member of Parliament (Morena)
Government of India

MESSAGE FROM

CHIEF PATRON

"Vision looks inward & becomes duty
Vision looks outward & becomes aspiration
Vision looks upward & becomes faith"

When the vision of duty, aspiration and faith become a reality, it becomes a proud moment for me and my team to see professionals, students and researchers come together to work collectively towards a better society.

The International Conference on "futuristic Trends in Engineering, science, Humanities & Technology" is being organized with a view to provide platform to the professionals, scientists and students to work together for a just and better society.

I extend warm greetings to all those associated with the conference and wish the conference a grand success.

Smt. Shobha Mishra

Chairperson

IPS Group of Colleges

MESSAGE FROM

PATRON

Education is simply the soul of society as it passes from one to another.

G.K. Chesterton

The world is moving very fast & new technologies are coming every week. We need to be proactive & enthusiastic in learning about these cutting edge tools and research.

New technology is bringing opportunities along with new set of skills and new challenges. Interaction in person is the best mode of communication to know the development taking place in Science, Technology & Engineering.

IPS constantly strives to meet challenges of future by fostering education and technical advancement. This conference is an effort in similar direction. It aims at keeping pace with technological development taking place globally and bridging the technology gaps.

I am quite optimistic about the success of the conference and wish it gives a qualitative outcome for global educational and development.

Best wishes....!!!

Dr. Arun Kumar Tyagi

Director
IPS Group of Colleges

MESSAGE FROM

PATRON

I am delighted to know that the IPS CTM is organizing an International Conference on "Smart Material, Manufacturing and Characterization Techniques."

Knowledge is liberating force which helps in removing the barriers of prejudices and ignorance and facilitates eliminating the various disparities between human beings. Knowledge has also come a long way, from being power to becoming powerful vision.

I am sure this conference will prove a step – ahead in the same direction and achieve the ultimate target of global academic success.

I offer my best wishes and greetings to all participants and wish good luck and grand success.

Mr. Ashwini Mishra

Working President

IPS Group of Colleges

MESSAGE FROM

CONFERENCE CHAIR

It is with immense pleasure and pride that I extend my warm greetings to all the distinguished participants, scholars, researchers, and experts contributing to the International Conference on "Smart Materials, Manufacturing and Characterization Techniques."

At IPS College of Technology and Management, we are committed to fostering an environment of academic excellence and intellectual collaboration. We believe that conferences like these play an essential role in encouraging knowledge exchange, advancing research, and creating opportunities for cross-disciplinary interaction among the brightest minds from around the world.

I am grateful to the associate of ICMMCT 2024, the Institution of Engineers (Gwalior Local Chapter) for their generous support in organizing this conference.

I would like to express my sincere appreciation to all the organizing members, speakers, participants, and volunteers who have made this conference a reality. Your contributions will undoubtedly have a lasting impact on the research community and beyond.

I wish everyone an enriching experience, stimulating discussions, and fruitful outcomes throughout the course of this conference.

Anurag Garg

Principal

IPS College of Technology and Management

MESSAGE FROM

CONFERENCE CHAIR

On behalf of the academic community, I am pleased to extend my warm greetings to all participants of this distinguished conference on "Smart Materials, Manufacturing, and Characterization Techniques."

As we continue to push the boundaries of innovation and technology, the role of smart materials and their advanced manufacturing techniques becomes increasingly central in shaping industries across the globe. The convergence of interdisciplinary fields such as material science, mechanical engineering, and nanotechnology presents unparalleled opportunities to enhance the functionality and adaptability of materials for a range of applications.

This conference provides an excellent platform for sharing cutting-edge research, insights, and future directions in the development and application of smart materials. It also plays a crucial role in fostering collaboration between scholars, researchers, and industry experts, all of whom are dedicated to advancing our understanding of these transformative materials.

We look forward to the continued growth of this exciting field and to the new possibilities that will emerge as a result of your dedicated efforts.

Best wishes for sharing the work of learner participants to the world through these proceeding. May these proceedings reach a wide audience and receive the recognition of good work.

Dr. Jyoti Mishra

Dean-Academic
IPS College of Technology and Management

MESSAGE FROM

CONVENER

It gives us immense pleasure to publish the proceedings of Smart Material, Manufacturing and Characterization Techniques (ICSMMCT – 2024) held on during November 23 & 24, 2024 in IPS College of Technology & Management.

One of the major objectives of the present International Conference was to provide a platform for Scientists, Technocrats and Researchers to share and exchange views on the opportunity and challenges offered by the ever-increasing technological advancement that are taking place in the world.

There has been excellent response from various sections which is evident from the contributions received through valuable articles. We sincerely acknowledge and express our gratitude to the reviewers for their great contribution in selecting the worthy articles and facilitating the process of publication.

We take this opportunity to thank International and National Advisory Committee members and reviewers for their guidance and timely help. We also appreciate the efforts of my colleagues, members of the staff and students to make this event successful. We hope that the proceedings will get your appreciation.

Dr. Manoj Narwariya

Dean-Research
IPS College of Technology and Management

CHIEF PATRON

Mrs. Shobha Mishra,
Honorable Chairperson, IPS GOC, Gwalior

PATRONS

Dr. Arun Tyagi
Director, IPS GOC, Gwalior

Mr. Ashwini Mishra
Working President, IPS GOC, Gwalior

Mr. P. K, Ghosh
CAO, IPSGOC, Gwalior

CONFERENCE CHAIR

Dr. Anurag Garg,
Principal, IPS CTM , Gwalior

Dr. Jyoti Mishra
Dean-Academic, IPS CTM

CONVENER

Dr. Manoj Narwariya,
Dean, Research, IPS CTM

CO-CONVENER

Mr. Vineet R S Kushwaha,
Associate Professor, IPS CTM

ORGANIZING SECRETARY

Dr. Snehika Shrivastava
Professor, IPS CTM

Dr. Vijay Verma
Associate. Professor, BIET, Jhansi

TREASURERS

Mr. Sushil Chaturvedi
Assistant Professor, IPS CTM

Mr. Prem Prakash Pandit
Assistant Professor, IPS CTM

ADVISORY COMMITTEE

Dr. Elammaran Jayamani
Associate Professor
Swinburne University of Technology, Malaysia

Dr. V. K. Jain
Former Professor. CSIR-CBRI
IIT Kanpur, India

Dr. Kamal K Kar
Professor, Department of Mechanical Engineering
IIT, Kanpur, India

Dr. R.K. Mandal
Professor, Department of Mechanical Engineering
IIT(BHU), Varanasi, India

Dr. Sunil Mohan
Professor, Department of Metallurgical Engineering
IIT(BHU), Varanasi, India

Dr. N.C. Santhi Srinivas
Professor, Department of Metallurgical Engineering
IIT(BHU), India

Dr. Manoj Kumar Harbola
Professor, Department of Physics
IIT Kanpur, India

Dr. Jawar Singh
Professor, Department of Electrical Engineering
IIT, Patna, India

Dr. Anand Parey
Professor, Department of Mechanical Engineering
IIT, Indore, India

Dr. Pankaj R Sagdeo
Professor, Department of Physics
IIT, Indore, India

Dr. Prashant K. Jain
Professor, Department of Mechanical Engineering
IIITDM, Jabalpur, India

Dr. Pradeep Kumar
Associate Professor, Department of Mechanical Engineering, IIT, Mandi, India

Dr. Anil Kumar Sachan
Professor, Department of Civil Engineering
MNNIT, Allahabad, India

Dr. Yogendra Kumar Prajapati
Professor, Department of Electronics & Communication Engineering
MNNIT, Allahabad, India

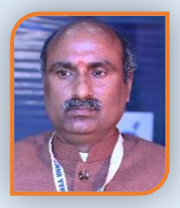

Dr. Avanish Kumar Dubey
Professor, Department of Mechanical Engineering
MNNIT, Pragyagraj, India

Dr. Mukul Shukla
Professor, Department of Mechanical Engineering
MNNIT, Pragyagraj, India

Dr. Manoj Chouksey
Professor, Department of Mechanical Engineering
SGSITS, Indore, India

Dr. Vinod Patidar
Professor, Physics, University of Petroleum and Energy Studies, **Dehradun, Uttarakhand,** India

Dr. S. M. Narulkar
Professor & Head, Department of Civil Engineering
SGSITS, Indore, India

Dr. Avadesh K Sharma
Associate Professor, Department of Mechanical Engineering, Rajkiya Engineering College
Mainpuri, U.P., India

Dr. Chaitanya Sharma
Associate Professor, Department of Mechanical Engineering, B.I.T.,Sindri, Dhanbad, India

Dr. Arun Kumar Pandey
Associate Professor, Department of Mechanical Engineering, B.I.E.T., Jhansi, India

Dr. Mukal Pastor
Associate Professor, Department of Mechanical Engineering, Bundelakhand University, Jhansi, India

Dr. Nitin Narang
Associate Professor, Department of Electrical and Instrumentation Engineering,
Thapar Institute of Engineering & Technology, India

Dr. R. Prasad
Assistant Professor, Department of Mechanical Engineering, HCST, Mathura, India

Mr. Prabhat Bhargava
President, IE(India) Gwalior Chapter
Institution of Engineers, India

Mr. R K Khetan
Vice-President, IE(India) Gwalior Chapter
Institution of Engineers, India

TABLE OF CONTENTS

International conference on Smart Material, Manufacturing and Characterization Techniques – 2024

Paper ID: ICSMMCT-01006

Biocompatibility and corrosive resistance of Magnesium based biomedical implants: A brief discussion

Ayush Saxena[1], Dr. Vaibhav Trivedi[2], Dr. Ankur Goel[3], Bhavana Singh[4]

[1]*Research Scholar Mechanical Engineering Department, IFTM University, Moradabad 244001, India*
[2]*Professor Mechanical Engineering Department, IFTM University, Moradabad 244001, India*
[3]*Orthopedic & Joint replacement surgeon Sri sai superspeciality Hospital, Moradabad 244001, India*
[4]*Research Scholar Mechanical Engineering Department, IFTM University, Moradabad 244001, India*

Abstract
In this current study a comprehensive analysis of the latest research on magnesium (Mg)-based bio composites and bio alloys has been conducted. This study highlights their potential applications in biomedical fields, particularly in orthopedics. Mg-based alloys which are known for their excellent compatibility as biomaterials, biodegradability, and non-toxic properties, making them suitable materials for the retention of bone healing and implant applications. However, the degradation rate of the Mg alloys remains to be enhanced, necessitating further research and development. This review also examines the factors influencing the degradation of magnesium (Mg) based alloys, including composition, microstructure distribution, and surface films. Mg alloys, which can remain in vivo for 12-18 weeks without toxicity, form $Mg(OH)_2$ on their surface during corrosion, which dissolves due to Cl-, leading to a pH increase. Adding zinc (Zn) and the interaction of Mg-Zn-Sr phases can accelerate corrosion, while calcium promotes a dendritic grain structure. The biodegradation and biocompatibility of Mg-based alloys are emphasized, with studies showing that Mg alloys, particularly Mg-Ca alloys, exhibit strong cyto-compatibility and are fully degradable within 18 weeks. Despite their potential as biodegradable implant materials, the rapid corrosion rate of Mg alloys necessitates further research to align with the typical bone soothing process, which can take several weeks for healing.

Keywords: Biocompatibility; Corrosive resistance ; Biodegradation ; Bio electrodes

1. Introduction

Biomaterials find extensive applications across various medical fields, including implants which further branch out into heart valves, grafts, and stents dentistry involving implants and tissue repairing or replacing, biosensors, bioelectrodes, synthetic blood vessels and thedrug delivery systems [1 – 3]. Consequently, the excellent biomaterials must possess good physical and mechanical properties, besides being biocompatible, bio-functional, and bio adhesive [4]. Additionally, they should exhibit resistance to corrosion, support osteoconduction, with low friction coefficients and wear rates [5].Table 1 shows the properties required for the biomaterial. Several materials including ceramics, composites, polymers, metals and their alloys falls in the category of the biocomposite materials [6]. However, metal based bio composites such as stainless steel, cobalt-chromium alloys, titanium alloys, and magnesium, find common use in medical applications like orthopedic and cardiovascular transplants [7, 8]. Also, Mg-based biocompsites are gaining significant attention from the researcher due to their excellent biocompatibility, biodegradability and corrosion-resistant properties [9], which are discussed in the later section. Also, the incorporation of nano particles to manipulate their properties is quite common. Therefore, it must be studied carefully for better implementation in the future.

Table 1.Properties required for feasible biomaterials

Properties	Comments	REFERENCES
Biocompatibility	Biomaterials must not induce any toxicity while interacting with the body. They should be able to function without causing negative impact on the human body such as inflammation or rejection.	[10]
Biofunctionality	The material should performs its function within the provided environment, such as supporting tissue growth, delivering drugs, or facilitating healing, without degrading or losing its effectiveness.	[11]
Mechanical Strength	Such biomaterials must be resistant enough from a mechanical point of view to provide the necessary support for the forces	[12]

Published online on: ***February01, 2025***
Corresponding Author's E-mail ID: ayushsaxena.me@gmail.com

	that act through them in the body.This includes tensile strength, compressive strength, and fatigue resistance, depending on the application.	
Osteocondutivity	For applications like bone grafts and implants, biomaterials should support the growth of new bone tissue by providing a scaffold that encourages bone cell attachment and proliferation.	[13]
Corrosion resistance	Biomaterials, especially those used in implants, should resist corrosion caused by bodily fluids. Corrosion can lead to the release of harmful ions and the degradation of the material's structural integrity.	[14]
Wear resistance	Biomaterials used in applications subject to mechanical stress, such as joint prosthetics, need to resist wear over time to maintain their function and prevent the release of wear particles that could cause inflammation.	[15]
Bioadhesiveness	In some applications, such as wound dressings or tissue adhesives, the biomaterial should adhere effectively to biological tissues without causing damage or irritation.	[16]
Sterilizability	Biomaterials must be capable of being sterilized without losing their properties or becoming compromised. This is essential to prevent infections when they are implanted or used in medical devices.	[17]
Chemically stable	Biomaterials should maintain their properties and structure over time when exposed to the body's chemical environment, including enzymes, pH levels, and bodily fluids.	[18]
Non-toxic Degradation	If a biomaterial is designed to degrade over time, it should do so in a controlled manner, releasing non-toxic byproducts that it—afterwards—either can be safely degraded or removed by the body over the time without any significant problems.	[18]
Cost-effectiveness	Finally, biomaterials should be economically viable for production and use in medical applications, ensuring that they are accessible and affordable for widespread use.	[18]

2. Metallic Biomaterials

Metallic biomaterials have wide range of application in the medical field. These are mainly used in surgeries to replace hard tissues namely hip joints, bones, and dental implants due to attributed properties through mechanical reliability [19]. It has been found that among various metallic biomaterials ‘Ti’ and ‘Mg’ based biomaterial is highly biocompatible. Along with this, it is not bioactive which makes it suitable for transplants [20]. Few other materials are thoroughly discussed here for better knowledge.

2.1 Cobalt alloys

These are generally used for wear resistance application, for the fabrication of medical devices for e.g., artificial hip joint [21]. These Co alloys are basically divided as wroth alloys and cast alloys. These contain significant amounts of Ni (1 mass %) and C (0.35 mass %), improving its workability and durability due to easy casting [22]. The considerable amount of carbon also improves the wear resistance properties and makes it more durable [23]. According to some previous literature reports, both a Co-Cr-Mo alloys, having excellent strength and ductility can be obtained by processing in the ‘γ’ phase region. Afterwards subsequently rapid cooling was provided through the brittle ‘γ’ phase, which later becomes quite steady below the ‘ε’ phase temperature. While in most cases, wear resistance is improved due to dispersion of carbides due to low carbon content, but here it improved due to the deformation-induced transformation of metastable ‘γ’ phase into ‘ε’ martensite. [24].

2.2 Stainless Steel alloys

Stainless steels (SS) are among the most widely used biomaterials due to their practical applications. SS 316L has gained its

utility as a biomedical application, an austenitic SS, is currently the only SS employed in biomedical applications [25]. However, because SS 316L contains a significant amount of nickel (Ni), there is a risk of Ni-induced allergic reactions [26]. As a result, research and development efforts are focused on creating Ni-free stainless steels. One of the early developments in Ni-free stainless steel involved the incorporation of nitrogen (N) and manganese (Mn), both of which are effective austenite stabilizers, similar to Ni [27]. Therefore, Ni-free SS is being used in the biomedical industries for better implementation.

2.3 Titanium (Ti) alloys

Titanium (Ti)material has high tensile strength, coupled with very light weight and excellent biocompatibility. [28]. Further, Ti and its alloys are very corrosion resistance; additionally, they are non-magnetic and can be used for orthopaedic applications. Despite the mentioned favourable properties, the tribological behavior of Ti alloys still needs to be improved. Ti mostly comes in grade 4 and grade 5 forms because both of them have very admirable chemical and mechanical properties. [29]. To make Ti ideal choice for implant applications, non-toxic elements such as niobium (Nb), tantalum (Ta), molybdenum (Mo), and zirconium (Zr) have been added to lower its elastic modulus without losing its strength. [30]. However, since the aforementioned elements are very expensive, current research is oriented toward cheaper substitutes for Mn, Fe, Al, Cr, and Sn to reduce the overall cost of the titanium-based implant [31].

2.4 Magnesium (Mg) alloys

Pure or alloys of Mg have found significant application in biomedical applications since 1892. Mg has excellent biodegradable properties which degrades inside the human body after its application [32]. The selection of particular Mg alloys is based on their application. Mg alloys have superior biocompatibility, bioactive, and biodegradability in long-term usage. The major application of Mg-based alloys can be seen as a stents in cardiovascular surgery during angiography which considerably minimizes the chances of heart attack by opening the shrinkage blood vessels [34]. Also, it has been evident that magnesium-based alloys have low density similar to human bones i.e., 1.8 to 2.1 g/cm3 which increases its utility [34]. Mechanical Properties of Mg-based composites with different reinforcement materials can be seen from figure 1.

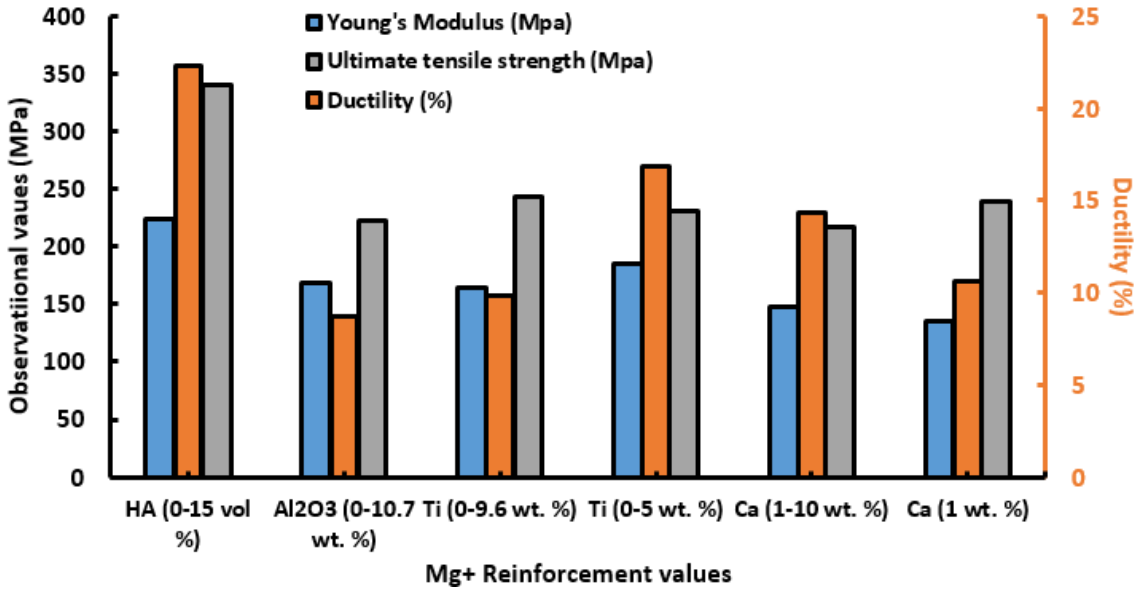

Fig 1. Mechanical Properties of Mg-based composites with different reinforcement materials [35 – 40]

3. Corrosion mechanism in Mg-based alloys

Three major factors influence the degradation rates of alloys: (1) composition, (2) microstructure distribution and (3) surface films respectively. Mg alloys can stay in vivo for the range of 12-18 weeks without exhibiting any kind of toxicity [41]. Based on the recent published literature, it was observed that Mg(OH)2 was formed over the surface, that was later

dissolved by Cl-resulting in sudden increase in the pH value [42]. Also, an intermetallic phase was found over the addition of Zn upto 9 wt. % which makes Mg51Zn20prone to corrosion. The increasing galvanic coupling between Mg-Zn-Sr phases increases the degradation rate with in the composites [43]. According to a study published by Zumdick [44], observed the lowest corrosion rate for Mg-0.6Ca-xZn (x ¼ 0.8, 1.8 wt.%) alloys. Additionally, it was observed that calcium promotes a more dendritic grain structure, whereas zinc had no impact on the grain shape. Adding to this Lu et al. [45] observed that providing heat treatment and grain size can significantly affect the corrosion rate within the secondary phases.

4. Biodegradation and Biocompatibility of Mg- based alloys

Every implant material should be compatible with the human body and must be nontoxic. For finding the feasibility of Mg-alloys medical studies and degradation process must be examined thoroughly. Figure 2, physical and mechanical Properties of biomaterials as compared to that human bones. Literature [46, 47] suggests Mg-Cd alloy produces hard callous in the fracture area during repairing. Four different Mg alloys rods were fabricated by Witee et al. [48]. In their study they observed degradation rate are within the limits influencing the bone mass surroundings. Furthermore, literature [49] observed Mg implants are completely degraded within 18 weeks. Zheng et al. [50] examined a biomedical binary Mg–xCa (x=1–3 wt.%) alloy. The cytotoxicity test by L-929 cells indicated good cytocompatibility of this Mg–1Ca alloy, with a cell survival rate higher than the control group in the extraction medium culture. Moreover, during the in vitro and in vivo corrosion reactions, a mixture of $Mg(OH)_2$ and HA would form on the surface of the Mg–1Ca alloy. These findings demonstrates the Mg–Ca alloy is a highly biocompatible material with potential application as a biodegradable implant material. Mg and its alloys are biocompatible and non-toxic, which initially makes them very attractive for use in bone healing applications in orthopedics. Currently, the corrosion rate of magnesium or magnesium-based alloys is too high to match the normal process of bone healing, which takes a minimum of 12 weeks. Further research is necessary to reduce the corrosion rate of magnesium and the alloys of magnesium. [51-53].

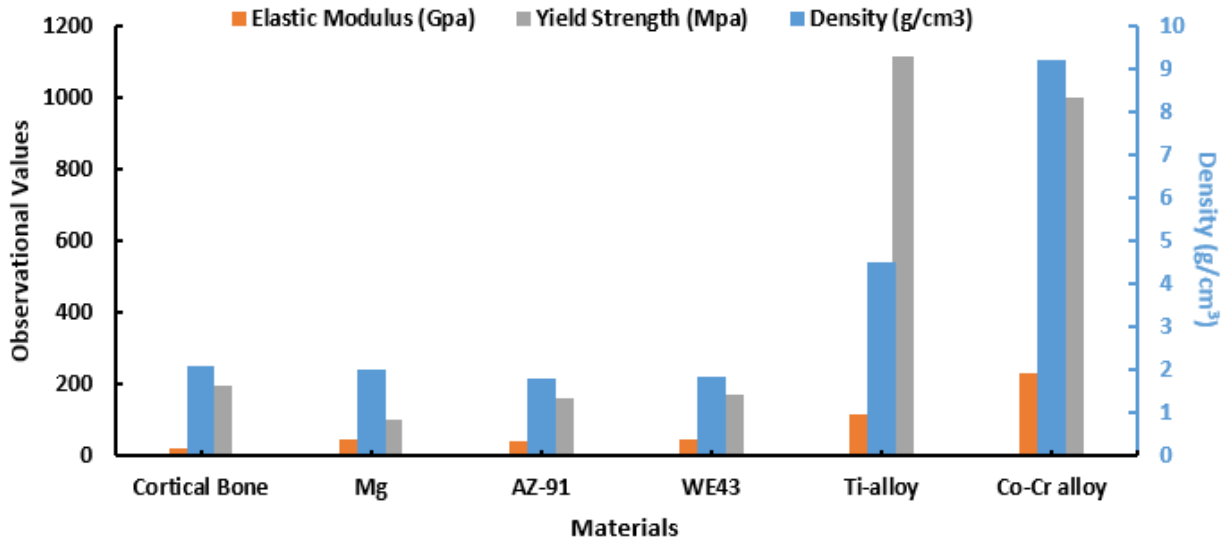

Fig. 2. Physical and Mechanical Properties of various biomaterials and human bone [54]

5. Conclusion and Future Research Potential

1. This review highlights the latest advancements in Mg-based bio-composites and bio-alloys.
2. Mg composites show promise in addressing the rapid degradation of the Magnesium alloys while preserving mechanical integrity.
3. Metallic and ceramic reinforcement, its grain size, and proper biocompatibility are important to be selected to add more value to these materials. Mechanical properties are significantly influenced by processing techniques, heat treatments, and plastic deformation methods.

4. Processing techniques together with heat treatments and plastic deformation methods are very influential on the mechanical properties of these materials.
5. Mechanical performance of Magnesium-based alloys can be greatly enhanced by the optimization of processing techniques and parameters.
6. Further addition of rare earth elements can increase mechanical properties and enhance creep resistance.
7. Various Artificial Neural Networks and optimization techniques can help in predicting the output.

References

[1] Hedayati, R., Ahmadi, S. M., Lietaert, K., Tümer, N., Li, Y., Yavari, S. A., & Zadpoor, A. A. (2018). Fatigue and quasi- static mechanical behavior of biodegradable porous biomaterials based on magnesium alloys. *Journal of Biomedical Materials Research Part A*, *106*(7), 1798-1811.

[2] Ali, M., Hussein, M. A., & Al-Aqeeli, N. (2019). Magnesium-based composites and alloys for medical applications: A review of mechanical and corrosion properties. *Journal of Alloys and Compounds*, *792*, 1162-1190.

[3] Olvera, D., & Monaghan, M. G. (2021). Electroactive material-based biosensors for detection and drug delivery. *Advanced Drug Delivery Reviews*, *170*, 396-424.

[4] Dey, A., Bhattacharya, P., & Neogi, S. (2021). Bioadhesives in biomedical applications: A critical review. *Progress in Adhesion and Adhesives*, *6*, 131-153.

[5] Geetha, M., Singh, A. K., Asokamani, R., & Gogia, A. K. (2009). Ti-based biomaterials, the ultimate choice for orthopedic implants–a review. *Progress in Materials Science*, *54*(3), 397-425.

[6] Akter, M., Uddin, M. H., & Tania, I. S. (2022). Biocomposites based on natural fibers and polymers: A review on properties and potential applications. *Journal of Reinforced Plastics and Composites*, *41*(17-18), 705-742.

[7] Ozturk, S., Ayanoğlu, F. B., Parmaksiz, M., Elçin, A. E., & Elçin, Y. M. (2020). Clinical and surgical aspects of medical materials' biocompatibility. In *Handbook of Biomaterials Biocompatibility* (pp. 219-250). Woodhead Publishing.

[8] da Silva, L. R. R., Sales, W. F., Campos, F. dos A. R., de Sousa, J. A. G., Davis, R., Singh, A., Coelho, R. T., & Borgohain, B. (2021). A comprehensive review on additive manufacturing of medical devices. *Progress in Additive Manufacturing*, *6*(3), 517-553.

[9] Mehdizade, M., Eivani, A. R., Tabatabaei, F., Mousavi Anijdan, S. H., & Jafarian, H. R. (2023). Enhanced in-vitro biodegradation, bioactivity, and mechanical properties of Mg-based biocomposite via addition of calcium-silicate-based bioceramic through friction stir processing as resorbable temporary bone implant. *Journal of Materials Research and Technology*, *26*, 4007-4023.

[10] Marin, E., Boschetto, F., & Pezzotti, G. (2020). Biomaterials and biocompatibility: An historical overview. *Journal of Biomedical Materials Research Part A*, *108*(8), 1617-1633.

[11] Ariga, K., Hill, J. P., & Ji, Q. (2008). Biomaterials and biofunctionality in layered macromolecular assemblies. *Macromolecular Bioscience*, *8*(11), 981-990.

[12] Prasadh, S., & Wong, R. C. W. (2018). Unraveling the mechanical strength of biomaterials used as a bone scaffold in oral and maxillofacial defects. *Oral Science International*, *15*(2), 48-55.

[13] Suzuki, K., Anada, T., Miyazaki, T., Miyatake, N., Honda, Y., Kishimoto, K. N., Hosaka, M., Imaizumi, H., Itoi, E., & Suzuki, O. (2014). Effect of addition of hyaluronic acids on the osteoconductivity and biodegradability of synthetic octacalcium phosphate. *Acta Biomaterialia*, *10*(1), 531-543.

[14] Eliaz, N. (2019). Corrosion of metallic biomaterials: A review. *Materials*, *12*(3), 407.

[15] Hussein, M. A., Mohammed, A. S., & Al-Aqeeli, N. (2015). Wear characteristics of metallic biomaterials: A review. *Materials*, *8*(5), 2749-2768.

[16] Saha, N., Saha, N., Sáha, T., Toksoy Öner, E., Vrabič Brodnjak, U., Redl, H., von Byern, J., & Sáha, P. (2020). Polymer-based bioadhesive biomaterials for medical application—a perspective of redefining healthcare system management. *Polymers*, *12*(12), 3015.

[17] Lerouge, S., & Simmons, A. (Eds.). (2012). *Sterilisation of biomaterials and medical devices.* Elsevier.

[18] Kumar, A., Sharma, G., Naushad, M., Ala'a, H., García-Peñas, A., Mola, G. T., Si, C., & Stadler, F. J. (2020). Bio-inspired and biomaterials-based hybrid photocatalysts for environmental detoxification: A review. *Chemical Engineering Journal*, *382*, 122937.

[19] Prasad, K., Bazaka, O., Chua, M., Rochford, M., Fedrick, L., Spoor, J., Symes, R., et al. (2017). Metallic biomaterials: Current challenges and opportunities. *Materials*, *10*(8), 884.

[20] Sezer, N., Evis, Z., Kayhan, S. M., Tahmasebifar, A., & Koç, M. (2018). Review of magnesium-based biomaterials and their applications. *Journal of Magnesium and Alloys*, *6*(1), 23-43.

[21] Merola, M., & Affatato, S. (2019). Materials for hip prostheses: A review of wear and loading considerations. *Materials*, *12*(3), 495.

[22] Acharya, S., Soni, R., Suwas, S., & Chatterjee, K. (2021). Additive manufacturing of Co–Cr alloys for biomedical applications: A concise review. *Journal of Materials Research*, 1-15.

[23] Chiba, A., Kumagai, K., Takeda, H., & Nomura, N. (2005). Mechanical properties of forged low Ni and C-containing Co-Cr-Mo biomedical implant alloy. In *Materials Science Forum* (Vol. 475, pp. 2317-2322). Trans Tech Publications Ltd.

[24] Kumagai, K., Nomura, N., Ono, T., Hotta, M., & Chiba, A. (2005). Dry friction and wear behavior of forged Co–29Cr–6Mo alloy without Ni and C additions for implant applications. *Materials Transactions*, *46*(7), 1578-1587.

[25] Ali, S., Irfan, M., Niazi, U. M., Abdul Rani, A. M., Rashedi, A., Rahman, S., Khan, M. K. A., et al. (2022). Microstructure and mechanical properties of modified 316L stainless steel alloy for biomedical applications using powder metallurgy. *Materials*, *15*(8), 2822.

[26] Li, M., Yin, T., Wang, Y., Du, F., Zou, X., Gregersen, H., & Wang, G. (2014). Study of biocompatibility of medical grade high nitrogen nickel-free austenitic stainless steel in vitro. *Materials Science and Engineering: C*, *43*, 641-648.

[27] Talha, M., Behera, C. K., & Sinha, O. P. (2013). A review on nickel-free nitrogen-containing austenitic stainless steels for biomedical applications. *Materials Science and Engineering: C*, *33*(7), 3563-3575.

[28] Zou, Z., Ismail, B. B., Zhang, X., Yang, Z., Liu, D., & Guo, M. (2023). Improving barrier and antibacterial properties of chitosan composite films by incorporating lignin nanoparticles and acylated soy protein isolate nanogel. *Food Hydrocolloids*, *134*, 108091.

[29] Eliasa, C. N., Fernandesa, D. J., Resendea, C. R. S., & Roestel, J. (2015). Mechanical properties, surface morphology and stability of a modified commercially pure high strength titanium alloy for dental implants. *Dental Materials*, *31*, 1-13.

[30] Farrahnoor, A., & Zuhailawati, H. (2021). Review on the mechanical properties and biocompatibility of titanium implant: The role of niobium alloying element. *International Journal of Materials Research*, *112*(6), 505-513.

[31] Straumal, B. B., Gornakova, A. S., Kilmametov, A. R., Rabkin, E., Anisimova, N. Y., & Kiselevskiy, M. V. (2021). β-Ti-based alloys for medical applications. *Russian Journal of Non-Ferrous Metals*, *62*, 54-63.

[32] Haghshenas, M. (2017). Mechanical characteristics of biodegradable magnesium matrix composites: A review. *Journal of Magnesium and Alloys*, *5*(2), 189-201.

[33] Korei, N., Solouk, A., Nazarpak, M. H., & Nouri, A. (2022). A review on design characteristics and fabrication methods of metallic cardiovascular stents. *Materials Today Communications*, *31*, 103467.

[34] Kumar, S., & Katyal, P. (2022). Factors affecting biocompatibility and biodegradation of magnesium-based alloys. *Materials Today: Proceedings*, *52*, 1092-1107.

[35] Del Campo, R., Savoini, B., Muñoz, A., Monge, M. A., & Garcés, G. (2014). Mechanical properties and corrosion behavior of Mg–HAP composites. *Journal of the Mechanical Behavior of Biomedical Materials*, *39*, 238-246.

[36] Wong, W. L. E., Karthik, S., & Gupta, M. (2005). Development of high-performance Mg–Al_2O_3 composites containing Al_2O_3 in submicron length scale using microwave-assisted rapid sintering. *Materials Science and Technology*, *21*(9), 1063-1070.

[37] Hassan, S. F., & Gupta, M. (2002). Development of ductile magnesium composite materials using titanium as reinforcement. *Journal of Alloys and Compounds*, *345*(1-2), 246-251.

[38] Umeda, J., Kawakami, M., Kondoh, K., Ayman, E.-S., & Imai, H. (2010). Microstructural and mechanical properties of titanium particulate reinforced magnesium composite materials. *Materials Chemistry and Physics*, *123*(2-3), 649-657.

[39] Zheng, Y. F., Gu, X. N., Xi, Y. L., & Chai, D. L. (2010). In vitro degradation and cytotoxicity of Mg/Ca composites produced by powder metallurgy. *Acta Biomaterialia*, *6*(5), 1783-1791.

[40] Li, Z., Gu, X., Lou, S., & Zheng, Y. (2008). The development of binary Mg–Ca alloys for use as biodegradable materials within bone. *Biomaterials*, *29*(10), 1329-1344.

[41] Song, G., & Atrens, A. (2007). Recent insights into the mechanism of magnesium corrosion and research suggestions. *Advanced Engineering Materials*, *9*(3), 177-183.

[42] Li, Z., Gu, X., Lou, S., & Zheng, Y. (2008). The development of binary Mg–Ca alloys for use as biodegradable materials within bone. *Biomaterials*, *29*(10), 1329-1344.

[43] Hong, D., Saha, P., Chou, D.-T., Lee, B., Collins, B. E., Tan, Z., Dong, Z., & Kumta, P. N. (2013). In vitro degradation and cytotoxicity response of Mg–4% Zn–0.5% Zr (ZK40) alloy as a potential biodegradable material. *Acta Biomaterialia*, *9*(10), 8534-8547.

[44] Zander, D., & Zumdick, N. A. (2015). Influence of Ca and Zn on the microstructure and corrosion of biodegradable Mg–Ca–Zn alloys. *Corrosion Science, 93*, 222-233.
[45] Lu, Y., Bradshaw, A. R., Chiu, Y.-L., & Jones, I. P. (2015). Effects of secondary phase and grain size on the corrosion of biodegradable Mg–Zn–Ca alloys. *Materials Science and Engineering: C, 48*, 480-486.
[46] Bergmann, C., Lindner, M., Zhang, W., Koczur, K., Kirsten, A., Telle, R., & Fischer, H. (2010). 3D printing of bone substitute implants using calcium phosphate and bioactive glasses. *Journal of the European Ceramic Society, 30*(12), 2563-2567.
[47] Bose, S., Vahabzadeh, S., & Bandyopadhyay, A. (2013). Bone tissue engineering using 3D printing. *Materials Today, 16*(12), 496-504.
[48] Witte, F., Kaese, V., Haferkamp, H., Switzer, E., Meyer-Lindenberg, A., Wirth, C. J., & Windhagen, H. (2005). In vivo corrosion of four magnesium alloys and the associated bone response. *Biomaterials, 26*(17), 3557-3563.
[49] Suchanek, W., & Yoshimura, M. (1998). Processing and properties of hydroxyapatite-based biomaterials for use as hard tissue replacement implants. *Journal of Materials Research, 13*(1), 94-117.
[50] Li, Z., Gu, X., Lou, S., & Zheng, Y. (2008). The development of binary Mg–Ca alloys for use as biodegradable materials within bone. *Biomaterials, 29*(10), 1329-1344.
[51] Zhao, D., Huang, S., Lu, F., Wang, B., Yang, L., Qin, L., Yang, K., et al. (2016). Vascularized bone grafting fixed by biodegradable magnesium screw for treating osteonecrosis of the femoral head. *Biomaterials, 81*, 84-92.
[52] Lee, J.-W., Han, H.-S., Han, K.-J., Park, J., Jeon, H., Ok, M.-R., Seok, H.-K., et al. (2016). Long-term clinical study and multiscale analysis of in vivo biodegradation mechanism of Mg alloy. *Proceedings of the National Academy of Sciences, 113*(3), 716-721.
[53] Windhagen, H., Radtke, K., Weizbauer, A., Diekmann, J., Noll, Y., Kreimeyer, U., Schavan, R., Stukenborg-Colsman, C., & Waizy, H. (2013). Biodegradable magnesium-based screw clinically equivalent to titanium screw in hallux valgus surgery: Short-term results of the first prospective, randomized, controlled clinical pilot study. *Biomedical Engineering Online, 12*, 1-10.
[54] Li, L., Zhang, M., Li, Y., Zhao, J., Qin, L., & Lai, Y. (2017). Corrosion and biocompatibility improvement of magnesium-based alloys as bone implant materials: A review. *Regenerative Biomaterials, 4*(2), 129-137.

Acknowledgements

We would like to express our heartfelt gratitude to Dr. Vaibhav Trivedi for their valuable guidance, support, and constructive feedback throughout the development of this work.

We also extend our thanks to IFTM University Moradabad for providing the necessary resources that made this research possible.

Special thanks to our colleagues and Dr. Ankur Goel, whose insights and discussions significantly contributed to the quality of this paper.

Finally, we are grateful to the organizers and reviewers of ICSMMCT 2024 for their efforts in creating an opportunity to share and improve this work.

Investigating the Effects of Nano-clay Incorporation on Soil Engineering Properties: A Machine Learning Approach to Soil Stabilization and Behavior Analysis

Khushboo Akbar Wani[1], Plaban Deb[2]

[1,2]*Department of Civil Engineering, Chandigarh University, Mohali, 140413, India*

Abstract

This research looks at how adding nanoclay affects soil's engineering characteristics. This is because nanoclay particles are both lightweight and porous. The soil is reclassified from clay with moderate plasticity to silt with high plasticity when the addition of nano-soil increases the values of the Liquid Limit (LL) and Plastic Limit (PL), while a lower PI is the consequence of a higher fraction of nanoclay. In addition, the dry density increases with increasing nanoclay percentages, which means that the soil is compacted better. The impact of axial strain and nanoclay concentration on soil strength is shown by mechanical testing, which shows that compressive strength varies with these variables. The results are corroborated by scanning electron microscopy (SEM) examination, which shows that the addition of nanoclay changes the microstructure of the clay. In conclusion, this research sheds light on the substantial effect of nanoclay on mechanical behaviour and soil characteristics, which is useful for engineering and soil stabilisation purposes.

Keywords: Soil, Clay, Strength, Compression, Stress, Strain

1. Introduction

The stability of soil is a significant challenge to civil engineers and builders since it is the foundation of our constructed environment [1]. Because of their high compressibility and low shear strength, soft soils are notoriously problematic for building. Settlement, erosion, and low load-bearing capacity are infamous problems with these soils, which necessitates expensive and time-consuming solutions [2, 3]. Engineers and academics looking for long-term geotechnical fixes have focused on nanotechnology, namely the use of nano-silica and nano-clay, to shore up soft soils' intrinsic deficiencies. Traditional methods of soil stabilization often include the use of chemical additives such as cement and lime; however, these materials are not always the best choices and may have harmful impacts on the environment. As an alternative, one might lessen the environmental effect of soft soils while increasing their geotechnical properties by utilizing nano-silica and nano-clay. Researchers have shown that soils with nano-silica, or very small particles of silicon dioxide, have much better mechanical properties. Its high surface area and reactivity make it an excellent candidate for soil reinforcement. The unique qualities of nano-clay, which are made of mineral particles on the nanometer scale, may be used to modify the behavior of soft soils. These properties include a high cation exchange capacity and swelling potential. Researchers looked at the efficacy of using cement and high calcium fly ash to stabilize fine-grained clayey soils (CL, CH) [4, 5]. After soaking soil samples for 90 days with different ratios of fly ash and cement, they were examined for various characteristics such as uniaxial compression, splitting tension, flexure, modulus of elasticity, and CBR values. Pavement designs with higher subgrades achieved by in situ stabilization using cement and fly ash were compared to traditional flexible pavements without improved subgrades. Pavement thickness, especially in the asphalt course. With cement added, setting and hardening are much better, and early and ultimate strength are both increased. The research does concede, however, that in order to offer more accurate estimates for the mechanical characteristics of the stabilised layer under real-world field circumstances, laboratory findings must be validated by in situ experiments [4]. Researchers looked into nucleation seeding, which uses nano-silica to provide C-S-H seeds nucleation sites and speed up cement hydration. Experiments with varying particle sizes and surface areas show that the acceleration is directly related to the surface area of nano-silica particles. An increase in the early consumption of C3S during hydration, a larger silica surface, and accelerated portlandite formation are all outcomes of mixing conventional Portland cement with nano-silica [6]-[9]. This proves that nano-silica indeed speed up

Published online on: ***February 01, 2025***
Corresponding Author's E-mail ID: khushbooakbarwani@gmail.com

C3S hydration, and that the amount of surface area that the silica particles have is the main factor that controls this acceleration. Furthermore, nano-silica injection causes the early development of sulphate-type AFm. Therefore, it can be concluded that nano-silica plays a crucial role in cement hydration events involving sulphate-containing phases. Possible causes include silica's ion-absorption capabilities, which alter the specific sulphate equilibrium and, hence, the amount of time required to produce sulphate-type AFM. Researchers looked at nanotechnology's role in geotechnical engineering, focussing on nanomaterials (NM) and its effects on soil stability and improvement. Particles smaller than 100 nm are called nanoparticles (NP), while even smaller things are called nanoobjects. These two types of particles make up nanomaterials [10]-[14]. Methods for studying soil nanostructures using state-of-the-art instruments are detailed in the paper. Additionally, it emphasises the possibilities of nanotechnology in geotechnical engineering, specifically in two important areas: investigating soil structures on a microscopic size and modifying soil on a molecular or atomic level by including nanoparticles [15]-[18].

Nanoparticles react strongly with other particles in the soil due to their enormous specific surface area. Nanoparticles, even in minute quantities, have the potential to drastically alter soil engineering properties like as strength, permeability, indices, and resistance. Ultimately, this research emphasises the practical applications of nanoscience in geotechnical engineering, particularly in the creation of nanotechnological tools for regulating and comprehending soil dynamics on a microscopic scale.

The novel technique of stabilising soil using nano-silica and nano-clay is discussed in this article. We explore the cutting-edge methods used to incorporate these nanomaterials into sandy soils as well as the underlying processes. Furthermore, we investigate the geotechnical benefits of nano-silica and nano-clay, which include increased shear strength, decreased compressibility, and better durability. In addition to discussing the technical details, this study highlights the financial and ecological benefits of using nano-materials for soil stabilisation. One way to encourage sustainable practices in infrastructure construction is to lessen the reliance on soil stabilisation procedures that are both energies demanding and environmentally damaging.

2. Methodology

2.1. Sample preparation

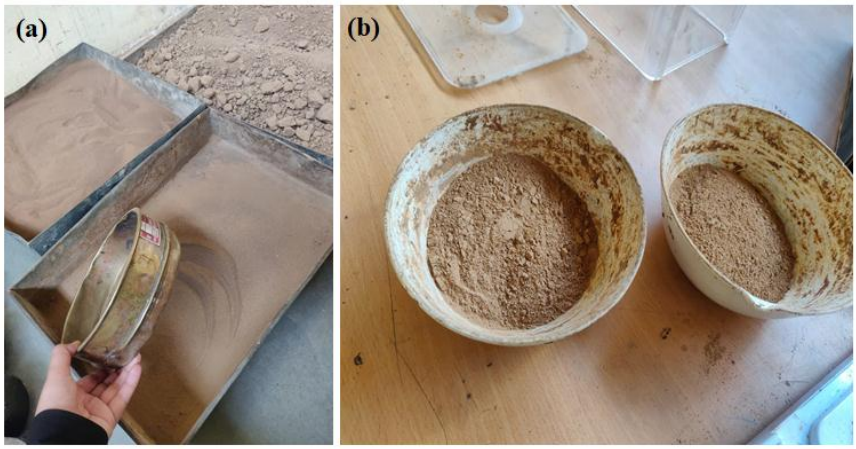

Figure 1 Preparation of sample

Five samples were made, as shown in Table 1. The first sample, which was soft soil, was used as the basis sample, and the second sample was created by combining 1% nanoclay with the soft soil. In order to create the third, fourth, and fifth samples, 3%, 4%, and 5% of nanoclay were mixed with the soft soil, respectively. Combinations of soft soil and nano clay samples were prepared according to the optimal content of moisture. The unconfined compressive test (UCT), the compaction test, and the Atterberg border examination were three primary evaluations. Standard BS 1377:1990 served as the foundation for all of the tests. Compression testing and the consolidated drained test were performed by compacting the material into a mold. Wrapping and storing the specimen samples at room temperature prevented moisture content loss before they were analyzed for the UCT and compaction test. Soil samples and those with 1%, 3%, 4%, and 5% nanoclay were able to react in this way.

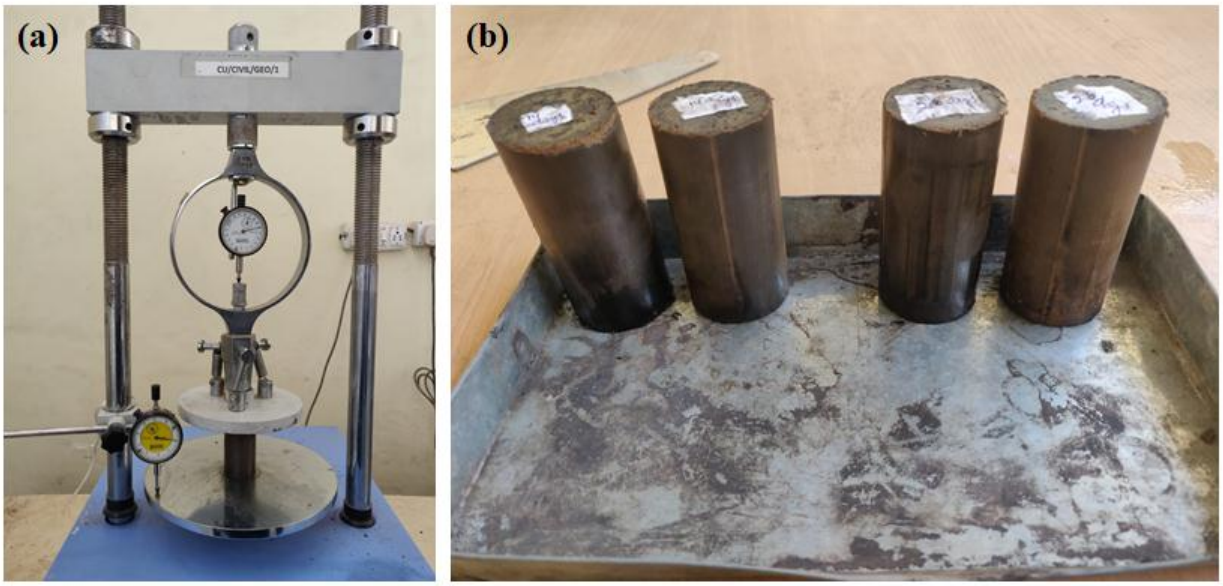

Figure 2 Compaction used for preparation of samples

Table 1 Sample nomenclature

Sample ID	Constituents
SS	Soft soil
1% NC	Soft soil + 1% nanoclay
3% NC	Soft soil + 3% nanoclay
4% NC	Soft soil + 4% nanoclay
5% NC	Soft soil + 5% nanoclay

2.2. Process of experimentation

Nano-Clay and soft soil are the two materials that must be utilised together in order to conduct experiments. Before conducting tests with different combinations of Nanoclay and Soft soil, the two must be mixed separately according to ASTM and applicable Indian Standard regulations.

2.3. Machine Learning Algorithm

Many disciplines, including geotechnical engineering and soil mechanics, rely on machine learning (ML) algorithms to forecast intricate correlations between factors. Such algorithms are priceless for jobs like forecasting soil dry density from input parameters like water content and nanoclay (NC) percentages because they can find patterns in the data and make reliable predictions. This section will focus on the application of machine learning algorithms for response prediction, namely SVM, decision trees, random forests, and linear regression. Using NC percentages and water content, machine learning methods provide robust solutions for soil dry density predictions. Linear regression provides both simplicity and interpretability, in contrast to decision trees and random forests, which capture non-linear correlations and interactions between variables. Despite their high processing requirements, support vector machines are effective at dealing with data that has many dimensions. The precise needs of accuracy, interpretability, and processing resources in the particular research setting determine which method is best.

3. Result and Discussion

3.1. Result analysis for specific gravity

Specific gravity results show (fig. 3) a decrease in specific gravity as the percentage of nanoclay increases.

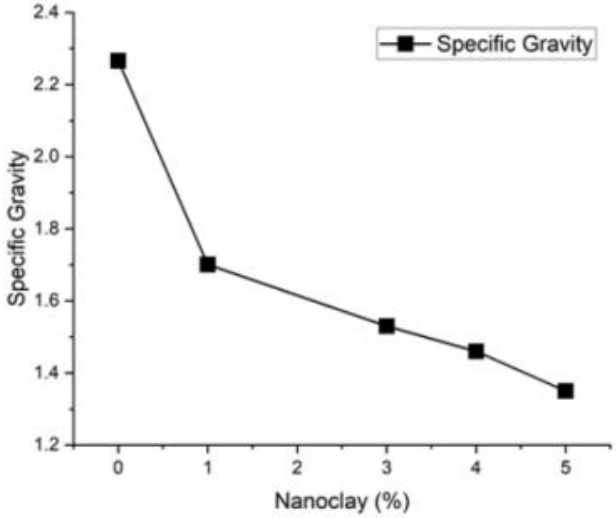

Figure 3 Nanoclay% v/s specific gravity illustration

The present graphical trend (figure 3) demonstrates that the density of the soil falls as the quantity of nanoclay in the soil rises. This could be because, when added in greater amounts, the lightweight and porous character of nanoclay particles lowers the soil's total density.

3.2. Analysis of Atterberg limits

The study's findings indicate that when the amount of nanosoil increases, the liquid limit and plastic limit results marginally rise.

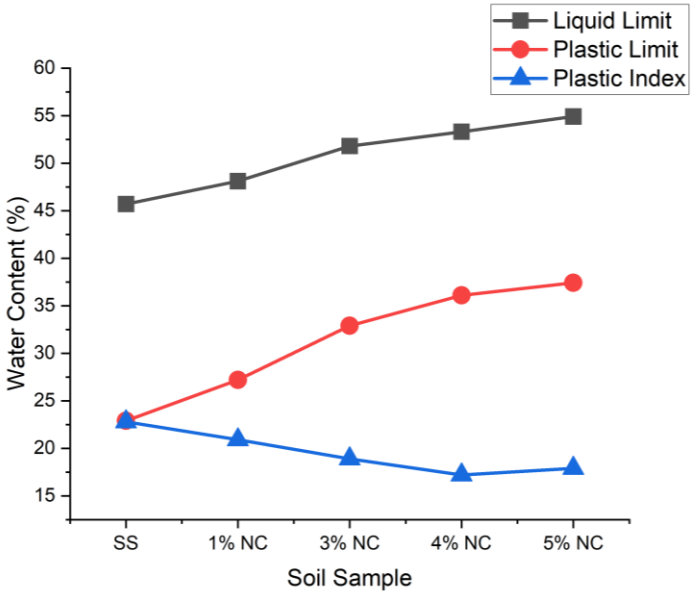

Figure 4 Samples' liquid, plastic, and plastic index limits in relation to water content

In contrast, the plasticity index decreased as the amount of nanosoil increased. As the increasing percentage of nano-clay compared to unstabilized soft soil, which was classed as clay of intermediate plasticity, the silt of high plasticity was assigned to the soft soil stabilised with nano-clay based on the plasticity chart classification. According to Taha (2009), the lowering of the plasticity index is one sign of soil stabilisation and improvement of soil qualities. The Liquid Limit (LL) and Plastic Limit (PL) values rise when nano-clay is added. The Plastic Index (PI) typically falls as the proportion of nano-soil rises. The soil with the addition of nanosoil (3%, 4%, and 5%) is categorised as "Silt of high plasticity," whilst the control soft soil is designated as "Clay of Intermediate plasticity." This implies that adding additional nano-soil changes the properties of soil plasticity, changing it from a clay type to a greater plasticity silt type.

3.3. Analysis of compaction test

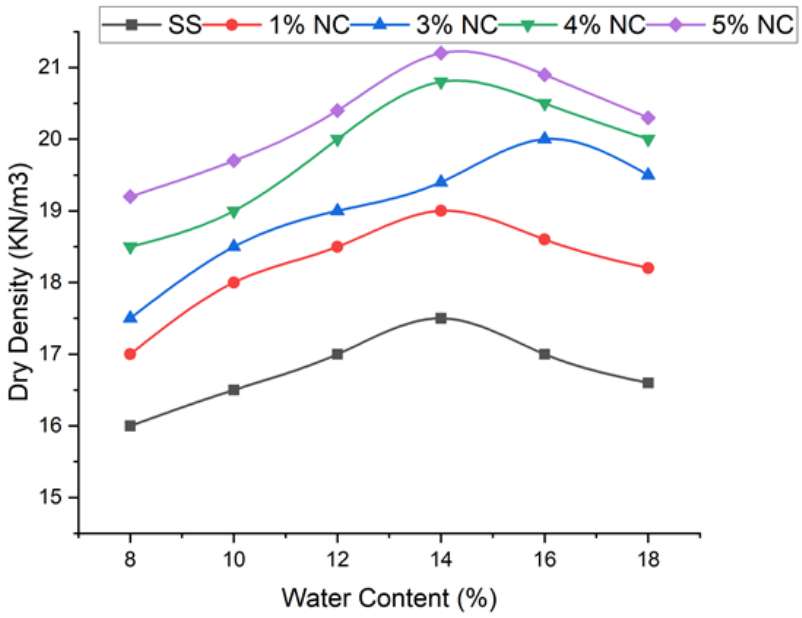

Figure 5 Compaction response with different percentage of nanoclay

The figure 5 presents data on water content (%) and dry density (in kilonewtons per cubic meter, KN/m³) for different soil compositions varying percentages of nanoclay (1%, 3%, 4%, and 5%).

As the water content increases from 8% to 18% (figure 4.3), there's a trend of increasing dry density across all compositions. Comparing the dry densities of soft soil and soft soil with nanoclay additions. For the same water content, the introduction of nanoclay increases the dry density compared to the soft soil alone. The dry density tends to increase with higher percentages of nanoclay, indicating that nanoclay incorporation contributes to higher soil compaction and density. The variations in dry density at different water contents and nanoclay percentages highlight the influence of these factors on the overall density and compaction characteristics of the soil mixtures.

3.4. UCS test

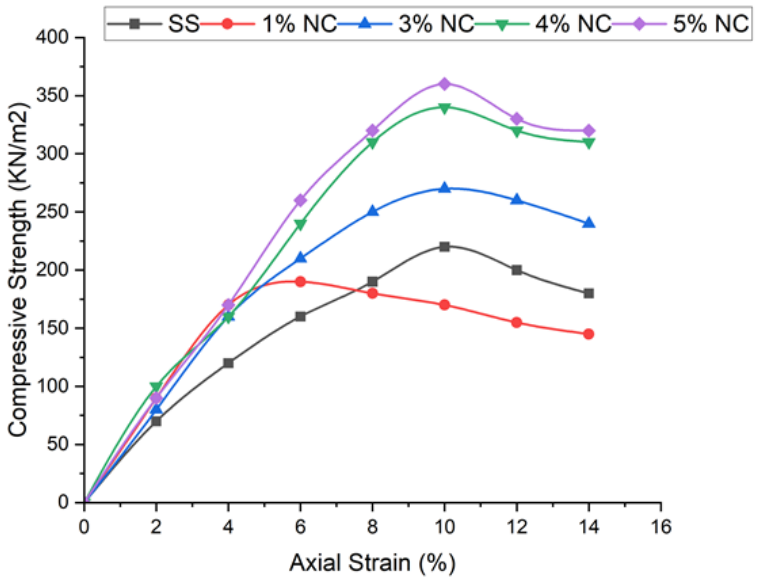

Figure 6 Axial strength v/s Compressive strength (UCS test) for different percentage of nanoclay

The table provides data on axial strain (%), which represents the deformation of the soil sample under axial compression, and compressive strength (in kilonewtons per square meter, KN/m²) for different soil compositions.

As the axial strain increases from 0% to 14%, representing increased compression on the soil sample, the compressive strength generally increases across all compositions.

Comparing the compressive strengths of soft soil and soft soil with nanoclay additions, the inclusion of nanoclay often results in a higher compressive strength than only soft soil at the same degree of axial strain.Higher percentages of nanoclay tend to enhance compressive strength, suggesting that adding nanoclay improves the properties of soil mixes' compressive strength.

The variations in compressive strength at different levels of axial strain and nanoclay percentages demonstrate how these factors influence the overall mechanical behavior and strength of the soil samples under compression.

3.5. SEM and XRD characterization of samples

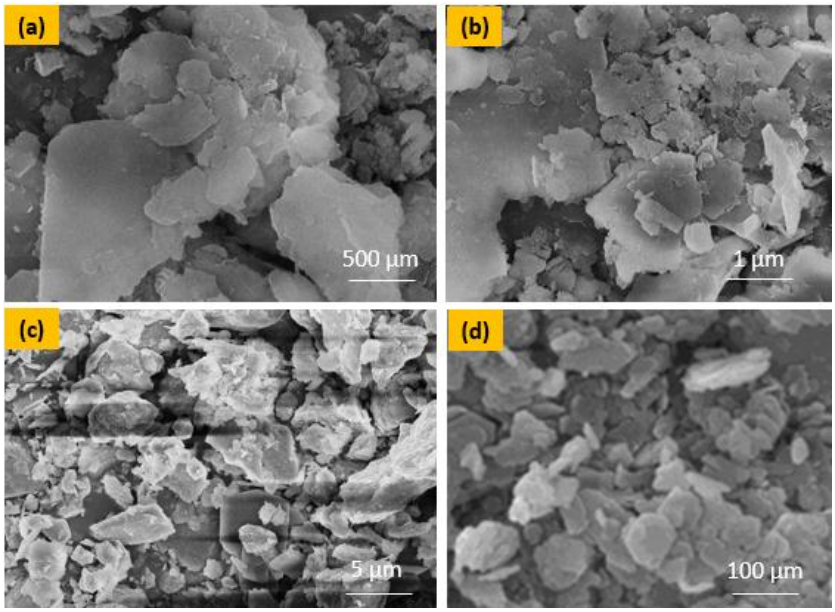

Figure 7 SEM images at 500x (a) Soft soil (b) Soft soil+1% Nanoclay (c) Soft soil+3% Nanoclay (d) Soft soil+4% Nanoclay (e) Soft soil+5% Nanoclay

Scanning electron microscopy (SEM) images only show the surface of the material, it could be challenging to derive meaningful inferences from them. After 28 days of curing, samples of1%,3%,4%, and 5% were placed on the treated soil for scanning electron microscopy (SEM) evolution imaging. The results were shown using SEM. The soil hydration system is affected by several things, including how the samples are prepared and even the images that are taken by the operators. For instance, since very small particles are used to capture images after they have been magnified, the operator may alter the measurements without realizing it or understanding the significance of the photographs. The first photo shows soil that has been adequately hydrated, whereas the second shows dirt that has been inadequately hydrated. The prior assumption was supported by the results of the SEM analysis, which showed the microstructures of the clay. Figure 7, a scanning electron micrograph (SEM) of soil containing varying percentages of clay taken at various points throughout. It is possible for pozzolanic reactions to take place between hydrated products and clay fine minerals even in the absence of clay particles, as seen in the images, which highlight the relationship between clay particles and stabilized clay structure. Remarkably, stabilized clay contains silt and sand particles in its matrix due to the binding of sand particles to the clay's surface by products of cement hydration, such as CSH. We know from prior research that only a small percentage of clay and silt particles form inert mixtures.

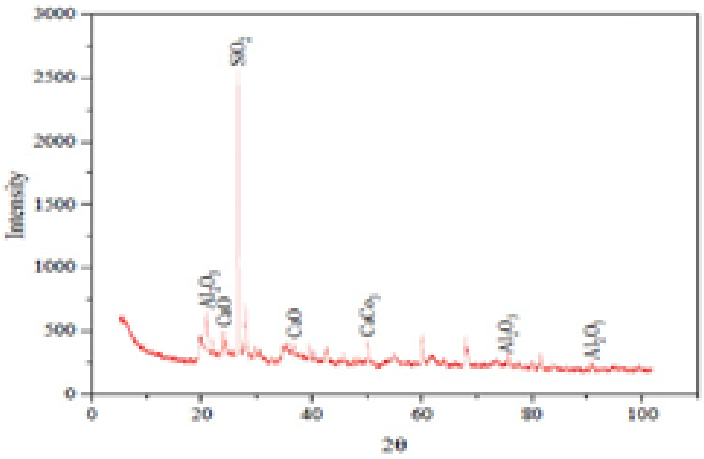

Figure 8 XRD pattern of soft soil

After 28 days of curing, X-ray diffraction analyses were performed on samples with four different percentages (1%, 3%, 4%, and 5%). These analyses helped determine the substances' period texture and identified the main reactive compounds, The spectrum reveals a reduction in the crystalline phases, which is a result of the increased material used for particle bonding development.

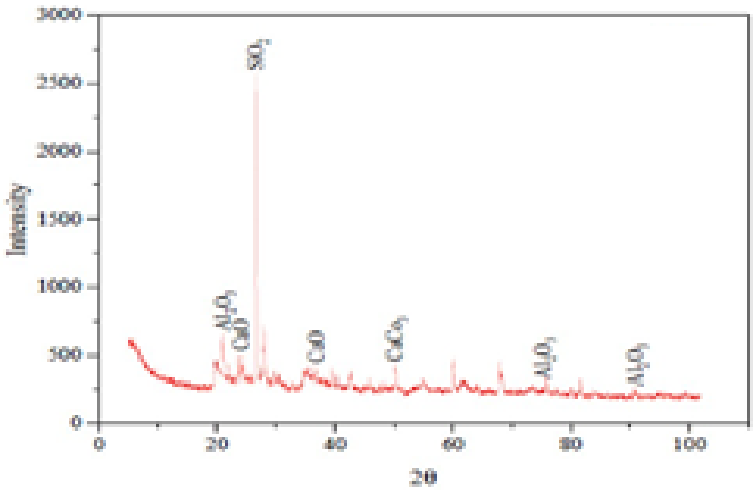

Figure 9 XRD pattern (a) Soft soil+1% Nanoclay (b) Soft soil+3% Nanoclay (c) Soft soil+4% Nanoclay (d) Soft soil+5% Nanoclay

3.6. Machine Learning Model Results for Dry Density Prediction

The linear regression model fits a line to the data for each nanoclay (NC) percentage (1%, 3%, 4%, and 5%) to predict the density of dried samples on content of water. Scatter plots shown in fig. 10 shows the actual data points for dry density versus water content for each NC percentage. The regression lines (dashed lines) indicate the predicted relationship between dry density and water content according to the linear regression model. The regression lines for different NC percentages will have different slopes (coefficients) and intercepts. For varying NC percentages, the prediction equations and high R^2 values show a robust linear connection between water content and dry density. The dry density drops with increasing water content for all NC percentages, albeit the exact rate of drop varies with each NC %.

The high R^2 values suggest that the linear regression models are good fits for the data, meaning water content is a significant predictor of dry density for these soil samples.

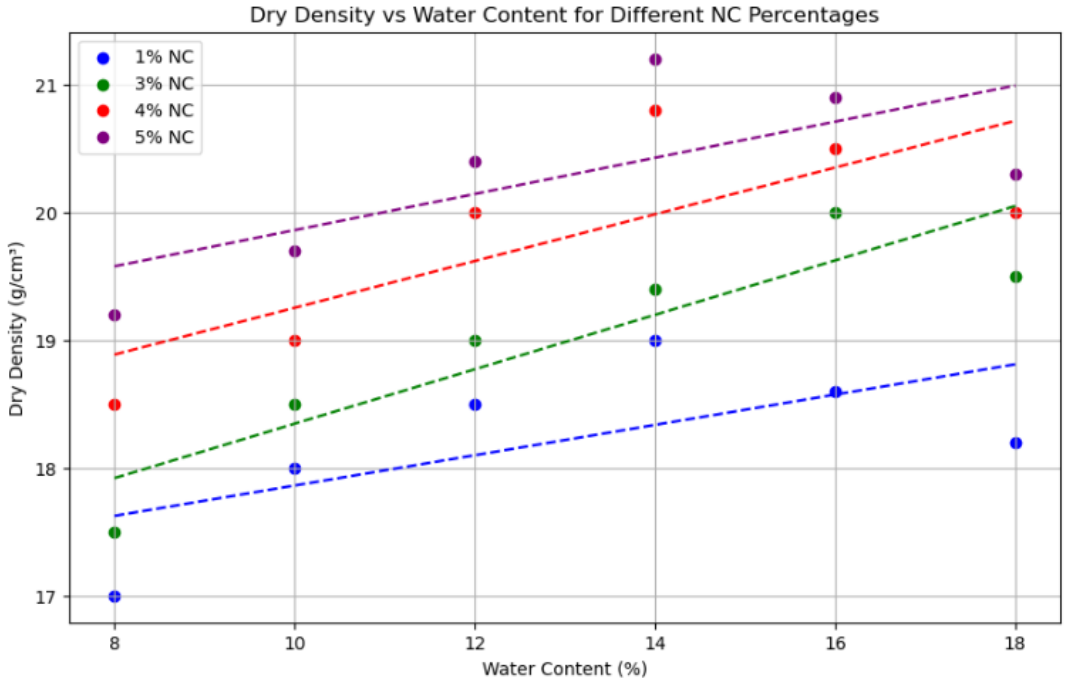

Figure 10 Scatter plot of Dry density v/s Water content

The mathematical equations for calculation of dry density as a function of water content are given in equation (i), (ii), (iii) and (iv):

For 1% Nanoclay content:

Dry Density=0.1186*Water Content+16.6752……. (i)

For 3% Nanoclay content:

Dry Density=0.2129*Water Content+16.2162……..……(ii)

For 4% Nanoclay content:

Dry Density=0.1829*Water Content+17.4229……..…. (iii)

For 5% Nanoclay content:

Dry Density=0.1414*Water Content+18.4448…… ……(iv)

4. Conclusion

The current graphical trend indicates, as volume of nanoclay in soil surges, soil's density decreases. This reduction in density is likely due to the lightweight and porous nature of nanoclay particles, which reduce the overall density when incorporated in larger quantities. When nanoclay is added to soil, it raises the values of Liquid Limit (LL) and Plastic Limit (PL). Plastic Index (PI) values tend to fall as nanoclay percentages become higher. Soil with 3%, 4%, or 5% additional nanoclay is referred to as "Silt of high plasticity," in contrast to the control soft soil, which is categorized as "Clay of Intermediate plasticity." This suggests that the soil's plasticity changes when nanoclay is applied, going from a clay type to a greater plasticity silt type. Soil compaction and density are both improved by adding nanoclay, as the dry density rises as the proportion of nanoclay increases. Compressive strength variations with axial strain and nanoclay % show how these parameters affect the mechanical behavior and compressive strength of soil samples. The microstructures of the clay were shown by SEM investigation, which lends credence to this. The linear link between water content and dry density for varying percentages of nanoclay is strongly shown by predictive equations and good R^2 values.

References

[1] Ikeagwuani, C. C., & Nwonu, D. C. (2019). Emerging trends in expansive soil stabilisation: A review. *Journal of Rock Mechanics and Geotechnical Engineering*, *11*(2), 423-440.

[2] Afrin, H. (2017). A review on different types of soil stabilization techniques. *International Journal of Transportation Engineering and Technology*, *3*(2), 19-24.

[3] Nabil, M., Mustapha, A., & Rios, S. (2020). Impact of wetting-drying cycles on the mechanical properties of lime-stabilized soils. *International Journal of Pavement Research and Technology*, *13*(1), 83-92.

[4] Jawad, I. T., Taha, M. R., Majeed, Z. H., & Khan, T. A. (2014). Soil stabilization using lime: Advantages, disadvantages and proposing a potential alternative. *Research Journal of Applied Sciences, Engineering and Technology*, *8*(4), 510-520.

[5] Rivera, J. F., Orobio, A., de Gutierrez, R. M., & Cristelo, N. (2020). Clayey soil stabilization using alkali-activated cementitious materials. *Materiales de Construcción*, *70*(337), e211-e211.

[6] Cabezas, R., & Cataldo, C. (2019). Influence of chemical stabilization method and its effective additive concentration (EAC) in non-pavement roads: A study in andesite-based soils. *Cogent Engineering*, *6*(1), 1592658.

[7] Ikeagwuani, C. C., & Nwonu, D. C. (2019). Resilient modulus of lime-bamboo ash stabilized subgrade soil with different compactive energy. *Geotechnical and Geological Engineering*, *37*(4), 3557-3565.

[8] Phanikumar, B. R., & Nagaraju, T. V. (2019). Swell and compressibility of GGBS–clay mixes in lumps and powders: Effect of 4% lime. *Indian Geotechnical Journal*, *49*(2), 161-169.

[9] Bring, J. K. (2021). Developing a sustainable post-fire soil restoration technique using pulp mill fly ash and agreeing polymer (Doctoral dissertation, University of British Columbia).

[10] Iyengar, S. R., Masad, E., Rodriguez, A. K., Bazzi, H. S., Little, D., & Hanley, H. J. (2013). Pavement subgrade stabilization using polymers: Characterization and performance. *Journal of Materials in Civil Engineering*, *25*(4), 472-483.

[11] Ikeagwuani, C. C., & Nwonu, D. C. (2019). Emerging trends in expansive soil stabilisation: A review. *Journal of Rock Mechanics and Geotechnical Engineering*, *11*(2), 423-440.

[12] Balasubramaniam, A. S., Bergado, D. T., Buensuceso Jr, B. R., & Yong, W. C. (1989). Strength and deformation characteristics of lime-treated soft clays. *Geotechnical Engineering*, *20*, 49-65.
[13] Holtz, W. G., & Gibbs, H. J. (1956). Engineering properties of expansive clays. *Transactions, ASCE*, *121*, Paper No. 2814.
[14] Bell, F. G. (1988). Stabilization and treatment of clay soils with lime. Part 1: Basic principles. *Ground Engineering*, *21*, 10-15.
[15] Moses, G., Saminu, A., & Oriola, F. O. P. (2012). Influence of compactive efforts on compacted foundry sand treated with cement kiln dust. *Civil and Environmental Research*, *2*(5), 11-24.
[16] Zhang, Y., Sappinen, T., Korkiala-Tanttu, L., Vilenius, M., & Juuti, E. (2021). Investigations into stabilized waste foundry sand for applications in pavement structures. *Resources, Conservation and Recycling*, *170*, 105585.
[17] Siddique, R. (2007). *Waste materials and by-products in concrete.* Springer Science & Business Media.
[18] Yadu, L., Tripathi, R. K., & Singh, D. (2011). Comparison of fly ash and rice husk ash stabilized black cotton soil. *International Journal of Earth Sciences and Engineering*, *4*(06), 42–45.
[19] Lamb, T. W., & Whitman, R. V. (1969). *Soil mechanics.* John Wiley & Sons Publishing.
[20] Zhang, G. (2007). Soil nanoparticles and their influence on engineering properties of soils. In *Advances in Measurement and Modelling of Soil Behavior.* ASCE.
[21] Yalamanchili, M. R., Veeramasuneni, S., Azevedo, M. A. D., & Miller, J. D. (1998). Use of atomic force microscopy in particle science and technology research. *Colloids and Surfaces A*, *133*, 77–88.
[22] Kollensperger, G., Friedbacher, G., Krammer, A., & Grasserbauer, M. (1999). Application of atomic force microscopy to particle sizing. *Journal of Analytical and Bioanalytical Chemistry*, *363*(4), 323–332.
[23] Feynman, R. (1960). There is plenty of room at the bottom. *Engineering and Science (California Institute of Technology*, *23*, 22–36.
[24] Booker, R., & Boysen, E. (2005). *Nanotechnology for dummies.* Wiley Publishing.
[25] Zhu, R., & Lau, S. (2010). A high-resolution TEM investigation of nanoparticles in soils. *Journal of Molecular Environmental Soil Science, Interfaces Earth Critical Zone*, 282–284.
[26] Jha, K. K. (2012). *An energy-based nano mechanical properties evaluation method for cementitious materials* (Ph.D. dissertation). Florida International University, Miami, FL, USA.
[27] Mohamadzadeh Sani, M., Arabani, M., Haghi, A. K., & Chenari, R. J. (2010). Effect of nanoclay additive on the geotechnical properties of silty sands. In *Proceedings of the 4th International Conference on Geotechnical Engineering and Soil Mechanics*, Tehran, Iran, 2–3 November (in Persian).
[28] Arabani, M., Haghi, A. K., Mohamadzadeh Sani, A., & Kambozia, N. (2012). Use of nanoclay for improvement of the microstructure and mechanical properties of soil stabilized by cement. In *Proceedings of the 4th International Conference on Nanostructures (ICNS4)*, Kish Island, Iran, 12–14 March.
[29] Khalid, N., Arshad, M. F., Mukri, M., Mohamad, K., & Kamarudin, F. (2015). Influence of nano-soil particles in soft soil stabilization, *20*, 731–738.
[30] Lou, H. L., Hsiao, D. H., & Lin, C. K. (2012). Cohesive soil stabilized using sewage sludge ash/cement and nano aluminum oxide. *International Journal of Transportation Science and Technology*, *1*(1), 83–100.
[31] Nikookar, M., Bahari, M., Nikookar, H., & Arabani, M. (2013). The strength characteristics of silty soil stabilized using nanoclay. In *Proceedings of the 7th Symposium on Advances in Science & Technology (7thSASTech)*, Bandar-Abbas, Iran, 7–8 March.
[32] Majeed, Z. H., & Taha, M. R. (2012). Effect of nanomaterial treatment on geotechnical properties of a Penang soft soil. *Asian Scientific Research*, *2*(11), 587–592.

Detection of Crack Location by Using Impedance Technique-A Review

Angoori Lodhi [1], Manoj Narwariya[2]

[1]*Research scholar, Mechanical Engineering Department, IPS College of Technology and Management, Gwalior-474001 (MP), India*
[2]*Professor, Mechanical Engineering Department, IPS College of Technology and Management, Gwalior-474001 (MP), India*

Abstract This paper explores the challenges to fatigue stress and cyclic loading in engineering surfaces, particularly focusing on metal surfaces and plates where crack often initiate at the microscopic level. Crack detection methods are categorized into two primary approaches: destructive testing and non-destructive testing (NDT). Through visual examination and various surveying tools, surface condition deficiencies can be assessed. Automated crack detection is facilitated by several NDT techniques, including thermal testing and infrared, ultrasonic testing, radiographic testing and laser testing. Recent advancements in computer hardware and software, particularly the emergence of multi-core processors and the utilization of graphic processing units (GPUs), have significantly enhanced the efficiency of training deep neural networks. These techniques are further classified into four categories: integrated algorithms, percolation-based methods, practical techniques and morphological approaches. This is achieved using dedicated software packages in environments such as NVIDIA, Python, MATLAB, as well as cloud-based platforms like Amazon and Google. The methodology presented in this study enables the identification of occurrence, location and size of single and multiple cracks in metal structures. However, given that the impedance response is localized, multiple piezoelectric (PZT) sensors must be employed for effective detection of multiple cracks.

Keywords*: Enter your keywords her Keywords*: piezoelectric transducers; impedance-based detection of crack location; metal surface; piezoelectric sensors; impedance analyzer; actuator.

1. Introduction

The review aims provide a thorough understanding of the advancements in EMI technology over the past decade, highlighting theoretical foundations, practical applications, and future challenges. Address issues related to the long-term durability of the bond between the sensor and the structure, which can affect measurement reliability. Discuss the potential degradation of piezoelectric materials over time and its impact on sensor performance. Examine the constraints in the spatial resolution and sensing range of EMI, proposing solutions or technological advances that could mitigate these limitations. Explore the challenges in establishing baseline impedance signatures, which are critical for effective damage detection. Discuss techniques for adapting reference signatures in real-time monitoring scenarios. ANNs are used to analyze impedance data and identify damage patterns. Include examples of successful implementations of ANNs in damage detection through EMI, etimphasizing their effectiveness compared to traditional methods.

Destructive testing (DT) method involves testing the material until it fails, which allows for a comprehensive understanding of its properties and limits, but Non-destructive testing (NDT) methods allow for crack detection without causing any damage to the structure and they are crucial for regular inspections and maintenance. NDT techniques: Visual inspection is the most basic method; involves examining the surface for visible cracks or anomalies, ultrasonic testing uses high-frequency sound waves to detect internal flaws by measuring the time it takes for the wave to return and magnetic particle testing detects surface and near-surface defects in ferromagnetic materials by applying a magnetic field and observing magnetic particle patterns.

Early detection of cracks can significantly enhance safety and reliability, reduce repair costs, and extend the lifespan of structures. By utilizing a combination of visual inspection and advanced NDT techniques, engineers can effectively monitor structural integrity and implement preventive measures before cracks lead to catastrophic failures. Automatic crack detection techniques are infrared and thermal testing technique detects temperature variations. on the surface of materials, which can indicate subsurface flaws or defects, ultrasonic testing uses high-frequency sound waves to detect internal flaws, laser testing uses employs laser scanning technology to create high-resolution surface maps and detect cracks, radiographic testing involves using X-ray or gamma rays to inspect the internal structure of materials etc.

1.1. Advances in computer hardware and software

The combination of advance hardware and sophisticated software frameworks has revolutionized the field of deep

Published online on: ***February 01, 2025***
Corresponding Author's E-mail ID: drmanoj.academic@gmail.com

learning, enabling researchers to train more complex models with larger datasets in significantly shorter time frames. This progress continues to expand the horizons of what's possible in artificial intelligence, impacting various domains such as healthcare, finance, autonomous systems, and more. Recent advancements in computer hardware and software, particularly the emergence of multi-core processors and the utilization of graphic processing units (GPUs), have significantly enhanced the efficiency of training deep neural networks. This is achieved using dedicated software packages in environments such as NVIDIA, Python, MATLAB, as well as cloud-based platforms like Amazon and Google.

1.2. Principle of EMI technology

EMI technology leverages the interaction between electrical and mechanical systems. When a piezoelectric sensor is attached to a structure, it can convert mechanical vibrations into electrical signals and vice versa. The mechanical impedance of the structure influences the electrical impedance of the piezoelectric sensor. When the structure experiences damage, its mechanical properties change, resulting in measurable alteration in the sensor's impedance. Signal processing is advanced algorithms analyze impedance data to extract features indicative of structural damage and emerging methods employ machine learning techniques to classify and predict damage based on historical data and impedance patterns. Environmental factors are variations in temperature, humidity, and other environmental conditions can affect the impedance readings, necessitating careful calibration and interpretation. The effectiveness of EMI depends on proper sensor placement to ensure that it accurately reflects the structural condition.

This section can delve into the fundamental principles behind EMI, including the mechanics of piezoelectric materials, the relationship between mechanical and electrical impedance, and how these principles are utilized in structural health monitoring. Discuss practical steps for deploying EMI, such as sensor selection, bonding techniques, and experimental setup for impedance measurements. Review a variety of applications where EMI has been effectively employed, such as in civil engineering structure, aerospace components, and mechanical systems. Highlight how different frequency ranges affect the sensitively and accuracy of damage detection. Discuss how researchers utilize FEM to simulate the structural response and predict the effects of damage on impedance signatures.

EMI technology is a powerful tool in the field of structural health monitoring, offering a sensitive, non-destructive means of detecting and assessing damage. As technology continues to evolve, its integration with other monitoring method and data analytics will enhance its effectiveness and reliability in ensuring structural safety.

.

2. EMI Technique in Prediction of crack

B.P. Nandwana et al. (1997): The study by author presented an innovative approach to detect cracks in a stepped cantilever beam using natural frequency measurements. In this method, cracks were modeled as rotational springs, allowing for the analysis of how crack location influences the stiffness of the beam across different natural modes. The crack was modeled as a rotational spring, which simplifies the analysis of its effect on the beam stiffness. The method relied on measuring the natural frequencies of the beam in three different modes. This provided a basis for determining the stiffness associated with the crack at various locations. By solving the characteristic equation, plots of stiffness versus crack location were generated for the three modes. Once the crack location was identified, the size of the crack can be computed using established relationships between stiffness and crack size. This method offers a systematic way to pinpoint and quantify cracks in structural elements, which was crucial for maintenance and safety assessments in engineering applications [1].

O. S. Salawu et al. (1997): Author emphasized that while vibration monitoring using natural frequencies offers a promising approach for structural assessment, careful consideration must be given to the factors that can impact its effectiveness. The paper advocates for further research to enhance the reliability of this technique and expand its applicability in real-world scenarios. The paper identified several factors that can hinder the successful application of vibration monitoring for damage detection, including environmental influences, sensor placement and structural complexity. The paper discussed how systematic analysis of frequency data can help in identifying and quantifying structural damage. Frequency changes could serve as indicators of issues such as cracks, fatigue, and other forms of deterioration [2].

Giurgiutiu et al. (1998): Author contributed valuable insights into the E/M impedance method for structural health monitoring, demonstrating its potential for predicting remaining life based on stiffness changes. This work underscored the method's applicability in real-world settings, where understanding the relationship between loading conditions and structural integrity was vital for effective maintenance strategies. The study established a correspondence between the stiffness loss of structures and their remaining life under fatigue loading. This relationship is crucial for assessing structural integrity and predicting failure. The authors argue that the observed relationship was not limited to specific

condition but could be generalized to any repetitive fatigue-loading spectrum. This means the finding can be applied across different loading scenarios in structural assessments. The electromechanical impedance method was highlight as a viable technique for monitoring structural health. By calibrating the method, it can provide quantitative indications of the remaining life of structure under defined loading conditions [3].

Park et al. (2003): The study by author highlighted the advantages of the impedance method for non-destructive evaluation (NDT) in monitoring structural health. The impedance method operated in a high-frequency range, making it highly sensitive to early signs of damage in structures. This allowed for the detection of incipient issues before they develop into significant problems. The method was well-suited for autonomous monitoring systems. its data acquisition process can be automated requiring minimal user intervention. This feature allowed for continuous health monitoring of structures, enhancing safety and maintenance efficiency. Overall the impedance method presented a promising alternative to conventional NDE approaches, particularly for ongoing assessments in dynamic environments [4].

Verma et al. (2003): The study by author discussed the advantages of the electro-magnetic inspection (EMI) technique in non-destructive evaluation (NDE). EMI operates over a wide range of frequencies, significantly enhancing its sensitively to variations in the properties of the host material. This allowed for the detection of subtle changes that may indicate damage. The technique supports ongoing monitoring at regular intervals, enabling the collection of extensive data over time. This long-term data can be instrumental in assessing the aging and deterioration of structures. Overall, the EMI technique offers a robust method for ongoing structural assessment, enhancing safety and maintenance strategies in civil engineering [5].

Bhalla et al. (2008): The study by author presented the new EMI-based technique outperforms existing methods, such as ultrasonic techniques, for predicting concrete strength. This improvement highlights its effectiveness in assessing structural integrity. The study also demonstrated the feasibility of using EMI to monitor the curing process of concrete. This capability allowed for real-time assessment of curing conditions, which was crucial for achieving optimal concrete strength. The EMI technique exhibits significantly higher sensitivity compared to conventional non-destructive evaluation (NDE) methods, enabling more accurate detection of variations in concrete properties. Overall, this research highlighted the potential of EMI as a superior tool for both assessing concrete strength and monitoring curing contributing to better quality control in construction practices [6].

Yang et al. (2008): The study by author investigates the influence of external excitation on the admittance signature of piezoelectric transducers (PZT). The research emphasized that the effect of external vibrations cannot be overlooked, especially when the frequencies of the external excitation and the PZT actuation are comparable. The paper derived a fundamental formulation of the Electro-Magnetic inspection (EMI) model for a simply supported beam subjected to external excitations. This theoretical framework set the stage for the experimental investigation. The study involved testing an aluminum beam specimen bonded with a PZT sensor. Various external excitations were applied, and the corresponding admittance signatures of the PZT sensor were measured to analyze the impact of these vibrations. Overall this research provides valuable insights into how external vibrations affect PZT signatures, which was important for the effective use of PZT in structural health monitoring and non-destructive testing [7].

Liu et al. (2009): the study by author focused on enhancing the piezoelectric impedance-based technique for assessing damage in truss structures, particularly using longitudinal waves. The research highlighted the good performance of piezoelectric impedance methods in damage detection, especially when utilizing longitudinal wave modes. However, achieving a satisfactory longitudinal impedance output in practical applications could be challenging. The authors previously discovered that appropriate selection of PZT patches can effectively generate longitudinal vibration modes. This finding motivated the current study, which aims to optimize patch design for improved impedance response. The paper explored the influence of various PZT patch design parameter on the impedance response through theoretical analysis. Finally, the study applied the optimized longitudinal modes for damage assessment, specifically investigating crack detection in beams through both experimental and analytical methods. Overall, this research contributed to refining the piezoelectric impedance technique, making it more viable for practical damage assessment in structural applications [8].

Soh et al. (2009): The study by author investigated the effectiveness of the Electro-Magnetic inspection (EMI) technique for detecting and characterizing fatigue-induced damage in structures. The research demonstrated that the EMI technique was highly effective in identifying incipient cracks through changes in the frequency of the admittance signature, even at the very early stages of crack initiation. The propagation of cracks could also be accurately reflected in the admittance plots, making the EMI technique a useful tool for tracking the progression of damage over time. The main objective of the study was to assess the feasibility of using the EMI technique with surface-bonded PZT patches for detecting and characterizing damage caused by fatigue. Experimental results supported the claim that the EMI technique excels in detecting incipient cracks and monitoring their development, highlighting it was potential for practical applications in structural health monitoring. Overall, This research underscored the reliability of the EMI technique for

early damage detection and characterization, contributing to safer and more efficient maintenance practices in engineering structures [9].

Lim et al. (2010): The study by author examined the progressive nature of fatigue-induced damage in structure and the importance of monitoring for early detection of cracks. Fatigue-induced damage was characterized by a gradual process of crack initiation, propagation, and eventual fracture, especially in structures subjected to numerous loading cycles. The research highlighted the effectiveness of smart materials, particularly piezo-impedance transducers, in conjunction with the electromechanical impedance (EMI) technique and wave propagation techniques for detecting incipient damage. The study shown that progressive shifts in admittance signatures measured by PZT patches correspond to an increase in loading cycles, demonstrating the EMI technique's capability to track the progression of fatigue damage. By applying Linear Elastic Fracture Mechanics (LEFM), the research suggested that it was possible to predict the remaining life of a structure based on the number of loading cycles, further emphasizing the practical implications of the monitoring techniques. Overall, This study underscored the significance of advanced monitoring methods in understanding and managing fatigue damaged in structural components [10].

Zhang et al. (2011): The study by focused on enhancing the electro-mechanical impedance technique by developing an analytical model for better damage identification in cracked beam structures. The authors presented a quantitative EMI model specially for predicting the electromechanical impedance of a cracked beam structure. This model considered various boundary and continuity conditions. The paper emphasized that while the EMI technique traditionally did not rely on analytical models for damage identification, having an accurate model was essential for obtaining detailed information about damage. An analytical expression for the admittance of the PZT patch was derived, allowing for a more precise assessment of the structure's condition. Overall, this research contributed to improving the EMI technique by providing a structured analytical framework, which aids in more accurately detecting and characterizing structural damage [11].

Zhou et al. (2018): The paper by author described a method for detecting damage in plate structures using an array of piezoceramic transducers. By identifying multiple reflection points, the boundary of the damage was mapped. The envelope of these reflection points was used to approximate the shape of the damage. When there was damage, waves generated by an actuator reflect off the boundary of the damaged area. The point of reflection lied on an ellipse whose foci were the positions of the actuator and sensor. The method was tested experimentally using 12 piezoceramic transducers attached to an aluminum plate. These tests involved detecting the size and shape of bonded masses. This method provided a useful way to detect structural damage in materials by using reflected wave pattern and could be beneficial in fields such as aerospace, civil engineering, and mechanical engineering. The experimental results showed that the proposed method can accurately determine the size and shape of the damage with minimal error [12].

Wang et al. (2018): The paper by author explored the use of high-frequency ultrasound to assess the local stress state of structures. The study highlighted that high-frequency signals, particularly in the megahertz range, are highly sensitive to local stress states in a structure. In this experiment, a tensile load was applied to an aluminum beam, and the corresponding changes in resonant and anti-resonant frequencies were observed. The study demonstrates the effectiveness of using very high-frequency ultrasound for monitoring structural stress states and provides a foundation for non-destructive testing methods in various engineering applications, such as aerospace, civil, and mechanical engineering [13].

Wongi et al. (2018): The paper by author discusses the Electro-mechanical impedance (EMI) technique, highlighting it was potential and ongoing research challenges. The EMI technique is recognized as a powerful tool for structural health monitoring (SHM). It had been the focus of numerous studies, offering solutions to detect and assess damage in various structures by analyzing changes in impedance. Although many studies had shown the effectiveness of the EMI technique, most had been conducted under controlled laboratory conditions. The authors emphasized the need for future research to focus applying the technique to real-world structures to uncover critical challenges and make technology more practical for field use. With the continuous development of computational tools and techniques, especially Finite Element Method (FEM) simulations, the authors believe that the technique will improve in term of accuracy and applicability. This paper stressed the importance of bridging the gap between laboratory research and real-world applications, while also recognizing the role of technology advancements in enhancing the EMI technique for broader use in structural health monitoring [14].

Ye et al. (2020): The paper by author investigated the application of the Electromechanical Impedance technique, using a PZT (Lead Zirconate Titanate) transducer, for structural health monitoring. Over the past two decades, the EMI technique had proven to be a cost-effective and highly sensitive method for detecting structural damage. This study built on that research to examine its application in real-world scenarios. The research focused on tunnel invert concrete subjected to high traffic cyclic loading. To simulate different levels of initial damage, the researchers created six damage levels in the specimens by applying impacts with a free-falling iron ball. This controlled damage was used to assess how the EMI technique responds to varying damage levels under cyclic stress. This paper contributed to the practical application of the EMI technique in real-world infrastructure monitoring, showing its potential for use in tunnel

maintenance and assessment under demanding operational conditions [15].

Hamzeloo et al. (2020): The paper by presented a theoretical model for damage detection in L-shaped beams using the Electromechanical Impedance (EMI) method. The EMI technique was recognized as an effective approach within the field of nondestructive evaluation for structure health monitoring. The study focused on L-shaped beams with embedded piezoelectric wafer active sensor (PWAS). The model calculated the electromechanical impedance response of the structure based on its excitation and natural frequencies, which appear as resonance frequencies in the impedance spectrum. The theoretical predictions were validated through experiments, demonstrating good agreement between the model's impedance spectra and the actual experimental data. This confirmed the model's accuracy in predicting damage detection. The study shown that the electromechanical impedance response was sensitive to changes in the structural state, particularly at resonance frequencies The successful application of statistical algorithms for comparing pristine and damaged states confirms the efficacy of the proposed model for damage detection. Overall, the paper introduced a cost-effective theoretical approach for using the EMI method in structural health monitoring, specifically for L-shaped beams, and demonstrates its practicality by showing good alignment with experimental results [16].

Wang et al. (2021): The paper by author focuses on the use of piezoelectric admittance to detect cracks in structures, with specific attention to the peak frequency in the imaginary part of the piezoelectric admittance spectrum. The study demonstrated that the peak frequency in the imaginary part of the piezoelectric admittance spectrum was highly sensitive to the presence of a crack. As the crack length increases, the peak frequency decreases. The experimental results align with the predictions from Finite Element Model (FEM) simulations, confirming the accuracy and validity of the FEM in modeling the behavior of cracks in structures This agreement suggested that FEM can be a reliable tool for predicting structural responses in future applications. The paper proposed that future studies should use FEM to identify the resonant frequencies of complex structures. The peak frequency shift in the admittance signature can than be used to judge the degree of structural change or damage. In summary, author presented a promising method for crack detection that relies on tracking peak frequency shifts in the piezoelectric admittance spectrum. The combination of experimental results and FEM simulation reinforces the technique's potential for real-world applications, particularly in detecting small crack with high sensitively [17].

Zhu et al. (2022): the paper by author explored the use of the Electromechanical Impedance (EMI) method to measure the dynamic stress state of structural elements, with a particular focus on its application in the railroad industry. The EMI method demonstrated the ability to measure the stress state of structural elements, including identifying the zero-stress state, which is of significant interest in the railroad industry for ensuring safety and structural integrity. The capacitive responsed of the PZT, represented by susceptance, was predominantly controlled by the frequency input from the structure. The research demonstrated the potential of the EMI method, particularly through susceptance, as a stable and effective means of measuring structural dynamics and stress states. Its ability to accurately identify the zero-stress state was valuable for industries like railroads, where maintaining the integrity of structural elements was critical [18].

Singh et al. (2022): The paper by author focused on the structural health monitoring of manholes in the sewerage system, which were prone to damage due to concrete corrosion from hydrogen sulfide gas in sewage and vehicular loading. Manholes were critical components of urban infrastructure, and their failure can lead to accidents. Due to the significant number of accidents caused by damaged manholes, there was a pressing need to monitor their condition to ensure timely replacement before critical failure. The Electromechanical Impedance technique was employed to quantify the damage in the manholes. The Root Mean Square Deviation (RMSD) was used to analyze the impedance signatures at different damage stages. This allowed for effective detection and quantification of structural damage in the manholes. The paper highlights the used of the EMI technique for damage assessment of manholes, which weer crucial for maintaining road safety. The ability to predict the remaining life of manholes through structural health monitoring could be helped prevent accidents and ensure timely maintenance or replacement [19].

Roy et al. (2023): The paper by author focused on detecting and addressing small-depth cracks in beam-type structural elements using piezoelectric materials and steady-state vibration analysis. The study aims to both locate cracks and restore the dynamic response of the cracked beams. An open crack in a beam creates a discontinuity in the rotational displacement curve, making it a useful parameter for crack detection. The study revealed that a bending piezoelectric sensor could effectively detect the rotational displacement discontinuity caused by crack. This was because the voltage output from the sensor depends on the difference in rotational displacement at the two ends of the piezoelectric patch. The sensor's ability to detect this voltage variation allows it to identify the presence and location of a crack. The paper presented a novel method for detecting small-depth cracks in beams by utilizing piezoelectric sensors to measure rotational displacement discontinuities. Additionally, the use of piezoelectric materials to produce a local moment near the crack helps restore the dynamic response of the structure. The combination of theoretical modeling and experimental validation demonstrates the potential for this approach in structural health monitoring [20].

3. Conclusion

The paper presents a nondestructive method for detecting cracks in metal structure, utilizing a combination of electromechanical impedance (EMI) responses and artificial neural networks (ANNs). The others propose a new approach for identifying and conducting nondestructive evaluation (NDE) of structures. This approach is based on identifying an equivalent system through the EMI technique, simplifying the diagnostic process. A significant benefit of the proposed method is that the equivalent system can be identifying solely from experimental data, eliminating the need for a pre-existing model of the structure. This feature enhances the method's practicality and adaptability across various applications. The proposed method effectively detects not only the presence of cracks but also provides information on their location and size.

This research introduces a promising nondestructive method for crack detection in metal structures, combining EMI responses and artificial neural networks for effective real-time monitoring. Its applicability in both aerospace and civil engineering domains underscores its potential to improve structural integrity assessments and maintenance strategies. A significant consideration is that the impedance response obtained from the piezoelectric sensors (PZT) is inherently a local sensing technique. While the method presents a robust approach for crack detection in metal structures, the need for multiple sensors to monitor large areas and the potential for future applications in civil engineering are key considerations that can drive subsequent research efforts in this field.

4. References

[1] Nandwana, B. P., & Maiti, S. K. (1997). Modeling of vibration of a beam in the presence of an inclined edge or internal crack for its possible detection based on frequency measurements. *Engineering Structures*, *19*(3), 193–205.

[2] Salawu, O. S., et al. (1997). Detection of structural damage through changes in frequency: A review. *Engineering Structures.*

[3] Giurgiutiu, V., Ionita, A., & Dillard, D. A. (1998). Details of the integral equation method to the analysis of an adhesive layer crack. *International Journal of Solids and Structures.*

[4] Singh, S. K., & Maurya, K. K. (2022). Prediction of remaining life of RCC sewer manhole using smart material-based EMI technique for a sustainable environment. *Environmental Science and Pollution Research.*

[5] Ye, Y., Peng, L., Lin, Y., Lue, J., Lei, M., & Fei, R. (2020). EMI technique for monitoring the damage evaluation of initially damaged tunnel invert concrete subjected to high traffic cycle loading. *Advances in Civil Engineering.*

[6] Lim, Y. Y., & Soh, C. K. (2010). Estimation of fatigue life using electromechanical impedance technique. *Civil and Environmental Engineering, Nanyang Technological University.*

[7] Yang, Y., et al. (2008). Practical issues related to the application of the electromechanical impedance technique in the structural health monitoring of civil structures. *Smart Materials and Structures.*

[8] Zhang, Y., Xu, F., Chen, J., Wu, C., & Wen, D. (2011). Electromechanical impedance response of a cracked Timoshenko beam. *Sensors.*

[9] Hamzeloo, S. R., Barzegar, M., & Mohsenzadeh, M. (2020). Damage detection of an L-shaped beam structure with a crack by electromechanical impedance response: Analytical approach and experimental validation. *Journal of Nondestructive Evaluation.*

[10] Bhalla, S., & Soh, C. K. (2008). Electro-mechanical impedance technique for structural health monitoring and non-destructive evaluation.

[11] Wang, T., Wei, D., Shao, J., Li, Y., & Song, G. (2018). Structural stress monitoring based on piezoelectric impedance frequency shift. *Journal of Aerospace Engineering.*

[12] Zhou, M., Li, Y., Feng, Q., & Lu, G. (2018). Detecting damage size and shape in a plate structure using PZT transducer array. *Journal of Aerospace Engineering.*

[13] Roy, G., Panigrahi, B. R., & Pohit, G. (2022). Identification of crack by vibration analysis and restoration of dynamic response in beams using PZT sensor/actuator. *Nondestructive Testing and Evaluation.*

FEA Study the effect of load on factor of safety of Clevis fastener

Sonu Parihar[1], R P Singh[2]

[1,2] *Mechanical Engineering Department, IPS College of Technology and Management, Gwalior, MP – 474001 (India)*

Abstract

This study presents a detailed tensile load analysis of a clevis pin using ANSYS finite element analysis (FEA) software. Clevis pins play a pivotal role in mechanical assemblies, often subjected to tensile loads that can lead to potential failure if not properly designed. The primary objective is to understand the mechanical behaviour and performance of the clevis pin under tensile loading conditions to ensure its reliability and safety in practical applications. The study underscores the significance of utilizing ANSYS for tensile load analysis, aiding in the optimization of clevis pin design to enhance its tensile strength and overall performance. By understanding the behaviour of the clevis pin under tensile loads through FEA, designers and engineers can make informed decisions to ensure the component's reliability and longevity in mechanical assemblies

Keywords*: FEA analysis; Clevis fastener; Factor of safety; Equivalent Stress and total deformation.*

1. Introduction

Clevis pins are essential fasteners widely employed in mechanical linkages to connect and articulate various components, ensuring the smooth operation of machinery and structural systems. Their pivotal role necessitates a thorough understanding of their mechanical behaviour under different loading conditions, with tensile loading being one of the primary concerns due to its direct impact on the pin's integrity.

Most of literatures emphasize to optimize the clevis joint to improve performance and reduce weight while maintaining strength and durability in the vehicle's steering system. The literature, which highlight the importance of optimizing the clevis joint to improve performance and reduce weight while maintaining strength and durability in the vehicle's steering system, are less in open domain. Here's detailed literatures review.

William H. Greene et al. [1988] The investigation into the Space Shuttle Challenger accident highlighted a critical failure in the tang-clevis joint of the right solid rocket motor (SRM). The relative motion between the inner arm of the clevis and the O-ring sealing surface on the tang was identified as a potential factor in the failure. Authors proposed two modifications to address the relative motion issue i.e. Capture Feature and External Stiffening Rings. Both modifications proved effective in controlling the relative motion within the joint, potentially preventing similar failures in the future.

Jesse R. Crookston and Steven L. Folkman [1997] investigated the dynamic behavior of a three-bay cantilevered truss that includes eight tang/clevis-type joints with clearance fit pins. These clearance fit joints alter the dynamic behavior of the truss, in contrast to the other tightly clamped joints which exhibit linear stiffness and low damping characteristics.

According to Zienkiewicz et al. (2000), FEA has become the cornerstone for stress and structural analysis, significantly improving design processes in engineering Clevis Fasteners: Design and Applications. A clevis fastener is a U-shaped fastener with a pin or bolt through its open ends, commonly used in mechanical linkages to allow motion. Clevises are utilized in numerous applications, from aerospace to heavy machinery, where they act as pivot points.

Chang and Tang's [2001] cohesive design methodology incorporates manufacturing costs into the design process. They realize that Design problems must balance objective functions and manufacturing costs.

Brain Pechatsko et al.[2003] studied the stress distribution in pin and clevis connections. The analysis involved creating a computer model of the components and applying the expected loads to simulate real-world conditions. The author found the highest stressed region in the clearance gap between the blade and clevis. This gap can amplify stress concentrations, making it a focal point for failure analysis.

Rajkumar Roy et al.[2008] discussed automation in manual optimization processes and challenges in scalability and Emphasized on new optimization approaches like genetic algorithms (GAs) and the need for exploration in topology design, computational power, and effective optimization for large-scale problems.

The application of load on a fastener like a clevis is associated with the generation of stress concentrations, particularly around the pin holes and areas subjected to bending. As highlighted by Peterson (2008), stress concentration factors

Published online on: ***February 01, 2025***

Corresponding Author's E-mail ID: pariharsonu142@gmail.com

significantly influence the overall strength and performance of fasteners under load. Studies show that varying the load direction (tensile, shear, or combined loading) results in different stress distributions within the fastener. FEA simulations are widely employed to predict these stress concentrations and ensure that the clevis fastener design maintains a sufficient factor of safety (FOS) to prevent failure.

J. H. Argyris and R. W. Clough [2011] showed that Finite Element Analysis (FEA) is widely used for analyzing stress, strain, and deformation in mechanical parts under various loading conditions and also realised that FEA is a reliable method for examining the effects of complex loading on factors such as material properties, geometry, and connection types in components like clevis fasteners.

Rajendran et al.[2013] focused on designing optimized steering knuckles from scratch. They Utilized structural, topology, and shape optimization to achieve optimal load cases and intermediate concept models.

The factor of safety is a critical design parameter, representing the ratio between the ultimate load a structure can handle and the applied load. A higher FOS indicates a more conservative design. For clevis fasteners, ensuring an appropriate FOS involves not only understanding the material properties but also how stress is distributed under operational loads. According to Norton (2013), fasteners like clevises must maintain a FOS of 2 to 4 in typical mechanical applications to account for uncertainties such as material defects, unanticipated loading, or environmental factors.

Judong Liu et al.[2014] studied on the cylindrical plunge grinding and intermittent axial feed grinding experiment which revealed important insights into the grind-hardened layer structure and properties of the loader clevis pin done. Key findings include the presence of arc-shaped medium/high-temperature tempered zones and annular unhardened zones on the external circumference surface. These features are attributed to the temperature gradient, induced grinding heat during circumferential feed, and axial grinding heat conduction. The temperature gradient and heat conduction patterns play a crucial role in determining the final microstructure and properties of the grind-hardened layer, affecting the performance and durability of the loader clevis pin.

Amir Javidinejad [2016] examined the failure testing of clevis-pin attachments, comparing full-length symmetric configurations to partial-length asymmetric configurations. Theoretically and analytically, it is shown that higher stress levels in the partial-length asymmetric pin clevis configuration lead to earlier failure compared to the full-length symmetric configuration. The study highlights the importance of configuration in the durability and performance of clevis-pin attachments, with significant implications for design and engineering practices.

N. Patel and M. Patel [2016] did research on the FoS for clevis fasteners which emphasized understanding how variations in load conditions (e.g., tensile, shear, and combined loading) influence FoS values. The aim was to ensure that designs can withstand extreme load scenarios without failure.

Niraj Kulkarni and Pratik Maid [2017] focused on the design and analysis of a custom clevis joint. Design software such as CATIA and SolidWorks were employed to create the clevis joint, while ANSYS was used to perform a thorough analysis of the component. The study aims to optimize the clevis joint to enhance the vehicle's steering performance despite the increased weight due to additional features.

Li and Zhou (2017) explored the stress distribution in clevis fasteners under tensile and shear loading using FEA. Their findings revealed that tensile loading produced more uniform stress distributions, whereas shear loading induced stress concentrations at the pinhole. This caused the FOS to decrease significantly under shear conditions compared to tensile loading.

Kumar et al. (2018) conducted an FEA study on clevis fasteners under tensile loading and found that increasing the load reduced the FOS due to the higher stress concentrations near the pin contact area. They also noted that modifying the fastener’s geometry (e.g., increasing the arm thickness or using stronger materials) could enhance the FOS.

M. Kumar, S. N. Yadav, and R. Singh [2018] explored how different loads affect fastener safety using FEA. Their studies focused on simulating real-world stresses in 3D models and analyzing stress distribution, deformation, and potential failure points. They showed that under increasing loads, clevis fasteners exhibit varying stress concentrations at contact points, which is crucial for FoS calculations.

R. Shah and D. Kumar [2019] indicated that using high-strength materials and optimizing geometrical parameters (such a s pin diameter, hole size, and clevis thickness) can significantly increase the FoS under varied loading conditions.

Aniket Sawant et al.[2020] The research focused on designing the clevis joint for an all-terrain vehicle (ATV) with the objectives of reducing weight and increasing steering stability, while ensuring a satisfactory safety factor for both handling and performance. The first step involved modeling the clevis joint based on operational considerations and various design constraints. That was followed by stress analysis using finite element software, which was employed to make design adjustments that decrease weight without compromising structural strength.

Feng et al. (2020) conducted a parametric study on clevis fasteners using FEA and demonstrated that increasing the pin diameter relative to the clevis thickness significantly improved the FOS by reducing the stress concentration at the pinhole. This optimization led to a more uniform stress distribution, particularly under combined loading conditions.

Similarly, Sharma and Verma (2020) explored the impact of varying the clevis arm thickness and pin material on the FOS. Their FEA results showed that thicker arms reduced the peak stresses around the pinhole, enhancing the FOS, while using high-strength materials (such as titanium alloys) further improved the overall safety margin of the fastener.

K. Monika et al. (2024) modified a pull rod and clevis unit using CRE-O design software and performed static structural analysis in ANSYS Workbench 15.0, utilizing advanced materials. The modeled part was converted into an IGES file for import into ANSYS Workbench, where static structural analysis was conducted under a 10 kN pressure load. Various materials, including Aluminum Alloy and special alloy steel, were applied in the analysis. This approach helped assess the stresses, strains, and total deformation focused on the pull rod and clevis unit, with the factor of safety also determined. These parameters aid in evaluating the component's safety for practical use.

2. Methodology

Clevis Pin is modelled in SOLODWORKS and analysed in ANSYS, Figure 1 shows the SOLIDWORKS Model. In the study, the one end is treated as fixed and the force is applied on the end. The force applied is varied in the present case to study the effect of loading on the stress, deformation and factor of safety is considered as monitoring parameter.

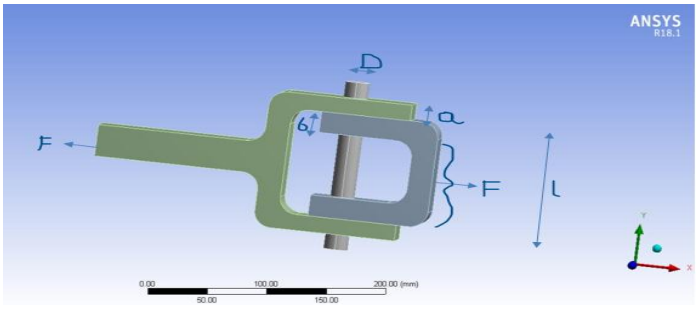

Fig. 1. Solid Works Model

Where, a = 15 mm, D = 20 mm, b = 15 mm, L = 100 mm

2.1. Material properties

Structural steel is used as a material. The thermal and mechanical properties of the structural steel are listed in table 1 and table 2 respectively.

Table 1. Material thermal properties.

S. No.	Property	Value
1	Isotropic coefficient of thermal expansion	1.2×10^{-5} /^{0} C
2	Specific Heat	4.34×10^5 mJ/kg^0 C
3	Isotropic Thermal Conductivity	6.05×10^{-2} W/mm^0 C
4	Isotropic Resistivity	1.7×10^{-4} ohm-mm

Table 2. Material mechanical properties.

S. No.	Property	Value
1	Density	7850 kg/m^3
2	Modulus of Elasticity	2×10^{11} Pa
3	Poisson's Ratio	0.3

4	Bulk Modulus	1.6667×10^{11} Pa
5	Shear Modulus	7.6293×10^{10} Pa
6	Tensile yield strength	2.5×10^{8} Pa
7	Compressive yield strength	2.5×10^{8} Pa
8	Tensile ultimate strength	4.6×10^{8} Pa
9	Compressive ultimate strength	0

2.2. Mesh Generation

In order to accurate simulations in ANSYS, effective meshing plays the important role. The Model is meshed with minimum edge length of 15 mm. The meshed model is shown in figure 2.

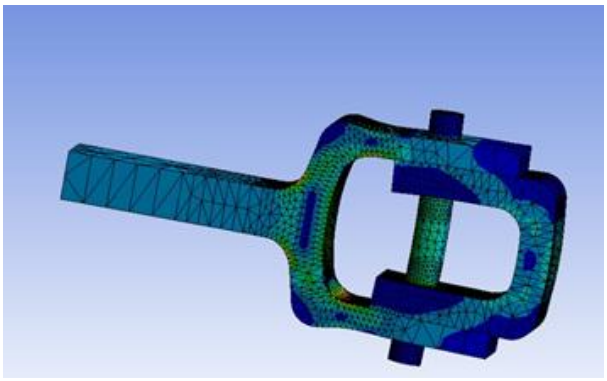

Fig. 2 Meshed geometry

2.3. Loading condition

Figure 3 shows the loading condition of the clevis pin model with following details:

- The left end A of yock is fixed
- Pressure is applied on B which are respectively 9 MPa,12MPa and15 MPa

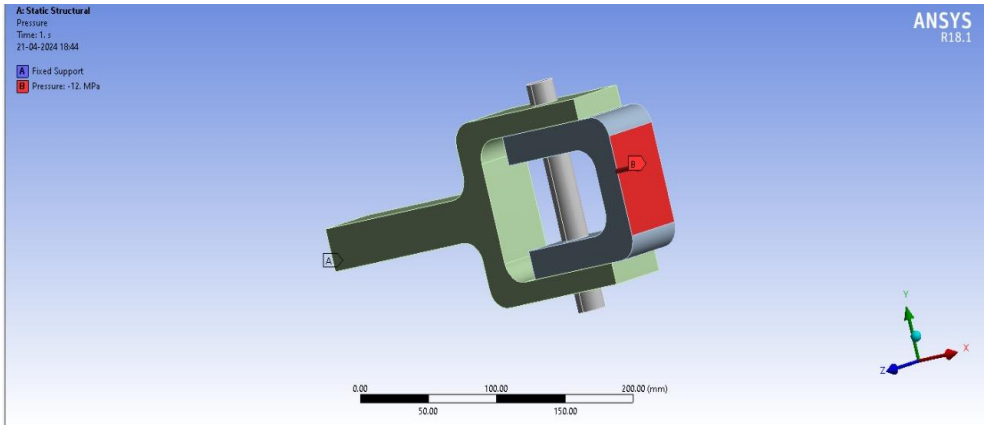

Fig. 3 Loading Conditions

3. Result and Discussion

The study on the clevis pin subjected to different loads provides insightful data on how stress, strain, deformation, and safety factor are affected by increasing applied loads. This analysis is critical for understanding the mechanical behaviour and safety limits of the clevis pin in practical applications.

The study is carried under the following three different cases.

- Case 1: When load of 9 MPa is applied
- Case 2: When load of 12 MPa is applied
- Case 3: When load of 15 MPa is applied

3.1. Case:1 When load of 9 MPa is applied

When a pressure force of 9 MPa magnitude is applied on the clevis pin model at the right end, the following value are obtained as listed in table

Table 3 Obtained Result

load (MPa)	Maximum Equivalent Stress (MPa)	Equivalent Elastic Strain (mm/mm)	Total Deformation (mm)	Factor of Safety
9	115.65	0.00057912	0.07461	2.1618

The nodal solutions of above results are presented in figure 4 to figure 7.

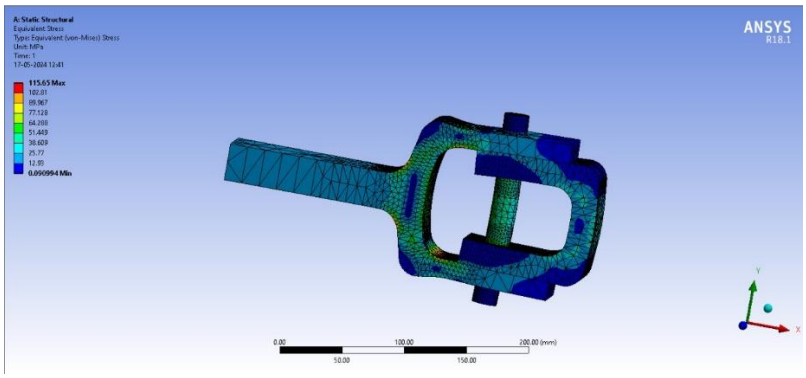

Figure 4: Equivalent Stress (Von Mises) For Structural Steel

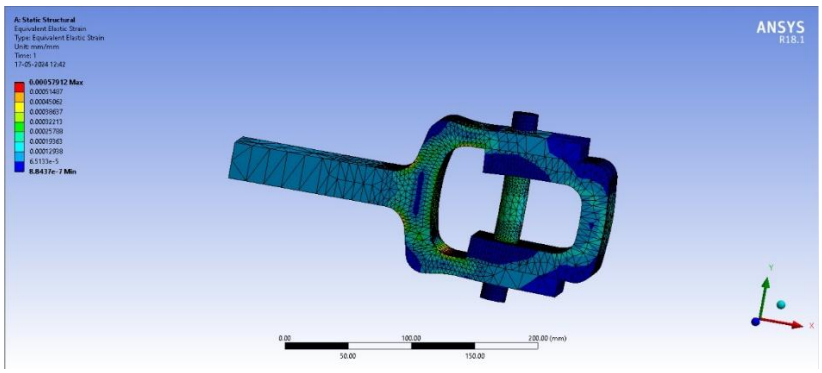

Figure 5: Equivalent Elastic Strain for Structural Steel

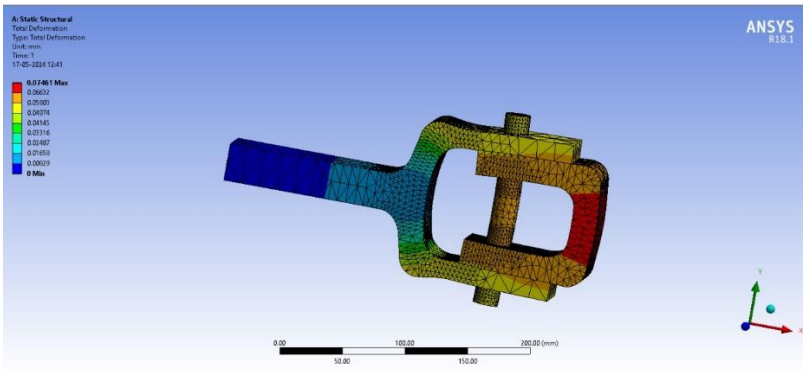

Figure 6: Total deformation For Structural Steel

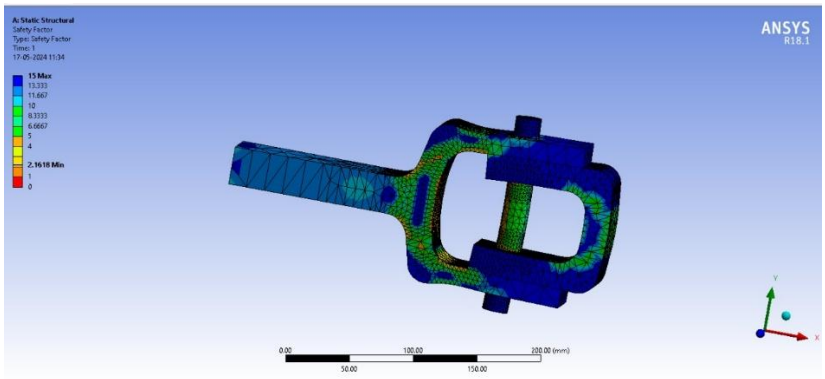

Figure 7: Factor of Safety for Structural Steel

3.2. Case:2 When load of 12 MPa is applied

When a pressure force of 12 MPa magnitude is applied on the clevis pin model at the right end, the following value are obtained as listed in table 4.

Table 4 Obtained Result

load (MPa)	**Maximum Equivalent Stress (MPa)**	**Equivalent Elastic Strain (mm/mm)**	**Total Deformation (mm)**	**Factor of Safety**
12	154.2	0.00077216	0.09948	1.6213

The nodal solutions of above results are presented in figure 8 to figure 11.

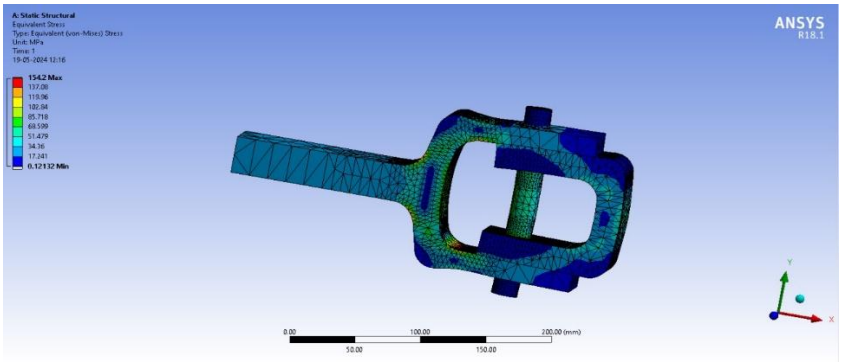

Figure 8: Equivalent Stress (Von Mises) For Structural Steel

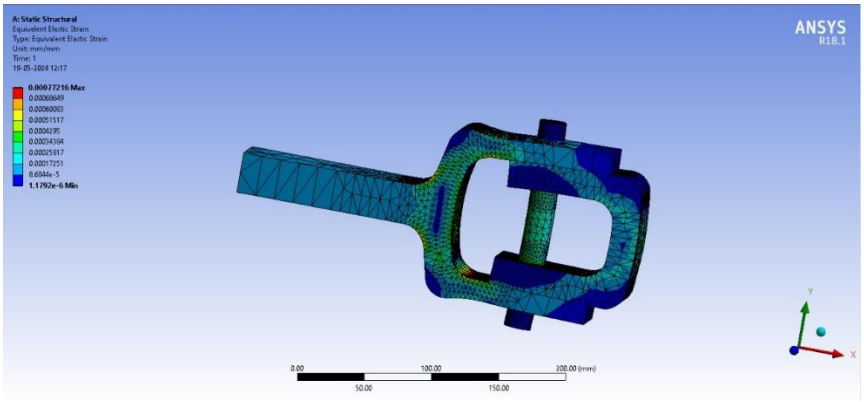

Figure 9: Equivalent Elastic Strain for Structural Steel

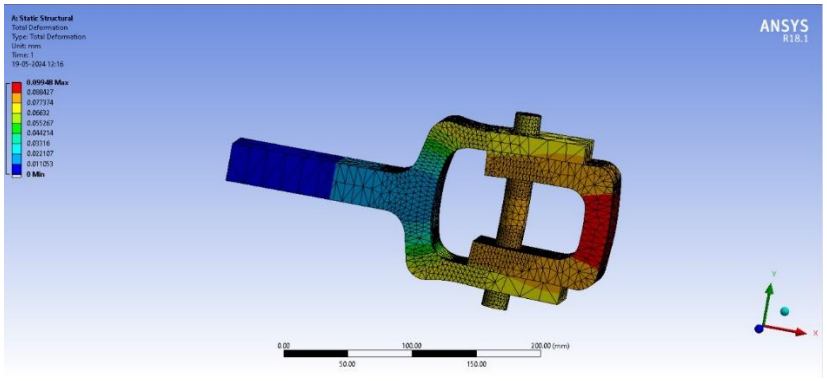

Figure 10: Total deformation For Structural Steel

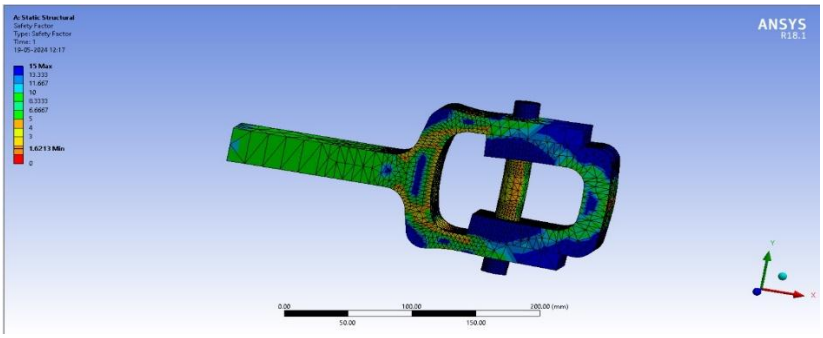

Figure 11: Factor of Safety for Structural Steel

3.3. Case:3 When load of 15 MPa is applied

When a pressure force of 15 MPa magnitude is applied on the clevis pin model at the right end, the following value are obtained as listed in table 5.

Table 5 Obtained Result

load (MPa)	Maximum Equivalent Stress (MPa)	Equivalent Elastic Strain (mm/mm)	Total Deformation (mm)	Factor of Safety
15	192.4	0.0009652	0.12435	1.2971

The nodal solutions of above results are presented in figure 12 to figure 15.

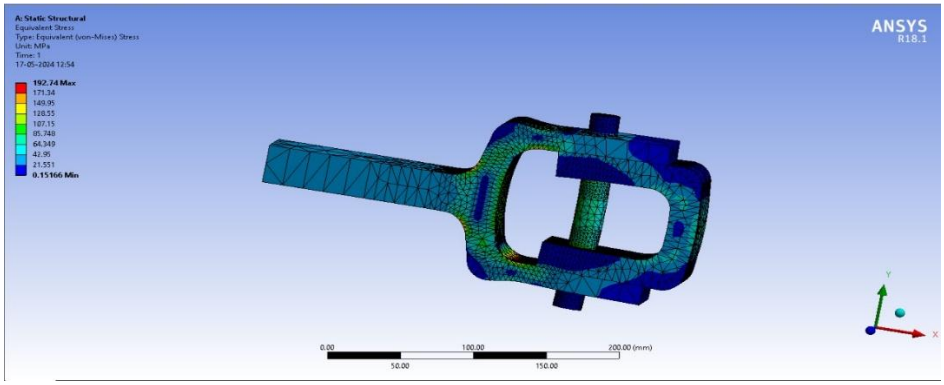

Figure 12: Equivalent Stress (Von Mises) for Structural Steel

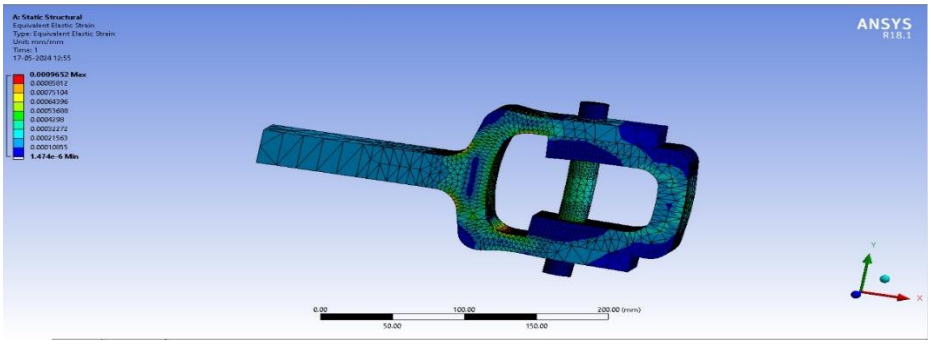

Figure 13: Equivalent Elastic Strain for Structural Steel

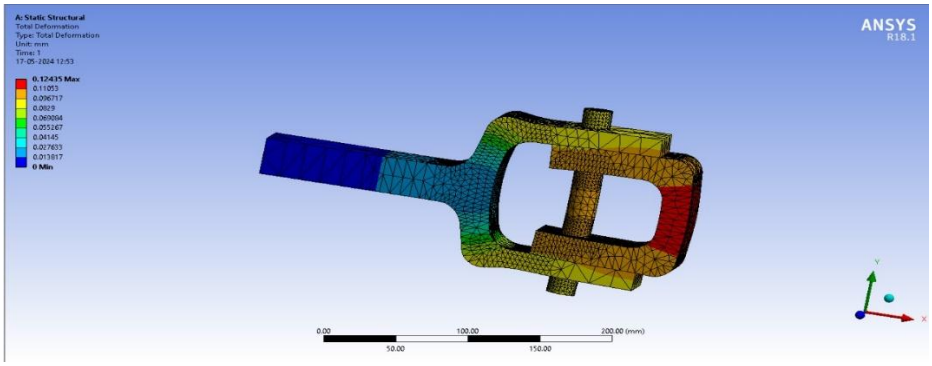

Figure 14: Total Deformation For Structural Steel

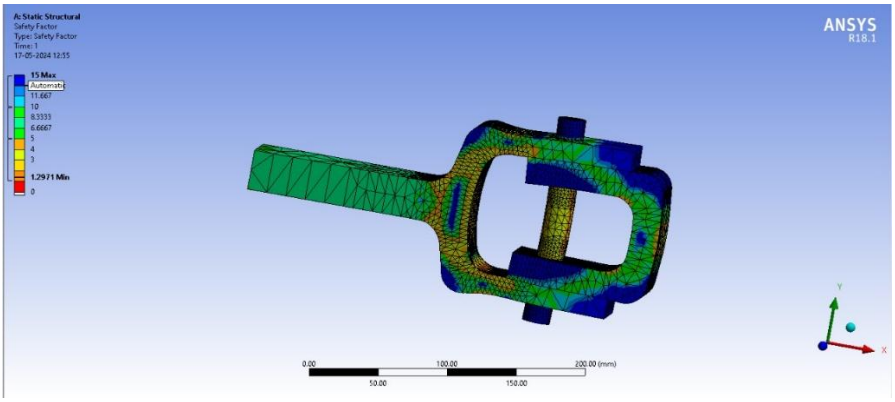

Figure 15: Factor of Safety for Structural Steel

4. Comparison of Results with different loads

4.1. Maximum Equivalent Stress:

- The maximum equivalent stress experienced by the clevis pin increases proportionally with the applied load as shown in figure 16. At 9 MPa, the stress is 115.65 MPa. This stress rises to 154.2 MPa at 12 MPa load and reaches 192.4 MPa at 15 MPa load.
- The increasing stress indicates the material's response to higher loads, reflecting the stress distribution within the pin. Higher stress values suggest that the pin is closer to its yield point as the load increases.

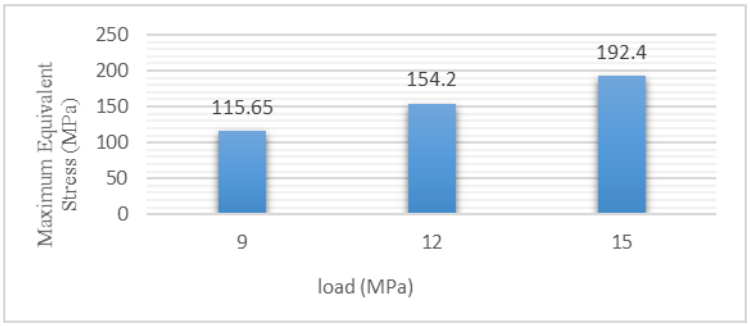

Figure 16: Comparison chart of Maximum Stress for different loads

4.2. Equivalent Elastic Strain:

- Similar to stress, the equivalent elastic strain also shows a proportional increase with the applied load as shown in figure 17. The strain values are 0.00057912 mm/mm for 9 Mpa, 0.00077216 mm/mm for 12 Mpa, and 0.0009652 mm/mm for 15 Mpa.
- This strain measurement reflects the deformation per unit length of the material. Higher strain values indicate that the material undergoes more significant deformation under increased loads.

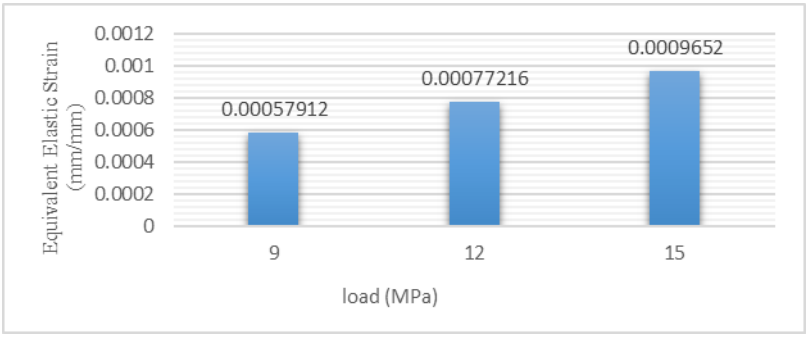

Figure 17: Comparison chart of Elastic Strain for different loads

4.3. Total Deformation:

- Total deformation measures the overall change in the shape of the clevis pin. As the applied load increases, the total deformation also increases. The values recorded are 0.07461 mm at 9 MPa, 0.09948 mm at 12 MPa, and 0.12435 mm at 15 MPa as shown in figure 18.
- The growing deformation with higher loads is expected as the material stretches and compresses more under greater forces.

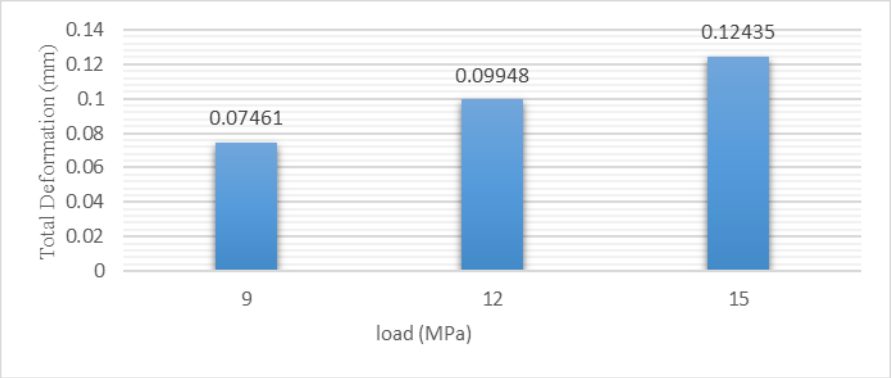

Figure 18: Comparison chart of Total Deformation for different loads

4.4. Factor of Safety:

- The factor of safety decreases as the applied load increases. This factor is 2.1618 for 9 MPa, 1.6213 for 12 MPa, and 1.2971 for 15 MPa as shown in figure 19.
- The factor of safety is a crucial parameter indicating how much load the structure can handle beyond the applied load before failure. A decreasing factor of safety implies that the clevis pin becomes less reliable and closer to failure as the load increases.

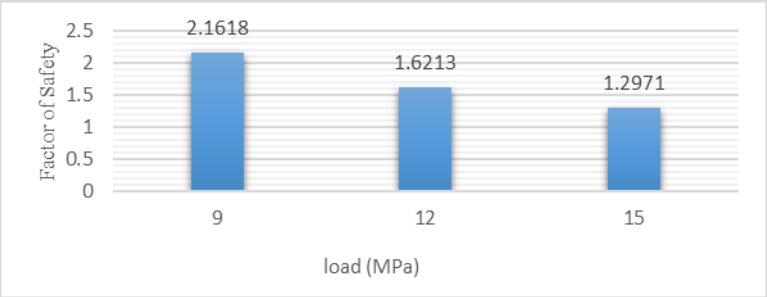

Figure 19: Comparison chart of Factor of Safety for different loads

The results indicate a clear trend as the load applied to the clevis pin increases, the stresses and strains within the material also increase, leading to greater total deformation. Consequently, the factor of safety decreases, highlighting a reduced margin between the applied load and the load that would cause failure.

From an engineering perspective, these findings underscore the importance of designing components with adequate safety margins. The clevis pin must be designed to withstand expected operational loads while maintaining a sufficient factor of safety to ensure reliability and prevent failure. The data suggests that while the clevis pin can handle loads up to 15 Mpa, the factor of safety at this load is relatively low (1.2971), indicating limited tolerance for unexpected loads or material imperfections. It is seeming from above discussion that minimum factor of safety are on yoke and as we increase load the factor of safety decreases and the factor should be greater than 1.5 but at load more than almost 13 Mpa the Factor of safety decreases 1.5. We are Working on those condition where loads less than 13 Mpa only.

5. Conclusion

The analysis of a clevis pin under tensile load using ANSYS provides valuable insights into the structural behaviour and performance of the component. Through Finite Element Analysis (FEA), we were able to evaluate the stress distribution, deformation, and safety factors to ensure the clevis pin's integrity and reliability in various

operating conditions. In conclusion, the ANSYS analysis of the clevis pin under tensile load provides a comprehensive understanding of its structural behaviour and performance. By identifying stress concentrations, evaluating deformation, and calculating safety factors, we can make informed decisions to optimize the design, enhance reliability, and ensure the clevis pin's functionality in its intended application. Continuous improvement and validation through simulation are essential to meet the design requirements and ensure the safety and efficiency of mechanical components like clevis pins in engineering applications. In conclusion, the study provides valuable insights into the mechanical performance of the clevis pin under varying loads. Understanding these parameters helps engineers design safer and more efficient components, ensuring that they can withstand operational stresses while maintaining structural integrity. Balancing applied loads with material capabilities and safety factors is essential for optimal design and reliable performance in practical applications.

6. References

[1] Greene, W. H., Knight, N. F. Jr., & Stockwell, A. E. (1988). Structural behavior of the Space Shuttle SRM Tang-Clevis joint. *Journal of Propulsion, 4*(4), 317–327.

[2] Crookston, J. R., & Folkman, S. L. T. (1997). An approach for modeling a truss using clearance fit pinned joints. *American Institute of Aeronautics and Astronautics, Inc.*, 586–596.

[3] Zienkiewicz, O. C., Taylor, R. L., & Zhu, J. Z. (2000). *The finite element method: Its basis and fundamentals.* Butterworth-Heinemann.

[4] Chang, K. H., & Tang, P. S. (2001). Integration of design and manufacturing for structural shape optimization. *Advances in Engineering Software, 32*, 555–567.

[5] Pechatsko, B., Stambolia, J., Shields, E. B., Davenport, J. B., & Orning, A. D. (2003). Stress analysis of a pin and clevis assembly. In *Proceedings of PVP2003, Pressure Vessels and Piping Conference* (July 20–24, 2003), Cleveland, Ohio, USA.

[6] Roy, R., Hinduja, S., & Teti, R. (2008). Recent advances in engineering design optimization: Challenges and future trends. *CIRP Annals - Manufacturing Technology, 57*, 697–715.

[7] Peterson, R. E. (2008). *Stress concentration factors.* John Wiley & Sons.

[8] Argyris, J. H., & Clough, R. W. (2011). Finite element analysis: Its basis and fundamentals. In *The finite element method* (6th ed., pp. 120–145). Butterworth-Heinemann.

[9] Rajendran, R. S., & Sadalaimuthu, S. (2013). Knuckle development process with the help of optimization. *Advanced Engineering Software, 32*, 555–567.

[10] Norton, R. L. (2013). *Machine design: An integrated approach.* Pearson.

[11] Liu, J., Zhuang, J., & Xu, Z. (2014). Study on the grind-hardening of the loader clevis pin. *Key Engineering Materials, 621*, 140–145.

[12] Javidinejad, A. (2016). Full-length symmetric versus partial-length un-symmetric pin loading failure and analysis for clevis attachments. *Journal of Failure Analysis and Prevention, 16*, 67–74.

[13] Patel, N., & Patel, M. (2016). Analysis of the effect of different loading conditions on the factor of safety of bolted and riveted joints. *Journal of Mechanical and Civil Engineering, 12*(3), 45–51.

[14] Kulkarni, N., & Maid, P. (2017). Structural design & analysis of steering clevis joint of an ATV for weight reduction & steering stability. *International Journal of New Technology and Research (IJNTR), 3*(7), 35–37.

[15] Li, X., & Zhou, L. (2017). Stress analysis and safety assessment of clevis fasteners using FEA. *Journal of Mechanical Design, 139*(5), 1–10.

[16] Kumar, A., Sharma, P., & Verma, S. (2018). Finite element analysis of clevis fasteners under tensile loading. *International Journal of Engineering Research and Applications, 8*(2), 54–60.

[17] Kumar, M., Yadav, S. N., & Singh, R. (2018). FEA-based study of load impact on safety factor for mechanical fasteners. *International Journal of Engineering Science and Technology, 9*(4), 525–533.

[18] Shah, R., & Kumar, D. (2019). Effect of material and geometry on factor of safety of fastening elements. *Engineering Failure Analysis, 34*, 150–161.

[19] Sawant, A., Patil, D., Joshi, V., Trisal, A., & Chel, A. (2020). Design and analysis of steering clevis joint for optimization and steering stability. *Recent Trends in Mechanical Engineering.*

[20] Feng, Y., Zhao, H., & Li, W. (2020). Parametric design optimization of clevis fasteners using FEA. *Journal of Advanced Mechanical Engineering, 12*(4), 23–30.

[21] Sharma, R., & Verma, S. (2020). Material and geometrical optimization of clevis fasteners using FEA. *Materials Science and Engineering, 957*(2), 44–53.

[22] Lewis, P. (2021). Role of advanced FEA tools in enhancing mechanical component design. *Mechanical Design Journal, 20*(2), 82–90.

FEA Analysis of factor of safety of Tata Ace leaf spring

Kapil Sen[1], Sudhir Sharma[2]

[1,2] *Mechanical Engineering Department, IPS College of Technology and Management, Gwalior, MP – 474001 (India)*

Abstract

The present study is focused about the analysis of the leaf spring of the TATA Ace commercial vehicle with 1 ton rated load capacity. The 3D model of leaf spring is designed using commercial package solid work and the analysis is conducted in Ansys commercial FEA software. The eye ends were considered as fixed with restriction of all moments and displacement. The load is applied at the center point of the leaf spring where it will seat on the tie rod. A load of 8093.25 N is taken in the calculation for determining the output parameters. The result indicate that the leaf spring is strong and safe enough at the desired maximum load with factor of safety as 15. On increasing the load the factory of safety decreases

Keywords: *FEA analysis, Leaf spring, Von-Mises stress, Factor of safety.*

1. Introduction

In automobiles, the leaf spring is key components for comfortable ride and stability to the vehicle. In recent years multiple researches, on metallic and different materials were carried out to study the application of leaf springs and revealed that the use of different materials in vehicle suspension can have accountable significance.

Patunkar and Dolas create a FE model for composite mono leaf spring (GFRP) by using Pro-E and conducted Analysis by using ANSYS [1].

Gowd and Goud analyzed the safe load of the leaf spring of TATA-407 light commercial vehicle using ANSYS. Author found the care required (selection of material, design, fabrication etc.) for leaf spring at the inner portion of eye section because author observed the maximum stress at this section.[2].

Kothari and Patel conducted an extensive review on composite leaf spring of its design and fabrication. The author suggests that a composite leaf spring is better replacement of steel spring. Further the author also reviews some papers for other materials. A Fiberglass (FRP) material was suggested by author due to its light weight and greater strength characteristic as compare to steel for leaf spring. [3].

Ismaeel worked on composite leaf spring reinforced by mono-fiber. Author discussed the effects of shear moduli on fibres, matrix etc. by changing the material of a leaf spring from steel to monofibre reinforced composite by using different software of modeling and analysis [4].

Nutalapati compared the conventional leaf spring with composite one by taking parameters of stresses, deformations, weight etc. Pro/ENGINEER was used for modelling of leaf springs and ANSYS 12.0 software used for analysis. Glass fiber reinforced polymer (E-glass/epoxy) was used for composite leaf spring [5].

Triveni and Babu concluded that Carbon fiber–reinforced leaf spring is more suitable as compared to conventional steel spring after conducting a static and dynamic analysis using FEA software package ANSYS. [6]

Jacob and Deepak aimed to fabricate a leaf spring for various loading conditions. Analysis has been conducted to compare the strength for various reinforcement angles between mild steel and composite material glass/carbon.[7].

Salman et al. conduced FEM analysis of leaf spring for four different composite materials at full load condition. The comparison was done to find the light weighted material with adequate improvement of the mechanical properties [8].

Chintada et al. made a comparison study between steel and different composite materials leaf springs to find the suitable material according to the weight, total deformation, von-mises Stress distribution and strain energy are considered as performance measuring parameters [9].

Ashwini and Rao summarized the results obtained by thorough study of literature available in open domain for composite leaf spring. Authors concluded that A conventional mono steel leaf spring can be replaced by composite one due to its better performance for comfort ride [10].

Dey et al. compared conventional leaf spring with E-glass/Epoxy leaf spring for various parameters i.e. weight, stress, deformation etc. [11]. Krishnamurthy et al. did the FEA analysis of leaf springs to find the stress and deflection. The

Published online on: ***February 01, 2025***

Corresponding Author's E-mail ID: kapilsen516@gmail.com

results were validated by conducting comparison experimentally and numerically. [12].

Thillikkani and Nataraj focused on analyzing and understanding the premature failure of both existing and proposed bracket models under dynamic loading conditions. The study seeks to simulate the early failure of bracket models subjected to dynamic loading, which helps in identifying weak points in the design and improving durability. The use of generalized force elements in the analysis captures the variety of dynamic loads that the bracket experiences during real-world operations, especially in suspension systems. A Scanning Electron Microscope (SEM) was utilized to identify failure-prone areas in the brackets, providing a microscopic view of surface defects and crack initiation points. The findings show that cyclic loads in the suspension system, primarily due to vibrations and bumps on rural roads, are significant contributors to fatigue failure. These conditions accelerate the wear and tear of the bracket, leading to premature failure.[13]

Mahajan and Patil investigated the strength of a semi-elliptic multi-leaf spring made of steel material to obtain a von mises stress for various loads [14].

Zou et al. established a FE model of the composite leaf spring and investigated the results for stiffness and damping [15].

Indrajit Salunke et al. worked on structural leaf spring and compared results for three different materials and found that the maximum stress and deflection in leaf spring is observed for the titanium alloy the structural steel has minimum deflection [16]

Satish M. Silaskar et al. The study conducted static structural analysis on both steel and composite leaf springs, comparing their stress, displacement, deflection, and load carrying capacities using analytical methods and ANSYS. Composite leaf springs, particularly those made of Kevlar Fiber, showed significant weight reductions (37.92% for carbon fiber, 45.67% for Kevlar fiber, and 28.18% for E-glass Epoxy compared to 55Si2Mn90 steel), making Kevlar Fiber a preferable choice for lightweight vehicles due to minimized unsprung mass. [17]

Many literature is available in open domain dealing with the type of material which can be utilized for better leaf spring from the common or conventional steel to the modern unconventional composite material. The composite material is good option to have light weight, higher stiffness, leaf spring but the limitation is that the cracking of fibers at the fiber matrix interface and transversely to the load axis are the common problem associated with composite material. The majority of the analysis was concentrated on the strength and stiffness of the leaf spring. As per the author knowledge till date no such literature is available in open domain which concentrates their study on the factor of safety.

2. Selection of material

A structural steel is used for this analysis. Property of structural steel are shown in table 1.

Table 1. Properties of structural Steel

Properties	Values
Density	7850 kg/m^3
Young Modulas	2×10^5 MPa
Poison Ratio	0.3
Shear Modulus	7.9615×10^{10} Pa
Bulk modulus	1.725×10^{11} Pa
Tensile yield strength	2.5×10^8 Pa
Tensile Ultimate strength	2.5×10^8 Pa

3. Design and calculation

3.1. Leaf spring Parameters

Length of different leaves of a leaf spring and radius of curvature are shown in figure 1. All dimensions are taken in mm.

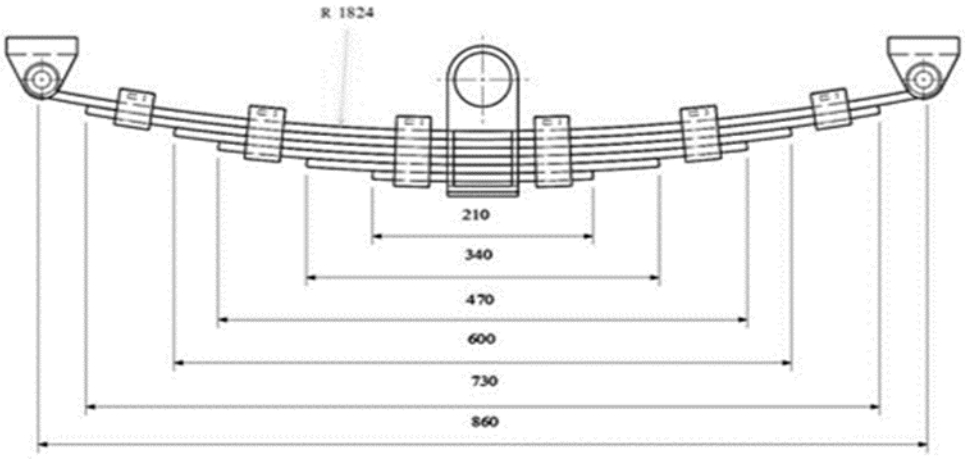

Fig. 1 Dimensions of Leaf Spring

3.2. Weight calculation

In this study, a light commercial four wheeler "TATA ACE" vehicle is taken for analysis. The maximum load on each springs are calculated as follows:

- Weight of vehicle = 980 kg
- Max. load capacity = 1700 kg
- Driver weight = 70 kg
- Total weight = 1000 + 1700+70
  = 2750 kg
- Acceleration due to gravity (g) = 9.81 m/s2
- Load acting on leaf spring = 2750 x 9.81
  = 26977.50 N
- Rear suspension = 60% of Total weight
  = 0.60 × 26977.50 N
  = 16186.50 N
- Therefore Total weight = 16186.50 N

Since rear suspension consists of 2 springs therefore the load on 1 spring = 16186.50/2 = 8093.25 N
So, Maximum load given on each spring is 8093.25 N

4. Methodology

Leaf spring of TATA ACE vehicles is taken for modeling and analysis. The 3D modeling of leaf spring is carried out using SOLIDWORKS. Figures 2 shows one of the models of leaf spring used in analysis. Analysis part is done using ANSYS.

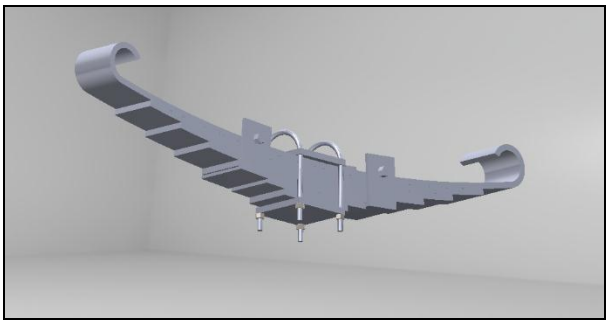

Figure 2: Solid works Model

4.1. Meshing

Figure 3 shows the meshed model of leaf spring. Meshing is an important process of an analysis and it should be performed on the leaf spring structure. Meshing is the procedure of dividing the created model in wide variety of elements or factors which includes nodes.

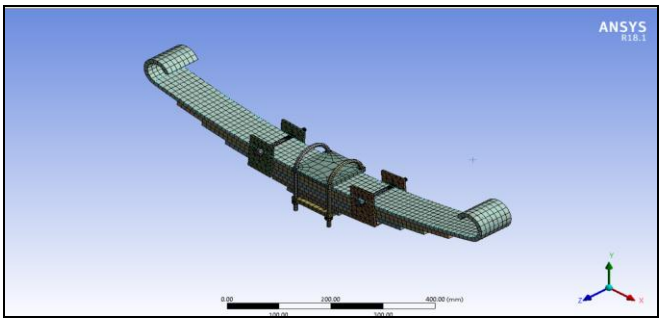

Figure 3: Meshed Model

4.2. Boundary Conditions:

Figure 4 and 5 show the boundary conditions which are applied for structural analysis. The boundary conditions are as follows:

A. Fixed Support: - The notation in the figure 4 shows the points where leaf spring fixed i.e. all degrees of freedom are locked.

B. Moment: - This means the calculated load for required deceleration is applied on both eye surface of the leaf spring.

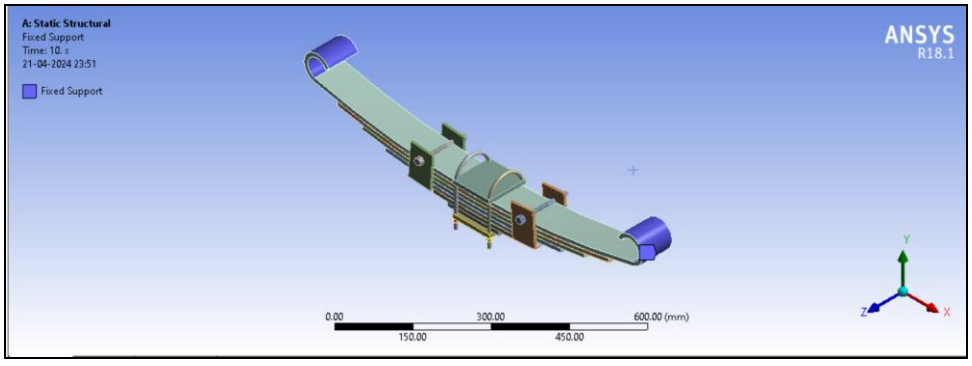

Figure 4: Fixed Support

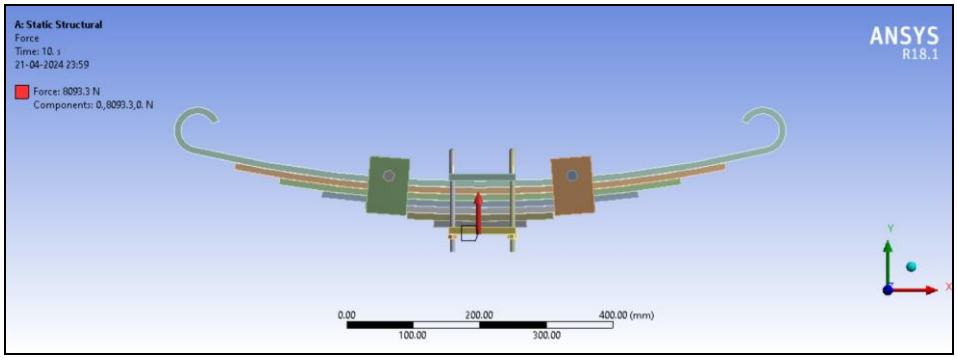

Figure 5: Application of force

5. Result and Discussion

Structural analysis of leaf spring is carried out for following three different cases.

Case 1: when low load of 8093.3 N is applied
Case 2: when low load of 12140 N is applied
Case 3: when low load of 16189 N is applied

For each cases, stress, elastic strain and deformation are calculated in ANSYS and the results of each leaf spring have been discussed.

5.1. Case: 1 when low load of 8093.3 N is applied.

The results are listed in table1.

Table 1: Obtained results for applied load of 8093.3 N

Force	Values	Max.	Min.
8093.30 N	Equivalent Von-Mises stress (MPa)	36.28	6×10^{-9}
	Total Deformation (mm)	7.94×10^{-2}	0
	Elastic strain	1.82×10^{-4}	6.98×10^{-14}
	Factor of safety	15	6.89

The nodal solution for above values are shown in figure 6 to figure 8 respectively.

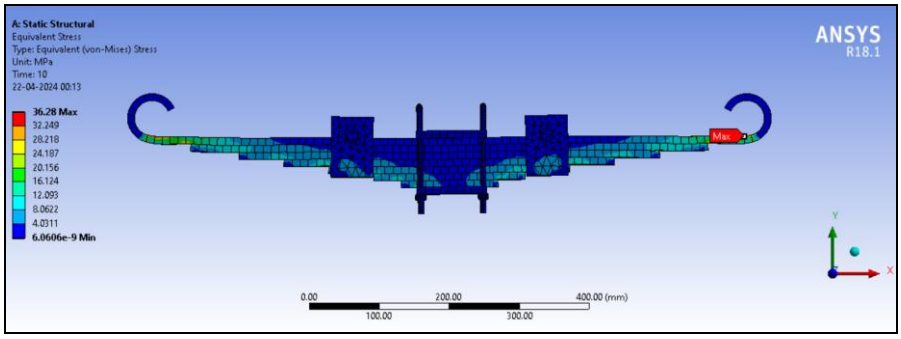

Fig. 6 Equiv. Von-Mises stresses for steel leaf spring

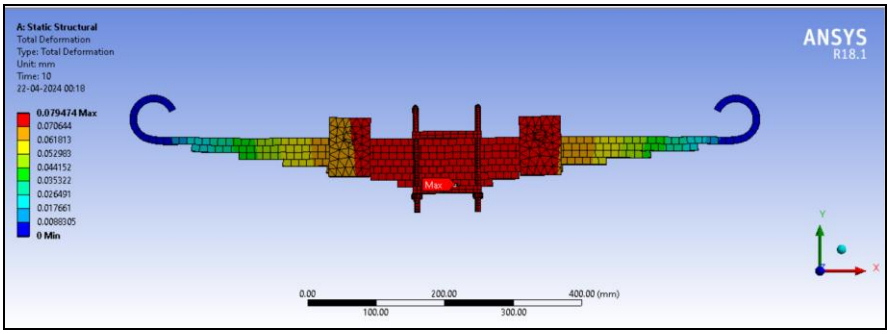

Fig. 7 Deformation for steel leaf spring

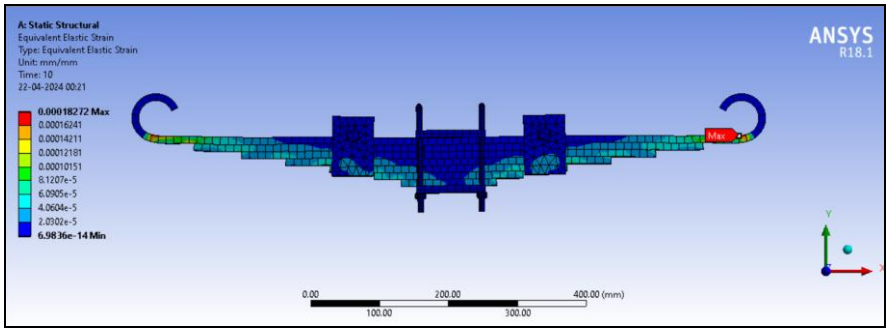

Fig. 8 Equiv. elastic strain for steel leaf spring

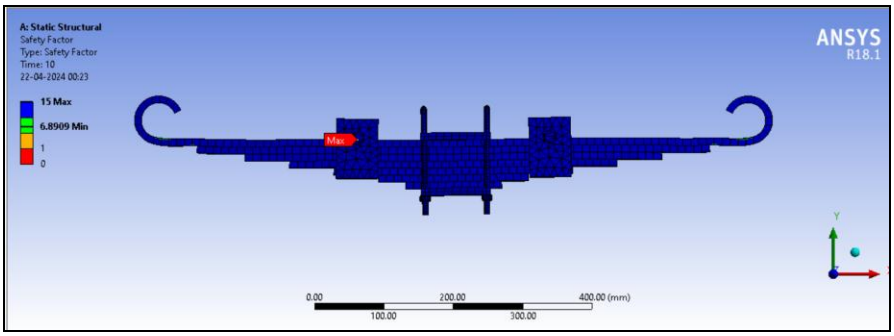

Fig. 9 Factor of safety for steel leaf spring

5.2. Case 2 when low load of 12140 N is applied

The results are listed in table 2.

Table 2: Obtained results for applied load of 12140 N

Force	Values	Max.	Min.
12140.00 N	Equivalent Von-Mises stress (MPa)	54.42	9.1×10^{-9}
	Elastic strain	2.74×10^{-4}	1.0438×10^{-13}
	Total Deformation (mm)	0.119	0
	Factor of safety	15	5.59

The nodal solution for above values are shown in figure 10 to figure 13 respectively.

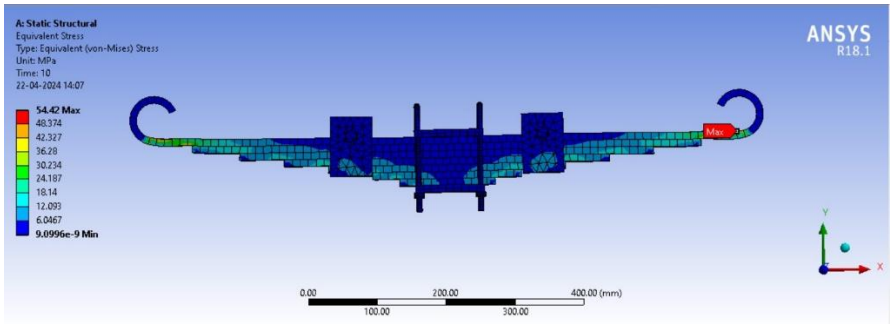

Fig. 10 Equiv. Von-Mises stress for steel leaf spring

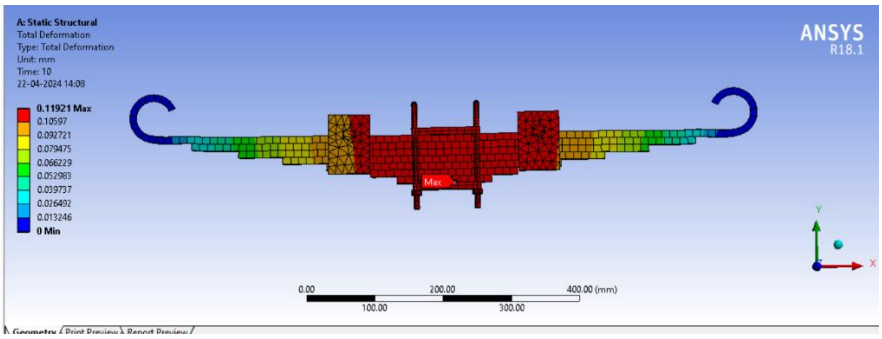

Fig. 11 Deformation for steel leaf spring

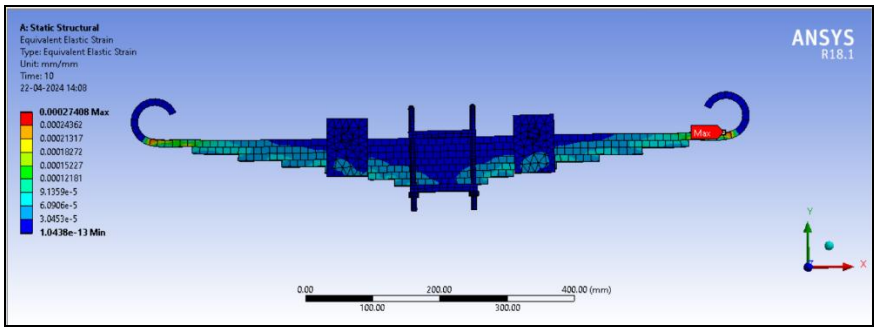

Fig. 12 Equiv. elastic strain for steel leaf spring

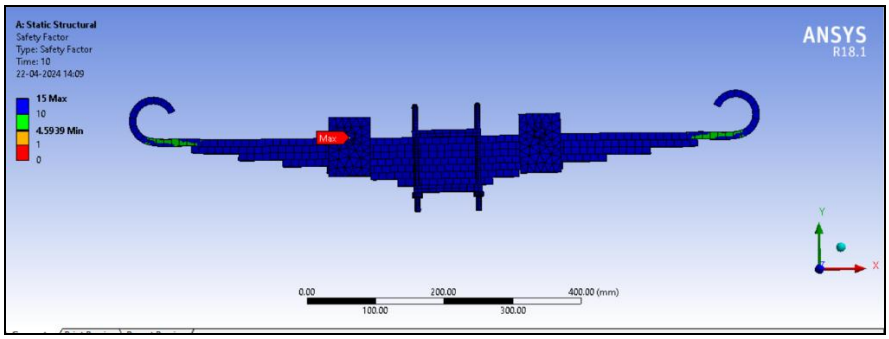

Fig. 13 Factor of safety for steel leaf spring

5.3. Case 3 when low load of 16187 N is applied

The results are listed in table3.

Table 3: Obtained results for applied load of 16187 N

Force	Values	Max.	Min.
16187.00 N	Equivalent Von-Mises stress (MPa)	72.56	1.2105×10^{-8}
	Elastic strain	3.654×10^{-4}	1.39×10^{-13}
	Total Deformation (mm)	0.1589	0
	Factor of safety	15	3.445

The nodal solution for above values are shown in figure 14 to figure 17 respectively.

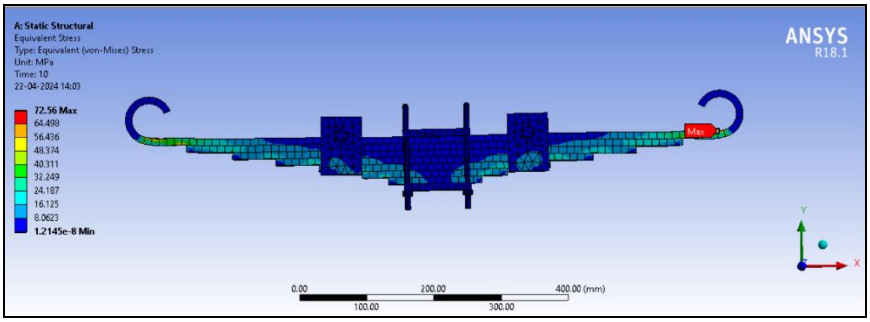

Fig. 14 Equiv. Von-Mises stress for steel leaf spring

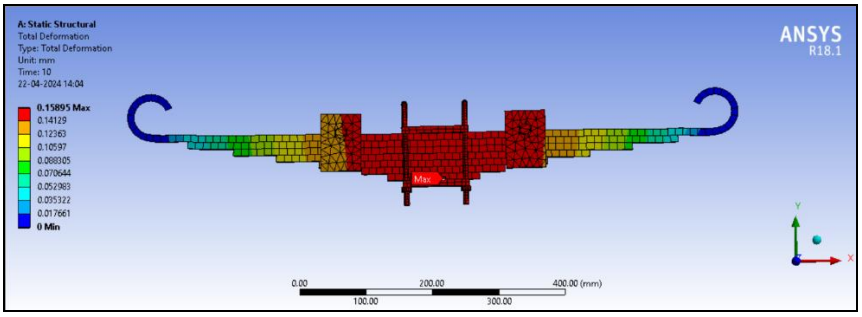

Fig. 15 Deformation for steel leaf spring

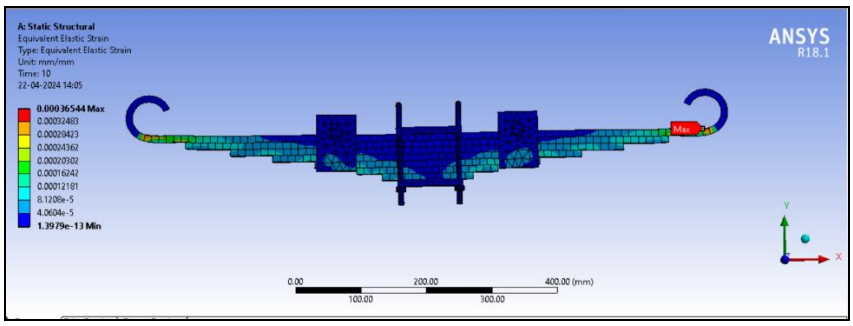

Fig. 16 Equiv. elastic strain for steel leaf spring

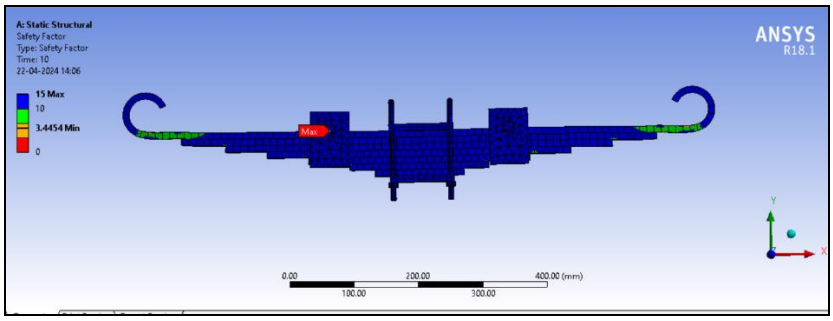

Fig. 17 Factor of safety for steel leaf spring

6. Conclusion

This paper was focused to design a leaf spring minimum stress, elastic strain, deformation and factor of safety at an acceptable range. Therefore modified leaf spring was used by changing the design. In the present work, a structural leaf spring is chosen because of its high strength and minimum deflection for the same load.

- A semi-elliptical multi leaf spring is designed for a four wheel automobile under same loading condition using three different load conditions.
- The maximum stress and deflection in leaf spring is observed for the spring having highest load i.e. double the designed load.
- Therefore there's extensive distinction within side the stresses and deflection in leaf springs under the same static load conditions. Stresses and deflection in structural steel leaf spring found to be less as compared to the increased in load level.
- From above analysis it is concluded that the structural steel leaf spring having more number of plates are more efficient compared to the normal spring having less number of plates [13 & 17].

Reference

[1] Patunkar, M. M., & Dolas, D. R. (2011). Modelling and Analysis of Composite Leaf Spring under the Static Load Condition by using FEA. *International Journal of Mechanical and Industrial Engineering*, 1–4. https://doi.org/10.47893/ijmie.2011.1001

[2] Harinath Gowd, G., & Venugopal Goud, E. (2012.). Static analysis of leaf spring. *International Journal of Engineering Science and Technology*, 4(8), 3794-3803.

[3] Kothari, P., & Patel, A. (n.d.). *A Review Paper on Design & Analysis of Leaf Spring*. www.ijert.org

[4] Ismaeel, L. M. A. (2015). Optimization and Static Stress Analysis of Hybrid Fiber Reinforced Composite Leaf Spring. *Advances in Materials Science and Engineering*, *2015*. https://doi.org/10.1155/2015/374609

[5] Nutalapati, S. (2015). Design and Analysis of Leaf Spring by Using Composite Material For Light Vehicles. *International Journal of Mechanical Engineering and Technology*, *6*(12), 36–59. http://iaeme.com/Home/issue/IJMET?Volume=6&Issue=12http://iaeme.com/Home/issue/IJMET?Volume=6&Issue=12http://iaeme.com/Home/journal/IJMET37

[6] Triveni, Z., & Babu, B. A. (n.d.). *FINITE ELEMENT ANALYSIS ON LEAF SPRING MADE OF COMPOSITE MATERIAL*.

[7] Joshua Jacob, G., & Assistant professor, M. (n.d.). Design And Analysis Of Leaf Spring In A Heavy Truck. In *IJITR) INTERNATIONAL JOURNAL OF INNOVATIVE TECHNOLOGY AND RESEARCH* (Issue 5). http://www.ijitr.com

[8] kashif Salman, M., Singh, A. P., Roy, S., & Banerjee, J. (n.d.). *Fem Analysis of Leaf Spring for Different Composite Materials at Full Load Condition*. www.ijesi.org

[9] Babu, C. V., Rao, M. V., & Sudhakar, U. (2017). Analysis of Composite Leaf Spring: A Comparison. *International Journal of Mechanical Engineering and Technology (IJMET)*, *8*(6), 688–694. http://www.iaeme.com/IJMET/index.asp688http://www.iaeme.com/IJMET/issues.asp?JType=IJMET&VType=8&IType=6http://www.iaeme.com/IJMET/issues.asp?JType=IJMET&VType=8&IType=6

[10] Ashwini, K., & Mohan Rao, C. V. (2018). Design and Analysis of Leaf Spring using Various Composites-An Overview. *Materials Today: Proceedings*, *5*(2), 5716–5721. https://doi.org/10.1016/j.matpr.2017.12.166

[11] Dey M, Uniyal S. Dhillon, S. S., Rauthan and Sharma M (2019). *Design and Analysis of Leaf Spring Using ANSYS*. International Journal of Applied Engineering Research 14(10), 67-70

[12] Krishnamurthy, K., Ravichandran, P., Shahid Naufal, A., Pradeep, R., & Sai HarishAdithiya, K. M. (2020). Modeling and structural analysis of leaf spring using composite materials. *Materials Today: Proceedings*, *33*, 4228–4232. https://doi.org/10.1016/j.matpr.2020.07.346

[13] Thillikkani S. and Nataraj (2020), *Fatigue life prediction of heavy vehicle suspension system under varying load conditions*, Advances in Mechanical Engineering, 12(11) 1–10.

[14] Mahajan R. R. and Patil A. V. (2021) *Design and Analysis of Automobile LEAF Spring*, International Journal of Engineering and Applied Sciences (IJEAS), 8(9), 5-8.

[15] Zou, X., Zhang, B., & Yin, G. (2022). Analysis of stiffness and damping performance of the composite leaf spring. *Scientific Reports*, *12*(1). https://doi.org/10.1038/s41598-022-11055-5

[16] Indrajit Salunke I., Patel A., Date D and Mane V., (2023). *Structural Analysis of Leaf Spring by Using Different Material for Automotive Vehicle,* International Research Journal of Modernization in Engineering Technology and Science, 5(10), 3132-3142.

[17] Silaskar S. M., Nikhade S., Davane P. and Alone P. (2023), *Design, Analysis and Optimization of a Light weight Vehicle's Leaf Springs,* SAMRIDDHI, 15(1), 16-19.

Evaluation of constants K0, K1, K2, K3 of pure ferromagnetic crystal anisotropy energy balance based on α, α*, η texture of ideal fibers

Sudhakar Geruganti[1] and Gautam Jai Prakash[2]

[1]*PhD Research Scholar, SEST, The University of Hyderabad , Gachibowli Hyderabad 500046, Telangana (India))*
[2]*Professor, SEST, The University of Hyderabad , Gachibowli Hyderabad 500046, Telangana (India))*

Abstract
Texture factor, A* and magnetocrystalline anisotropy energy density K0, constants K1, K2, K3, are important for pure metals. The former represents the rapid bulking of crystals with associated preferences and the latter represents simple and complex instructions. Evaluation of defects of pure metal and electrical metal can reduce metal loss in transformers and rotating motors and increase electrical efficiency. In this research paper, an attempt has been made to calculate the magnetocrystalline anisotropy energy density of pure metals based on the beauty of ideal fibers

Keywords: *texture, anisotropy, core loss.*

1. Introduction

Their importance depends on chemical composition, crystal structure and thermomechanical processing history. Texture is similar to the K0, K1, K2 and K3 values that determine the preference of the grain, and overall texture is a quantitative measure of texture.

1.1. Standard Equations

$$E^* = K0 + K1 (\sum \alpha 21\ \alpha 22) + K2 (\prod \alpha 21) + K3 (\sum \alpha 21\ \alpha 22)2;$$

$$E^* = K0 + K1 (\sum \alpha 21\ \alpha 22) + K2 (\prod \alpha 21) + K3 (\sum \alpha 21\ \alpha 22)2$$

2. Estimation of magnetic anisotropy constants K0, K1, K2, K3 Evaluation of pure metals:

The anisotropy properties of magnetocrystals are usually expressed by the expansion of the cosine of the magnetization directions α1, α2, α3 with respect to the crystallographic axis.

$$E^* = K0 + K1 (\sum \alpha 21\ \alpha 22) + K2 (\prod \alpha 21) + K3 (\sum \alpha 21\ \alpha 22)2$$

$$E^* = 0.355A^* + (0.163 - 0.013A^*)[wt\%Si] - 1.898$$

For pure iron,

$$E^* = 0.355A^* - 1.898;$$

Texture Factor, A* for η fibre is <001> // RD is 27.88
Texture Factor, A* for α fibre is <110> // RD is 30.06
Texture Factor, A* for α* fibre is <112> // RD is 30.77

E* for η fibre is <001> // RD is => E* = 0.355 * 27.88 – 1.898 = 7.9994
E* for α fibre is <110> // RD is => E* = 0.355 * 30.06 – 1.898 = 8.7733
E* for α* fibre is <112> // RD is => E* = 0.355 * 30.77– 1.898 = 9.02535

Published online on: ***February 01, 2025***
Corresponding Author's E-mail ID: smecsudhakar@gmail.com

E* = K0 + K1 (± 21 ± 22) + K2 (± 21) + K3 (± 21 ± 22)2 [I] ;
For [100] directions, α1= 1, α2 = 0, α3=0

E*[100] = K0 = 7.9994 ….[II]

E* = K0 + K1 (∑α21 α22) + K2 (∏α21)+ K3 (∑α21 α22)2 [I];

FOR [110] directions, α1 =1/√2, α2 =1/√2, α3=0

8.7733 = 7.9994 + K1/4 + K3/16

4 K1 + K3 = 12.3824 ……..[III]

E* = K0 + K1 (± 21 ± 22) + K2 (± 21) + K3 (± 21 ± 22)2 [I];

FOR [112] directions, α1 =0.408248, α2 =0.408248, α3=0.816496;

COS<112>,<100> = α1= (1.0+2.0)/(√6 * √1) = 0.408248

COS<112>,<010> = α2 =(0.1+1.1+2.0)/(√6 * √1) = 0.408248

COS<112>,<001> = α3 =(0.1+1.0+2.1)/(√6 * √1) = 0.816496

(∑α21 α22) =0.24999928; (∏α21) = 0.0185184

E* = 7.9994 + K1 [0.24999928] + K2 [0.0185184] + K3 [0.06249964]

9.02535 = 7.9994 + K1 [0.24999928] + K2 [0.0185184] + K3 [0.06249964]

DIVISON BY [0.06249964] L.H.S,R.H.S

16.415294 = 4 K1 + K2 [0.2962961] + K3

4 K1 + K3 = 12.3824 FROM ……..[III]

K2 [0.2962961] = 16.415294 - 12.3824 =4.032894

K2 [0.2962961] = 4.032894

K2 = 13.611032 ……..[IV]

4 K1 + K3 = 12.3824 FROM ……..[III]

4*3 + 0.3824 = 12.3824

K1 = 3; K3 = 0.3824 ……..[V]

FINAL GENERAL EQUATION, IS GIVEN BY

E* = K0 + K1 (∑α21 α22) + K2 (∏α21)+ K3 (∑α21 α22)2

Substituting the values of K0 = 7.9994; K1 = 3; K2 = 13.611032; K3 = 0.3824

$E^* = 7.9994 + 3(\sum \alpha_{21}\ \alpha_{22}) + 13.611032(\prod \alpha_{21}) + 0.3824(\sum \alpha_{21}\ \alpha_{22})2$ ……..[VI]

CRYSTAL DIRECTION	MAGNETOCRYSTALLINE ANISOTROPY ENERGY DENSITY
[10] $\alpha_1 = 1, \alpha_2 = 0, \alpha_3 = 0$	7.9994
[110] $\alpha_1 = 1/\sqrt{2}, \alpha_2 = 1/\sqrt{2}, \alpha_3 = 0$	8.7733
[112] $\alpha_1 = 0.408248$,$\alpha_2 = 0.408248$, $\alpha_3 = 0.816496$	9.02535

2.1. Discussion

The <100> // Optical fiber has self-distribution During the rotating lamination With the in-plane rotating cubic texture components, the magnetic flux line in the plane of the paper has a simple magnetization direction. <112> and <110>//RD fiber orientations have relatively high anisotropy properties, and therefore it is undesirable for objects to form in pure metals.

3. ESTIMATION OF PURE METAL CONSTANTS K0,K1,K2, K3

$E^* = 7.9994 + 3(\sum \alpha_{21}\ \alpha_{22}) + 13.611032(\prod \alpha_{21}) + 0.3824(\sum \alpha_{21}\ \alpha_{22})2$ ……..[VI]

$E^* = 0.355A^* - 1.898;$

$0.355A^* = 1.898 + 7.9994 + 3(\sum \alpha_{21}\ \alpha_{22}) + 13.611032(\prod \alpha_{21}) + 0.3824(\sum \alpha_{21}\ \alpha_{22})2$

$0.355A^* = 9.8974 + 3(\sum \alpha_{21}\ \alpha_{22}) + 13.611032(\prod \alpha_{21}) + 0.3824(\sum \alpha_{21}\ \alpha_{22})2$

$A^* = 27.88 + 8.450704(\sum \alpha_{21}\ \alpha_{22}) + 38.3409352(\prod \alpha_{21}) + 1.077183(\sum \alpha_{21}\ \alpha_{22})2$

FOR direction <hundred> $A^* = 27.88 \Rightarrow A^* = 27.88$ for η fibre <100>//RD

FOR direction <one hundred & ten> , $\alpha_1 = 1/\sqrt{2}, \alpha_2 = 1/\sqrt{2}, \alpha_3 = 0$, $A^* = 27.88 + 8.72/4 + 1.077183/16 = 30.06$ $\Rightarrow A^* = 30.06$ for α fibre <110>//RD

FOR <112> direction , $\alpha_1 = 0.408248, \alpha_2 = 0.408248, \alpha_3 = 0.816496$,
$(\sum \alpha_{21}\ \alpha_{22}) = 0.24999928$; $(\prod \alpha_{21}) = 0.0185184$; $(\sum \alpha_{21}\ \alpha_{22})2 = 0.06249964$

4. Conclusions

The anisotropic direction [100] has the least energy, and the [110] and [111] directions are stronger. Therefore, the [100] direction is the easiest magnetization direction of the pure metal, the [112] direction is the hardest magnetization direction of the pure metal, and the [110] direction is the complex magnetization direction of the pure metals. The effective values of the balance equation are consistent with the theoretical requirements and are consistent with the effective values

of ideal fibers.

References

[1] Kestens, L., & Jacobs, S. (n.d.). Texture control and manufacturing in non-oriented electrical steel.
[2] Westerstrand, B., Nordblad, P., & Nordborg, L. (n.d.). The magnetocrystalline anisotropy constants of iron and iron-silicon alloys.
[3] Mehdi, M. (n.d.). Texture evolution of non-oriented electrical steels during thermomechanical processing.
[4] Kloseka, V. (n.d.). Crystallographic textures. *CEA, IRAMIS, Laboratoire Léon Brillouin*, 91191 Gif-sur-Yvette Cedex, France.

Recent Advances in optimization of keyhole closure techniques in friction stir spot welding of dissimilar Al-Alloys: A Review

Dinesh Singh[1], Vijay Verma[2]

[1,2]*Department of Mechanical Engineering, Bundelkhand Institute of Engineering and Technology, Jhansi, 284128, Uttar Pradesh, India.*

Abstract

This study investigates various keyhole closure techniques in Friction stir spot welding (FSSW) of dissimilar Al-alloys to address the detrimental effects of conventional-FSSW. Keyhole closure/repair techniques such as Refill-FSSW, pinless-FSSW, interlayer-FSSW, protrusion-FSSW, active-passive FSSW and others are critically reviewed. Their impact on microstructure, grain size and mechanical properties of the welds are analysed. The study found that keyhole closure is crucial for achieving high strength, defects free sound welds. It enhances material mixing, bonding and fracture behavior.

Keywords: *Friction stir spot welding, Al-alloys, Keyhole closure techniques, Grain size, Optimization.*

1. Introduction

The global climate is currently teetering on the edge of a catastrophic event. In order to mitigate climate change and its consequences, it will be necessary to reduce emissions by over 50% by the year 2030. Prompt and revolutionary measures are required in all sectors to fulfil the obligations outlined in the United Nations' sustainable development goals (SDGs). The vehicle, shipbuilding, and aerospace sectors now prioritise material selection based on emission control and increased fuel economy [1]. Aluminium or magnesium alloys, which are lightweight and without containing iron, have been substituting dense steel alloys made of traditional ferrous elements. Therefore, by decreasing the release of exhaust gases such as carbon dioxide (CO2) and nitrogen oxides (NOx), it is possible to achieve a reduction in emissions and minimise the environmental consequences. Aluminium and its alloys are extensively utilised in high-performance structural applications, including door panels, protection covers, and lift gates [2, 3] due to their favourable characteristics such as a high strength-to-weight ratio, resistance to stress corrosion cracking, excellent cryogenic properties, and superior weldability compared to steels [4]. The International Council on Clean Transportation has demonstrated that ambitious targets of 95 g CO2/km for harmful vehicle emissions can be achieved through the use of lightweight materials. The diverse range of material properties in multi-material vehicle structures offers a prominent solution for enhancing fuel economy, reducing emissions, improving performance, and optimising design flexibility. However, achieving this requires extensive research and development of a dependable and cost-effective welding technique for dissimilar materials [5].

2000 series and 7000 series Al-alloys for structural applications are mainly joined by Resistance spot welding (RSW) and fusion welding techniques, susceptible to weld cracking [6, 7], welds formed in these materials by fusion welding are prone to solidification shrinkage, porosity, hot cracks or distortion due to residual stresses induced from high coefficient of thermal expansion. Coursed and dendrite microstructure has been formed in fusion welding due to solidification and grain growth in weld nugget or fusion zone, resulting in poor weld strength and reduced fatigue resistance [8, 9].

Above mentioned problems can be avoided by a newly developed cost effective solid-state welding technique, FSSW[10]. FSSW, shows several advantages over traditional welding techniques in the automotive industry such as less heat input, little distortion, short cycle time, long tool life and restrict intermetallic formation. Since the maximum temperature during FSSW is always less than the melting point of the different base materials which diminishes formation of intermetallic compounds, cracking and thermal distortions [11]. Hence, improved mechanical properties, higher corrosion resistance and much lower energy consumption(90% energy savings and 40% cost reduction) [12, 13].

From the concepts of FSW, FSSW was developed to spot weld two or more overlapping plates of steel, aluminum, magnesium, titanium, and other alloys. The Welding Institute in the UK created FSW in 1991[14]. 2003 saw the invention of FSSW solid state joining by Mazda Motor Corporation. After being used in the rear door panels of the Mazda RX-8 in 2003, conventional-FSSW was used to attach the aluminum trunk lid to the steel bolt retainers for the 2005 Mazda MX-5 sports car. It is also used for the decklid and hood of the Prius gasoline/electric hybrid. A non-consumable rotating tool is lowered at a predetermined depth and speed into overlapping sheets for FSSW. The revolving tool stays in place for a set

Published online on: ***February 01, 2025***

Corresponding Author's E-mail ID: dineshme.iitr@gmail.com

amount of time when it reaches the plunge depth.

Retracting the spinning tool from the welded joint immediately or after a dwell period leaves a keyhole at the weld centre after FSSW. See FSSW schematic in Fig.1. The rotating pin creates circumferential and axial material flow and softens the metal with frictional heat. Forging pressure, heating, and material flow generate a solid state metallurgical bond around the pin with a fine-grained microstructure and high-angle grain boundaries around the rotating tool [15]. FSSW parameters affect microstructure, bond area, weld strength, and failure mode [16].

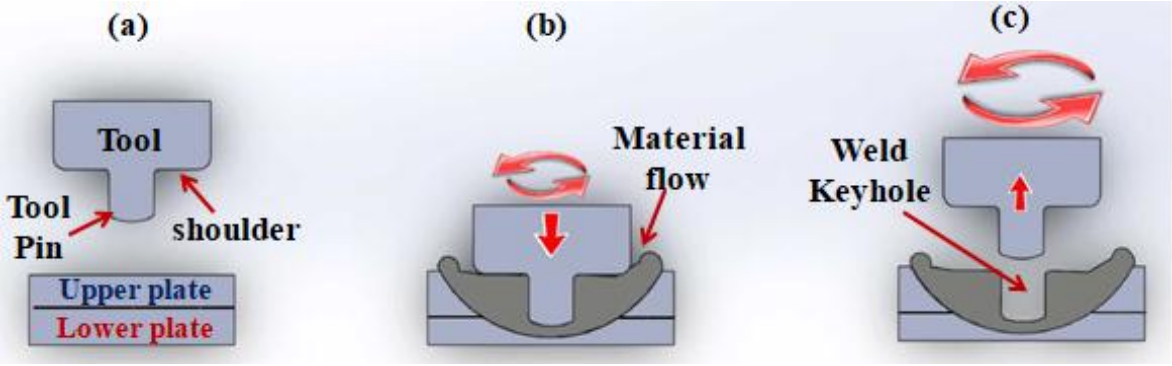

Fig.1 Schematic of conventional-FSSW showing (a) Plunging (b) Stirring and (c) Retraction of the tool

Earlier many researchers reported that different micro structural zones in FSSW, such as, the weld nugget/stir zone (SZ) at the weld center. The region adjacent to SZ, thermo-mechanical affected zone (TMAZ), which is followed by heat affected zone (HAZ) during the FSSW, the typical schematic of microstructural zones in FSSW is as shown in Fig.2. The classical formation was shown by the FSSW of Al-alloys. Considering the elliptical "onion"-like microstructure in the weld nugget zone, thin and elongated grains in the TMAZ as a result of continuous mixing were described, and very fine equiaxed grains as a result of plastic deformation and dynamic recrystallization. Although there was no plastic deformation in HAZ, there were noticeably coarser granules.

Fig.2 Typical schematic of microstructural zones in FSSW

2. Literature Survey

Keyholes concentrate stress and reduce the effective welding area during spot welds, reducing their tensile shear and fatigue strengths[17]. Since body paint cannot reach the keyhole bottom and rain water remains in the keyhole, anti-corrosion capabilities decrease [18]. Due to processing issues, typical keyhole closure methods and their effects on microstructure and mechanical behavior of FSSW of dissimilar Al-Alloys have not been extensively studied. The performance of such novel al-alloys in structural applications is little known. Therefore, the present review article is aimed to deal with detailed study on typical methods of keyhole closure and its influence on microstructure and mechanical behavior in FSSW of dissimilar Al-Alloys. **Table 1** shows the Abbreviations of technical terms used in this review.

Table 1. Abbreviations of technical terms used

Technical terms	Abbreviations
Friction Stir Spot Welding	FSSW
Refill-friction stir spot welding	RFSSW
Interlayer-friction stir spot welding	IL- FSSW
Filing-friction stir welding	FFSW
Active-passive filing friction stir welding	A-PFFSW
Rotational speed	RS
Plunge depth	PD

Weld time	WT
Dwell time	DT
Plunge speed	PS
Weld speed	WS
Plunge time	PT
Tensile shear failure load	TSFL

Shen et al. investigated RFSSW of dissimilar 2024/7075 aluminum alloys. They found that RFSSW produced keyhole-free joints with improved mechanical properties compared to conventional FSSW. The refilling process led to a fine-grained microstructure in the stir zone, enhancing strength and ductility [15].

Janga et al. analyzed RFSSW of thin AA7075-T6 sheets experimentally and numerically. Their results showed that RFSSW eliminated the keyhole and achieved joint strengths up to 77% of the base material [19].

Farhan and Guven studied the effects of interlayers on FSSW of stainless steel. They found that using a copper interlayer improved joint strength by 22% compared to joints without interlayers. The interlayer altered material flow and promoted metallurgical bonding [20]. Chu et al. developed a probeless friction stir spot welding technique for AA7075-T6. By optimizing tool geometry and process parameters, they achieved keyhole-free joints with strengths comparable to conventional FSSW [21]. Recent studies have focused on optimizing FSSW parameters for specific dissimilar alloy combinations to maximize strength and minimize defects. Understanding the link among welding parameters, microstructure, and joint properties is crucial for optimization.

Li et al. reviewed FSSW of aluminum and copper, emphasizing the role of intermetallic compounds in determining joint strength. They found that controlling heat input and material flow through parameter optimization was key to achieving sound joints [22]. Janga et al. combined experimental and numerical analysis to study RFSSW of thin AA7075-T6 sheets. Their coupled thermal-mechanical model provided insights into material flow and temperature distribution during welding. Such models enable rapid parameter optimization and process understanding [19].

ANNs have gained popularity for modeling complex relationships in FSSW. Kłonica et al. used machine learning techniques, including ANNs, to optimize friction stir welding of 2024-T3 aluminum alloy. Their ANN model accurately predicted joint strength with mean absolute percentage error below 5% [23]. **Fig.3** shows Artificial Neural Network (ANN) Modeling Flowchart.

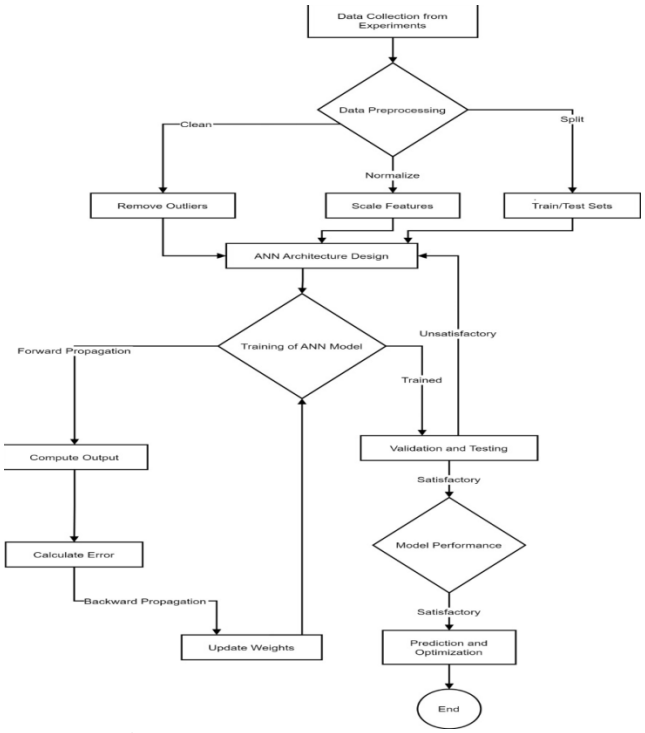

Fig.3 Artificial Neural Network (ANN) Modeling Flowchart

Recent advancements in friction stir welding for a range of industrial applications were evaluated by Bharti et al. They talked about how real-time monitoring and machine learning may be used to optimize welding conditions and provide adaptive control. This integration promises to enhance process robustness and joint quality. Optimizing FSSW processes for

energy efficiency and environmental impact has gained attention [24]. Rodrigues discussed recent developments in friction stir welding technology, highlighting the need for sustainable manufacturing practices. Optimization studies have begun to incorporate energy consumption and environmental factors alongside traditional mechanical property targets [25].

3. Keyhole closure/repair techniques

The current work attempts to address the keyhole issue related to traditional FSSW and its effects on the mechanical behavior, microstructure, and weld quality of friction stir spot welded dissimilar Al-Alloys. To address the aforementioned, a number of FSSW approaches are evaluated, including Refill-FSSW, Pinless/Probeless-FSSW, FSSW with Inter-layer, Protrusion-FSSW, Filling-FSSW, Active-passive Filling, and Stich and Swing FSW. **Table 2** shows the influence of various FSSW techniques used for keyhole closure.

Table 2. Summary of experimental techniques, joint configuration, tool geometries, FSSW constraints and key findings in FSSW of dissimilar Al-alloys

Technique	Al-alloy	Tool geometry	FSSW constraints	Key findings	Ref.
RFSSW	Alclad 7075-T6 100x25x0.8 mm^3	Clamp ring dia.- 15mm, Sleeve dia.- 9mm and Pin dia.- 6mm	RS-2100rpm, PD-0.85 to 1.1mm and WT-3 to 3.5s	Defect free welds with max. lap shear strength of 4.7 KN at WT of 3.5s and PD of 1.1 mm	[26]
RFSSW	AA7075-T651 Plate thickness- 6mm	MoV alloyed steel tool with Clamp ring dia.- 17mm, Sleeve dia.- 9mm, Pin dia.- 6mm	RS-1500 to 2100rpm, PD-5.85mm, DT-2 to 6s with AA cylindrical plugs as filler material	Efficient flawless weld with increased weld strength of 46 to 55% of BM and high heating rate with peak temperature of 540°C in NZ	[27]
RFSSW	AA7075-T6 210x30x1.6mm^3	RPS100 tool with Clamp ring dia.- 13.5mm, Sleeve dia.- 9mm , Pin dia.- 5.2mm	RS-3000rpm, PS upto 3.6mm/s, WT-1 to 1.5s Force-11KN	Defect free weld with increased lap shear strength	[28]
RFSSW	AA2014-O 75×25×2mm^3	Ring like grooved tool Clamp ring dia.- 14mm, Sleeve dia.-9mm, Pin dia.-5.2mm	RS-500 to 1800rpm, PD-1.57 to 1.97mm, DT-0 to 2.5s	Dispersion of grapheme nanosheet in Al-matrix	[29]
Pinless FSSW	AA6111-T4 100x25x0.91mm^3	Threaded 10° tapered pin H13 steel tool with Clamping ring dia.- 12mm, Tool shoulder dia.- 10 mm, Pin dia.- 4mm	RS-2000rpm, PD-0.2mm, PS-2.5mm/s, DT-2.5s	High quality welds with optimum shear strength is obtained	[5]
Pinless FSSW	AA6061-T6 138×60x2mm^3	L-shape grooved and scroll grooved H13 steel Tool with tool shoulder dia.- 10mm	RS-2000rpm, PD-1.1mm, PS-18.6mm/min , DT-6s	keyhole free welds and onion ring like microstructure with higher bond width	[30]
Pinless FSSW	AA 5052-H32 (upper plate) & AA 6061-T6 (lower plate)	Flat faced H13 Steel tool with Tool shoulder dia.- 14mm, Tool dia.- 10 to 18mm, Pin dia.- 4mm	RS-500rpm, PD-0.7mm , PS-0.002mm/sec	Elimination of keyhole and hook formation moderate bond width and minimum bulging	[31, 32]
IL- FSSW	Upper plate Cu and Bottom plate Al with Zn Interlayer (0.5 mm thickness)	H13 truncated cone (8°taper) Tool shoulder dia.- 16 mm, Pin dia.- 6mm, Axial force-1350N Penetration -1.5 to 6mm	RS-1400rpm, WS-3.4& 6.8mm/s, DT- 8s	Increased effective bond area therefore lap shear tensile strength and fracture strength improved	[33]
IL- FSSW	AA6061 (upper plate) AA2024 (lower plate) with AA6061 as interlayer (1mm thickness)	Pinless grooved Flat tool with Shoulder dia.- 10 mm	RS-900 to 1500rpm, PR-15 to 25mm/min , PD-0.7 to 0.9mm	Keyhole free welds with uniform spot appearance strength level reached double with refined microstructure in SZ	[34]
FSSW-Reinforced With Al_2O_3 Nano powder	AA2024-T3	**Step 1**-H13 hot work steel pinned tool Shoulder dia.- 14 mm, Pin dia.- 5mm **Step 2**-Pinless tool with Shoulder	RS-1120 and 1600rpm PD-2.5 and 2.75mm , DT-5 and 7s Al_2O_3 nano powder of	Keyhole free welds addition of Al_2O_3 powder 23% increase in weld strength and 7% in hardness. Rreinforced	[35, 36]

		dia.- 16mm	particle size 20-30nm	specimens have 5% smaller grain size	
Protrusion-FSSW	AA2024-T3 105×45x1mm^3	WC-based cylindrical pinless tool Clamp ring dia.- 16mm	RS-1000 to 2000rpm PD-0.1mm, DT-10s Protrusion height-0.2 to 0.6mm	Keyhole free welds Highest strength at 1600rpm and 0.6mm protrusion height Fine grains with size 5 µm in NZ	[37]
Protrusion-FSSW	AA5052 105×45x1mm^3	H13 cylindrical pinless steel tool with Shoulder dia.- 14mm	RS-800rpm, PD-0.2mm, DT -3 to 18s Protrusion height-0.4mm	Keyhole free welds by increasing dwell time from 3 to 18s, grain size increased from 5.3 µm to 10.5 µm	[38]
FFSW	AA5456-H321 (upper plate) and AA5456-O(lower plate)	Threaded and fluted AISI H13 consumable tool with Pin length-6.5mm , Shoulder dia.- 20mm, Pin dia.- 7mm, Pin cone angle- 8°	RS-400rpm in First pass 250rpm in Second pass WS-50mm/ min Indentation depth -0.3 mm, Tilt angle-5°	Keyhole free lap joints at 11° cone angle and 8 mm shoulder diameter	[39]
FFSW	AA7075-T6 and AA2219-T6 300x100x7.8mm^3	HSS Tool, AA7075, Pin length-10 to 12mm, Shoulder dia.- 22mm, Pin dia.- 10mm	RS-800rpm, WS-500mm/ min, PS-0.5 to 8 mm/min, Indentation depth -0.1 mm, Tilt angle-2.5°	Keyhole free welds at lower plunge speed	[40]
A-PFFSW	AA-ZL210- T5 200x100x6 mm^3	H13 Grooved shoulder pinless tool with Shoulder dia.- 6 mm in **Stage-1** Active Filling and 10 mm in **stage-2** Active Filling Shoulder dia.- 14mm in Passive filling with Pin dia.-10mm	RS=1600rpm, PS=2mm/min, DT=5s, Tilt angle= 2.5°	Keyhole free welds with 6-spiral grooves Shoulder peak temperature and material flow speed increased by increasing number of grooves in shoulder	[41]
Stich & Swing FSSW	AA6022-T4	Steel tool and Aluminum C-frame Swing FSW gun Shoulder dia.- 8mm Pin dia.- 3mm	RS-2500 to 3500rpm Feed rate-100 to 500mm/min, Swing length-0.5 to 2.5mm, Cycle time-0.5s, Feed-0 to 2.5mm	Strong welds with 490N higher lap shear strength than FSSW at the same welding time	[42]

4. Conclusion:

The study investigated various keyhole closure techniques employed in Friction stir spot welding (FSSW) of dissimilar Al-alloys. Key findings of the review are-

1. The keyhole closure characteristics significantly impact on the characteristics of spot weld, including microstructure, grain size and mechanical properties.
2. Proper keyhole closure ensures sufficient material mixing and bonding between joining parts leads to high strength defect and void free welds compared to the conventional FSSW.
3. The Machine learning and Artificial Neural Network are gaining traction for modeling complex relationship in FSSW of Al-alloys.

5. Future outlook

FSSW and its variants are the promising opportunities for joining dissimilar Al-alloys without keyhole. Future research should focus on optimization of keyhole closure techniques and simulation of material flow and temperature distribution in stir zone incorporating AI for the process.

Acknowledgement

Authors declare that they have no known competing financial interests or personal relationships that could have appeared to influence the work reported in this paper.

References:

[1] Barbini, A., Carstensen, J., & dos Santos, J. F. (2018). Influence of a non-rotating shoulder on heat generation, microstructure and mechanical properties of dissimilar AA2024/AA7050 FSW joints. *Journal of Materials Science & Technology*, *34*(1), 119–127.

[2] Suryanarayanan, R., & Sridhar, V. G. (2020). Process parameter optimisation in pinless friction stir spot welding of dissimilar aluminium alloys using Multi-start algorithm. *Proceedings of the Institution of Mechanical Engineers, Part C: Journal of Mechanical Engineering Science*, *234*(20), 4101–4115.

[3] Bozkurt, Y., & Bilici, M. K. (2013). Application of Taguchi approach to optimize FSSW parameters on joint properties of dissimilar AA2024-T3 and AA5754-H22 aluminum alloys. *Materials & Design*, *51*, 513–521.

[4] Wallington, T. J., Sullivan, J. L., & Hurley, M. D. (2008). Emissions of CO2, CO, NOx, HC, PM, HFC-134a, N2O, and CH4 from the global light-duty vehicle fleet. *Meteorologische Zeitschrift*, *17*(2), 109–116.

[5] Piccini, J. M., & Svoboda, H. G. (2015). Effect of the tool penetration depth in friction stir spot welding (FSSW) of dissimilar aluminum alloys. *Procedia Materials Science*, *8*, 868–877.

[6] Mishra, R. S., & Ma, Z. Y. (2005). Friction stir welding and processing. *Materials Science and Engineering: R: Reports*, *50*(1–2), 1–78.

[7] Threadgill, P. L., Leonard, A. J., Shercliff, H. R., & Withers, P. J. (2009). Friction stir welding of aluminium alloys. *International Materials Reviews*, *54*(2), 49–93.

[8] Zhang, B., Chen, X., Pan, K., & Yang, C. (2019). J-integral-based correlation evaluation between microstructure and mechanical strength for FSSW joints made of automotive aluminum alloys. *Journal of Manufacturing Processes*, *44*, 62–71.

[9] Huang, Y. X., et al. (2011). New technique of filling friction stir welding. *Science and Technology of Welding and Joining*, *16*(6), 497–501.

[10] Bagheri, B., Abbasi, M., Abdollahzadeh, A., & Omidvar, H. (2020). Advanced approach to modify friction stir spot welding process. *Metals and Materials International*, *26*(10), 1562–1573.

[11] Mishra, R. S., De, P. S., & Kumar, N. (2014). *Friction stir welding and processing: Science and engineering*.

[12] Chen, K., Liu, X., & Ni, J. (2017). Keyhole refilled friction stir spot welding of aluminum alloy to advanced high-strength steel. *Journal of Materials Processing Technology*, *249*, 452–462.

[13] Sun, Y., Fujii, H., Zhu, S., & Guan, S. (2019). Flat friction stir spot welding of three 6061-T6 aluminum sheets. *Journal of Materials Processing Technology*, *264*, 414–421.

[14] Pradeep, S., Sharma, S. K., & Pancholi, V. (2012). Influence of friction stir processing parameters on anisotropic behavior property of 5086-O aluminum alloy. *Materials Science Forum*, *702–703*, 348–351.

[15] Shen, Z., Ding, Y., & Gerlich, A. P. (2020). Advances in friction stir spot welding. *Critical Reviews in Solid State and Materials Sciences*, *45*(6), 457–534.

[16] Sarkar, R., Pal, T. K., & Shome, M. (2016). Material flow and intermixing during friction stir spot welding of steel. *Journal of Materials Processing Technology*, *227*, 96–109.

[17] Li, G., Zhou, L., Luo, L., Wu, X., & Guo, N. (2019). Microstructural evolution and mechanical properties of refill friction stir spot welded Alclad 2A12-T4 aluminum alloy. *Journal of Materials Research and Technology*, *8*(5), 4115–4129.

[18] Xu, Z., Li, Z., Ji, S., & Zhang, L. (2018). Refill friction stir spot welding of 5083-O aluminum alloy. *Journal of Materials Science & Technology*, *34*(5), 878–885.

[19] Janga, V. S. R., & Awang, M. (2022). Influence of plunge depth on temperatures and material flow behavior in refill friction stir spot welding of thin AA7075-T6 sheets: A numerical study. *Metals*, *12*(6), 927.

[20] Raza, M. F., & Yapici, G. G. (2022). Effects of interlayer on the friction stir spot welding of stainless steel. *Materials Today: Proceedings*, *62*, 4291–4294.

[21] Chu, X., et al. (2020). Effects of shoulder geometry on microstructures and mechanical properties of probeless friction stir spot welded aluminum 7075-T651 sheets. *Metals*, *10*(12), 1605.

[22] Li, P., et al. (2020). Interfacial microstructure and mechanical properties of dissimilar aluminum/steel joint fabricated via refilled friction stir spot welding. *Journal of Manufacturing Processes*, *49*, 385–396.

[23] Kujawska, J., et al. (2023). Improved prediction of the higher heating value of biomass using an artificial neural network model based on the selection of input parameters. *Energies*, *16*(10), 4162.

[24] Bharti, S., et al. (2023). A review of recent developments in friction stir welding for various industrial applications. *Journal of Marine Science and Engineering*, *12*(1), 71.

[25] Hussein, S. A., et al. (2024). A review of recent improvements, developments, influential parameters, and challenges in the friction stir welding process. *International Journal of Automotive and Mechanical Engineering, 21*(2), 11438–11452.

[26] Shen, Z., Chen, Y., Hou, J. S. C., Yang, X., & Gerlich, A. P. (2015). Influence of processing parameters on microstructure and mechanical performance of refill friction stir spot welded 7075-T6 aluminium alloy. *Science and Technology of Welding and Joining, 20*(1), 48–57.

[27] Reimann, M., Goebel, J., & dos Santos, J. F. (2017). Microstructure and mechanical properties of keyhole repair welds in AA 7075-T651 using refill friction stir spot welding. *Materials & Design, 132*, 283–294. https://doi.org/10.1016/j.matdes.2017.07.013

[28] Kubit, A., Wydrzyński, D., & Trzepieciński, T. (2018). Refill friction stir spot welding of 7075-T6 aluminium alloy single-lap joints with polymer sealant interlayer. *Composite Structures, 201*, 389–397. https://doi.org/10.1016/j.compstruct.2018.06.070

[29] Wang, S., et al. (2020). Strengthening and toughening mechanisms in refilled friction stir spot welding of AA2014 aluminum alloy reinforced by graphene nanosheets. *Materials & Design, 186*, 108212. https://doi.org/10.1016/j.matdes.2019.108212

[30] Yazdi, S. R., Beidokhti, B., & Haddad-Sabzevar, M. (2019). Pinless tool for FSSW of AA 6061-T6 aluminum alloy. *Journal of Materials Processing Technology, 267*, 44–51. https://doi.org/10.1016/j.jmatprotec.2018.12.005

[31] Saju, T. P., & Narayanan, R. G. (2020). Dieless friction stir extrusion joining of aluminum alloy sheets with a pinless stir tool by controlling tool plunge depth. *Journal of Materials Processing Technology, 276*, 116416. https://doi.org/10.1016/j.jmatprotec.2019.116416

[32] Saju, T. P., Narayanan, R. G., & Roy, B. S. (2019). Effect of pinless tool shoulder diameter on dieless friction stir extrusion joining of AA 5052-H32 and AA 6061-T6 aluminum alloy sheets. *Journal of Mechanical Science and Technology, 33*(8), 3981–3997. https://doi.org/10.1007/s12206-019-0136-1

[33] "Interlayer FSSW Intermediate layer Optimization_2019.pdf."

[34] Ibrahim, I. J., & Yapici, G. G. (2018). Application of a novel friction stir spot welding process on dissimilar aluminum joints. *Journal of Manufacturing Processes, 35*, 282–288. https://doi.org/10.1016/j.jmapro.2018.08.018

[35] Enami, M., Farahani, M., & Farhang, M. (2019). Novel study on keyhole-less friction stir spot welding of Al 2024 reinforced with alumina nanopowder. *International Journal of Advanced Manufacturing Technology, 101*(9–12), 3093–3106. https://doi.org/10.1007/s00170-018-3142-z

[36] "FSW_Reinforcement with alumina particles_2018.pdf."

[37] Dourandish, S., Mousavizade, S. M., Ezatpour, H. R., & Ebrahimi, G. R. (2018). Microstructure, mechanical properties, and failure behavior of protrusion friction stir spot welded 2024 aluminium alloy sheets. *Science and Technology of Welding and Joining, 23*(4), 295–307. https://doi.org/10.1080/13621718.2017.1386759

[38] Farmanbar, N., Mousavizade, S. M., & Ezatpour, H. R. (2019). Achieving special mechanical properties with considering dwell time of AA5052 sheets welded by a simple novel friction stir spot welding. *Marine Structures, 65*, 197–214. https://doi.org/10.1016/j.marstruc.2019.01.010

[39] Han, B., Huang, Y., Lv, S., Wan, L., Feng, J., & Fu, G. (2013). AA7075 bit for repairing AA2219 keyhole by filling friction stir welding. *Materials & Design, 51*, 25–33. https://doi.org/10.1016/j.matdes.2013.03.089

[40] Wen, Q., Li, D., Ji, S., Dong, Z., Huang, R., & Liu, Z. (2020). Improving interfacial microstructures and tensile properties of active–passive filling friction stir repaired ZL210 aluminum alloys by optimizing shoulder morphologies. *Transactions of the Indian Institute of Metals, 73*(9), 2181–2190. https://doi.org/10.1007/s12666-020-02024-5

[41] Yang, X. W., Fu, T., & Li, W. Y. (2014). Friction stir spot welding: A review on joint macro- and microstructure, property, and process modelling. *Advances in Materials Science and Engineering, 2014*, 697170. https://doi.org/10.1155/2014/697170

[42] Okamoto, K., Hunt, F., & Hirano, S. (2005). Development of friction stir welding technique and machine for aluminum sheet metal assembly—Friction stir welding of aluminum for automotive applications. *SAE Technical Paper*, 724. https://doi.org/10.4271/2005-01-1254

A Review on Advancement of Metallic Biomaterials for Biomedical Implants

Bhavana Singh[1], Dr. Vaibhav Trivedi[2], Dr. Ankur Goel[3], Ayush Saxena[4]

[1]*Research Scholar Mechanical Engineering Department, IFTM University, Moradabad 244001, India*
[2]*Professor Mechanical Engineering Department, IFTM University, Moradabad 244001, India*
[3]*Orthopedic & Joint replacement surgeon Sri sai superspeciality Hospital, Moradabad 244001, India*
[4]*Research Scholar Mechanical Engineering Department, IFTM University, Moradabad 244001, India*

Abstract

The field of metallic biomaterials has undergone significant advancements over the past few decades, particularly in their application for biomedical implants. These materials, because of their remarkable mechanical characteristics, biocompatibility, and better resistance against corrosion and mechanical wear, have become the cornerstone of modern medical implants used in orthopedics, dentistry, and cardiovascular applications. Innovations in the design and fabrication of metallic biomaterials have led to improved implant performance, longevity, and patient outcomes. This review paper seeks to offer an all-compassing overview of the latest advancements in metallic biomaterials, focusing on novel alloys, surface modification techniques, and their impact on biocompatibility and mechanical performance. Additionally, the paper will explore emerging trends and future directions in this rapidly evolving field, highlighting the potential for next-generation implants to further enhance patient care and recovery.

Keywords: *Biomaterial, Metallic Alloys, Implant..*

1. Introduction

The American National Institutes of Health defines biomaterials as "Any substance or combination of substances, other than drugs, synthetic or natural in origin, which can be used for any period, which augments or replaces partially or any tissue, organ or function of the body, to maintain or improve the quality of life of the individual". A biomaterial holds significant performance in interacting with the biological system of a living organism to ensure proper function in medical applications and to facilitate healing following injury or disease. It is often used as an alternative to biological bone in cases where tissue inflammation or mechanical stability is compromised [1]. Metallic biomedical materials are essential in the creation of functional prosthetics and implants used in surgical interventions, with the primary intent to boost patient outcomes [2].Significant advancements in the domain of biomaterials research have expanded the applications of various orthopaedic as well as dental implants, including total bone replacements, devices to fix fracture, dental screws, joint arthrodesis, and more [3].The success of a metallic bioimplants mainly relies two important factors- their overall bulk properties and on the characteristics of the bioimplant's surfaces, which comes in direct interaction with the tissues of human body. Consequently, the development of bioimplants has advanced to the point where material selection is driven by the specific properties required for optimal performance [4]. At the start of the 1930s, stainless steel and cobalt-chromium alloys became recognized as viable biomaterials, followed by the introduction of polymers in the 1940s. The first fully developed total metallic hip implant was introduced in 1938, and in 1952, the first synthetic blood vessel, made from Vinyon and Co-polymer, was developed. Over the following years, significant advancements included the creation of vascular grafts in 1953, the first complete hip replacement in 1958, the development of heart valves in 1960, and the artificial heart in 1976 [5]. Among the metallic biomaterials used for biomedical implants low-carbon stainless steel with austenitic microstructure, especially AISI 316L, is widely utilized in biomedical applications due to its cost-effectiveness and versatility[6].Titanium alloys, magnesium alloys, high entropy alloys, Al-Si alloys, cobalt-chromium-molybdenum, and tungsten are commonly used in across different 0biomedical implants because of the unique properties of these alloys. Selecting the right material for implants is still a complex task, as it depends on the variety of factors such as the expected duration of biomedical implant, type of tissue of human body that directly come in contact with implant and the specific characteristics of the patient [7].Magnesium (Mg) alloys and composites possess mechanical properties that closely resemble those of bone, making them suitable for use as small fixation devices and load-bearing components. As a result, these materials minimize the risk of bone damage caused by stress shielding [8]. The alloys of Cobalt (Co) metal provide greater wear resistance properties as compared to titanium (Ti) alloys, enabling them to be particularly well-suited for metallic artificial orthopedic hip replacement joints [9].Aluminum based high entropy alloys and Al-Si alloys with enhanced corrosion resistance are also used for certain specialized applications in biomedical industry. However, Al-Si alloys are generally considered non-biocompatible due to their relatively low corrosion resistance [10]. Metallic implants are favored for their outstanding

Published online on: ***February 01, 2025***
Corresponding Author's E-mail ID: bhavnasingh15619@gmail.com

physical-mechanical attributes, wide availability, and low production costs. Historically, the use of gold and silver was commonly used in dental and skeletal implants. For an implant material to be effective, it must exhibit high corrosion resistance, excellent tissue compatibility, non-toxicity, and mechanical properties comparable to hard tissues [11]. Although alloys and metallic substances satisfy numerous biomedical needs, the bonding between the metallic surface and surrounding tissue or bone is often weak or non-existent. The failure or deterioration of a metallic implants typically occurs at the implant-tissue contact interface, where inadequate bonding between tissues and implant give rise to the development of a non-adherent layer and movement at the tissue-implant junction [12].Corrosive wear in biometallic implants can compromise the surface integrity and biocompatibility, triggering tissue reactions that release corrosion byproducts from the surface of implant, ultimately leading to early failure. Bioimplants are expected to last at least 15 to 20 years for older patients and over 20 years for younger patients [13]. To find a solution of these challenges and difficulties in metallic biomedical implants various physical and chemical surface modification techniques are employed to enhance the interfacial attributes and interactions of implant materials with the biological environment. Alloying is considered the most crucial method for strengthening mechanical characteristics and corrosion resistance of metallic biomedical implants. This review paper is meant to deliver a comprehensive overview of the latest advancements in metallic biomaterials, focusing on novel alloys, surface modification techniques, and their impact on biocompatibility and mechanical performance. Additionally, the paper will explore emerging trends and future directions in this rapidly evolving field, highlighting the potential for next-generation implants to further enhance patient care and recovery.

2. Properties of Metallic Biomaterials

A biomaterial must have the following properties to be best suited-

2.1 Mechanical Properties

The elastic modulus of elasticity (Young's modulus-specific to linear elasticity) of natural bones ranges between 10 and 40 GPa, and implant materials should ideally have a similar modulus. If the value of modulus of elasticity is too high, it can cause stress shielding, where inadequate load transfer to the bone prevents it from developing the strength needed to handle stress and load. Therefore, implants with a lower modulus of elasticity are favoured, as they disperse mechanical stress and load more evenly between the bone and the implant, helping to extend the implant's lifespan [14]. By aligning the flexibility module of biomaterials with bone, which ranges from 4 to 30 GPa, stress shielding can be prevented. Table 1shows the comparison of mechanical strength of commonly used biomaterials with the strength human bone [15].

Table 1 Comparison of mechanical strength of Bone with the commonly used metallic biomaterials

Material	Young's Modulus (GPa)	Yield Strength (MPa)	Tensile Strength (MPa)	Fatigue limit (MPa)
Stainless Steel	200	221-1213	586-1301	241-820
Co-Cr	210-253	448-1606	655-1896	207-950
Ti-6A-4V	116	896-1034	965-1103	620
Cortical Bone	15-30	30-70	70-150	

2.2 Biocompatibility

Biocompatibility is crucial for medical implants. It provides assurance that the material used does not cause any unfavorable biological responses in the body, such as toxicity, inflammation, or allergic responses. This involves evaluating how the material interacts with the surrounding biological tissues and fluids to ensure it is safe and effective for long-term use. Figure 1. Shows the comparison of biocompatibility of most commonly used alloys [16].

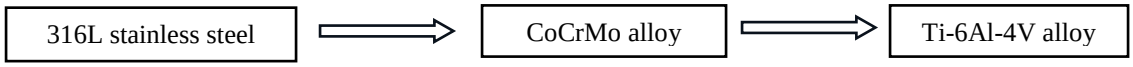

Fig.1 Increasing order of biocompatibility of commonly used alloys

2.3 Corrosion Resistance and Wear Resistance Property

Corrosive and mechanical wear in metallic implants often result in aseptic loosening and excessive release of metal ions, which can be harmful or toxic to the body. To address these issues and improve the implants' resistance to corrosion and wear, as well as their ability to integrate with bone and provide antibacterial effects, a range of surface modification techniques are essential [17].

2.4 Non-toxicity

The material should be free from genotoxicity (which can modify DNA) and cytotoxicity (which can harm cells). Biological responses of various metal elements on the human body are shown in Table 2.

2.5 Fatigue Strength

The material should exhibit superior resistance to stress-induced fatigue and failure to avoid implant malfunctions and ensure protection against fatigue fractures. Fatigue-related failures have been observed in hip prostheses, but titanium-based alloys offer superior fatigue resistance and strength.

To increase the desirable properties of biomaterial various alloying elements are added to the base metal. When selecting alloying elements for biomedical applications, it is crucial to consider factors such as biocompatibility, bioactivity, biodegradability, reduced stress shielding effectand non-toxicity, in addition to mechanical and corrosion properties [18,19]. Effect of high concentration of various alloying elements is shown in Table 2.

Table 2. Effect of high concentration of alloying elements on the human body

Metal Element	**Biological responses of High concentration on Human Body**
Nickel	Significantly impacts the skin, resulting in dermatitis [18].
Cobalt	Prevents iron (Fe) from being absorbed into the bloodstream, leading to anemia [18].
Vanadium	Extremely toxic to the human body in its elemental form [18].
Aluminum	Its buildup in the human body can lead to Alzheimer's disease and has been associated with epileptic effects [18].
Chromium	causes the formation of ulcers and disrupts the central nervous system [18].
Copper	High concentrations of copper (Cu) can lead to severe liver damage [19].
Molybdenum	Excess of Mo leads to developmental issues and an increase in uric acid levels [19].
Manganese	A significant quantity of manganese (Mn) leads to reduced absorption of iron (Fe) [19].

3. Metallic Biomaterial Alloy Compositions

3.1 Titanium and Its Alloys

Titanium and its alloys are suitable for use as permanent biomedical prosthetics and implants by virtue of their strong biocompatibility, superior ability to withstand corrosion, mechanical strength, and reliable stability [20]. Titanium can naturally form a highly resilient and a non-toxic titanium dioxide protective passivation layer, which effectively isolates the titanium from surrounding body fluids [21]. Spataru et al. developed a novel titanium alloy that includes molybdenum (Mo) and silicon (Si) through vacuum arc remelting (VAR), which enhanced the alloy's stability against chemical reactions as well asits biocompatibility [22]. Nitinol is a unique nickel-titanium metal alloy. It is best known for its unique thermal shape memory, super elasticity, and superior damping characteristics, making it extensively used in medical applications [23]. The shape memory effect allows it to 'remember" a specific shape and return to that shape when heated above a certain temperature. Recently, researchers have concentrated on using nitinol in cardiovascular devices because of its superior reversible deformation when compared to alternative metals. Its distinct characteristics make nitinol ideal for manufacturing functional stents, which can be implanted at the surgical site through minimally invasive techniques [24].Ti.6Al.4V alloy is one of the foremost desirable, widely employed and durable titanium alloys. It is composed of approximately 90% titanium, 6% aluminum (Al), and 4% of vanadium (V). This alloy possesses numerous favorable attributes that make it highly compatible for medical implant production. It offers excellent resistance against corrosion thanks to the creation of an layer of oxide on the implant's surface [25].Dentists favor Ti.6Al.4V implants for replacing damaged teeth and for creating shape

memory devices. This alloy is also utilized in the production of artificial hip joints, bone plates, artificial hearts, cardiac valve prostheses, knee joints, pacemakers, and fracture fixation screws [26]. A critical downside of Ti.6Al.4V alloy is that it releases vanadium metal ions. The human body may experience toxic effects from vanadium metal ions. Additionally, the presence of aluminum and vanadium can trigger negative immunological responses [27]. Ti-Zr is a titanium (Ti) based alloy with zirconium (Zr) with a composition of 84% of Ti and 16% of Zr. Zirconium, which is in the same group of the periodic table as titanium, shares chemically similar structures and characteristics with titanium. When dissolved in titanium, zirconium becomes neutral and non-toxic [28]. Sharma et al. explored the mechanical attributes of the Ti-Zr alloy and found that it had a reduced elastic modulus, improved hardness, and a refined grain structure with finer grain size compared to traditional titanium. They concluded that Ti-Zr alloy could be better fit for implants subjected to high loads. The Ti-Zr alloy exhibits exceptional corrosion resistance property because both titanium and zirconium form a layer of oxide on their surfaces when they exposed to oxygen [29]. Ou et al. in their work investigated the cytocompatibility of the Ti-Zr alloy, including aspects such as cytotoxicity, cell adhesion, and proliferation. They reached to the result that the Ti-Zr alloy is free from toxicity for biological systems and exhibits splendid biomechanical properties compared to conventional titanium [30].The major drawbacks of the alloy are that it has poor mechanical stability and high complexity involved in its procedures of processing and synthesis [31].Thus, Ti-Zr exhibits superior suits of properties and holds potential for various dental implant applications. However, further focused exploration and analysis is required to improve its mechanical stability and processing and manufacturing techniques on an industrial scale. Additionally, discovering effective and competent methods for developing and producing biomedical implants from Ti-Zr is crucial. Titanium-Nickel (Ti-Ni) is another desirable alloy with a nearly equal atomic proportional composition of 49% of nickel and 51% of titanium. This alloy boasts several unique combinations of properties. These unique combinations of properties make it highly valuable in the domain of medical industry. The alloy is super elastic, exhibits excellent biocompatibility, and has an elastic modulus comparable to that of human bone. Its corrosion resistance is enhanced by the formation of a protective TiO2 layer on its surface [32]. The shape memory effect of Ti-Ni alloy makes it particularly advantageous for creating braces used to correct the shape of teeth. Additionally, its superelastic property, which allows it to return to its original shape after deformation, is highly beneficial in endodontology, enabling the construction of curved root canals [33]. Ti-Ni alloys are also employed in the production of self-expandable vascular stents, which are used to treat atherosclerosis in coronary arteries, carotid arteries, and peripheral arteries [34]. Since nickel is highly toxic to the human body, prolonged use of the Ti-Ni alloy can result in the shadding of metal ions, potentially leading to allergic reactions and other health issues [35]. Li et al. investigated the microstructural properties and mechanical properties of Ti-Mo-Nb alloys for use in various biomedical applications [36].Ashkani, Omid, et al. conducted a simulation-based study on the impact of copper and aluminum alloying elements on the various mechanical traits of biocompatible Ti-Mo alloys. Their findings indicated that incorporating copper and aluminum elements significantly enhances the strength and as well as hardness of Ti-Mo alloys while reducing their elasticity [37].

3.2 Magnesium and Magnesium Alloys

Magnesium and various alloys of magnesium are regarded as best-suited materials for biodegradable metallic prosthetics and medical implants. Magnesium-based alloys can safely degrade in the body over time [38]. Bioresorbability makes Mg-alloys especially suitable for temporary implants. Costantino et al. discovered that Mg-based alloys, used as biomaterials, exhibited superior cell compatibility with macrophages. This interaction is crucial in the inflammatory process and can positively influence the healing of tissue and performance of implant, leading to quicker inflammation resolution and tissue repair [39]. Mao et al. developed a magnesium-based alloy by adding Neodymium (Nd), Zinc (Zn) and Zirconium (Zr) as alloying constituents (Mg-2.2Nd-0.1Zn-0.4Zr).This Mg-alloy has a stable degradation rate and long-term structural durability along with mechanical durability in vivo. Using human vascular endothelial cells (HUVECs), the magnesium extract's toxicity to cells was assessed in vitro [40]. Dvorsky et al. in their work suggested that the AM50 magnesium alloy could be a viable choice for biodegradable heart stent applications, owing to its appropriate corrosion rate of 1.2 mm/year and favorable cellular compatibility [41]. Magnesium and its alloys have been thoroughly investigated as potential biodegradable materials for orthopedic implants, such as fracture fixation. However, the high rate of corrosion of Mg-based alloys under physiological conditions presents a significant challenge that must be addressed for their effective therapeutic use. To enhance the mechanical attributes and achieve desirable resistance against corrosion in magnesium and its alloys while ensuring the biocompatibility of the medical implant through non-toxic features, it is essential to identify suitable alloying elements [42]. Changes induced by various alloying elements on the physical-mechanical properties of Mg-alloy are shown in Table 3.[43]

Table 3 Changes induced by the alloying elements on the mechanical properties of Mg alloy [43]

Alloying Element	Effect on properties
Al	Aluminum enhances tensile strength and hardness in alloys.
Zr	Zirconium offers excellent ductility, tensile strength, and damping capacity.
Sn	Adding tin increases both compressive and tensile strength.
Mn	The addition of manganese as alloying elements improves grain fineness and tensile strength.
Sr	Strontium, when added up to 3 wt%, increases strength while reducing ductility and enhances grain size refinement.
Zn	Zinc, when added up to 5% by weight, improves the mechanical attributes (strength)of the composite.

3.3 Cobalt (Co)-Chrome (Cr) Alloy

Cobalt-Chrome is also a widely used alloy primarily composed of cobalt (Co) and chromium (Cr). This alloy consists of main element cobalt with 27-30% of chromium, 5-7% of molybdenum, and small amounts of other alloying elements manganese, silicon (<1%), iron (<0.75%), nickel (<0.5%), along with traces of tungsten, carbon, phosphorus, nitrogen, sulphur, and boron [44].The Co-Cr alloy exhibits high corrosion resistance. The reason of high corrosion resistance property is that a passive protective film made of Cr2O3formed on its surface[45].Co-Cr alloys are superior wear-resistant as well as they possess high wear resistant surface. However, as a result of their lesser osseointegration in comparison to titanium and other alternative alloys, they are primarily used in the development of prostheses used for joint replacement, the one of the examples is the femoral component in total knee replacements and the femoral head in total hip replacements [46].Screws made of Co-Cr alloys have weak integration with human bone tissues. Due to this property Co-Cr alloys are also utilized as screws in trauma plating systems. Their poor bonding with human bone tissues allows for easy removal after the fracture in bone has healed. Along with this they are commonly used in orthopedic prosthesis, including implants for knees, dental implants and metal-to-metal hip joints[47]. Plecko et al. conducted an in-vivo study where several metallic screws were implanted in sheep. The study revealed that the torque required to remove the Co-Cr screws was considerably lower than that of titanium screws and screws coated with bioactive [48].Cobalt-Chrome alloys hold promise as materials for medical implants due to their advantageous and desirable properties and compatibility with bone. Future research could focus on enhancing the osteointegration of Co-Cr alloys by applying titanium or zirconium-based coatings or applying layer of bioceramic coatings on the material's surface. Additionally, efforts should be made to develop nickel-free Co-Cr alloys to reduce toxicity and improve safety regarding health of the human body [49].

3.4 Stainless steel alloys

Stainless steel is a group of ferrous alloys primarily composed of iron. The composition typically includes 70% iron, 16-18% chromium, 10-14% nickel, and 1% carbon [50]. Stainless steel when correctly heat-treated and finished, resists oxidation and corrosive attacks from corrosive media. Biomedical implants made up of Stainless steel are radiopaque, meaning it appears clearly on X-rays, so to enhance their radiopacity, uniform layers of noble metals like gold or platinum are coated to their surfaces [51]. The alloy exhibits promising resistance against corrosion as a result of the developement of a protective Cr2O3 layer on its surface [52]. Medical implants used temporarily for the replacement of hips, knees, or shoulders are typically made from stainless steel. Additionally, guide wires and sensor wires used in heart surgeries are commonly constructed from stainless steel [53]. In spite of its significant benefits, stainless steel has limited range of applications in medical implants due to its susceptibility to corrosion in chloride environments. This corrosion can lead to the shedding of metal ions, such as nickel and chromium, which are toxic to the human body [54]. Salahinejad et al. experimented with producing nickel-free austenitic stainless steel by substituting nickel with nitrogen. This modification enhanced the structural stability and improved the steel's strength. The results demonstrated that this nickel-free alloy offered higher strength, greater resistance against corrosion and wear, and improved biocompatibility compared to traditional nickel-

containing stainless steel. It has shown to be a highly effective alternative due to its reduced toxicity and enhanced properties [55].Stainless steel is best suited alloy for the manufacturing of medical implants because it is cost efficient and satisfactory physical-mechanical attributes. However, its tendency to erode in bodily fluids restricts its use to smaller medical implants, such as nails and wires.

3.5 High Entropy Alloys

High entropy alloys are composite materials made up of five or more constituents, each present in relatively equal concentrations of 5–35%, which contribute to the formation of a stable solid solution [56].High entropy alloys (HEAs) provide greater design flexibility, allowing for the integration of various medical features to meet diverse needs. These features include a decreased modulus of elasticity, optimal biocompatibility, and possible shape-memory properties [57]. Alagarsamy et al. investigated the potential use of the Al0.1CoCrFeNi high-entropy alloy as a peripheral vascular stent by evaluating its physical-mechanical attributes and making a comparison of them with those of commercial 316L stainless steel stent materials. The findings indicate that the high-entropy alloy either matched or surpassed 316L SS in several mechanical attributes, demonstrating improved fatigue resistance, which is advantageous for minimizing the failure rate and improving reliability of stent implants [58].Chen et al. developed a new Co40Fe35Cr16Ni8Ti1 high-entropy alloy for coronary stents. This alloy compiled with the physical-mechanical traits and corrosion resistive standards of regular coronary stent materials available in the market. It demonstrated superior elongation, as well as impressive yield strength and tensile strength [59]. Tanji et al. concluded that the TiHfZrNbx high-entropy alloy showed superior resistance against corrosion in the body's saline environment compared to standard CP-Ti and Ti6Al4V alloy biomaterials, making it a promising high-performance material for medical implants [60].

3.6 Aluminum-Silicon Alloys (Al-Si Alloys)

The unmodified Al–Si alloy is recognised and identifiable by silicon flakes. The existance of these silicon flakes result in poor ductility of the Al-Si alloy casting. Modifiers are commonly employed in eutectic as well as hypoeutectic Al–Si alloys to improve the refinement of the eutectic Si phase, changing it from angular platelets into finer fibers. This microstructural modification generates considerable enhancement in the mechanical attributes of the alloy [61].The aluminum-silicon alloy with magnesium as a constituent in it (AlSi7Mg), notable for its favorable mechanical properties, shows potential as metallic implant material for biomedical applications. The properties of this alloy are further refined and enhanced to meet strict standards for biomedical implants. The characteristics and attributes of the AlSi7Mg alloy were notably affected by means of adding alloying elements strontium(Sr) and zirconium (Zr) invarying concentration levels. Strontium (Sr) alters the eutectic silicon phase in aluminum-silicon alloys. It refines the silicon morphology from coarse needle-like or plate-like structures to a finer, more spherical nodule form. Along with it, Zirconium acts as a nucleation site, enhancing the transformation process that is induced by Sr and leading to a more potent refinement of the Si phase [62].

4. Conclusion

The field of metallic biomaterials has seen remarkable progress, driven by advancements in alloy composition and surface modification techniques that have significantly enhanced their application in biomedical implants. These materials, particularly magnesium, cobalt-chrome, titanium, stainless steel, high entropy alloys, and aluminum-silicon alloys, each offer unique properties that make them well-suited for various medical uses, including orthopedics, dentistry, and cardiovascular devices. Key considerations in developing these materials include mechanical strength, biocompatibility, corrosion resistance, non-toxicity, and fatigue resistance. While materials like titanium alloys and magnesium-based alloys have shown significant promise due to their biocompatibility and desirable mechanical attributes, challenges remain, such as the rapid corrosion of magnesium alloys and the potential toxicity of certain elements in titanium alloys. Emerging materials like high entropy alloys and aluminum-silicon alloys are beginning to show potential for next-generation implants, offering properties that could further enhance patient outcomes and implant longevity. However, further exploration and analysis is needed to enrich the mechanical stability and biocompatibility of these materials and to develop efficient manufacturing techniques for their use in clinical settings.In conclusion, the continuous evolution of metallic biomaterials promises to advance the capabilities of metallic biomedical implants, facilitating to better patient treatment, recovery, and overall standard of life. As research progresses, the development of more safe, more durable, and more effective biomaterials will continue to serve as a key factor in modern medicine.

References

[1] Prakasam, M., Locs, J., Salma-Ancane, K., et al. (2017). Biodegradable materials and metallic implants—A review. *Journal of Functional Biomaterials, 8*, 1–15.
[2] Mamo, H. B., Adamiak, M., & Kunwar, A. (2023). 3D printed biomedical devices and their applications: A review on state-of-the-art technologies, existing challenges, and future perspectives. *Journal of the Mechanical Behavior of Biomedical Materials.*
[3] Tang, G., Liu, Z., Liu, Y., Yu, J., Wang, X., Tan, Z., & Ye, X. (2021). Recent trends in the development of bone regenerative biomaterials. *Frontiers in Cell and Developmental Biology, 9*, 1001.
[4] Campbell, A. A. (2003). Bioceramics for implant coatings. *Materials Today, 6*, 26–30.
[5] Davis, R., et al. (2022). A comprehensive review on metallic implant biomaterials and their subtractive manufacturing. *The International Journal of Advanced Manufacturing Technology, 120*(3), 1473–1530.
[6] Nouri, A., & Wen, C. (2021). Stainless steels in orthopedics. In *Structural Biomaterials* (pp. 67–101). Woodhead Publishing.
[7] Teixeira, R. L. P., & Silva, P. C. D. (2024). Advancing metallic biomaterials for biomedical implants: A comprehensive integrative review. *Revista de Gestão Social e Ambiental, 18*(5), e05255-e05255.
[8] Gutiérrez Púa, L. D. C., et al. (2023). Biomaterials for orthopedic applications and techniques to improve corrosion resistance and mechanical properties for magnesium alloy: A review. *Journal of Materials Science, 58*(9), 3879–3908.
[9] Abraham, A. M., & Venkatesan, S. (2023). A review on application of biomaterials for medical and dental implants. *Proceedings of the Institution of Mechanical Engineers, Part L: Journal of Materials: Design and Applications, 237*(2), 249–273.
[10] Sathiyaseelan, G., et al. (2024). Enhancing the strength and structure of Al–Si alloys for biomedical applications through the addition of Sr and Zr grain refiners on secondary AlSi7Mg aluminum alloys. *Chemical Physics Impact, 8*, 100557.
[11] Zwawi, M. (2022). Recent advances in biomedical implants; mechanical properties, surface modifications, and applications. *Engineering Research Express, 4*(3), 032003.
[12] Goharian, A. (2019). Fundamentals in loosening and osseointegration of orthopedic implants. *Osseointegration in Orthopedic Implants, 1*, 1–26.
[13] Rodriguez-Gabella, T., Voisine, P., Puri, R., Pibarot, P., & Rodés-Cabau, J. (2017). Aortic bioprosthetic valve durability: Incidence, mechanisms, predictors, and management of surgical and transcatheter valve degeneration. *Journal of the American College of Cardiology, 70*, 1013–1028.
[14] Zwawi, M. (2022). Recent advances in biomedical implants; mechanical properties, surface modifications, and applications. *Engineering Research Express, 4*(3), 032003.
[15] Lawrence, K. J. (1980). Anisotropy of Young's modulus of bone. *Nature, 283*, 106–107.
[16] Manam, N. S., et al. (2017). Study of corrosion in biocompatible metals for implants: A review. *Journal of Alloys and Compounds, 701*, 698–715.
[17] Unune, D. R., Brown, G. R., & Reilly, G. C. (2022). Thermal-based surface modification techniques for enhancing the corrosion and wear resistance of metallic implants: A review. *Vacuum, 203*, 111298.
[18] Ali, S., et al. (2020). Biocompatibility and corrosion resistance of metallic biomaterials. *Corrosion Reviews, 38*(5), 381–402.
[19] Geetha, M., et al. (2009). Ti-based biomaterials, the ultimate choice for orthopedic implants—A review. *Progress in Materials Science, 54*(3), 397–425.
[20] Hazwani, M. R. S. N., et al. (2022). Fabrication of titanium-based alloys with bioactive surface oxide layer as biomedical implants: Opportunity and challenges. *Transactions of Nonferrous Metals Society of China, 32*(1), 1–44.
[21] Priyadarshini, B., et al. (2019). Bioactive coating as a surface modification technique for biocompatible metallic implants: A review. *Journal of Asian Ceramic Societies, 7*(4), 397–406.
[22] Spataru, M. C., et al. (2021). In-depth assessment of new Ti-based biocompatible materials. *Materials Chemistry and Physics, 258*, 123959.
[23] Katić, J., & Metikoš-Huković, M. (2010). Surface modification of nitinol by biocompatible passive films. *ECS Transactions, 28*(29), 65.
[24] Nagaraja, S., et al. (2018). Impact of nitinol stent surface processing on in-vivo nickel release and biological response. *Acta Biomaterialia, 72*, 424–433.

[25] Ding, R., Guo, Z. X., & Wilson, A. (2002). Microstructural evolution of a Ti–6Al–4V alloy during thermomechanical processing. *Materials Science and Engineering: A*, *327*(2), 233–245.
[26] Wu, C., et al. (2008). Novel sphene coatings on Ti–6Al–4V for orthopedic implants using the sol–gel method. *Acta Biomaterialia*, *4*(3), 569–576.
[27] Fojt, J. (2012). Ti–6Al–4V alloy surface modification for medical applications. *Applied Surface Science*, *262*, 163–167.
[28] Grandin, H. M., Berner, S., & Dard, M. (2012). A review of titanium zirconium (TiZr) alloys for use in endosseous dental implants. *Materials*, *5*(8), 1348–1360.
[29] Sharma, A., et al. (2021). Is titanium–zirconium alloy a better alternative to pure titanium for oral implant? Composition, mechanical properties, and microstructure analysis. *The Saudi Dental Journal*, *33*(7), 546–553.
[30] Ou, P., et al. (2021). Cytocompatibility of Ti–xZr alloys as dental implant materials. *Journal of Materials Science: Materials in Medicine*, *32*(5), 50.
[31] Chopra, D., et al. (2022). Advancing dental implants: Bioactive and therapeutic modifications of zirconia. *Bioactive Materials*, *13*, 161–178.
[32] Thompson, S. A. (2000). An overview of nickel–titanium alloys used in dentistry. *International Endodontic Journal*, *33*(4), 297–310.
[33] Sifakakis, I., & Bourauel, C. (2017). Nickel–titanium products in daily orthodontic practice. In *Orthodontic Applications of Biomaterials* (pp. 107–127). Woodhead Publishing.
[34] Sharma, N., Raj, T., & Jangra, K. (2015). Applications of nickel-titanium alloy. *Journal of Engineering and Technology*, *5*(1), 1.
[35] Hagemann, R., et al. (2015). Design, processing, and characterization of nickel titanium micro-actuators for medical implants. *Journal of Laser Applications*, *27*(S2).
[36] Li, P., et al. (2020). Microstructural and mechanical properties of β-type Ti–Mo–Nb biomedical alloys with low elastic modulus. *Journal of Alloys and Compounds*, *815*, 152412.
[37] Ashkani, O., et al. (2023). Influence of aluminum and copper on mechanical properties of biocompatible Ti-Mo alloys: A simulation-based investigation. *Micromachines*, *14*(5), 1081.
[38] Gai, X., et al. (2020). A novel method for evaluating the dynamic biocompatibility of degradable biomaterials based on real-time cell analysis. *Regenerative Biomaterials*, *7*(3), 321–329.
[39] Costantino, M. D., et al. (2020). Inflammatory response to magnesium-based biodegradable implant materials. *Acta Biomaterialia*, *101*, 598–608.
[40] Mao, L., et al. (2017). A promising biodegradable magnesium alloy suitable for clinical vascular stent application. *Scientific Reports*, *7*(1), 46343.
[41] Dvorsky, D., et al. (2019). High strength AM50 magnesium alloy as a material for possible stent application in medicine. *Materials Technology*, *34*(14), 838–842.
[42] Singh, B. P., et al. (2017). Fabrication of biodegradable low elastic porous Mg-Zn-Mn-HA alloy by spark plasma sintering for orthopedic applications. *IOP Conference Series: Materials Science and Engineering*, *225*(1).
[43] Sharma, S. K., et al. (2022). Significance of alloying elements on the mechanical characteristics of Mg-based materials for biomedical applications. *Crystals*, *12*(8), 1138.
[44] Marti, A. (2000). Cobalt-base alloys used in bone surgery. *Injury*, *31*, D18–D21.
[45] Haynes, D. R., Crotti, T. N., & Haywood, M. R. (2000). Corrosion of and changes in biological effects of cobalt chrome alloy and 316L stainless steel prosthetic particles with age. *Journal of Biomedical Materials Research*, *49*(2), 167–175.
[46] Sahoo, P., Das, S. K., & Davim, J. P. (2019). Tribology of materials for biomedical applications. In *Mechanical Behaviour of Biomaterials* (pp. 1–45). Woodhead Publishing.
[47] Babis, G. C., & Mavrogenis, A. F. (2013). Cobalt–chrome porous-coated implant-bone interface in total joint arthroplasty. In *Bone-Implant Interface in Orthopedic Surgery: Basic Science to Clinical Applications* (pp. 55–65). Springer London.
[48] Plecko, M., et al. (2012). Osseointegration and biocompatibility of different metal implants—A comparative experimental investigation in sheep. *BMC Musculoskeletal Disorders*, *13*, 1–12.
[49] Gautam, S., et al. (2022). Recent advancements in nanomaterials for biomedical implants. *Biomedical Engineering Advances*, *3*, 100029.
[50] Davis, J. R. (2003). *Handbook of materials for medical devices*.
[51] Mahmoudi Hashemi, P., Borhani, E., & Nourbakhsh, M. S. (2016). A review on nanostructured stainless steel implants for biomedical application. *Nanomedicine Journal*, *3*(4), 202–216.

[52] Reclaru, L., et al. (2001). Corrosion behavior of a welded stainless-steel orthopedic implant. *Biomaterials, 22*(3), 269–279.
[53] Bekmurzayeva, A., et al. (2018). Surface modification of stainless steel for biomedical applications: Revisiting a century-old material. *Materials Science and Engineering: C, 93*, 1073–1089.
[54] Ortiz, A. J., et al. (2011). Metallic ions released from stainless steel, nickel-free, and titanium orthodontic alloys: Toxicity and DNA damage. *American Journal of Orthodontics and Dentofacial Orthopedics, 140*(3), e115–e122.
[55] Salahinejad, E., et al. (2013). In vitro electrochemical corrosion and cell viability studies on nickel-free stainless steel orthopedic implants. *PLoS ONE, 8*(4), e61633.
[56] Feng, J., et al. (2022). Bio-high entropy alloys: Progress, challenges, and opportunities. *Frontiers in Bioengineering and Biotechnology, 10*, 977282.
[57] Liu, C., et al. (2022). Medical high-entropy alloy: Outstanding mechanical properties and superb biological compatibility. *Frontiers in Bioengineering and Biotechnology, 10*, 952536.
[58] Alagarsamy, K., et al. (2016). Mechanical properties of high entropy alloy $Al_{0.1}$CoCrFeNi for peripheral vascular stent application. *Cardiovascular Engineering and Technology, 7*, 448–454.
[59] Chen, X., et al. (2022). Bidirectional improvement of strength and ductility of CoCrFeNiTi ($Co_{40}Cr_{16}Fe_{35}Ni_8Ti_1$) high-entropy alloys suitable for coronary stents. *Journal of Materials Research and Technology, 18*, 1934–1946.
[60] Tanji, A., et al. (2022). Niobium addition improves the corrosion resistance of TiHfZrNbx high-entropy alloys in Hanks' solution. *Electrochimica Acta, 424*, 140651.
[61] Prach, O., et al. (2019). Effect of Zr, Cr, and Sc on the Al–Mg–Si–Mn high-pressure die casting alloys. *Materials Science and Engineering: A, 759*, 603–612.
[62] Sathiyaseelan, G., et al. (2024). Enhancing the strength and structure of Al–Si alloys for biomedical applications through the addition of Sr and Zr grain refiners on secondary AlSi7Mg aluminum alloys. *Chemical Physics Impact, 8*, 100557.

Acknowledgements

We would like to express our heartfelt gratitude to Dr. Vaibhav Trivedi for their valuable guidance, support, and constructive feedback throughout the development of this work.

We also extend our thanks to IFTM University Moradabad for providing the necessary resources that made this research possible.

Special thanks to our colleagues and Dr. Ankur Goel, whose insights and discussions significantly contributed to the quality of this paper.

Finally, we are grateful to the organizers and reviewers of ICSMMCT 2024 for their efforts in creating an opportunity to share and improve this work.

Magnetocrystalline Anisotropy Energy Density K0, K1, K2, K3, K4 Continuum Analysis of Electrical Steel Based on Electric Properties of θ,α,γ Ideal Fibers

Sudhakar Geruganti[1] and Gautam Jai Prakash[2]

[1]*PhD Research Scholar, SEST, The University of Hyderabad , Gachibowli Hyderabad 500046, Telangana (India))*
[2]*Professor, SEST, The University of Hyderabad , Gachibowli Hyderabad 500046, Telangana (India))*

Abstract
Texture factor, A* and magnetocrystalline anisotropy energy density K0, constants K1, K2, K3,K4 are important for pure metals. The former represents the rapid bulking of crystals with associated preferences and the latter represents simple and complex instructions. Evaluation of defects of pure metal and electrical metal can reduce metal loss in transformers and rotating motors and increase electrical efficiency. In this research paper, an attempt has been made to calculate the magnetocrystalline anisotropy energy density of pure metals based on the beauty of ideal fibers..

Keywords: *texture, anisotropy, core loss..*

1. Introduction

The values of magnetocrystalline anisotropy constants K0, K1, K2 and K3 ,K4determine the degree to which the material can be easily magnetized. Their results depend on the chemical composition, crystal structure and thermomechanical properties of the given material. Texture is similar to the values of K0, K1, K2 and K3,K4which determine the preference of the grain and the overall texture is a quantitative measure of the texture. Texture is an important microstructural parameter that directly determines the anisotropy level of most polycrystalline material bodies at the macro scale. Therefore, their properties are important and useful and should be done much before physical measurement or modeling. Neutron diffraction is the preferred tool for characterizing crystal structures. The data obtained are representative of many grains, allowing for a more accurate analysis of the texture. Texture measurement. This value represents what the texture pattern currently is. Cube texture (T.F = 22.5), Goss texture (T.F = 35.6), Gamma texture (T.F = 38.68) in a given product.

2. Steel

Magnetocrystalline anisotropy is usually expressed by the broadening of the crystal axis of the magnetic field compared to the cosine α1, α2, α3 directions.
$E^* = K0 + K1 (\sum\alpha21\ \alpha22) + K2 (\prod\alpha21) + K3 (\sum\alpha21\ \alpha22)2 + K4 (\sum\alpha21\ \alpha22)(\prod\alpha21)$ [I];

[uvw]	a	b	c	α_1	α_2	α_3	E
[100]	0	90^0	90^0	1	0	0	K_0
[110]	45^0	45^0	90^0	$1/\sqrt{2}$	$1/\sqrt{2}$	$1/\sqrt{2}$	$K_0 + K_1/4$
[111]	54.7^0	54.7^0	54.7^0	$1/\sqrt{3}$	$1/\sqrt{3}$	$1/\sqrt{3}$	$K_0 + K_1/3 + K_2/27$

According to REF 1 E* = 0.355A* +(0.163 – 0.013A) *)[wt%Si] - 1.898

A* for θ fiber <100>//ND 22.5 => E* = -0.5345 [wt%Si] + 6.0895
A* for α fiber <110>//ND 35.6 => E* = -0.9406 [wt%Si] + 10.74
A* for γ fiber <111> A* //ND 38.68 => E* = -1.03608 [wt%Si] + 11.8334

$E^* = K0 + K1 (\sum\alpha21\ \alpha22) + K2 (\prod\alpha21) + K3 (\sum\alpha21\ \alpha22)2 + K4 (\sum\alpha21\ \alpha22)(\prod\alpha21)$ …. [I];

For [100] directions, α1 = 1, α2 = 0, α3=0 => E = K0
For [100] directions, E* = 6.0895 => K0 = - 0.5345 [wt%Si] + 6.0895

Published online on: ***February 01, 2025***
Corresponding Author's E-mail ID: smecsudhakar@gmail.com

- For [110] directions, α1 = 1/β2, α2 = 1/β2, α3 = 0
- For [110] directions, E * = -0.9406 [wt%Si] + 10.74
- E*= -0.5345 [wt%Si] + 6.0895 + K1/4 + K3/16
- -0.9406 [wt%Si] + 10.74 = -0.5345 [wt%Si] + 6.0895 + K1/4+ K3/16
- 4.6505-0.4061[wt%Si] = K1/4 + K3/16
- 4K1 + K3 = 74.408 -6.4976[wt%Si] ……[II]

For the [111] direction, α1 = 1/β3, α2 = 1/â 3, α3= 1/ 3
For the [111] direction, E* = -1.03608 [wt%Si] + 11.8334

- -1.03608 [wt%Si] + 11.8334 = K0 + K1/3 + K2/27 + K3 /9 + K4 /81
- -1.03608 [wt%Si] + 11.8334 = -0.5345 [wt%Si] + 6.0895 + K1/3 + K2/27 + K3/9 + K4/81
- [-0.50158 [wt%Si] + 5.7439]*81 = 9(3K1 + K3) + (3K2 + K4)
- 9(3K1 + K3) + (3K2 + K4) = 465.2559 - 40.62798[wt%Si] => 9(51) + 6.2559 - 40.62798[wt%Si]
- 3K1 + K3 =51 ; 3K2 + K4 = 6.2559 -40.62798 [wt%Si] … [III]

Substracting [III] from [II]

- **K0 = -0.5345 [wt%Si] + 6.0895;K1 = 23.408-6.4976[wt%Si] ; K3= -19.224 + 19.4928[wt%Si] ; K2 =2 ; K4 =0.2559 - 40.62798 [wt%Si]**

GENERLIZED EQUATION FOR E*= K0 + K1 (∑α21 α22) + K2 (∏α21) + K3 (∑α21 α22)2 + K4 (∑α21 α22)(∏α21) …. [I];

- E* = -0.5345 [wt%Si] + 6.0895+(23.408-6.4976[wt%Si]) (∑α21 α22) + 2(∏α21) +(-19.224 + 19.4928[wt%Si]) (∑α21 α22)2
- + (0.2559 - 40.62798 [wt%Si]) (∑α21 α22)(∏α21) …. [IV]

- E* = Eiron* + [-0.5345[wt%Si] -6.4976 [wt%Si](∑α21 α22)+ 19.4928[wt%Si]](∑α21 α22)2- 40.62798 [wt%Si]) (∑α21 α22)(∏α21)]

- E** = [-0.5345[wt%Si] -6.4976 [wt%Si](∑α21 α22)+ 19.4928[wt%Si]](∑α21 α22)2-40.62798 [wt%Si]) (∑α21 α22)(∏α21] ……. [V]

- [V] Above is the Standard Magnetic Crystalline Anisotropic Energy Equation for Electrical Steels with four K0,K1,K2,K3 ,K4Constants

- [V] is the non-electron emission (NOES) and electron emission (GOES) material Basic equation).

- E* = Eiron* + E**

- E** = E* - E*iron

CRYSTAL DIRECTION	MAGNETOCRYSTALLINE ALL ANISOTROPY ENERGY DENSITY
[100] α_1 =1,α_2 =0, α_3=0	**$E^*_{[100]}$ = 6.0895 - 0.5345 [wt%Si]**
[110] α_1 =1/√2,α_2 =1/√2, α_3=0	**$E^*_{[110]}$ = 10.74 - 0.9406 [wt%Si]**
[111] α_1 =1/√3,α_2 =1/√3, α_3=1/√3	**$E^*_{[111]}$ =11.8334 -1.03608 [wt%Si]**

S.NO.	Standard Crystallographic Directions	Magneto-Crystalline Anisotropy Value E*	Magneto-Crystalline Anisotropy Value E*	Magneto-Crystalline Anisotropy Value E* for Fe-0.51%Si	Magneto-Crystalline Anisotropy Value E* for Fe-1.38%Si	Magneto-Crystalline Anisotropy Value E* for Fe-	Magneto-Crystalline Anisotropy Value E* for Fe-

		For Pure Iron				2.8%Si	3.2%Si
1	[100]	$E^*_{[100]}$ = 6.0895	$E^*_{[100]}$ = -0.5345 ([wt%Si])+6.0895	5.816905	5.35189	4.5929	4.3791
2	[110]	$E^*_{[110]}$ = 10.74	$E^*_{[110]}$ = -0.9406 [wt%Si] + 10.74	10.260294	9.441972	8.10632	7.73008
3	[111]	$E^*_{[111]}$ = 11.8634	$E^*_{[111]}$ = -1.03608 [wt%Si] + 11.8634	11.3349992	10.4336096	8.962376	8.547944

3. Discussion

<100>//ND fibers have the lowest anisotropic strength because the flux lines are uniformly distributed in the plane of the rotated laminate, have a simple magnetization direction, and also have a cubic texture component rotated into a plane. In contrast, the α and <011>//ND fiber orientations have relatively high anisotropy properties and therefore the presence of particles is undesirable in electrical steels. K2, K3, K4 constants of steel.

4. Estimation Of Texture Factor K0, K1,K2,K3, K4 Constants For Electrical Steels

From [II], we have E* = (0.355 -0.031Si) A* - 1.898 + 0.163Si

- (0.355 -0.031Si)A* - 1.898 + 0.163Si
- = 0.5345 [wt%Si] + 6.0895+(23.408-6.4976[wt%Si]) (∑α21 α22) + 2(∏α21) +(-19.224 + 19.4928[wt%Si]) (∑α21 α22)2
- + (0.2559 - 40.62798 [wt%Si]) (∑α21 α22)(∏α21)

TEXTURE EQUATION, A*= K0 + K1 (∑α21 α22) + K2 (∏α21)) + K3 (∑α21 α22)2 [I]

- (0.355 -0.031Si) A* = -0.6975 [wt%Si] + 7.9875 +(23.408-6.4976[wt%Si]) (∑α21 α22) + 2(∏α21) +(-19.224 + 19.4928[wt%Si]) (∑α21 α22)2
- + (0.2559 - 40.62798 [wt%Si]) (∑α21 α22)(∏α21) …. [IV]

- A* = [K0] + [K1](∑α21 α22) [K2] (∏α21) + [K4] ∑α21 α22) + [K5] (∑α21 α22)(∏α21)

- A* =(-0.6975 [wt%Si] + 7.9875) *P+ (23.408-6.4976[wt%Si]) *P (∑α21 α22) + (2)*P (∏α21) + (-19.224+19.4928 [wt%Si])*P ∑α21 α22)2 + (0.2559 - 40. 62798 [wt%Si]) *P (∑α21 α22)(∏α21)

- Above is the Standard Generalized equation for Texture Factor for Electrical Steels

- Where P= 1 / (0.355 -0.031Si)

- [K0] = (-0.6975 [wt%Si] + 7.9875) *P

- [K1] = (23.408-6.4976 [wt%Si]) , *P

- [K2] = 2 *P ,

- [K3] = (-19.224+19.4928[wt%Si])*P

- [K4] = (0.2559 – 40.62798 [wt%Si])*P

S.NO.	TEXTURE FACTOR CONSTANTS	ELECTRICAL STEELS Fe + 0.51%[wt%Si]	ELECTRICAL STEELS Fe + 1.38%	ELECTRICAL STEELS Fe + 2.8%	ELECTRICAL STEELS Fe + 3.2%

			[wt%Si]	[wt%Si]	[wt%Si]
1.	K_0	22.50	22.50	22.50	22.50
2.	K_1	59.24179	46.2566	19.4434	10.2254
3.	K_2	5.8964	6.40614	7.45712	7.81860
4.	K_3	-27.36717	24.587	131.8263	168.698
5.	K_4	-60.333	-178.7658	-423.2007	-507.2464

$$\Rightarrow A^*_{0.51\%Si} = 22.5 + 59.24179\,(\sum\alpha^2_1\,\alpha^2_2) + 5.8964\,(\prod\alpha^2_1) - 27.36717\sum(\alpha^2_1\,\alpha^2_2)^2 - 60.333\,(\sum\alpha^2_1\,\alpha^2_2)(\prod\alpha^2_1)$$

$$\Rightarrow A^*_{1.38\%Si} = 22.5 + 46.2566(\sum\alpha^2_1\,\alpha^2_2) + 6.40614\,(\prod\alpha^2_1) + 24.587\sum(\alpha^2_1\,\alpha^2_2)^2 - 178.7658\,(\sum\alpha^2_1\,\alpha^2_2)(\prod\alpha^2_1)$$

$$\Rightarrow A^*_{2.8\%Si} = 22.5 + 19.4434\,(\sum\alpha^2_1\,\alpha^2_2) + 7.45712\,(\prod\alpha^2_1) + 131.8263\sum(\alpha^2_1\,\alpha^2_2)^2 - 423.2007\,(\sum\alpha^2_1\,\alpha^2_2)(\prod\alpha^2_1)$$

$$\Rightarrow A^*_{3.2\%Si} = 22.5 + 10.2254\,(\sum\alpha^2_1\,\alpha^2_2) + 7.81860\,(\prod\alpha^2_1) + 168.698\sum(\alpha^2_1\,\alpha^2_2)^2 - 507.2464\,(\sum\alpha^2_1\,\alpha^2_2)(\prod\alpha^2_1)$$

S.NO.	CRYSTALLOGRAPHIC DIRECTIONS	DIRECTIONAL COSINE RELATIONSHIP	TEXTURE FACTOR FOR A* IDEAL FIBER	TEXTURE FACTOR FOR $A^*_{0.51\%Si}$	TEXTURE FACTOR FOR $A^*_{1.38\%Si}$	TEXTURE FACTOR FOR $A^*_{2.8\%Si}$	TEXTURE FACTOR FOR $A^*_{3.2\%Si}$
1	direction <100>	$\alpha_1=1$, $\alpha2=0$, $\alpha_3=0$	**22.5** Θ fibre <100>//ND	**22.5**	**22.5**	**22.5**	**22.5**
2	direction <110>	$\alpha_1=1/\sqrt{2}$, $\alpha2=1/\sqrt{2}$, $\alpha_3=0$	**35.6** fibre //ND	**35.6**	**≈35.6**	**≈35.6**	**≈35.6**
3	direction <111>	$\alpha_1=1/\sqrt{3}$, $\alpha2=1/\sqrt{3}$, $\alpha_3=1/\sqrt{3}$	**38.68** ϒ fibre <111>//ND	**38.68**	**≈38.68**	**≈38.68**	**≈38.68**

5. CONCLUSION:

[100] direction has the smallest magnetocrystalline anisotropy energy density value and [110] and [111] directions have more values. Therefore, [100] direction is the easiest magnetization direction of pure metal, [111] direction is the easiest magnetization direction of pure metal is the direction of the strongest magnetization and the [110] direction is the complex magnetization direction of pure metals. The positive values of the balance equation are consistent with the expected model and are consistent with the positive values of ideal fibers.

References

1. Author Nagy, B. and F. Koesdjojo, P The texture modification process of electrical and magnetic properties of non-oriented high voltage silicon materials were investigated. , Kim, Pablo Rodriguez Calvillo, Edgar Gomes, Juergen Schneider,
https://doi.org/10.1016/j.matchar.2012.06.006
2. Pure metal rolling cold and suction flux generation Research on shielding
Nitin Satpute, Prakash Dhoka, Pankaj Karande, Siddharth Jabade, Marek Iwaniec
https://doi.org/10.3390/ma15072630
3. Texture of non-orientational electronics Steel Control and Manufacturing Leo Kestens1 and Sigrid Jacobs2
• DOI: 10.1155/2008/173083
4. The Magneto crystalline Anisotropy Constants of Iron and Iron-sil icon Alloys
Björn Westerstrand1, Per Nordblad1 and Lars Nordborg1
DOI 10.1088/0031-8949/11/6/010
5. Mehdi, Mehdi, "Non-orientational texture evolution during thermomechanical processing of electrical steel" 2019 Electronic Thesis. a 7648".
https://scholar.uwindsor.ca/etd/7648

International conference on Smart Material, Manufacturing and Characterization Techniques – 2024

Paper ID: ICSMMCT-01026

An Experimental Evaluation on Physical and Mechanical Properties of Marble Dust Filled Natural Fiber Reinforce Hybrid Polymer Composite

Hemant Kumar[1], M Kanan[2] and Sachin Tejyan[3]

[1]*Research Scholar, Quantum University, Roorkee-247667 (Uttarakhand)*
[2]*Quantum University Roorkee-247667 (Uttarakhand)*
[3]*G. B. Pant Institute of Engineering & Technology, Ghurdauri Pauri Garhwal-246194(Uttarakhand)*

Abstract

Much interest has been paid to developing natural fiber/particulate-reinforced hybrid polymer composites in recent years due to resource scarcity and growing environmental concerns. To improve the mechanical and wear characteristics of the polymer composites, this work focused on developing bauhinia Vahlii (BV) natural fiber reinforced and marble dust-filled hybrid polymer composites. The composite samples were fabricated by hand lay-up technique utilizing 10, 20, and 30 wt.% of bauhinia Vahlii natural fiber with a fixed amount of 5 wt.% of marble dust waste. The findings of the experimental investigation showed that 30 wt.% Bauhinia Vahlii fibers with 5 wt.% marble dust-filled polymer composites improve hardness by 22% and increase impact energy by 31% compared to 10 wt.% BV fiber reinforced composite. Whereas 40% and 60% improvement were found in the composites' flexural strength and tensile strength. The experimental results show that all the mechanical properties improve by adding fiber content in an epoxy matrix. Moreover, increased water absorption is also reported with incrementing the fiber weight percentage in composites.

Keywords: *Natural Fiber, Composite, Bahaunia vahlii, Mechanical Properties*.

1. Introduction

Composite materials are engineered by combining two or more distinct substances, resulting in a material that possesses unique and enhanced properties compared to its individual components. Common types of composite materials include vinyl ester, epoxy, and polyester, which exhibit thermosetting properties. These materials typically comprise a matrix (the continuous phase) and a reinforcement phase, which can be fibers or particulates. The reinforcement, often in the form of fibers, enhances the mechanical properties of the composite. Common synthetic fibers used as reinforcements include glass, aramid, carbon, and graphite fibers. Due to their lightweight nature and favorable mechanical properties, composites are extensively used in the aerospace and automobile industries. Recently, researchers have been interested in natural fiber composites, driven by the ease of processing, biodegradability, and low cost of these materials. This shift is part of a broader movement towards more sustainable materials for both structural and tribological applications. Natural fiber-reinforced polymer composites have emerged as a distinct class of materials due to their exceptional specific strength and modulus [1]. While natural fibers are typically lighter and less expensive than their synthetic counterparts, their mechanical properties often fall short. However, natural fibers still present strong mechanical properties, wide availability, and cost-effectiveness, making them a viable alternative to traditional synthetic reinforcements [2, 3]. To overcome the limitations in mechanical performance, researchers have explored the addition of nanofillers or the use of hybrid fibers. One such natural fiber that holds promise for composite applications is Bauhinia Vahlii, which is abundantly found in Asian countries. There is potential for this fiber to be incorporated into novel composites for a wide range of technical applications. Additionally, integrating waste materials, such as construction debris, into composites has gained attention as a method to enhance strength and durability while promoting environmental sustainability. Marble dust is one such waste material that has been explored as a filler. In India alone, approximately 3172 thousand tons of marble dust are generated annually [4], and repurposing this waste can help mitigate its negative economic and environmental impacts. Previous research has shown that combining natural fibers with various industrial wastes, such as red mud [5], blast furnace slag [6], Linz-Donawitz slag [7], granite powder [8], and aluminum powder [9], can significantly improve the durability and strength of polymer composites. For instance, Boopalan et al. investigated the effects of fiber treatment on the mechanical properties of composites. They found that NaOH-treated jute and sisal fiber-reinforced epoxy composites exhibited better mechanical performance compared to untreated fibers [10]. The incorporation of treated fibers has enhanced mechanical properties, driving the increased use of natural fiber composites in various applications [11]. Other studies have also explored hybrid composites. For example, Jeyanthi et al. developed a natural fiber composite using Kenaf and Glass fibers mixed with an epoxy resin matrix. These hybrid composites, created using the hot impregnation process, demonstrated good mechanical properties, although their impact strength was slightly lower, a characteristic that could be improved with

Published online on: ***February 01, 2025***
Corresponding Author's E-mail ID: smecsudhakar@gmail.com

the addition of suitable additives [12]. Similarly, Lebrun et al. examined the tensile and impregnation properties of unidirectional hemp/paper/epoxy and flax/paper/epoxy composites. Their results showed that adding a thin sheet of paper to the reinforcing layers improved the composite's strength, though it marginally reduced Young's modulus [13]. Research by Fiore et al. [14] concluded that treating sisal fibers for 120 hours was optimal for achieving strong interfacial adhesion and enhanced mechanical properties when combined with an epoxy matrix. Furthermore, Vijaya Ramnath et al. [15] explored the mechanical properties of hybrid natural fiber composites made of Banana and Jute fibers within an epoxy matrix. Their findings revealed that the hybrid composites had superior mechanical properties compared to composites fabricated using individual fibers. Building on these developments, Surendra et al. [16] created a hybrid composite with a combination of okra, jute, and sisal fibers and a polyester resin matrix. The blend consisted of 35% sisal, 35% jute, and 30% okra fiber, and the resulting hybrid Composite demonstrated superior mechanical characteristics compared to polypropylene composites reinforced with sisal fibers alone. Despite the extensive research on hybrid natural fiber composites, there is a notable lack of studies that explore the use of marble dust in conjunction with Bauhinia Vahlii fibers. This gap in the literature provides an opportunity for further exploration. The present study seeks to address this by investigating the incorporation of Bauhinia Vahlii fibers and marble dust into an epoxy matrix to develop a novel type of hybrid polymer composite. This research aims to evaluate these hybrid composites' mechanical and physical properties to determine their potential as lightweight alternatives to traditional materials used in engineering applications.

2. Materials and Methodology

2.1. Materials

This study used Bauhinia Vahlii fibers (density: 1.47 g/cm³), collected from a nearby village, as the reinforcing material. The fibers were cleaned using a 10% NaOH solution (purchased from Chemical Industry, Roorkee) to enhance fibre-matrix bonding to remove dust, dirt, and impurities. The matrix material consisted of epoxy resin E-51 (density: 1.221 g/cm³) and hardener H-51, sourced from Amtech Esters Private Limited, Delhi, India. The resin-to-hardener ratio was set at 10:3 (by volume), meaning 10 milliliters of epoxy resin were combined with 3 milliliters of hardener, based on prior experience, to ensure optimal curing. Marble dust, with a particle size of 20-30 µm and a density of 2.68 g/cm³, was used as the filler material, and it was obtained from Rajasthan Stone-Cutting Industries, Rajasthan, India. The incorporation of marble dust as a filler aims to enhance the mechanical strength of the composite while promoting the sustainable use of industrial waste materials.

2.2. Method of fabrication

The hand lay-up moulding process was employed to fabricate the epoxy composites reinforced with natural fibers. A 210 mm x 210 mm x 10 mm mould, constructed from wood, was used to create composites. A plastic sheet was placed and securely positioned inside the mould to facilitate easy removal of the composite material after curing. A mould-releasing agent was then applied to the surface to prevent the composite from sticking to the mould during curing. At room temperature, the epoxy resin, hardener, and marble dust were mixed in fixed proportions for all samples. The mixture consisted of 9 wt% epoxy resin, 3 wt% hardener, and 5 wt% marble dust, as outlined in Table 1. Once thoroughly mixed, the composite was laid into the prepared mould, allowing the fibers to be evenly distributed within the resin matrix. The process was completed by allowing the composite to cure at room temperature before being removed from the mould.

Table 1: Composition of Pure reinforced Natural Fibre Composite

Table 1: Composition of Pure reinforced Natural Fibre Composite:			
Designation	Reinforcement Fiber (wt%)	Filler (Marble dust) (wt%)	Epoxy with hardener wt%)
Bv 10	10	5	85
Bv 20	20	5	75
Bv30	30	5	65

Bv mat Bv 10 Bv 20 Bv30

Fig1: Fabricated mat and composite

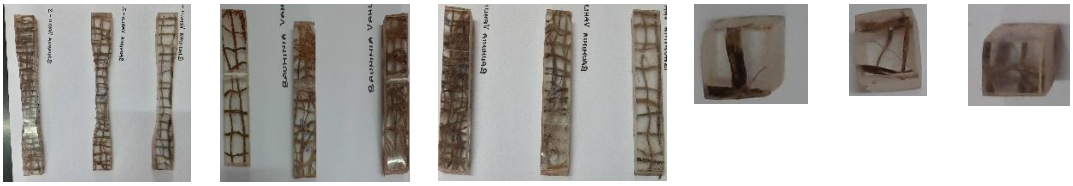

Figure 2: Composite specimens for the tensile, impact, flexural tests, and hardness

The Bauhinia Vahlii-based composites (Bv) fiber mat was positioned horizontally in the mold following the resin layer. Similarly, the second and third composites were fabricated by taking two mats and three mats of Bauhinia vahlii in another mold and allowed them to solidify. When the composite specimens are solidified, samples are taken out from the mold and cut to the appropriate dimensions per ASTM standards for various mechanical tests. Table 2 displays the dimensions of the samples for the different mechanical tests conducted in the research.

Table 2: Test sample Dimension

Sr.No	Type of Test	ASTM standard	Sample dimension(mm)
1	Tensile	ASTM D638	165×20×44
2	Impact	ASTM D256	64 x 12.7 x 3.2
3	Flexural	ASTM D790	127x12.7x3.4
4	Hardness	ASTM E 384	0.25 minimum

2.3. Physical and mechanical characterization

The Agarwal and Broutman method were used to calculate the theoretical density of the composite, and The primary water immersion method was used to find the density in an experimental setting. Meanwhile, the theoretical and actual densities were normalized to determine the void content. The theoretical density of composite materials was computed using equation (2) regarding weight fractions.

The density (ρ) and weight fraction (W) are shown, respectively, indicating the composite's theoretical density.

The sample (figure 3) size for the moisture absorption investigations was a one-inch square that were either 0.125" or 0.250" thick, by ASTM D 570-98 standards. Before exposing the samples to regular water, their weights were recorded. The specimens were removed from the damp environment after being exposed for 24 hours, and any remaining surface moisture was wiped off using tissue paper or a clean, dry cloth. Within a minute of being taken out of the environment room, the specimens were weighed again using an electronic digital scale, this time to the closest 0.001 mg. Regular weight checks were performed on the specimens at 12, 24, 36 48, 60, 72, 84, 96, 108, 120, 132, 144, 156, 168, and 180 hours of exposure. The weight difference was used to determine the moisture absorption.

Fig3: composite specimen for Water Absorption

As per ASTM-D638 and ASTM-D790 standards, rectangular samples(Shown in Figure 2) are frequently used for tensile and flexural testing using a Universal Testing Machine (Model No. H25K-S, Hounsfield Test Equipment Limited, England). The tensile strength means value is determined by averaging the results of three independent samples of the same composition for each test.

According to ASTM E92 standards, the micro-hardness of composite specimens (shown in Figure 2), was measured using a computerized Micro-Vickers Hardness Tester (Models: MV-1 PC). The hardness of the samples was determined using an automated Vicker's hardness tester. Every sample was put through all four tests, and the mean results are included in the publication. A weight of 1 kg was applied to the material's surface for 15 seconds to record a test result, allowing a diamond intender with an apical angle of 136° to develop.

An impact tester (Veekay -Model-I 91), was used to conduct the Charpy impact test. with a 55 x 10 x 10 mm3 size and a 3.33 mm (t/3 mm) notch depth at a 45 ° angle were tested in compliance with ASTM E23 guidelines. The tester in joules shows the impact energy absorbed by the samples. The test was conducted three times for every composite type, and the average result was considered.

3. Results and discussion

3.1. Physical test:

The Composite was subjected to the following physical examinations, as detailed below:

3.1.1 Void content

Table 3 and Figure 4 present the composites' experimental and theoretical densities and the corresponding void content percentages. The void content is significant in composite materials because even slight variations can significantly influence their mechanical performance. When Bahaunua vahlii fiber was incorporated into the epoxy resin, it resulted in a notable decrease in void content, with the highest recorded void fraction at 5.24% observed in the composite with 10% fiber loading. Several mechanisms can explain this reduction in void content. Firstly, the improved fiber-matrix interfacial bonding is a significant factor. Bahaunua vahlii fibers exhibit good adhesion with the epoxy matrix, which minimizes the spaces where voids typically form. This improved bonding ensures that the fibers integrate more seamlessly with the resin, creating a more vital, cohesive fiber-matrix interaction that reduces the likelihood of air pockets or gaps. Secondly, adding marble dust as a filler within the composite contributes to void reduction. Marble dust particles are fine and can occupy tiny spaces within the matrix that might otherwise remain as air pockets, resulting in a denser, more compact material. Research has shown that fillers such as marble dust can effectively reduce void content by filling microvoids, thus reducing the overall porosity and contributing to better mechanical properties. Lastly, natural fibers like Bahaunua vahlii have a cellular structure containing lumens, which can act as microvoids within the composite. However, optimizing the fiber loading and incorporating marble dust makes these lumens less likely to contribute to void content, as the filler material can further occupy these potential voids. Studies on similar natural fiber-reinforced composites support these observations, showing that composites with strong matrix bonding and filler materials tend to exhibit lower void content. Consequently, these structural improvements from reduced voids enhance the mechanical characteristics of the composite material.[17]

Table 3:- Theoretical and experimental densities of the Bauhinia Vahlii composites with void content

Fiber Loading	Experimental Density(g/cm^3)	Theoretical density(g/cm^3)	Void content %
BV 10	1.012067(±0.0506)	1.068	5.237203496 (±0.26186)
BV 20	1.297347(±0.06487)	1.361	4.676953221(±0.23385)
BV30	1.458457(±0.07292)	1.519	3.985704881(±0.19929)

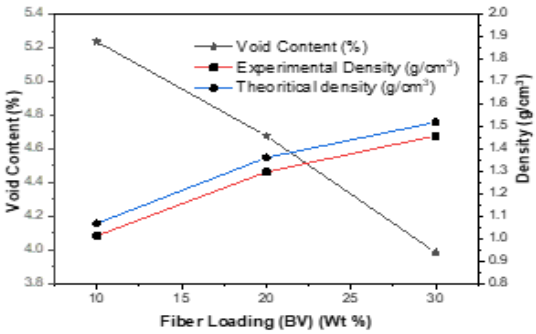

Figure 4: Density and void content of the Bv fabricated composites

Figure 5 illustrates the water absorption behaviour of composites as a function of immersion time. It shows that water absorption increases with time and fiber loading, reaching a saturation point after 156 hours. Specifically, the composite BV30, with 30% fiber loading, exhibited the highest water absorption rate at 0.464% after 156 hours, while BV10, with 10% fiber loading, showed the lowest at 0.1884%. This trend can be attributed to Bauhinia vahlii fibres' hydrophilic nature and the composite structure's inherent porosity, which allows water molecules to penetrate. The water absorption test critically evaluates composite materials, especially those intended for structural applications in humid or aquatic environments. This test measures how much moisture a composite can absorb, which is essential since absorbed moisture can weaken the fiber-matrix bond, leading to deterioration in mechanical performance, dimensional stability, and longevity of the material. In general, composites with high water absorption tend to have lower resistance to environmental exposure, which may restrict their use in outdoor or underwater applications. Natural fiber-reinforced composites are more prone to moisture absorption than synthetic fiber-reinforced composites due to the natural fibers' hydrophilic cellulose content, which attract water molecules. Similar research has documented these effects. Studies on other natural fiber-reinforced composites, such as jute-epoxy or sisal-polyester systems, also show that higher fiber content increases water absorption. Researchers observed that jute fiber composites increased water uptake with fiber loading, showing a saturation point after a similar time frame. This increase in water absorption with fiber content is often linked to the more significant presence of hydrophilic groups and microvoids in the composite, which allow for more water penetration. While some water absorption can be acceptable in composites, depending on their intended use, high water absorption is typically undesirable for structural applications. Excessive water absorption can result in swelling, dimensional instability, and decreased mechanical properties like tensile and flexural strength. Studies suggest that water absorption for composites should generally stay below 0.5% to minimize these issues, although the acceptable limit may vary depending on specific application requirements and environmental exposure.

In summary, the water absorption test helps in understanding the moisture resilience of natural fiber composites like those using Bauhinia vahlii fiber and allows for comparisons with similar materials. By identifying and understanding the absorption limits, manufacturers can make informed decisions about the suitability of these composites in different applications, potentially opting for fiber treatments or matrix modifications to enhance water resistance where needed. The samples' percentage weight gain was computed at different periods using the following equation:

$$W\% = \frac{Ww - Wd}{Ww} x100 \qquad (2)$$

where Wd is the specimen's dry weight and Ww is its wet weight at a specific immersion period

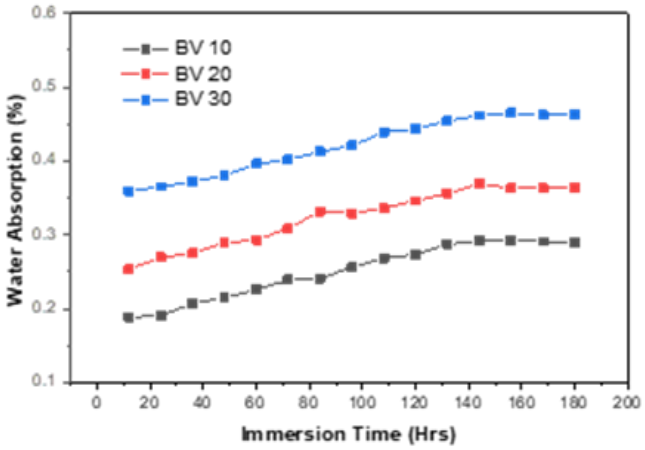

Figure 5: Water absorption with time for the Bv fabricated composites

3.2. Mechanical test

3.2.1 Tensile Test and Flexural Test

In Figure 6, the tensile and flexural test results reveal that adding marble dust to Bauhinia vahlii fiber composites (BV10, BV20, and BV30) significantly enhances their mechanical properties. Specifically, the tensile strength of these composites increased from 17.02 MPa for BV10 to 24.725 MPa for BV20 and 28.50 MPa for BV30—an improvement of approximately 45%. Similarly, the flexural strength of the BV30 composite, with 30% fiber content, was found to be 24.57% higher than that of BV10, which contains only 10% fiber. This enhancement in both tensile and flexural properties is attributed to the improved fiber-matrix bonding and the addition of hard marble dust particles, which contribute to a more densely packed and structurally cohesive composite. The increase in tensile and flexural strength observed here aligns with findings from other studies on natural fiber composites. Research on jute and sisal fiber-reinforced composites has also shown that adding fillers, such as silica or marble dust, improves interfacial bonding and load transfer between fibers and the matrix, resulting in enhanced tensile and flexural properties. Studies by Ramesh et al. (2020) on jute fiber composites found that incorporating silica particles increased tensile strength by 30%, while flexural strength improvements reached nearly 25%. These enhancements were primarily attributed to the filler particles' ability to reduce voids and reinforce the matrix, similar to the role of marble dust in the Bauhinia vahlii fiber composites. The improvements in the tensile and flexural properties of the Bauhinia vahlii composites, particularly with higher fiber and marble dust loading, suggest that these composites could be well-suited for applications requiring moderate structural strength. However, while marble dust enhances mechanical performance by creating a compact, densely packed structure, the final composite properties depend on achieving optimal filler and fiber balance to avoid excessive brittleness. Overall, the results from these tensile and flexural tests indicate that Bauhinia vahlii fiber composites with marble dust reinforcement perform competitively compared to other natural fiber composites. However, synthetic fiber composites or further reinforcement strategies might be considered for high-strength applications. This study demonstrates the viability of Bauhinia vahlii fiber composites for applications where moderate tensile and flexural strength is acceptable. It highlights the beneficial role of marble dust in enhancing these mechanical characteristics.

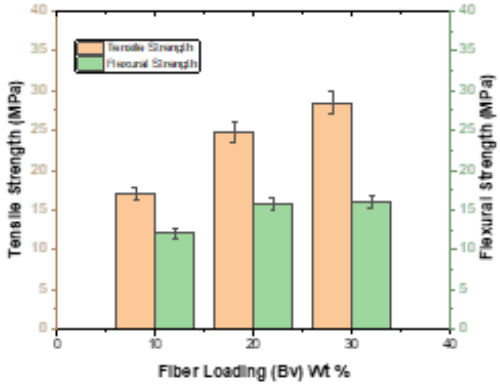

Figure 6: Effect of fiber loading on composites' Tensile strength and Flexural Strength

3.2.2 Hardness Test and Impact Test

The test results for hardness and impact energy, shown in Figure 7, indicate that both properties improve with increased fiber loading and marble dust addition in Bauhinia vahlii fiber composites. Hardness values rose from 11.874 HV for the BV10 composite (10% fiber by weight) to 15.245 HV for the BV30 composite (30% fiber by weight). This increase is partly due to adding 5% scrap marble dust, which contributes to a harder composite matrix. Similarly, impact energy improved with higher fiber content, reaching 10.24 J for the BV30 composite, up from 8.67 J for BV10. The GB30 hybrid composite, incorporating both 30% fiber and marble dust, exhibited the highest value for both hardness (15.245 HV) and impact energy (10.24 J). These hardness and impact energy enhancements align with prior research on natural fiber composites with filler materials. Studies on hybrid composites, such as those reinforced with sisal and jute fibers and filled with calcium carbonate or silica, similarly observed that adding rigid particles enhances the composite's structural properties. For instance, researchers found that including silica particles in a sisal-jute hybrid composite matrix improved hardness by 20% and increased impact resistance due to the more densely packed matrix, which limited micro-crack propagation and enabled more excellent energy absorption. The increase in hardness and impact energy in the Bauhinia vahlii composites can be explained by the reduction in interparticle spacing with marble dust addition, resulting in a more compact structure that resists deformation. The marble dust particles, being stiff and rigid, enhance the matrix's load-bearing capability and reinforce the composite against impact forces, like the effects documented in the studies by Singh et al. [20]. This denser, stiffer composite structure enables the material to absorb higher energy before failure, making it suitable for applications requiring moderate hardness and impact resistance. Combining Bauhinia vahlii fibers with marble dust creates a more robust composite capable of resisting surface wear and absorbing impact effectively, a characteristic validated by other research on hybrid natural fiber composites. These findings suggest that BV30 composites, especially those with additional marble dust, can be highly effective in applications where enhanced hardness and impact resistance are critical.

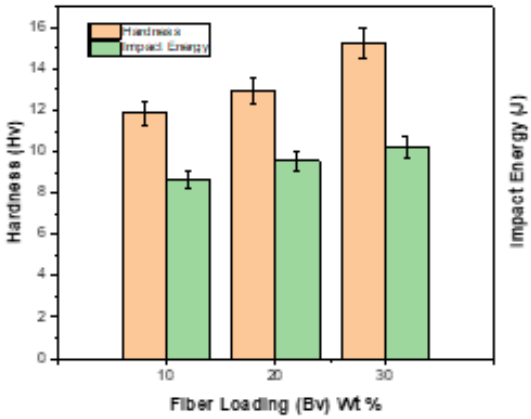

Figure 7: Effect of fiber loading on composites' hardness and impact energy.

4. Conclusions

The experimental analysis of Bauhinia Vahlii (BV) fiber-reinforced polyester composites have demonstrated significant findings about the relationship between fiber loading and the composites' mechanical properties.

Water Absorption: The study revealed that as fiber loading increased, so did water absorption, peaking at 0.464% for the Bv 30 composite, which contains 30% fiber loading. This behaviour can be attributed to the natural fibre's increased surface area and porous structure, which tends to attract water. Although higher fiber loadings can enhance specific mechanical properties, they also introduce higher hydrophilicity due to the natural fiber's structure, as noted in prior studies on water absorption trends in natural fiber composites.

Density and Void Content: Higher fiber loading was associated with increased density and reduced void content in the composites. For instance, as fiber loading rose from 10% (Bv 10) to 30% (Bv 30), the void content was reduced, indicating improved fiber-matrix adhesion. The densification effect observed here aligns with findings from studies that show how fillers and fiber interactions in hybrid composites enhance packing and minimize voids.

Hardness: The hardness value of the Bv 30 composite reached 15.245 HV, marking a 22% increase compared to the Bv 10 composite. This improvement is primarily due to the added stiffness from both fiber and marble dust fillers, which create a more compact and rigid composite matrix. Similar studies on natural fiber composites with fillers show that increased fiber-matrix interlocking and filler material can significantly boost hardness values.

Impact Energy: The impact energy for the Bv 30 composite was 10.24 J, approximately 15.3% higher than the Bv 10 composite. This result indicates the composite's increased capacity to absorb impact energy, which benefits applications requiring resilience against sudden forces. Marble dust further contributes to energy absorption by reducing interparticle spacing, a factor seen in similar research on hybrid composites where fillers support energy dissipation under impact conditions.

Flexural Strength: The Bv 30 composite showed 24.57% greater flexural strength than the Bv 10 composite. This enhancement suggests that higher fiber content significantly improves resistance to bending forces, an essential requirement for structural applications. The combined effects of Bauhinia Vahlii fiber and marble dust filler in reinforcing the matrix contribute to this improvement, as supported by prior research indicating that hybrid fiber composites with mineral fillers display greater flexural rigidity.

Including Bauhinia Vahlii fibers and marble dust fillers at higher loadings, they consistently enhanced the composite's mechanical properties, demonstrating the suitability of these materials for applications demanding increased strength, hardness, and impact resistance. These findings contribute to understanding natural fiber composites and align with broader research trends in hybrid composites, providing a pathway for eco-friendly and mechanically robust materials.

Acknowledgements:

Authors are thankful to Dr. Amit Dixit, Dean of Research, Quantum University, Dr. A. Gupta Hod, Mechanical Engineering, G. B. Pant Institute of Engg. & Tech., Dr Brijesh Gangil Hod, Mechanical Engineering, H.N.B Garhwal University Srinagar and my colleagues for help and support. The authors are grateful to H.N.B Garhwal University for testing and measurements.

References:

[1] Vishwanath, B., Verma, A. P., & Rao, C. K. (1993). Effect of reinforcement on friction and wear of fabric reinforced polymer composites. *Wear, 167*, 93–99.
[2] Singh, A. A., & Palsule, S. (2014). Coconut fiber reinforced chemically functionalized high-density polyethylene (CNF/CF-HDPE) composites by Palsule process. *Journal of Composite Materials, 48*(29), 3673–3684.
[3] Girge, A., et al. (2020). Industrial waste filled polymer composites – A review. *Materials Today: Proceedings, 47*, 2852–2863.
[4] O'Dogherty, M. J., et al. (1995). A study of the physical and mechanical properties of wheat straw. *Journal of Agricultural Engineering Research, 62*(2), 133–142.
[5] Prabu, V. A., et al. (2012). Investigations on the mechanical properties of red mud filled sisal and banana fiber reinforced polyester composites. *Materials Physics and Mechanics, 15*(2), 173–179.
[6] Zhang, J., et al. (2018). Mechanical performance of jute fiber-reinforced micaceous clay composites treated with ground-granulated blast-furnace slag. *Materials, 12*(4), 576.
[7] Pati, P. R., & Satapathy, A. (2015). Processing and characterization of glass-epoxy composites filled with Linz-Donawitz (LD) slag. *Universal Journal of Mechanical Engineering, 3*(1), 7–11.
[8] Pawar, M. J., et al. (2017). Investigation on mechanical and thermo-mechanical properties of granite powder filled treated jute fiber reinforced epoxy composite. *Polymer Composites, 38*(4), 736–748.
[9] Fogagnolo, J. B., et al. (2003). The effects of mechanical alloying on the compressibility of aluminium matrix composite powder. *Materials Science and Engineering: A, 355*(1-2), 50–55.
[10] Boopalan, M., Umapathy, M. J., & Jenyfer, P. (2012). A comparative study on the mechanical properties of jute and sisal fiber reinforced polymer composites. *Silicon, 4*, 145–149.
[11] Sanjay, M. R., & Yogesha, B. (2016). Studies on mechanical properties of jute/E-glass fiber reinforced epoxy hybrid composites. *Journal of Minerals and Materials Characterization and Engineering, 4*(1), 15–25.
[12] Jeyanthi, S., & Rani, J. J. (2012). Improving mechanical properties by kenaf natural long fiber reinforced composite for automotive structures. *Journal of Applied Science and Engineering, 15*(3), 275–280.
[13] Lebrun, G., Couture, A., & Laperriere, L. (2013). Tensile and impregnation behavior of unidirectional hemp/paper/epoxy and flax/paper/epoxy composites. *Composite Structures, 103*, 151–160.
[14] Fiore, V., et al. (2016). A new eco-friendly chemical treatment of natural fibres: Effect of sodium bicarbonate on properties of sisal fibre and its epoxy composites. *Composites Part B, 85*, 150–160.
[15] Ramnath, B. V., et al. (2015). Experimental determination of mechanical properties of banana-jute hybrid composite. *Fibers and Polymers, 16*, 164–172.
[16] Surendra, I. V., Rao, K. V., & Chandu, K. V. P. P. (2015). Fabrication and investigation of mechanical properties of sisal, jute & okra natural fiber reinforced hybrid polymer composites. *International Journal of Engineering Trends and Technology, 19*(2), 116–120.
[17] Pawar, M. J., Patnaik, A., & Nagar, R. (2017). Investigation on mechanical and thermo-mechanical properties of granite powder filled treated jute fiber reinforced epoxy composite. *Polymer Composites, 38*(4), 736–748.
[18] Mahendrakumar, N., et al. (2015). Mechanical and dynamic properties of nettle-polyester composite. *Materials Express, 5*(6), 505–517.
[19] Pokhriyal, M., et al. (2018). Influence of fiber loading on physical and mechanical properties of Himalayan nettle fabric reinforced polyester composite. *Materials Today: Proceedings, 5*(9), 16973–16982.
[20] Singh, T., et al. (2019). Fabrication of waste bagasse fiber-reinforced epoxy composites: Study of physical, mechanical, and erosion properties. *Polymer Composites, 40*(9), 3777–3786.
[21] Patnaik, P. K., et al. (2019). Investigation of mechanical and abrasive wear behavior of blast furnace slag-filled needle-punched nonwoven viscose fabric epoxy hybrid composites. *Polymer Composites, 40*(6), 2335–2345.

.

Smart Farming 4.0: Integrating AI, Machine Learning, and IoT to Drive Sustainable Agriculture

Jainam Jain[1], Meet Bhanushali[2], Suryendra N.[3], Vikas Gupta[4], Aruna Kadam[5], Archana Chaugule[6]

[1,2,3,4] *B. Tech Student, Department of Information Technology, Shah and Anchor Kutchhi Engineering College, Mumbai,(India)*
[5,6] *Assistant Professor, Department of Information Technology, Shah and Anchor Kutchhi Engineering College, Mumbai,(India)*

Abstract
This paper provides a comprehensive overview of Smart Farming 4.0, highlighting how the integration of Artificial Intelligence (AI), Machine Learning (ML), and the Internet of Things (IoT) can enhance sustainable agricultural practices. It discusses various applications of these technologies, such as monitoring soil conditions, managing irrigation systems, predicting crop yields, and controlling pests. By leveraging real-time data from sensors and advanced machine learning techniques, farmers can make informed decisions that enhance resource efficiency and increase productivity. The research includes a comparative analysis of different algorithms utilized in smart agriculture, focusing on their effectiveness, advantages, and drawbacks. The combination of AI, ML, and IoT holds the potential to transform agricultural practices, particularly in areas facing connectivity challenges. By prioritizing environmental sustainability and economic viability, Smart Farming 4.0 aims to address the rising global food demand.

Keywords: *Artificial Intelligence; Machine Learning; Internet of Things; Sustainable Agriculture; Crop Yield Prediction; Smart Farming; IoT Sensor Networks.*

1. Introduction

With the continuous rise in global population, the need for increased food production is becoming more urgent. Conventional farming methods frequently struggle to meet these growing demands due to their inherent inefficiencies and environmental challenges. The adoption of cutting-edge technologies, particularly Artificial Intelligence (AI), Machine Learning (ML), and the Internet of Things (IoT), presents a revolutionary solution for contemporary agriculture. These innovations facilitate real-time monitoring, comprehensive data analysis, and automated decision-making processes, thereby significantly boosting agricultural productivity and sustainability. This paper explores recent advancements in Smart Farming 4.0, emphasizing its capacity to improve resource management, enhance crop yields, and reduce environmental footprints.

2. Methodology

This research is based on the integration of AI, ML, and IoT systems to enhance agricultural sustainability. The methodology involves three primary phases: sensor network deployment for real-time data collection, machine learning model training for agricultural predictions, and implementation of smart irrigation and soil management systems. Data from soil sensors, weather stations, and drone imaging is analyzed using machine learning models, which are validated through real-time edge computing devices installed on farming machinery.

Fig. 1. AI and Smart Farming

Published online on: ***February 01, 2025***
Corresponding Author's E-mail ID: jainam.jain16523@sakec.ac.in

2.1. Data Collection

IoT sensors are essential for collecting data related to soil health, weather conditions, and crop vitality. Continuous monitoring of variables such as moisture content, temperature, pH levels, and nutrient availability provides farmers with vital insights into their agricultural practices. By integrating different types of sensors, a holistic view of farming environments is achieved, allowing for timely and effective interventions.

2.2. Machine Learning Model Development

The gathered data is processed using various machine learning algorithms to develop predictive models. These models are capable of forecasting crop yields, identifying diseases, and suggesting optimal irrigation strategies. Regular updates to these models, driven by new data, help enhance their accuracy and dependability.

2.3. AI-Driven Decision Support

The final component entails implementing these predictive models within decision support systems that guide farmers in making informed decisions regarding crop management, pest control, and resource distribution, ultimately improving operational efficiency.

3. IoT Sensor Networks for Precision Agriculture

IoT sensor networks form the backbone of precision agriculture by enabling detailed monitoring of agricultural variables.

3.1. Soil and Crop Monitoring

IoT sensors deliver real-time insights into essential soil characteristics, allowing farmers to refine their irrigation and fertilization strategies. By employing these sensors, timely actions can be taken to improve crop health and increase yields. For example, soil moisture sensors can activate irrigation systems only when necessary, thereby conserving water resources.

3.2. Weather Stations

On-farm weather stations outfitted with IoT sensors gather data on atmospheric conditions. This information is crucial for making well-informed decisions regarding irrigation and planting, helping to mitigate risks linked to extreme weather phenomena.

3.3. Challenges and Opportunities

Despite the considerable advantages that IoT technologies offer in agriculture, challenges such as high implementation costs, energy demands, and connectivity issues persist. Focusing on the development of energy-efficient sensors and investigating alternative communication technologies could help to address these obstacles. Tackling these challenges is essential for promoting the widespread adoption of IoT solutions in rural communities.

4. Machine Learning for Agricultural Insights

Machine learning has emerged as a pivotal tool in agriculture, offering numerous applications that can enhance productivity.

4.1. Crop Yield Prediction

ML models analyze historical data and current conditions to predict crop yields accurately. These predictions guide farmers in planning planting and harvesting schedules, ultimately maximizing profits. Advanced techniques such as deep

learning have shown promising results in enhancing prediction accuracy through the analysis of complex datasets.

4.2. Disease and Pest Detection

Artificial intelligence-driven systems employ image recognition technology to detect crop diseases and pest infestations. By identifying these issues early, farmers can implement targeted interventions that decrease reliance on broad-spectrum pesticides. This proactive strategy not only minimizes chemical application but also supports environmental sustainability.

4.3. Soil Health Management

Machine learning algorithms help maintain soil health by recommending appropriate fertilizer applications and irrigation strategies based on real-time soil data. This ensures long-term sustainability and productivity. Monitoring soil nutrient levels and implementing precision agriculture practices can significantly improve yields.

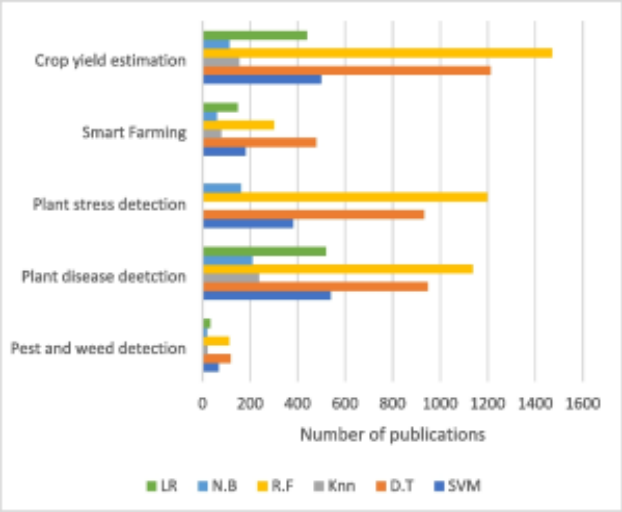

Fig. 2. Common Crop Application Algorithms

5. Algorithms Used in Smart Agriculture

A variety of machine learning algorithms have been employed in smart agriculture. Below is a comparative analysis of selected algorithms:

5.1. Linear Regression

Linear regression is a statistical approach used to model the relationship between a dependent variable and one or more independent variables. This method is straightforward to apply and easy to interpret, featuring a quick training process.

However, it operates under the assumption of linearity, which may not apply to more complex datasets, thus limiting its effectiveness in certain agricultural scenarios.

5.2. Decision Trees

Decision trees are analytical models that utilize a branching diagram to represent decisions and their potential outcomes. They are user-friendly and can effectively manage both numerical and categorical data. Nevertheless, decision trees are susceptible to overfitting and can be sensitive to noisy data, which may compromise their reliability in agricultural applications.

5.3. Random Forest

Random Forest is an ensemble learning technique that builds multiple decision trees and combines their outputs to

enhance accuracy and mitigate overfitting. This method is resilient to overfitting and can efficiently manage large datasets, making it well-suited for applications in smart agriculture. However, its complexity can make it more difficult to interpret and it demands greater computational resources compared to simpler models.

5.4. Support Vector Machines (SVM)

Support Vector Machines are supervised learning algorithms that identify a hyperplane to differentiate data into distinct classes. They perform well in high-dimensional spaces and are capable of handling unstructured data effectively. However, SVMs can consume significant memory and may be less efficient on extremely large datasets, presenting challenges for real-time monitoring in agriculture.

5.5. K-Nearest Neighbors (KNN)

K-Nearest Neighbors is a non-parametric method that classifies data based on the closest training examples in the feature space. It is simple and effective, with no training phase required. However, KNN can be computationally expensive during prediction and is sensitive to irrelevant features, which may complicate its application in diverse agricultural environments.

5.6. Neural Networks

Neural networks are a set of algorithms modeled loosely after the human brain, designed to recognize patterns. They can capture complex relationships in data, offering high flexibility and power. However, neural networks require a large amount of data and computational power, making them less accessible for smaller farms or operations. Additionally, they can be difficult to interpret, which may hinder their acceptance among traditional farmers.

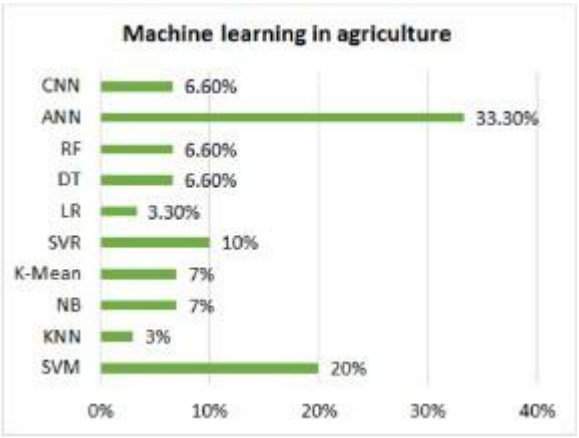

Fig. 3. Machine Learning Algorithms in Agriculture

5.7. Gradient Boosting Machines (GBM)

Gradient Boosting Machines represent an ensemble learning approach that constructs models in a sequential manner, with each new model designed to correct the errors of its predecessors. GBMs are known for their high accuracy and strong predictive capabilities, effectively managing missing data. However, if not appropriately tuned, they may overfit the training data and generally require longer training times than other algorithms, potentially limiting their effectiveness in rapidly changing agricultural environments.

This theoretical analysis sheds light on the advantages and drawbacks of various machine learning algorithms, emphasizing their relevance and application within smart agriculture.

6. Impact of Smart Farming 4.0 on Sustainability

The adoption of Smart Farming 4.0 technologies is poised to transform agricultural practices and enhance sustainability.

Fig. 4. Revolutionizing Crop Growth

6.1. Resource Efficiency

By leveraging IoT and AI technologies, farmers can optimize the use of water, fertilizers, and pesticides. This not only leads to cost savings but also minimizes environmental impact. Efficient resource management is crucial in combating issues like water scarcity and soil degradation.

6.2. Enhanced Crop Resilience

Through precise monitoring and predictive analytics, farmers can implement strategies that enhance crop resilience against diseases, pests, and climate variability. By adapting to changing conditions, farmers can secure their yields and maintain productivity.

6.3. Economic Viability

The integration of smart technologies can improve the economic viability of farming operations, particularly for smallholder farmers. By increasing productivity and reducing input costs, farmers can achieve better profitability, thereby ensuring their livelihoods and contributing to local economies.

7. Emerging Technologies in Smart Farming

Recent advancements in technology are set to play a crucial role in enhancing Smart Farming practices.

7.1. Drones and Remote Sensing

Drones equipped with advanced cameras and sensors are capable of gathering data on crop health, soil conditions, and irrigation requirements from an aerial perspective. This data can be analyzed using artificial intelligence to provide farmers with valuable insights, facilitating improved decision-making and more effective resource management.

7.2. Big Data Analytics

The growing amount of data produced by IoT devices offers a valuable opportunity to utilize big data analytics in agriculture. By examining extensive datasets, farmers can identify patterns and trends that can guide their practices, from forecasting market demand to refining planting schedules.

Fig. 5. Harnessing the Power

7.3. Autonomous Machinery

The advancement of autonomous tractors and other farming machinery has the potential to greatly improve operational efficiency. These machines can carry out various tasks, including planting, harvesting, and monitoring, without the need for human oversight, thereby reducing labor costs and enhancing precision.

8. Future Directions and Research

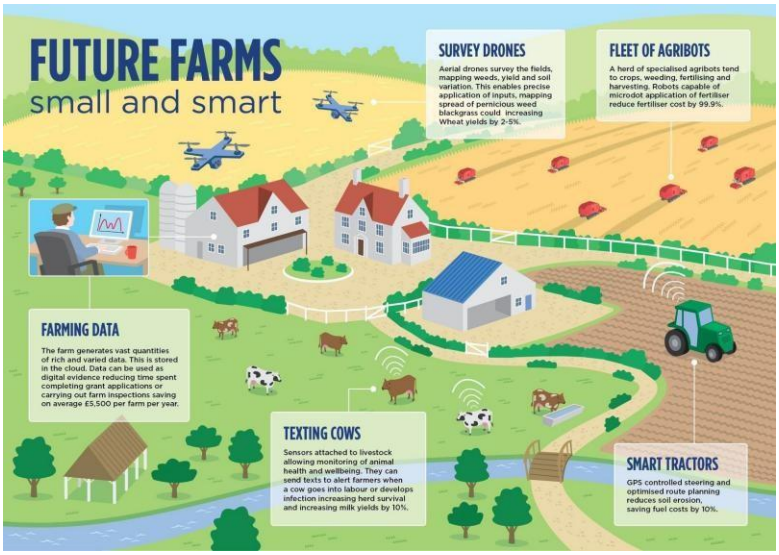

Fig. 6. Future of Smart Agriculture

As the agricultural sector continues to evolve, several areas warrant further research and development.

8.1. Integration of Blockchain Technology

Incorporating blockchain technology alongside IoT and AI has the potential to improve transparency and traceability within agricultural supply chains. This integration could build trust among various stakeholders and enhance food safety.

8.2. Development of Low-Cost Solutions

To promote the widespread adoption of Smart Farming technologies, research should concentrate on creating affordable, energy-efficient IoT devices. This focus is especially vital for smallholder farmers in developing regions, where resources are often scarce.

8.3. Collaboration Between Stakeholders

Future research should prioritize collaboration between academic institutions, industry players, and policymakers to establish supportive ecosystems for Smart Farming initiatives. By nurturing partnerships, stakeholders can exchange knowledge, resources, and best practices, fostering innovation in the agricultural sector.

9. Conclusion

The incorporation of AI, ML, and IoT technologies into agriculture marks the beginning of a new era known as Smart Farming 4.0. By utilizing these advanced technologies, farmers can enhance resource efficiency, increase crop yields, and lessen their environmental footprint. The potential for real-time decision-making and predictive analytics provides significant advantages, particularly in regions facing connectivity challenges. Continued advancements in these fields can contribute to sustainable agricultural practices, ultimately helping to secure food production for future generations.

References

[1] Shyam, G. K., & Chandrakar, I. (2023). A novel approach to edge-fog-cloud based smart agriculture. *2023 International Conference on New Frontiers in Communication, Automation, Management and Security (ICCAMS)*, Bangalore, India, 1–5.

[2] Nimmala, S., Ramchander, M., Mahendar, M., Manasa, P., Kiran, M. A., & Rambabu, B. (2024). A recent survey on AI enabled practices for smart agriculture. *2024 International Conference on Intelligent Systems for Cybersecurity (ISCS)*, Gurugram, India, 1–5.

[3] Sharma, R., Vaidya, P., & Sharma, B. (2024). A review on plant growth monitoring using artificial intelligence and the Internet of Things. *2024 11th International Conference on Computing for Sustainable Global Development (INDIACom)*, New Delhi, India, 140–145.

[4] AlZubi, A. A., & Galyna, K. (2023). Artificial intelligence and Internet of Things for sustainable farming and smart agriculture. *IEEE Access*, *11*, 78686–78692.

[5] Nalwanga, R., Nsenga, J., Rushingabigwi, G., & Gatare, I. (2021). Design of an embedded machine learning-based system for an environmental-friendly crop prediction using a sustainable soil fertility management. *2021 IEEE 19th Student Conference on Research and Development (SCOReD)*, Kota Kinabalu, Malaysia, 251–256.

[6] Kumar, S., Shinde, V. D., Goradiya, U. B., Patil, A. A., Verman, S. P., & Tembhurne, V. K. (2024). Improved crop yields and resource efficiency in IoT-based agriculture with machine learning. *2024 International Conference on Automation and Computation (AUTOCOM)*, Dehradun, India, 119–125.

[7] Subudhi, M., Bhuyan, K. C., & Dastidar, A. (2022). IoT assisted farming using ML techniques. *2022 IEEE 2nd International Symposium on Sustainable Energy, Signal Processing and Cyber Security (iSSSC)*, Gunupur, Odisha, India, 1–5.

[8] Hasan, A., Diya, N. S., & Sultana, S. (2024). IoT based smart agriculture management system. *2024 3rd International Conference on Advancement in Electrical and Electronic Engineering (ICAEEE)*, Gazipur, Bangladesh, 1–5.

[9] Mahmood, M. R., Matin, M. A., Goudos, S. K., & Karagiannidis, G. (2024). Machine learning for smart agriculture: A comprehensive survey. *IEEE Transactions on Artificial Intelligence*, *5*(6), 2568–2588.

[10] Bhanu, K. N., Jasmine, H. J., & Mahadevaswamy, H. S. (2020). Machine learning implementation in IoT-based intelligent system for agriculture. *2020 International Conference for Emerging Technology (INCET)*, Belgaum, India, 1–5.

[11] Prathap, C., Sivaranjani, S., & Sathya, M. (2024). ML-based yield prediction in smart agriculture systems using IoT. *2024 5th International Conference on Innovative Trends in Information Technology (ICITIIT)*, Kottayam, India, 1–7.

[12] M. M., P. P. I., S. S., P. R. K., & P. R. S. (2024). Smart fields: Enhancing agriculture with machine learning. *2024 2nd International Conference on Artificial Intelligence and Machine Learning Applications Theme: Healthcare and Internet of Things (AIMLA)*, Namakkal, India, 1–5.

[13] Pandey, S., Gehlot, A., Pandey, V., Kathuria, N., Chhabra, G., & Malik, P. K. (2023). Subsuming AI, IoT and big data in smart farm practices. *2023 IEEE Devices for Integrated Circuit (DevIC)*, Kalyani, India, 229–232.

Effect of Stacking Sequence on Tensile and Flexural Strength of Fiber Glass Laminates

Dilip Johari[1], Sandeep Agrawal[3], Puneet Mangla[3], Dinesh Kumar[2]

[1]*Research Scholar, Mechanical Engineering Department, Harcourt Butler Technical University, Kanpur, 208 002, India*
[2]*Assistant Professor, Mechanical Engineering Department, Hindustan College of Science & Technology, Farah, Mathura 281122, India*
[3]*Associate Professor, Mechanical Engineering Department, Hindustan College of Science & Technology, Farah, Mathura 281122, India*

Abstract
Because of their high strength and stiffness, fiber glass laminates are now thought to be used as reinforcing materials in polymer matrix composites. The mechanical characteristics of fiber glass laminates were assessed in this work. Here, fiber glass cloth and epoxy resin were used in a hand layup method to prepare the laminates. Gaining a better knowledge of the mechanical characteristics of fiber glass composites was the primary goal of this study. The impact of laminate fiber orientation has been studied. Tensile and flexural strength testing on a universal testing machine (UTM) is the focus of this inquiry. The test results' resulting graphs are recorded. According to this study, the mechanical characteristics primarily depend on the fiber orientation of laminated polymer composites.

Keywords: *Epoxy Resin, stacking sequence, Glass fiber, Tensile & Flexural Strength.*

1. Introduction

When two or more physically separate phases are appropriately ordered or distributed, the result is a material known as a composite. The continuous phase is termed the matrix, and the scattered phase is called the reinforcement. The primary goal of developing composite materials is to balance their qualities for a specific range of applications. There are many different materials that can be categorized as composites, and there are many different applications for which they are made. The matrix, reinforcement, and interface between them are the three factors that define a composite's properties. There are numerous types of reinforcement materials, including whiskers, particles, continuous and short fibers, and more. [1]

Two different levels are usually used to classify composites. The primary composite classes are organic-matrix composites (OMCs), metal-matrix composites (MMCs), and ceramic-matrix composites (CMCs). The initial level of classification is typically made in relation to the matrix constituent. Polymer-matrix composites (PMCs) and carbon-matrix composites (also known as carbon-carbon composites) are the two kinds of composites that are typically included in the phrase "organic-matrix composite." Usually, PMCs are converted into carbon-matrix composites by adding the additional processes of carbonization and densification to the initial polymer matrix. Inter-metallic matrix composites (IMCs) are occasionally categorized as something different from MMCs in the research and development community. However, there are currently no notable commercial uses for IMCs, and practically speaking, these materials don't offer a whole different set of characteristics in comparison to MMCs. Particulate reinforcements, whisker reinforcements, continuous fiber laminated composites, and woven composites are the reinforcing forms that fall under the second level of classification. Epoxy resins are made from chemicals that have an average of more than one epoxy group per molecule and can be transformed into useful thermosetting goods by means of these groups; the cured product and its low molecule predecessors are referred to as reins [3]. Low shrinkage, strong adhesive strength, exceptional chemical resistance, superior electrical characteristics, and exceptional heat resistance are among the benefits of epoxy resins [4].

The strength of the composites is significantly influenced by the fiber orientation. Fiber-reinforced composites have several special qualities, including the ability to be modified to create various loading scenarios [5]. The connection between the fibers and the matrix determines the fiber reinforced composite's tensile strength. The fibers are supported and held in place by the matrix, which also passes the weight to the strong fibers, shields them from breakage during manufacture, and stops the spread of fiber breaks [1, 2]. Hardness testing is popular because it is rapid and easy, even though it does not provide as much specific information as tensile testing.

2. Literature Review

During last few years, there has been a renewed interest in using the fibers as reinforcement materials, to some extent in

Published online on: ***February 01, 2025***
Corresponding Author's E-mail ID: dilipjohari@gmail.com

the plastic industry. A number of researchers have investigated the influence of fiber orientation & thickness of laminates of different sized glass fibers on the mechanical properties of glass fiber epoxy resin composites. Sreekala et al. [6] investigated the performance of mechanical properties of oil palm fiber with glass fiber and used phenol formaldehyde as resin. The investigation revealed that maximum mechanical performance occurs at 40 wt% loading. Kasama and Nitina [7] studied the effect of glass fiber hybridization on properties of sisal fiber–polypropylene composites. Incorporation of glass fiber increases the mechanical, thermal and water resistance properties. Chen and Sun [8] used the finite element method to examine the impact responses of the composite laminates with and without starting stresses. For straightforward situations and straightforward material architecture, the deflections generated are minimal. However, when sophisticated designs are taken into account, the deflections generated become more complex. One crucial method for determining a natural composite's strength is finite element analysis.

The failures under combined tension and bending loads were examined by Khoshbakht et al. [9], who also simulated the performance of the woven composites under various loading scenarios. It was discovered that the failure happened close to the fastener where the composite was bent to its greatest extent. Numerous studies have demonstrated that treating the fiber can increase the strength of natural composites.

Using a matrix-resin pre-impregnation technique and saline treatment, Herrera-Franco and Valadez-Gonzalez [10] enhanced the short fiber laminates' tensile, flexural, and shear characteristics while leaving the tensile and flexural moduli unchanged. Dash et al. investigated the mechanical characteristics of jute fiber-unsaturated polyester composites made by solution impregnation and hot curing techniques; they discovered that bleached fibers outperformed unbleached fibers in terms of mechanical properties at 60% weight loading. Alwar [11] investigated the characteristics of date palm fiber that underwent various treatment procedures. While HCl treatment caused its attributes to deteriorate, 1% NaOH treatment increased its mechanical qualities. Glass/polypropylene and glass/polyester composites have undergone significant tensile, flexural, and inter-laminar testing by Varatharajan [12].

Hitchen [13] investigated how the fiber length affected a short carbon/epoxy composite's fatigue. They demonstrated that at any peak load, fatigue life is independent of fiber length. According to research by Craig D. Snyder [14] of Bayer Corporations, the flexural modulus of low density polyurethane structural form has risen with the addition of long glass fibers. A recent technological advancement that offers the composites sector new prospects is low density polyurethane composites. Using fibers of various cross sectional shapes, Deng [15] conducted a compressive experimental investigation to determine the impact of fiber cross sectional aspect ratio on the tensile and flexural characteristics as well as the failure modes of glass fiber/epoxy composites. K. Mohamed Kaleemulla [16] looked at how an epoxy resin component's fiber content and orientation affected its mechanical properties. Examining how fiber orientation affects mechanical qualities was the primary goal of the current work.

3. Experimental Work

There are many factors which affects the mechanical properties of the fiber glass laminates. Some of them are as follows:

- Length of the fiber
- Orientation of the fiber
- Shape and size of the fiber
- Stacking sequence of fiber layers
- Distribution of the fiber in the matrix
- Properties of the fiber

In the present paper, our main focus is on the orientation of the fiber, because the orientation of fiber directly affects the mechanical properties of fiber glass laminates. For this purpose, we have selected four different stacking sequences in which eight layers of the glass fabric are placed one over other having different orientations. The four different laminates having stacking sequence of the glass fabric are as:

1. 0/0/0/0/0/0/0/0
2. 0/90/0/90/0/90/0/90
3. 0/+45/-45/0/0/+45/-45/0
4. 0/45/90/0/0/45/90/0

3.1. Sample Preparation:

Four types of samples are prepared by using hand layup method based on the above stacking sequences. For preparing the laminate sheets, we have used Epoxy resin (LY556) and hardener (HY758). The glass fabric of 600 GSM is supplied by Kay Kay enterprises, New Delhi. For each sample, the glass fabric was cut down in eight layers of dimension 305 mm x 305 mm. These fabric layers are then placed one over another in required stacking sequence by applying the prepared mixture of epoxy resin and hardener in a ratio of 10:1 by weight as recommended. Then, the samples are cured at room temperature and constant pressure for 24 hours. Finally, the laminated sheets are cut down by a wire cutting machine and the edges are grinded. The appropriate standards are followed for preparing the specimens for test.

3.2. Mechanical Testing of the samples

The several variables listed above affect the mechanical characteristics of fiber glass laminates. For a particular matrix, even little modifications to the fiber's physical characteristics can have a significant impact on the laminates' overall mechanical characteristics. The fiber glass laminates can be subjected to a number of mechanical tests, including tensile, compression, hardness, impact, flexural strength, fatigue, and more. Tensile and flexural strength testing are conducted on the laminates in this article. A universal testing equipment is used to perform these tests at a temperature of 25±2˚C and a relative humidity of 65±5%. In order to determine the specimen's dimensions for tensile testing in accordance with IS: 1608 criteria, the laminates are cut with a saw cutter. Samples 1, 2, 3, and 4 are the four distinct sorts of specimens that are prepared according to the orientation that is used. Tension is applied to the specimens until they fracture while they are in the grip of the tensile testing apparatus. Tensile stress is measured in relation to strain increase. In accordance with IS: 13360 standards, the flexural test is conducted on the same tensile testing apparatus. The test specimen is loaded halfway between the supports and continues to be loaded until it breaks and fractures. Through this test, the specimen's behavior under basic beam loading is ascertained. The maximum stress generated in the outermost fiber is ascertained by the flexural test.

4. Results & Discussion

According to the experimental findings, reinforcements are always placed in the direction of load when designing laminates. Investigating the laminate's mechanical behavior becomes more crucial, though, if the load direction is changeable and not parallel to the fibers. Four distinct configurations are chosen for this study in order to examine the impact of the stacking sequence. The same procedures as previously mentioned are used to create specimens with various stacking sequences. The experimental findings demonstrate that the fiber orientation has a considerable impact on the tensile and flexural strengths. The effects of different stacking sequences on the aforementioned mechanical properties will be examined in the following section. The following tables list the outcomes of all the tests that were performed on the individual samples in accordance with a standard procedure:

Sample No.1

- Stacking Sequence:- 0/0/0/0/0/0/0/0
- Environmental Temperature:- 25±2˚C
- Relative humidity(RH):- 65±5%

Table1. Testing Results of Sample No. 1

S. No.	Parameter	Test Method	Result	Unit
1	Tensile Strength	IS : 1608	150	MPa
2	Elongation	IS : 1608	21.4	%
3	Flexural Strength	IS : 13360	258.7	Mpa

Sample No.2

- Stacking Sequence:- 0/90/0/90/0/90/0/90
- Environmental Temperature :- 25±2˚C
- Relative humidity(RH):- 65±5%

Table2. Testing Results of Sample No. 2

S. No.	Parameter	Test Method	Result	Unit
1	Tensile Strength	IS : 1608	160	Mpa
2	Elongation	IS : 1608	24.7	%
3	Flexural Strength	IS : 13360	250.5	Mpa

Sample No.3

- Stacking Sequence:- 0/+45/-45/0/0/+45/-45/0
- Environmental Temperature :- 25±2˚C
- Relative humidity(RH):- 65±5%

Table3. Testing Results of Sample No. 3

S. No.	Parameter	Test Method	Result	Unit
1	Tensile Strength	IS : 1608	110	Mpa
2	Elongation	IS : 1608	19.2	%
3	Flexural Strength	IS : 13360	202	Mpa

Sample No.4

- Stacking Sequence:- 0/45/90/0/0/45/90/0
- Environmental Temperature :- 25±2˚C
- Relative humidity(RH):- 65±5%

Table4. Testing Results of Sample No. 4

S. No.	Parameter	Test Method	Result	Unit
1	Tensile Strength	IS : 1608	116	Mpa
2	Elongation	IS : 1608	14.7	%
3	Flexural Strength	IS : 13360	198.76	Mpa

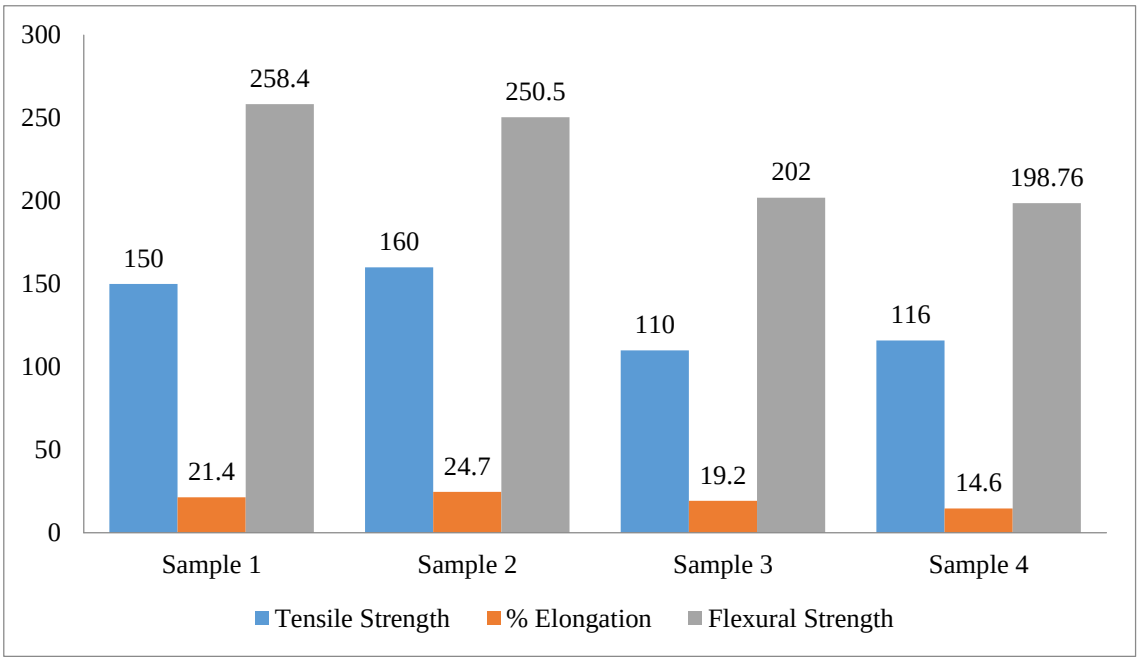

Fig. 1 Comparison of test results of all samples

The material can sustain itself for longer than other orientations because, as shown in Figure 1, the sample with the 0/+45/-45/0/0/+45/-45/0 stacking sequence has the lowest tensile strength but the most elongation and significant flexural strength, which may be applicable for variable loading. Configurations such as 0/0/0/0/0/0/0/0/0/0 and 0/45/90/0/0/45/90/0

demonstrate how the orientation of the pile up layer manages the applied load in redistribution from one layer to another layer. The sample with configuration 0/90/0/90/0/90/0/90/0/90/0/90 has good tensile strength and remarkable elongation with sufficient flexural strength that may be applicable for bearable tensile loading. According to observations, if we take into account the fundamental principle of stress and strain as measured by cross-sectional area, then each layer's commutative impact is concerned with another layer's change in relative orientation. Choosing an efficient arrangement of pile-up laminates one above the other is a crucial component of laminated composite design, given their load application and retain ability ratio.

5. Conclusion

The experimental work's findings suggest that altering the order in which different glass fiber layers stack can improve the mechanical qualities of fiber glass laminates. Whether or not their direction of load is taken into consideration, this observation has led to the conclusion that the orientation of pile-up laminates one above the other should have particular significance for object applications and load bearing capacity under subjected conditions with region-able changes in orientation, making it versatile for future aspects of research. This work uses glass fibers, epoxy resin, and a hardener to create various fiber glass laminates. The following conclusions were reached after an investigation into their mechanical characteristics, such as tensile strength, percentage elongation, and flexural strength.

Sample number two has a comparatively higher tensile strength than the rest. 160 MPa is its value. In tensile testing, sample number two also exhibits a higher percentage elongation than other laminates. As a result, in tensile testing, the laminates in that stacking sequence may bear greater strain before failing. The composite's flexural strength decreases with sample numbers 1, 2, 3, and 4. At 258.4 MPa, sample number one has the highest flexural strength. Compared to traditional wood-based plywood or particle boards, fiber glass laminates are undoubtedly a very promising material for the production of lightweight materials used in the packaging sector, office furniture, vehicle body building, partition panels, etc.

Additional stacking sequences and mechanical characteristics, such as compressive strength, hardness, impact strength, etc., can be investigated using this approach. The mechanical properties can be examined in various operating environments, and improved designs that support the idea of a green environment may be proposed.

References

[1] Meyers, M. A., & Chawla, K. K. (1999). *Mechanical behavior of materials*. Prentice-Hall.
[2] Courteny, T. H. (2000). *Mechanical behavior of materials*. McGraw Hill.
[3] John Wiley & Sons, Inc. (1967). *Encyclopedia of polymer science and technology* (Vol. 6). U.S.A.
[4] Clements, L. L., & Moore, R. L. (2007). Study of tensile strength and hardness property for epoxy reinforced with glass fiber layers. *Composites Engineering & Technology*, *25*(8), 988–997.
[5] Hall, D. (1981). *An introduction to composite material*. Cambridge University Press.
[6] Sreekala, M. S., George, J., Kumaran, M. G., & Thomas, S. (2002). The mechanical performance of hybrid phenol-formaldehyde-based composites reinforced with glass and oil palm fibers. *Composites Science and Technology*, *62*, 339–353.
[7] Jarukumjorn, K., & Suppakarn, N. (2009). Effect of glass fiber hybridization on properties of sisal fiber–polypropylene composites. *Composites Part B: Engineering*, *40*, 623–627.
[8] Chen, J. K., & Sun, C. T. (1985). Dynamic large deflection response of composite laminate subject to impact. *Composite Structures*, *4*, 59–73.
[9] Khoshbakht, M., Chouwdhury, S. J., Seif, M. A., & Khashaba, U. A. (2009). Failure of woven composites under combined tension–bending loading. *Composite Structures*, *90*, 279–286.
[10] Herrera-Franco, P. J., & Valadez-Gonzalez, A. (2005). A study of mechanical properties of short natural fiber reinforced composites. *Composites Part B: Engineering*, *36*, 597–608.
[11] Alawar, A., Hamed, A. M., & Al-Kaabi, K. (2009). Characterization of treated date palm tree fibre as composite reinforcement. *Composites Part B: Engineering*, *40*, 601–606.
[12] Varatharajan, R., et al. (2006). Mechanical and machining characteristics of GF/PP and GF/polyester composites. *Materials Science and Engineering B*, *132*, 134–137.

[13] Hitchen, S. A., Login, S. L., & Smith, P. A. (1995). Effect of fiber length on fatigue of short carbon fiber/epoxy composite. *Composites*, *26*(4), 303.

[14] Snyder, C. D., et al. (2002). Low density polyurethane composites. *Composites 2002 Convention and Trade Show*, September 25–27, Atlanta, Georgia, USA.

[15] Deng, S., Ye, L., & Mai, Y. W. (1999). Influence of fiber cross-sectional aspect ratio on mechanical properties of glass fiber/epoxy composites 1: Tensile and flexure behavior. *Composites Science and Technology*, *59*(9), 1331–1339.

[16] Kaleemulla, K. M., & Siddeswarappa, B. (2010). Influence of fiber orientation on the in-plane mechanical properties of laminated hybrid polymer composites. *Journal of Reinforced Plastics and Composites*, *29*(12), 1900–1914.

Surface Morphology of Hot Dip Galvanizing Coating

Amit Pal[1], Chaitanya Sharma[1]*, M. G. Walunj[2]

[1]*M. Tech Scholar, Mechanical Engineering Department, BIT Sindri, Dhanbad, Jharkhand, 828123*
[1*]*Associate Professor, Mechanical Engineering Department, BIT Sindri, Dhanbad, Jharkhand, 828123*
[2]*Sr. Scientist, CSIR-National Metallurgical Laboratory, Jamshedpur, 831007*

Abstract
In this study, the galvanizing ability of dual phase (DP) steel and its surface morphology is studied. The micro structural analysis was done by the optical microscope (OM) and scanning electron microscope (SEM). We see zinc enrich grain boundaries with the help of optical microscope. The EDS spectra show the 99% of zinc presence and small amount of iron (Fe) present in the top surface of the coating.

Keywords: *Galvanizing, Zinc enrichment, Scanning electron microscope (SEM), Dual phase steel*.

1. Introduction

Hot Dip Galvanizing coating is most widely used in our modern industrial application for better corrosion protection, paintability, weldability, formability of cold rolled steel substrate. Galvanizing process involves zinc and zinc-alloy coating to the substrate to protect the substrate through sacrificial or galvanic mechanism[1]. The zinc coating is non homogeneous in nature and composed many intermetallic in the substrate and coating interface. In comparison of HSS grade the use of Dual phase (DP) steel use increased in automobile sector in future. Dual phase (DP-590) steel is used as a substrate and this steel have a microstructure of soft ferrite with islands of martensite offers good strength and ductility. Due to the metallurgical reactions between steel substrate and zinc the hot dip galvanizing process consist heterogeneous assembly of Fe-Zn intermetallic compounds[2].After solidification the outer layer consist pure 100% of zinc (η-eta layer) and inner layers consisting Fe-Zn intermetallic phases such as zeta(ζ) layer (94% Zn -6% Fe), delta ( ) layer (90% Zn-10% Fe) and gamma(Γ) layer (75% Zn- 25% Fe)[3]. These inner intermetallic phases are harder than the outer layer and give good protection from coating damage[4][5].With the increase of galvanizing temperature and immersion time the Fe-Zn intermetalliclayer thickness also increases and the thickness is also affected by adding additives in the bath[6].In galvanizing small amount of aluminum(Al) is mixed with bath to reduce the relative thickness of the Fe-Zn layer and solubility and diffusion of iron in zinc in the coating. An inhibition layer (Fe2Al(5-x)Znx(0<x<1)) is developed between the interface of substrate and coating[7]. Aluminumreacts with iron (Fe) and zinc (Zn) and formed inhibition layer which slow down the diffusion of iron (Fe) into the zinc (Zn), thereby ductility of the coating increasing since the iron- zinc is brittle in nature.The thickness of the coating layer is depended on the bath temperature and the dipping speed of the substrate into the bath.The current study intends to study the surface morphology with the help of optical microscope(OM), scanning electron microscope(SEM) and energy dispersive X-ray spectroscopy(EDS).

2. Experimental methods

The substrate cut as per desired dimension (220mm×110mm) from the cold roll sheets with the longitudinal direction. Dual phase steel(DP-590) was used with the thickness of 1mm as a substrate and main alloying elements are shown in Table 1[8].

Table1: Main alloying element composition of DP590

Concentration (wt.%)							
Grade	%C	%Mn	%Si	%P	%S	%Al	%Nb
DP590	0.094	1.779	0.011	0.01	0.006	0.031	0.001

The surface of the substrate cleaned at first with the alkaline solution and then it is also cleaned by the distilled water. The substrate was further cleaned by pickling in an acid solution (30% HCL solution) and dried it in air-drier. The pickling process and its effect on developing coating is further discussed in several studies[9] For galvanization we can develop

Published online on: ***February 01, 2025***
Corresponding Author's E-mail ID: cs.me@bitsindri.ac.in, chaitanya.sharmaji@gmail.com

coating manually or by using hot dip process stimulator. Manually we cannot control annealing process, dipping time, coating thickness and more other properties precisely, thus we use Hot Dip Process Stimulator for developing galvanized coating. After cleaning put holder on the sample and attach a K- type thermocouple on the substrate by spot welding. After spot welding we kept the substrate in the loading chamber and connect it to the driving rod.

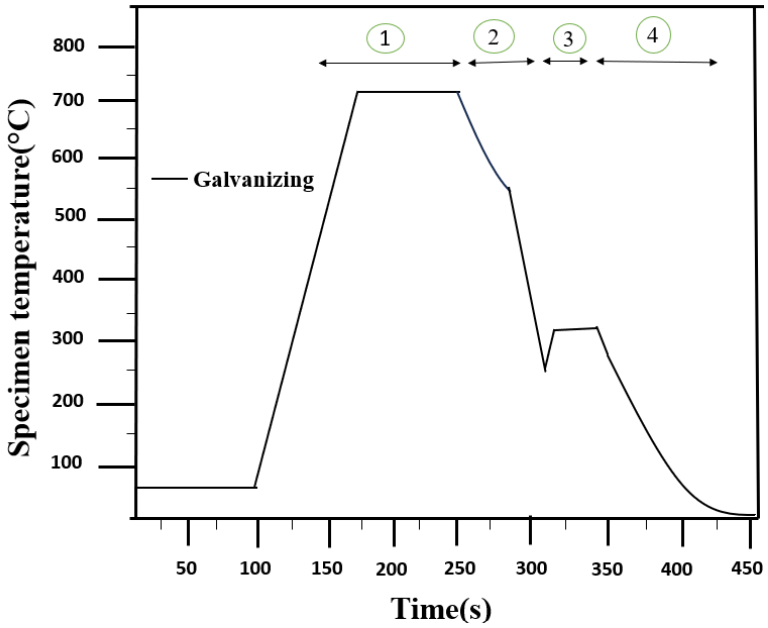

Fig.1. The temperature scheduled used for Galvanizing and Galvannealing. Specimens position in HDPS simulator is also shown in the profile: (1) Heating and soaking in IR-Furnace, (2) Controlled cooling section, (3) Dipping in the bath, (4) Controlled cooling section.

Before dipping we firstly heated the cold rolled specimen 750ºC at a constant heating rate 5°C/s in infra-red (IR) heating furnace and hold it for 60sec at this inter-critical temperature. Then the sample is cooled down to intermediate temperature 680°C at certain cooling rate 2°C/s. After reaching the intermediate temperature certainly we fast cooled at 15°C/s below the 400°C to obtain the dual phase microstructure.The mixture of hydrogen and nitrogen is used for fast cooling. Prior to dipping we isothermally heated the specimen at 2°C to obtain the bath temperature. After obtaining the bath temperature the specimen dipped into the bath at 475°C for 4sec and then the specimen is pulled out from the bath and excess liquid zinc skimmed off from the strip by nitrogen jet wiping to get desirable coating thickness of the specimen and finally cool it down to room temperature. In normal galvanizing process theiron (Fe%)cannot diffuse to the top surface of the substrate. Iron can diffuse at a certain thickness of the coating from the interface. For galvanized coating hot dip process stimulator was used. In stimulator we can regulate the annealing temperature (0-900) ºC, heating rate (0-40) ºC/s, cooling rate (0-250) ºC/s, dew point and uniform coating thickness. Coated substrate was cut into small pieces(3mm×4mm)for characterization study. The characterization of surface morphology was done using optical microscope (LEICA DM 2700M) and scanning electron microscope (ZEISS EVO-18) with an EDAX detector.

3. Result and Discussion

3.1. Macrostructure

Developed coating was somewhat rough with visible random texture with gray and shiny appearance. No visible discontinuity was observed in the coating. Sample top surface reflect the bright and shiny texture due to the presence of zinc (Zn) in the top surface and this is also confirmed by the Fig.2

Fig.2 Photograph of developed Galvanized coating

3.2. Microstructure

Surface morphology of galvanized coating is presented in Fig.3.Galvanizing coatings shows the grains of the zinc with well-defined grain boundaries. Inside the grain boundaries there are straight lines intersecting each other at equal angle whose thickness decrease gradually toward the outside from point of intersection. we can see clearly grain boundary of the zinc enrich phases which we can see inFig.4 of the galvanized coated sample. The grains are distributed both sides of the galvanized coating.

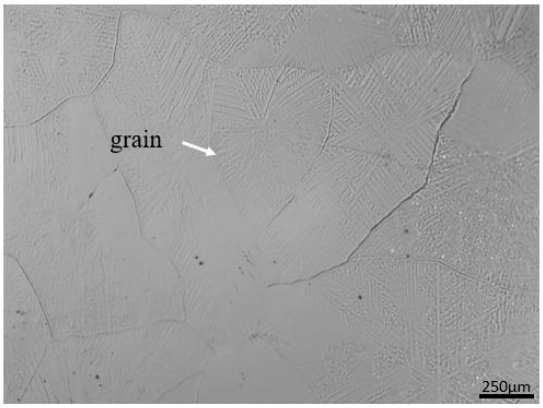

Fig.3 Structure evolution in galvanized coating

Figure 4 shows the high magnification SEM micrographs for understanding the structure evolution in coatings) with EDS spectra for understanding the element present in the top surface of the coating.

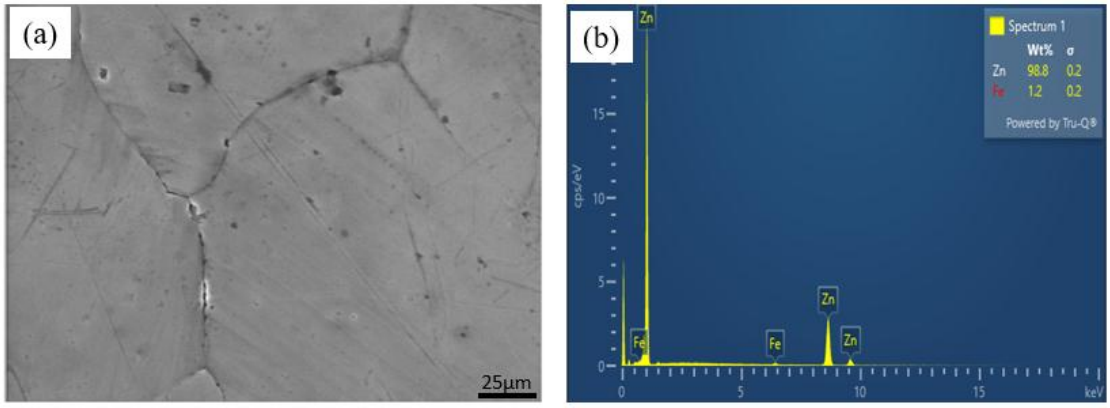

Fig.4 SEM image of galvanized coating with EDS spectra

SEM micrographs also confirmed the results of optical microscopy i.e. presence of Zn grains with well-defined boundaries in galvanizing coatings and provide in depth insight about the structure of developed coating. The EDS spectra show the 99% zinc (Zn) enrichment to the top surface of the coating and small amount of iron (Fe). So, we can conclude that galvanizing coating contains zinc at top surface mainly with very little Fe. There is no diffusion of iron (Fe) from the substrate to the top surface of the coating but there is iron diffusion into the zinc at the interface between the substrate and coating. The iron-zinc intermetallic layers are formed such as zeta(ζ),delta( ) gamma(Γ). A.Bakhtiari.et.al[10] suggested that the presence of the iron-zinc intermetallic at the interface of the substrate and coating and the outer surface of coating contains pure zinc(Zn).

4. Conclusion

Galvanizing coating has immense role on improving surface morphology and phase evolution. Galvanizing coating surface has bright and shiny texture on the top surface of the coating. In galvanizing the top surface enrich with zinc (Zn) and small amount of iron (Fe). There is no intermetallic Fe-Zn alloy formation on the top surface. In galvanizing the iron diffusion cannot occur to the top surface of the coated substrate. Iron-zinc intermetallic was present at the interface of the substrate and coating.

Reference

[1] Cook, D., & Grant, R. (1996). Iron-zinc intermetallics in commercial galvanneal steel coatings. In G. J. Long & F. Gd. (Eds.), *Mössbauer Spectroscopy Applied to Magnetic Materials Science* (Vol. 2, Ch. 10, pp. 225–271). Plenum Publishing Corporation. ISBN 0-306-45398-3.

[2] Shibli, S. M. A., Meena, B. N., & Remya, R. (2015). A review on recent approaches in the field of hot dip zinc galvanizing process. *Surface and Coatings Technology*, *262*, 210–215.

[3] Culcasi, J., Seré, P., Elsner, C., & Di Sarli, A. (1999). Control of the growth of zinc–iron phases in the hot-dip galvanizing process. *Surface and Coatings Technology*, *122*, 21–23.

[4] Rajak, P., Tewary, U., Das, S., Bhattacharya, B., & Chakraborti, N. (2011). Phases in Zn-coated Fe analyzed through an evolutionary meta-model and multi-objective genetic algorithms. *Computational Materials Science*, *50*(8), 2502–2516.

[5] Zhu, W., Jin, H. M., Wu, P., & Liu, H. L. (2004). Periodic density functional theory study of the crystal morphology of $FeZn_{13}$. *Physical Review B: Condensed Matter and Materials Physics*, *70*(16), 165419.

[6] Adetunji, O. (2010). Optimizing hot dip galvanizing operations of steel sheets for better quality. *Journal of Natural Science, Engineering and Technology*, *9*, 99–105.

[7] Mandal, G. (2011). Evolution of microstructures of galvanised and galvannealed coatings formed in 0.2 wt-% aluminium–zinc bath. *Materials Science and Technology*, *27*, 1265.

[8] Lin, C. S., Meshii, M., & Cheng, C. C. (1995). Phase evolution in galvanneal coatings on steel sheets. *ISIJ International*, *35*, 503.

[9] Díaz, B., Nóvoa, X. R., Pérez, C., & Silva-Fernández, S. (2021). Characterization of phosphate coatings: Influence of the acid pickling conditions. *Materials*, *14*(4), 1048.

[10] Bakhtiari, A., Toroghinejad, M. R., & Ashrafizadeh, F. (2014). The effect of zinc bath temperature on the morphology, texture, and corrosion behaviour of industrially produced hot-dip galvanized coatings. *Metallurgical and Materials Engineering*, *20*, 41–52.

.

International conference on Smart Material, Manufacturing and Characterization Techniques – 2024

Paper ID: ICSMMCT-01032

Evaluating the Effectiveness of TIG and ATIG Welding on Structural Integrity and Mechanical Performance of SS202 Stainless Steel

Anand Baghel[1], Chaitanya Sharma[2], Nasir Khan[3]

[1,3]*Department of Mechanical Engineering, Amity University Madhya Pradesh, Gwalior, India*
[2]*Department of Mechanical Engineering, BIT Sindri, Sindri Dhanbad, India*

Abstract
In this study, the effects of welding process viz. tungsten inert gas and activated tungsten inert gas welding on the microstructural and mechanical characteristics of bead-on-plate welds of SS202 stainless steel are investigated. SS202 beads were deposited by these processes using fixed welding parameters and various weld characteristics such as depth of penetration, weld and heat affected zone width, hardness and tensile strength were obtained to evaluate effect of welding techniques. Optical microscopy, hardness test and tensile test were conducted on defect free beads for microstructural and mechanical characterization. The results indicate that ATIG welding achieves deeper penetration, higher tensile strength, and reduced HAZ width compared to conventional TIG welding, demonstrating its potential as a superior method for high- performance applications requiring robust and precise welds.

Keywords: *Welding Processes, , Stainless steel, Bead profile, Microstructure, Hardness, Tensile strength*.

1. Introduction

Steel is currently the market's most adaptable engineering material. Steel makes a substantial contribution to the high standard of living in the world and is easy to weld and process [1, 2]. It has many uses, such as improved corrosion resistance in corrosive fluids and high-strength structural applications. The most prevalent type of stainless steel is austenitic. It has a totally austenitic steel structure with ductility, a broad range of application temperatures, high capacity, and non-magnetic weldability because it contains at least 7% nickel [3]. They might be more vulnerable to intermetallic precipitation and hot cracking than mild steels, depending on the microstructure of the weld metal. Applications for austenitic alloys in stainless steel are common [4]. There are no magnetic properties in the austenitic grades. Iron chromium-nickel steels, often referred to as the 300 series, and iron chromium-manganese steels, also known as the 200 series, are the most widely used austenitic alloys [5].

Due to its exceptional weldability, austenitic stainless steel (ASS202) finds extensive use in architectural facades, kitchenware, construction structures, industrial pipes and vessels, and containers [6, 7]. It is advisable to follow the standard welding guidelines that apply to SS304 steel when welding SS202 stainless steel. Because of their chemical makeup, stainless steels have a larger thermal elongation than mild steels [8-10].

In a single pass, TIG welding has a lower joint penetration rate for thick materials. Generally speaking, the depth of single pass TIG welding for stainless steel butt joints using argon as a shielding gas is restricted to 3 mm [11]. Enhancing TIG welding productivity and penetration is crucial. Using ATIG welding is among the most prominent methods. Acetone or ethanol is combined with powdered oxides, chlorides, and fluorides to produce an activating flux that has the viscosity of paint [12]. A thin coating of flux was applied to the joint's surface prior to welding. By increasing penetration by 200–300%, activated TIG welding can help manufacturers cut costs and weld times [13]. Weld bead width reduction is not as important as depth of penetration when using the activated TIG (ATIG) approach. For each welded joint, a bigger heat-affected zone results from a broader weld bead, which is undesired [14]. Before welding, a small layer of flux was applied to the surface of the joint to be welded. Activated TIG welding can increase penetration by 200-300%, leading to shorter weld times and lower costs for manufacturers[13]. The activated TIG (ATIG) technique prioritises depth of penetration over weld bead width reduction. A wider weld bead leads to a larger heat-affected zone, which is undesirable for any welded joint[14].

The current study intends to use welding parameters (current, speed and Electrode tip angle,) using TIG and ATIG welding and analyze their impact on weld macrostructure, hardness and tensile strength of SS202.

2. Experimental Procedure

300 mm × 150 mm × 5 mm SS202 plates were used as the base metal to make bead on plates welds by TIG and ATIG welding techniques. Following a manual grinding process to eliminate contaminants such as oil and grease, the plates were meticulously cleansed using acetone [15]. Welding was done using an air-cooled TIG welding machine with direct current

Published online on: ***February 01, 2025***
Corresponding Author's E-mail ID: cs.me@bitsindri.ac.in, chaitanya.sharmaji@gmail.com

electrode negative (DCEN) polarity (Electra-250, India)[16, 17], with argon shielding gasses and tungsten electrodes. The initial parameters of the pilot experiment were selected following a review of pertinent literature [16-19]. According to a pilot study, welding was successful when the current ranged from 85 A to 125 A. While currents above 125 A melted the 5 mm thick plate, currents below 85 A only allowed for shallow penetration. A mechanism was developed for automatic torch movement to maintain a constant arc gap and welding pace [19].

Table 1 lists the welding input parameters for the TIG and ATIG processes, such as current, speed, and electrode tip angle. I case of ATIG, a flux coating was placed to the steel weld plate surface where the weld must be done with a brush. For this flux and acetone were mixed in a certain ratio to create a paste. Since there are fewer options for a flux for ATIG welding, Cr2O3oxide flux is utilized for the experiment. After welding, defect free welds were cut with hand hacksaw to get samples for microstructural and mechanical characterization. Using normal metallographic procedures, samples with dimensions of 10 mm by 8 mm were prepared for microscopic examination using paper with grit sizes ranging from 120 to 2000. To analyse microstructure, polished samples were etched for 5 sec, with a solution of 2 g CuSO4, 5 ml H2SO4, 10 ml HCl, and 10 ml H2O.

Table 1: Welding parameters for experimental

Factors	Notation	Input value
Current (A)	I	125
Weld speed (mm/sec)	S	2
Electrode tip angle (Degree)	ETA	90

To determine the impact of welding procedures, measurements were made of DOP, weld and HAZ width, weld bead hardness, and tensile strength. The hardness at the weld bead on the weld plate was measured using a Vicker hardness tester (fig 2a). Evolution microstructure was examined and DoP, weld width, and HAZ width were measured using the Leica DM750 M optical microscope (Fig 2b). A tensile test conducted on a universal testing machine (25 kN INSTRON, UK) was used to determine the tensile properties (Figure 2c). Tensile tests were performed using flat test specimens prepared in accordance with ASTM recommendations (Figure 2d) at a stain rate of 1 mm/s crosshead speed. Three specimens were assessed for each condition in order to confirm repeatability, and the average tensile strength was discussed.

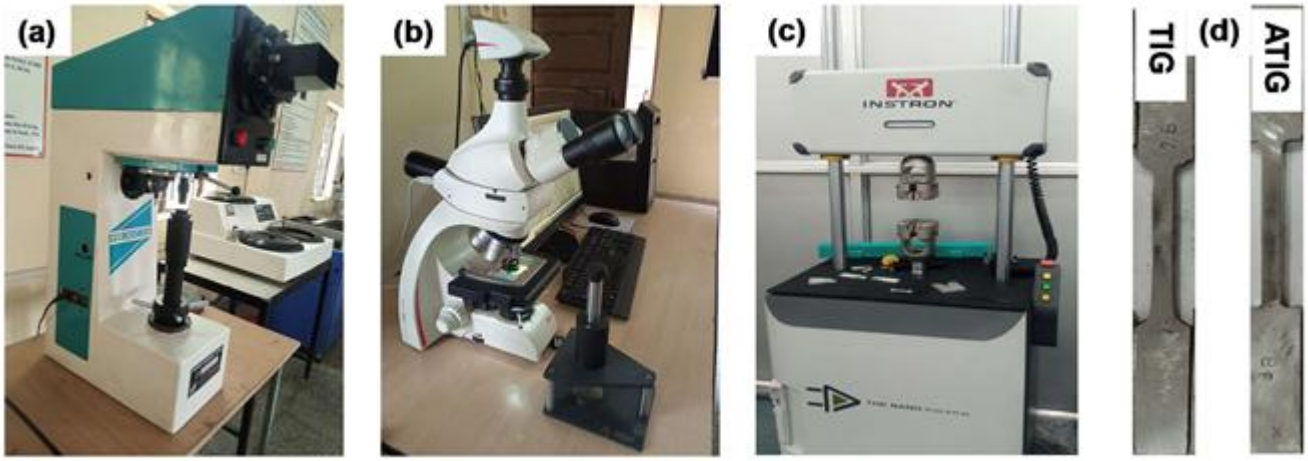

Figure 1: Testing equipment and specimen (a) Vicker hardness tester, (b) Leica Microscope, (c) Universal testing machine and (d) Tensile test specimen

3. Result and Discussion

3.1. Macrostructure

Welding process displayed significant influence on the bead morphology as evident from figure 2. Beads were of bowl shaped and size varied with the welding technique. Welding techniques affected the DoP, weld and HAZ width greatly.

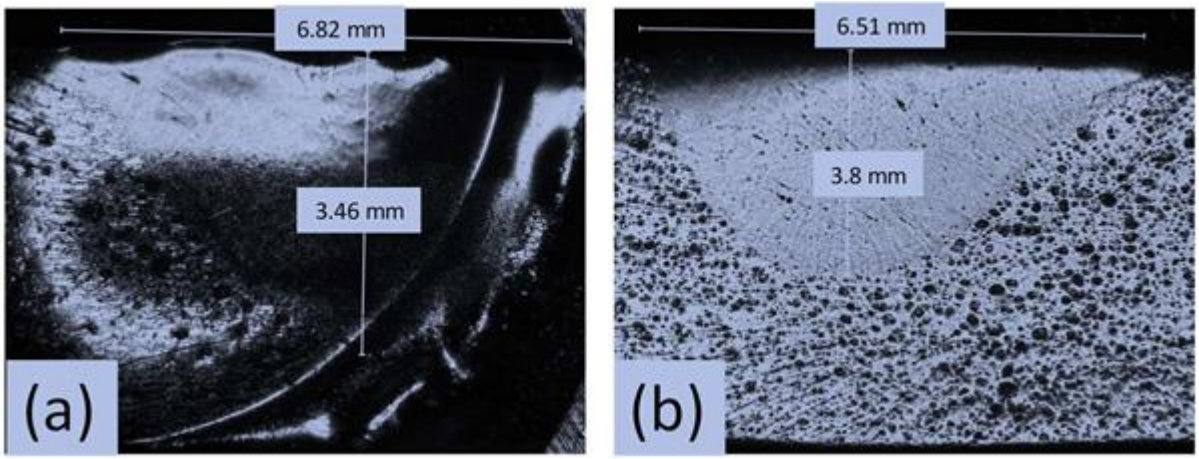

Figure 2 : Influence of welding process (a) TIIG and (b) ATIG on weld bead profiles

Figure 3 shows the influence of welding processes on various bead characteristics. DoP was higher for ATIG (3.8 mm) than TIG (3.46 mm) indicating the ability of ATIG process to make deeper penetration than TIG. ATIG process is more effective in achieving deeper welds, which can improve joint strength. Despite difference in DoP, the weld width remains nearly identical for both processes. Welding processes had most significant impact on the size of HAZ i.e. width. ATIG showed narrow HAZ than TIG. The HAZ width was 0.456 mm and0.741 mm for ATIG and TIG welds respectively. A smaller HAZ in ATIG welding suggests better control over heat input during welding, reducing the risk of thermal distortion or weakening of the material near the weld. On the side larger HAZ width in case of TIG welding reflects dispersion of heat to larger area. Use of activated flux change the flow behavior in molten pool, concentrating the heat along the plate thickness therefore grater is the DoP and smaller the HAZ width.

The aspect ratio, calculated as the depth-to-width (D/W) ratio, is another important factor when assessing weld quality. ATIG welding has a higher aspect ratio (0.58) compared to TIG welding (0.53). A higher aspect ratio implies a deeper, narrower weld, which can be desirable for certain applications where a strong, concentrated weld is required without excessive heat spread.

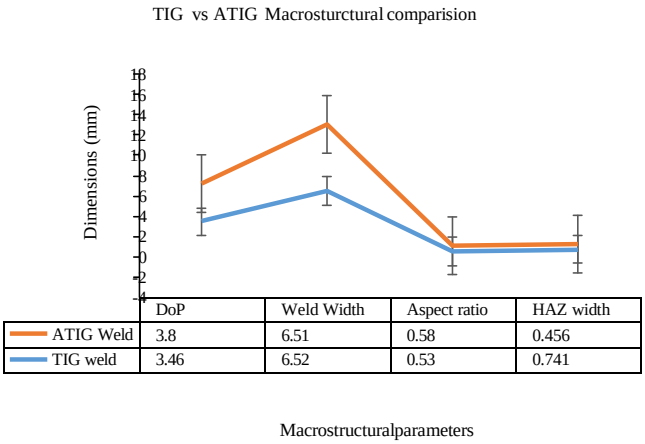

Figure 3: Variation bead characteristic with welding processes

3.2. Microstructure

The base metal SS202's microstructure is shown in Figure 4a. Grains were equiaxed and aligned randomly showing various constituent phases. In contrast, the TIG and ATIG welds have a specific weld bead microstructure showing the

development of various zones as shown in figure in 3b and 3c. No welding defects were present in the weld beads. Both the welding processes change the starting microstructure of base metal and created various zone owing to weld thermal cycle. Weld zone is just beneath the arc and subjected to highest temperature, sufficient to melt the base metal. Solidificaation of molten pool results in weld zone which exhibited cast dendritic grain structure. Next to weld zone, there is a region where base metal undergoes partial fusion leaving behind grains melted partially. This zone with partially melted grain is called partially melted zone and provide readymade nuclei for solidification of molten pool. On the other side of PMZ, base metal region is subjected to heating only thus changing the structure significantly. This region affected by heat only without melting is HAZ. Both the processes exhibited similar WZ and PMZ however different HAZ. HAZ grain structure is significantly coarser in case of conventional TIG then ATIG as evident in figure 4 b and c.

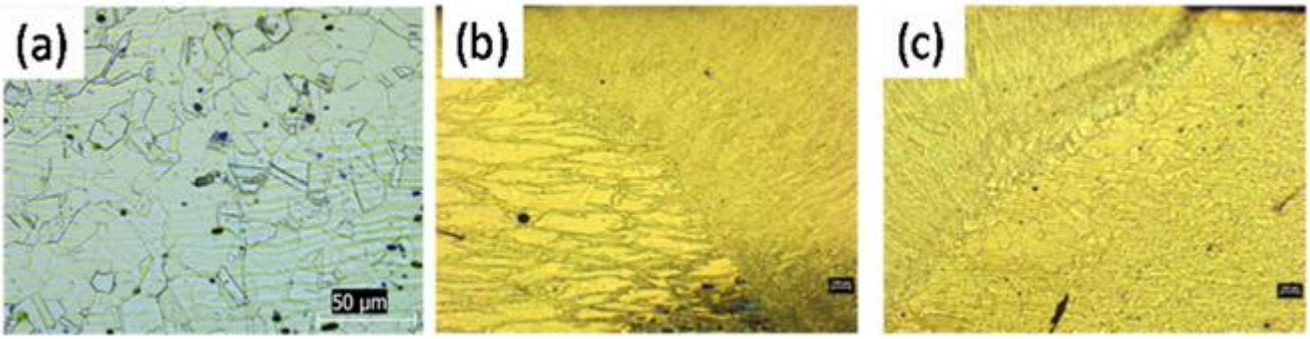

Figure 4 (a) Microstructure of base metal and (b) Region of Weld bead, HAZ and base metal under TIG weld & (c) ATIG weld

3.3. Mechanical Properties

Similar to bead morphology and microstructure welding processes is found to affect hardness and tensile strength of the bead on plate welds of SS202. Figure 5 depicts the variation bead hardness and tensile strength with the welding process. ATIG results in higher bead hardness and tensile strength than TIG process which are both indicators of improved mechanical properties in the final weld, making it stronger and more resistant to wear and deformation.

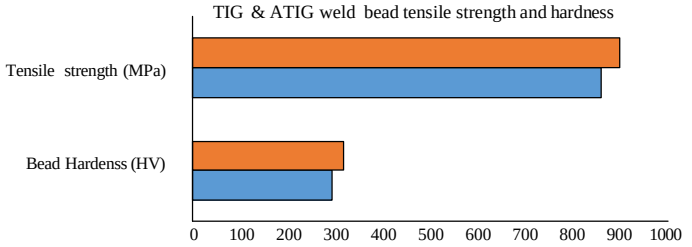

	Bead Hardenss (HV)	Tensile strength (MPa)
ATIG Weld	317	900
TIG weld	293	861

Figure 5: Variation of weld hardness and strength with welding processs

4. Conclusions

This study provides a comparative analysis of TIG and ATIG welding processes, highlighting significant improvements in weld quality and mechanical properties offered by ATIG welding. The findings indicate that ATIG produces a deeper and narrow weld than TIG. Surprisingly, weld size is found to be independent of welding process. Additionally, ATIG welds were stronger and harder than TIG welds. These results demonstrate that ATIG welding not only improves the mechanical performance of the weld but also minimizes heat-induced damage to the surrounding material, making it an ideal choice for applications requiring high-strength, precision welds. Future work could explore the optimization of ATIG process parameters to further enhance these benefits, as well as its application across different materials and industrial sectors. This study establishes ATIG as a promising alternative to traditional TIG welding, particularly in scenarios where weld strength and minimal thermal distortion are critical.

References

[1] Mulimbayan, F., & Mena, M. G. (2016). Comparative study of the corrosion behavior of low-nickel AISI 202 and conventional AISI 304 stainless steels in citric acid using electrochemical techniques. *Applied Mechanics and Materials*, *835*, 131–135.

[2] Effect of parameters on weld pool geometry in 202 stainless steel welded joint using tungsten inert gas (TIG) process. (n.d.).

[3] Baghel, A., Sharma, C., Rathee, S., & Srivastava, M. (2020). Influence of activated flux on microstructural and mechanical properties of AISI 1018 during MIG welding. *Materials Today: Proceedings*, *47*, 6947–6952.

[4] Schneider, C. F., Lisboa, C. P., de Almeida Silva, R., & Lermen, R. T. (2017). Optimizing the parameters of TIG-MIG/MAG hybrid welding on the geometry of bead welding using the Taguchi method. *Journal of Manufacturing and Materials Processing*, *1*(2), 1–17.

[5] Verma, V., Singh, A., Pandey, A. K., Sharma, C., Sonia, P., & Saxena, K. K. (2022). Experimental investigation of tensile properties and microstructure of TIG welded dissimilar joints of Al6061/Al5083 aluminium alloy. *Indian Journal of Engineering & Materials Sciences*, *29*(2), 262–270.

[6] Sharma, N., Abduallah, W. S., Garg, M., Gupta, R. D., Khanna, R., & Sharma, R. C. (2020). Optimization of TIG welding parameters for the 202 stainless steel using NSGA-II. *Journal of Engineering Research*, *8*(4), 206–221.

[7] Kumar, V., Rakesh, D., & Scholar, P. G. (2018). Optimization of TIG welding parameters for improvement of strength and hardness. *International Journal of Research in Engineering Applications and Management*, *4*(8), 8.

[8] Inoue, H., & Koseki, T. (2007). Clarification of solidification behaviors in austenitic stainless steels based on welding process. *Nippon Steel Technical Report*, *95*, 62–70.

[9] Singh, A., & Mittal, R. (2017). Experimental analysis on TIG welding process parameters of dissimilar metals SS304-SS202 using Taguchi method. *International Journal of Engineering and Manufacturing Science*, *7*(2), 249–258. Retrieved from http://www.ripublication.com.

[10] Bansal, A., Kumar, M. S., Shekhar, I., Chauhan, S., & Bhardwaj, S. (2020). Effect of welding parameter on mechanical properties of TIG welded AA6061. *Materials Today: Proceedings*, *37*(Part 2), 2126–2131.

[11] Baghel, A., Sharma, C., Rathee, S., & Srivastava, M. (2021). Proceedings: Influence of activated flux on microstructural and mechanical properties of AISI 1018 during MIG welding. *Materials Today: Proceedings*.

[12] Baghel, A., Sharma, C., Rathee, S., & Srivastava, M. (2021). Proceedings: Activated flux TIG welding of dissimilar SS202 and SS304 alloys—Effect of oxide and chloride fluxes on microstructure and mechanical properties of joints.

[13] Lu, S., Fujii, H., Sugiyama, H., Tanaka, M., & Nogi, K. (2002). Weld penetration and Marangoni convection with oxide fluxes in GTA welding. *Materials Transactions*, *43*(11), 2926–2931.

[14] Magudeeswaran, G., Nair, S. R., Sundar, L., & Harikannan, N. (2014). Optimization of process parameters of the activated tungsten inert gas welding for aspect ratio of UNS S32205 duplex stainless steel welds. *Defence Technology*, *10*(3), 251–260.

[15] Kulkarni, A., Dwivedi, D. K., & Vasudevan, M. (2018). Study of mechanism, microstructure, and mechanical properties of activated flux TIG welded P91 steel-P22 steel dissimilar metal joint. *Materials Science and Engineering A*, *731*, 309–323.

[16] Baghel, A., Sharma, C., Rathee, S., & Srivastava, M. (2020). Activated flux TIG welding of dissimilar SS202 and SS304 alloys: Effect of oxide and chloride fluxes on microstructure and mechanical properties of joints. *Materials Today: Proceedings*, *47*, 7189–7195.

[17] Abid, M., Parvez, S., & Nash, D. H. (2013). Effect of different electrode tip angles with tilted torch in stationary gas tungsten arc welding: A 3D simulation. *International Journal of Pressure Vessels and Piping*, *108–109*, 51–60.

[18] Baghel, A., Sharma, C., & Upadhyay, V. (2023). Optimization of process parameters for autogenous TIG welding of austenitic stainless-steel SS-304. *International Journal of Interactive Design and Manufacturing.*

[19] Baghel, A., Sharma, C., Singh, M. K., & Upadhyay, V. (2023). Modeling and optimization of bead geometry and hardness of bead on plate TIG welds of stainless steel SS202. *International Journal of Interactive Design and Manufacturing.*

[20] Assefa, A. T., et al. (2022). Experimental investigation and parametric optimization of the tungsten inert gas welding process parameters of dissimilar metals. *Materials*, *15*(13).

[21] Mishra, R. R., Tiwari, V. K., & R. S. (2014). A study of tensile strength of MIG and TIG welded dissimilar joints of mild steel and stainless steel. *International Journal of Advanced Materials Science and Engineering*, *3*(2), 23–32.

International conference on Smart Material, Manufacturing and Characterization Techniques – 2024

Paper ID: ICSMMCT-01056

Microstructure phases formation during firing of iron ore pellets –A surface morphology analysis

Gagan Kumar[1], Manoj Narwariya[2], Rakesh Prasad[3], Ganesh Pal Singh Jadon[4*]

[1]*M.Tech Scholar Mechanical Engineering Department, IPS College of Technology & Management, Gwalior, M.P. (474001)*
[2]*Professor, Mechanical Engineering Department, IPS College of Technology & Management, Gwalior M.P. (474001)*
[3]*Hindustan College of Science & Technology Farah Mathura U.P. India*
[4]*Assistant Professor, Mechanical Engineering Department, IPS College of Technology & Management, Gwalior M.P. (474001)*

Abstract

Microstructures are formed during the heating of iron ore pellets for heat hardening. Further required properties of pellets are dependent on various microstructure phases formation. Various phases of grain density Iron oxide phase density (IOPGD), Silicate grain density (SPGD), Pore phase density (PPGD)were studied for Cold compression strength (CCS) of pellets. For this optical images were analyzed through a tool to investigate the influence of the phase on pellets CCS. Pellets strength (CCS) is mainly dependent on slag phase bonding to hold iron oxides grains however higher pores structures fail to stabilize the structure.Various intermediate phases are also recoded like maghemite and wustite and higher temperature zone silicate melt is also responsible for the CCS of Pellets. Firing at 12000 C of pellet with 100 to 350 mesh no fineness of ore,pellets strength mainly dependent on slag and pores phase density but due 12000C is considered as low firing temperature slag phase is not taken under consideration.

Keywords: *Microstructure, Phases, Grain density, Iron ore pellets, Cold compression strength*

1. Introduction

Iron ore pellets are widely used in blast furnaces to produce pig iron. Due to the shortage of high-quality lump ore, the demand for iron ore pellets in steel production is increasing. The properties and behavior of iron ore pellets during agglomeration, and their use in blast furnaces, can be obtained by characterizing the microstructure. The most common mineralogy of iron ore can be identified with Reflective Light Microscopy (RLM) due to its unique reflectivity and is commonly used for the characterization of iron ores. RLM and digital image analysis are used as suitable tools for the characterization of these materials. Porosity and texture can be determined using this technique. Vale conducted a qualitative assessment to investigate the microstructure of low RLM iron ore grains concerning traditional quality parameters. Today, efforts are underway to develop RLM and digital image analysis between Vale and PUC Rio, establishing procedures for the qualitative and quantitative characterization of iron ore aggregates. Digital microscopy technology has been developed and used to enable this type of evaluation. These jigs puzzle scan samples with different diameters or cover the entire surface of the sample with a single image. Image analysis is then used to distinguish and measure the proportions of phase and porosity to establish their systematic spatial variation [1].

In the present work pellets which were prepared with iron ore fines in the form of balls. These balls were heated to high elevated temperature below melting point of iron ore. After cooling of these ball were tested for strength through crushing therefore this parameter is known as cold crushing strength CCS. In the present work it was investigated that the firing temperature 12000C is the optimum for this material and 100 to 350 mesh fineness provide enough strength.

2. Raw Materials for Blast Furnace Selection

2.1. Iron Ore Fines

The quality of iron ore balls also depends upon their chemistry if the iron ore is aluminous and siliceous again a secondary problem. The problem in making iron ore balls and their heat hardening at different temperatures decides the properties of iron ore pellets otherwise the desired properties of pellets will not be achieved. So this is very important to study the chemical behaviour of iron or balls during firing concerning various elements like MgO and CaO present inside the iron ore mixture [2].

The less than 1wt% of Al_2O_3 and higher-order more than 2 wt% is not suitable for pellets physical and physical-chemical properties. Similarly, SiO also should be in the nominal range as per the fineness of iron ore.

-1mm (30- 40%)

Published online on: ***February 01, 2025***
Corresponding Author's E-mail ID: ganeshjadon00@gmail.com

-3mm (35-38%)
+3,-5mm (28-45%)

Utilization of Iron Ore Fines, the Iron ore fines, which are produced as a waste material, can be utilized variously.

3. Objectives of the work

- Study of the effect of iron ore fine ness on the physical properties of iron ore pellets.
- Study of the microstructure of iron ore pellets during heat hardening by optical microscope
- Study of effect different phases pore phase and iron oxide phase formation and their impact on strength of pellets.
- Study of iron oxides, slag phase and pore phase grains density influence on CCS
- Study of grains distribution of various phases to explain pellets physical properties.

4. Methodology

4.1. Sample Collection

Indian iron ore from Kiruburu, Jharkhand has been chosen for the experiment, here ores around 100 mesh was taken and ground in a ball mill for variable mesh size. To prepare a perfect six fineness sample, sieves of 100, 150, 200, 250, 300, and 350 mesh were used.

Table 1

Chemistry (weight %)			
Fe	Sio_2	Al_2O_3	LOI
63.2	2.9	1.9	3.9

4.2. Sieve analysis

To confirm proper mesh size for study purpose to get optimal value of parameters for industrial prerequisite sieving help to make it feasible as shown in Fig. 1.

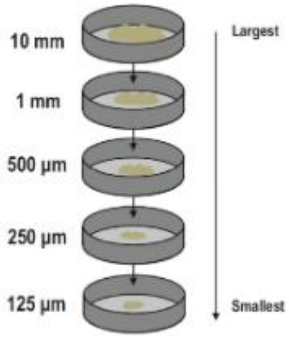

Fig. 1

4.3. Green Pellets Preparation

The iron ore and additives were mixed homogenously and then put inside the disc pelletizer to form balls of 8 to 18 mm diameter. Due to water sprinkler moisture amount had been introduced 8-10% of the total volume of pellets as shown in Fig 2.

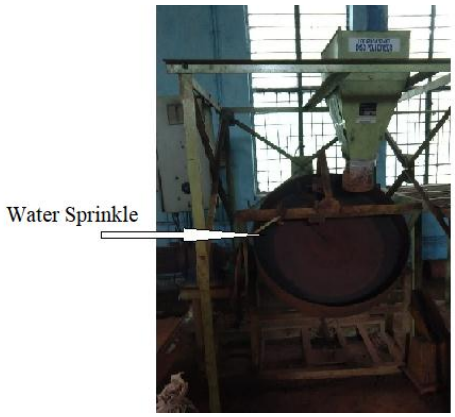

Fig. 2

4.4. Drying and Firing

After green ball formation heat hardening is proceeded in the RHF (raising hearth furnace). Pellets were fired at 12500C during its induration cycle.

For the use of pellets as raw feedstock in the blast, furnace pellets must have some porosity and cold compressive strength as well as some other properties but in the present work, only CCS and Porosity have been chosen. After firing roasted pellets were ready to test for CCS and characterization, as samples listed in the table 2.

. Table 2

Fired pellets	Pellet A	Pellet B	Pellet C	Pellet D	Pellet E	Pellet F
Mesh no	100	150	200	250	300	350
Sample	S1	S2	S3	S4	S5	S6

4.5. CCS testing and Specimen preparation for OM

Fired pellets were tested in the CCS testing machine for strength here 5 pellets in 3 batches were compressed and the average value of CCS was recorded. For further investigation characterization was aimed for this pellets were polished with sandpaper of 100 to 1200 grit size, after getting mirror polishing images were taken.

5. Pellets Characterization

Microstructure analysis through microscopic images is the popular technique to know inside the material to give a scientific explanation of physical properties dependencies. For this surface of a sample should be ground with emery papers of coarser to finer grit size and

Diamond polishing should be done for a better experience. An optical microscope is used to take a micrograph of a surface of pellets in 500 enlargements for 25 microns as shown in Figure 3.

For interpretation a technique is used to study; microstructure view on grayscale to bifurcate different phases from darker to lighter shades, pores to iron oxides respectively. For this thresholding is used to confine various phases in grey shades of phases such as pores in darker ones, moderate grey for slag phase and lighter for iron oxides. For this, a tool is used then the image of the micrograph is uploaded then a coloured image is converted to greyscale. After this area of interest has been confined then thresholding has been done based on prior experience. After thresholding particle analysis is done where a complete database has appeared on screen with full information of a particular typed phase grains size, area percentage, spheroidity, roundness etc at last a summary is given to take a note for fast assessment.

5.1. Optical images analysis

Phase confinement, their density and per millimeter distribution decide the physical properties of pellets. This is one of the simplest methods to study the separation study with their statics in the tabular form. Afterward graph has been plotted concerning CCS or any other physical properties which are to be studied.

In the present study phase of hematite, magnetite, silicate, porosity is considered for image analysis. For this image

analyser is used to analyse each phase of microstructure in the aspect of grain density, phase density was analysed for the optimum physical-chemical and physical properties. Because the properties always vary with the morphology and crystal structure of grains and phase existed and their thermal and composition stability. As shown in Fig 3. Optical microscopy images were taken for six types of pellets S1, S2, S3, S4, S5, S6.

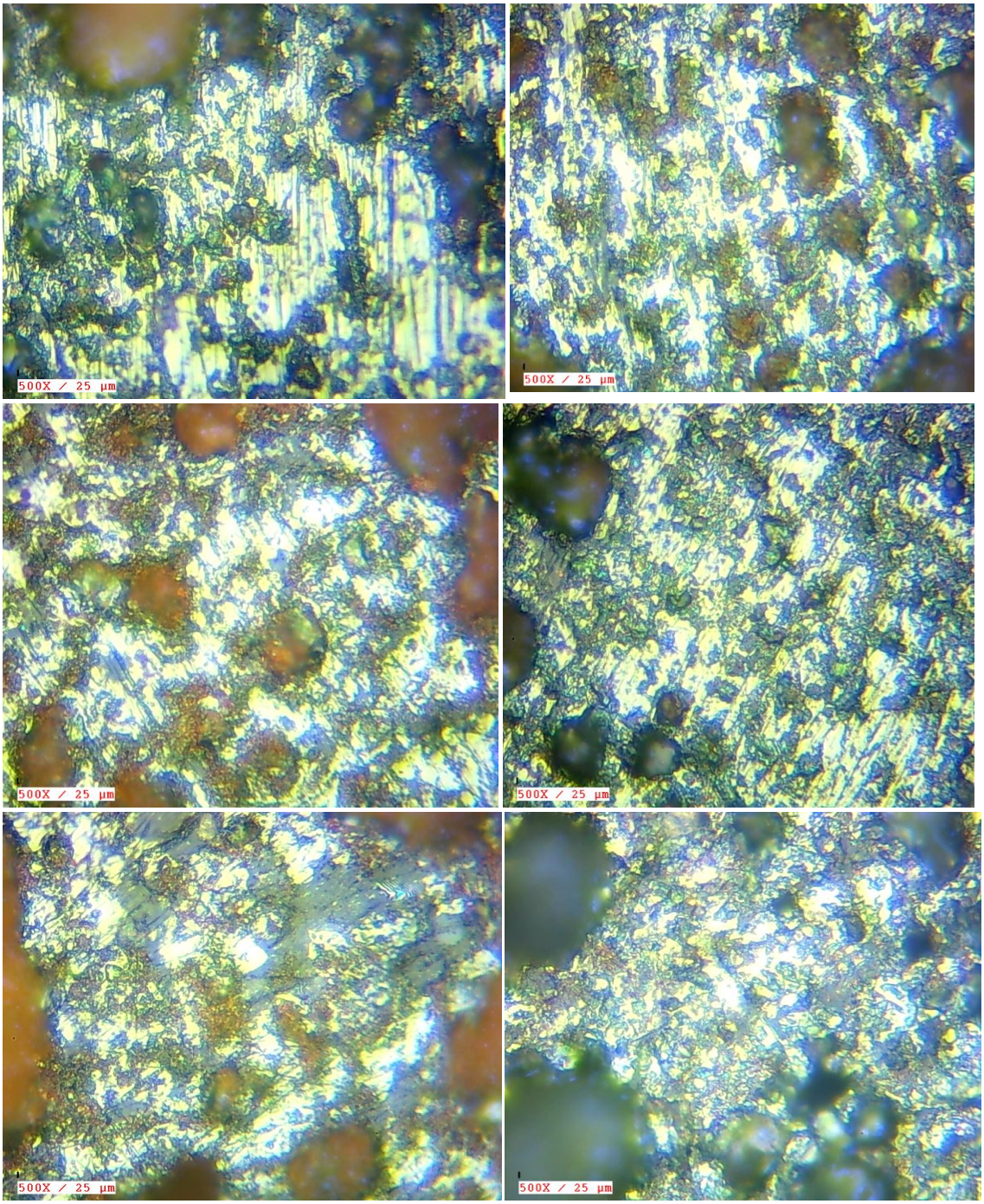

Fig. 3 Optical Images of Pellets S1, S2, S3, S4, S5 and S6

5.2. Image Analysis

A tool like ImagJ was taken for image processing to get thresholding for various phases here only two main phases pore (darker shade) and iron oxides (lighter shades) was used. Intermediate phase slag/silicate phase counted mathematically to save time here thresholding images with results are attached as per sample S1, S2, S3, S4, S5, S6 respectively on different pellets.

6. Result and Discussion

6.1. CCS

The grains packing and bonding phases between the ore grains provide compressive strength to pellets. Different grains mainly iron oxides are in the main matrix with 40% pores structure is formed and networking of this matrix is made by slag/silicate phases. The strength of pellets is tested by placing the sample on a fixed platform and moving pad lower down and crushed the pellets and reading of maximum applied KN load is recorded on a dial gauge. Noted readings of CCS of samples are tabulated in Table 3 and plotted on the graph shown in Fig.4.

Table 3

Sample	CCS(KN)
S1	2.4
S2	3.6
S3	4.1
S4	4.8
S5	5.2

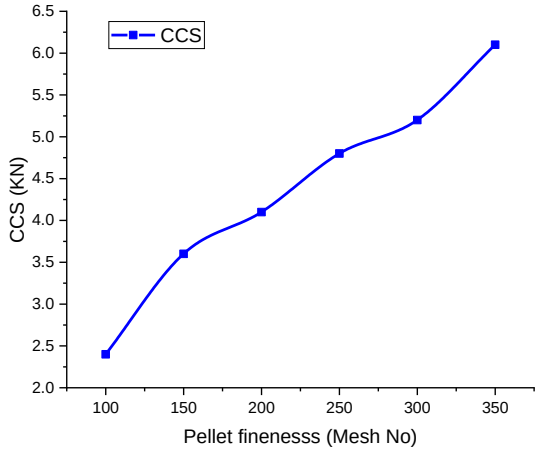

Fig.4 Fineness vs. CCS

As shown in Fig.4, CCS is increasing with increasing fineness of ore which shows compactness of grains in a matrix of slag/silicate phases with iron oxides are main particles with 40% pores. Here pores play an important role for CCS high the pores in the microstructure lower the strength becausethe structure of pellets become unstable to sustain iron oxides in the matrix with silicate bonding. As the pores will be more silicate bonding will not be stable and rigid to provide enough strength against crushing.Conversely, if higher porosity will reduce the reducing capability of pellet in blast furnace for the productivity of process and quality of iron as well [3]. Here CCS increases from 2.4 KN to 6.1 KN according to fineness inversely with pores phase decrement which will be showing in the next section of this report.

6.2. Grain Density

It is a very tedious task to evaluate pores size, their distribution, a percentage in silicate phase matrix and density also however with the image analysis of OM images an approximation can be done. This approximation is also validated with

the Optical Microscopic density result and duly asses by the ImageJ tool. Both the study affirms the physical testing result nicely. As shown in Fig.5 pore phase grain density decreases with increased fineness from 345 No. grains/ mm^2 PPGD to 151 No. grains/ mm^2 PPGD, towards higher fineness side pores density bit closer. This decreasing trend of PPGD shows strengthens of silicate matrix to retain all iron oxide within the network of slag bonding.

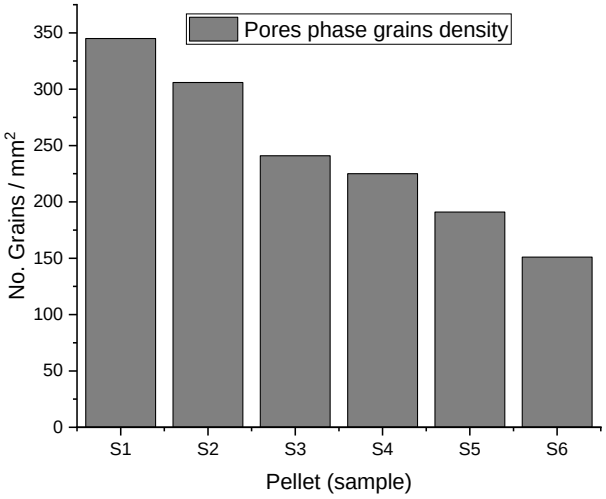

Fig.5 Pore grains density (PPGD)

Iron oxides grains phase are reinforced by slag matrix, silicate phase grains varied with heat treatment mainly as temperature goes up silicate phase get melt and weakening of pellets structure starts. Present work as the fineness increases slag phase (SPGD) increases proportionally and support more retention of iron oxides hence more strength of pellet. Here SPGD increases 182 No. grains / mm^2 to 758 No. grains / mm^2 corresponding to a fineness from 100 to 350 fineness of ores (S1 to S6) as shown in Fig. 6.

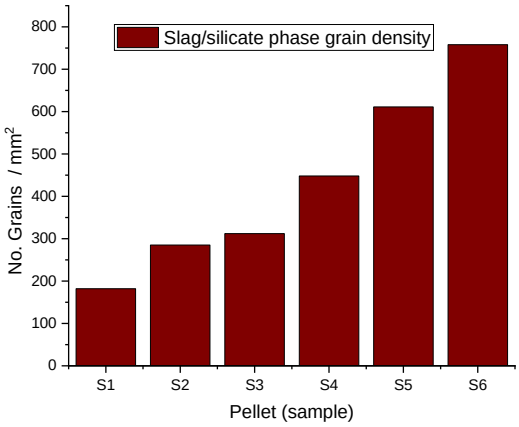

Fig. 6 Silicate phase grains density (SPGD)

Iron oxides are mainly hematite and magnetite phases are present in the silicate matrix more the number of oxides grains matrix network will be closely packed. In this situation, pellet stability at higher temperatures increases due to fuse bonding of iron grains with slag supports slag bonding along with oxide bonding to strengthening the structure of pellets. In the present study more fineness liberate more iron oxides grains which support high CCS but same time within the pellet structure reduction gas passage gets an abrupt and proper reduction of oxide during blast furnace operation get dissatisfactory [4-5]. As shown in Fig.7 IOPGD increases from 412 No. grains / mm^2 to 891 No. grains / mm^2 with increasing fineness.

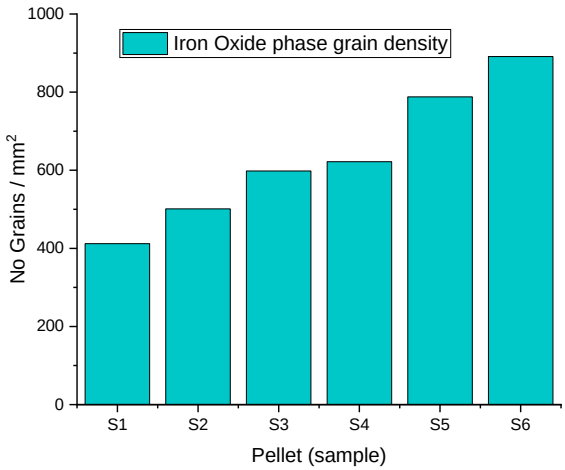

Fig. 7 Iron ore phase grains density (IOPGD)

Comparative study of phase percentage variability of pore and iron oxide obtained from image process shows the validation of analysis by tool ImageJ. As iron oxides phase percentage increases with fineness conversely pore phase grains percentage decreases to strengthen the structure of the pellet as shown in Fig.8.

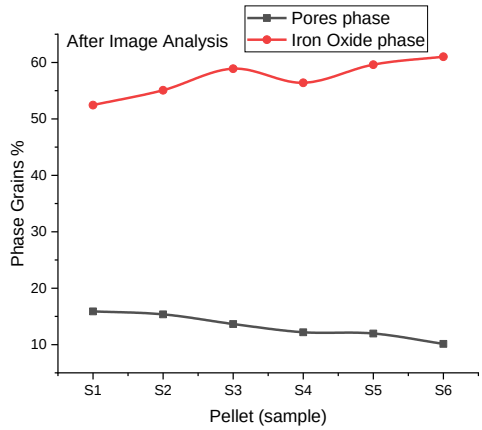

Fig. 8 Pore phase vs Iron oxide phase grains %

The recorded data for iron oxides phases' grain % with pore phase grains % is quite similar to variations obtained through ImageJ tool analysis, which shows that these facts support each other for the fulfilment of explanation of increases CCS with the fineness of ore [6-7]. Hence Fig. 9 is also included for the study of these main phase density calculations for verification of statement given through analysis of image processing by the software tool.

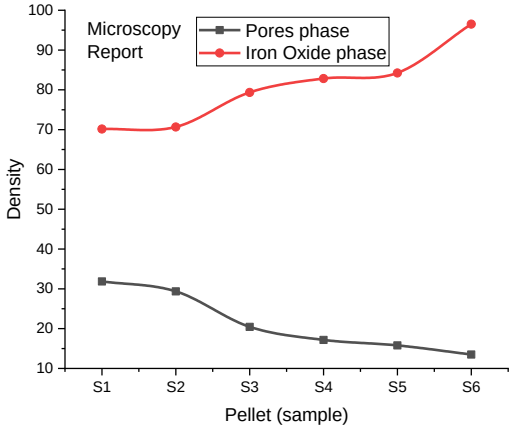

Fig. 9 Pore phase vs Iron oxide phase grains % (MR)

7. Conclusion

The following salient point related to this study is as follows.

(1) As per the fineness of ore, CCS varied proportionally due to increases iron oxides phase and silicate phase increasing at 12000C temperature.

(2) Phase grains density study for micrograph is a basic technique to define the physical properties of pellets.

(3) Pellets strength (CCS) is mainly dependent on slag phase bonding to hold iron oxides grains however higher pores structures fail to stabilize the structure.

(4) Various intermediate phases are also recoded like maghemite and wustite and higher temperature zone silicate melt responsible for CCS of Pellets

(5) Firing at 12000 C of pellet with 100 to 350 mesh no fineness of ore, pellets strength mainly dependent on slag and pores phase density but due 12000C is considered as low firing temperature slag phase is not taken under consideration but at the higher-order temperature, it has an important role to discuss strength.

References

[1] Pownceby, M. I., & Clout, J. M. F. (2003). Importance of fine ore chemical composition and high-temperature phase relations: Applications to iron ore sintering and pelletising.

[2] McCann, G., Strezov, V., Lucas, J. A., Evans, T., & Strezov, L. (2004). Iron ore characterisation during high-temperature thermal processing.

[3] Scarlett, N. V. Y., Madsen, I. C., Pownceby, M. I., & Christensen, A. N. (2004). In situ X-ray diffraction analysis of iron ore sinter phases.

[4] Mandal, A. K., & Sinha, O. P. (2015). Characterization of fluxed iron ore pellets as compared to feed material for blast furnace.

[5] Meyer, M., Lagoeiro, L. E., Graça, L. M., & Silva, C. J. (2016). Phase and microstructural characterization of iron ore pellet and their relation with cold crushing strength test.

[6] Koryttseva, A., Webster, N. A. S., Pownceby, M. I., & Navrotsky, A. (2017). Silico-ferrite of calcium and aluminum (SFCA) and SFCA-I phases form in iron ore sintering operations.

[7] Nicol, S., Chen, J., Pownceby, M. I., & Webster, N. A. S. (2018). A review of the chemistry, structure, and formation conditions of silico-ferrite of calcium and aluminum ('SFCA') phases.

[8] Liao, F., & Guo, X.-M. (2019). The effects of Al_2O_3 and SiO_2 on the formation process of silico-ferrite of calcium and aluminum (SFCA) by solid-state reactions.

International conference on Smart Material, Manufacturing and Characterization Techniques – 2024

Paper ID: ICSMMCT-01058

Examination of the Plan of Glass Fiber Strengthened Plastic Capacity Tank

Niranjan Singh Pawaiya[1] and Mr. Shatrughan Mishra[2]

[1,2]*Department of Mechanical Engineering, IPS College of Technology & Management, Gwalior, 474001,*

Abstract: There has been a outstanding rise within the request for composite materials in later a long time, ascribed to their different advantageous properties relative to other materials, counting chromium alloy . Glass woven mandering Fortified Plastics (GFRP) are a particular sort of composite fabric utilized within the development of capacity tanks. The central objective of this inquire about is to refine the plan of a vertical round and hollow capacity tank made from fiber strengthened plastic by altering the breadth of the round and hollow hull. The plan highlights a cover development that interchanges between stacks of fiberglass mat (CSM) and woven mandering (WM). The investigation is carried out utilizing ANSYS 19 program, and the discoveries for the GFRP capacity tank are compared with those of a comparative tank made from chromium- iron . This investigate is especially centered on the plan of a capacity tank for chemical fluids.

Keywords: *Glass Fiber Reinforced plastic; Capacity container; fiberglass mat ; WM.*

1. Introduction

Capacity tank are susceptible to significant inside pressures during operation, resulting in elevated stress levels. Ensuring the safety and reliability of these tanks is crucial due to the potential risks associated with high stress concentrations. Consequently, conducting a thorough stress examination is vital for evaluating the performance and guaranteeing the safe operation of capacity tanks. Glass woven mandering Fortified Plastics (GFRP) represent a distinct class of a combination of two or more materials, combining glass fibers as reinforcement within a resin matrix. Unlike traditional metallic materials, GFRP exhibits unique properties, falling between brittle and ductile categories. A key design consideration for GFRP is that breadth does not directly correlate with strength; instead, the quantity of glass content per unit weight is the determining factor. Additionally, plastic design necessitates incorporating high safety factors to account for variability in material behavior.

Modern engineering practices increasingly favor Glass Fiber Reinforced Plastics (GFRP) constructed with Epoxy Vinyl Ester Resins particularly in applications prone to chromium- iron corrosion. This material combination offers enhanced reliability and cost-effectiveness. While alternative materials may rival GFRP in upfront costs, their long-term maintenance expenses significantly inflate overall life cycle costs, making GFRP a more economical choice.

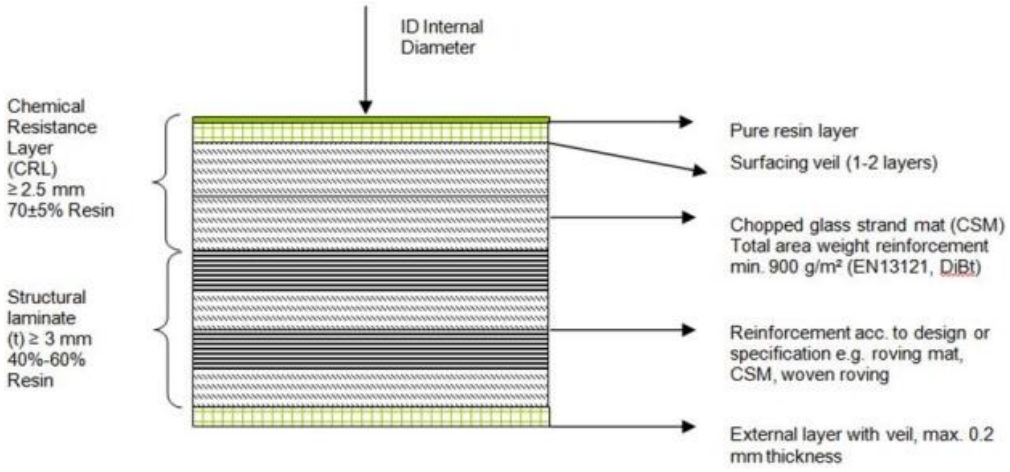

Fig. 1: Circular area of GFRP Materials [12].

The design and construction of tanks made from reinforced plastics, particularly those reinforced with glass fiber, have gained significant attention due to their potential advantages in terms of strength, durability, and lightweight properties. These materials are often employed in various industrial applications, such as water storage, chemical processing, and even

Published online on: ***February 01, 2025***
Corresponding Author's E-mail ID: niranjansinghpawaiya07@gmail.com

the storage of liquefied gases. A detailed review of existing literature highlights the importance of various design considerations, material properties, and the influence of different reinforcement strategies on the overall performance of Glass Fiber Reinforced Plastic (GFRP) tanks.

1.1. Standards for Glass Fiber Reinforced Plastic Tanks

British Standards Institution (1987) in BS 4994:1987 provides essential guidelines for the design and construction of vessels and tanks made of reinforced plastics. The standard emphasizes critical factors such as structural integrity, safety, and durability, specifically focusing on the materials used, construction techniques, and the potential challenges faced by reinforced plastic tanks. The proper application of such standards ensures that GFRP tanks can withstand high pressures and harsh environmental conditions while maintaining long-term performance. The document serves as a foundational reference for designing GFRP vessels, ensuring compliance with engineering best practices and material suitability.

1.2. Efficiency and Application of GFRP Tanks

Recent studies have highlighted the practical benefits of GFRP tanks, particularly in the context of rainwater harvesting. Kar and Gupta (2023) discuss the efficiency of GFRP tanks for storing rainwater, underscoring their advantages in terms of reliability and long-term sustainability. The study illustrates that GFRP tanks offer a cost-effective and efficient solution for enhancing water resources, particularly in regions with limited water availability. The lightweight and corrosion-resistant properties of glass fiber-reinforced polymers make them an ideal choice for this application, as they ensure the durability of the tanks over prolonged use.

1.3. Design and Optimization of Composite Pressure Vessels

The design of pressure vessels made from composite materials such as GFRP has been a subject of interest in several studies. Nair et al. (2015) provide a detailed analysis of laminated pressure vessels, exploring the optimal configurations that can enhance their structural strength. Their work discusses the benefits of using multiple layers of materials to resist internal pressures, ensuring the vessel's integrity. Similarly, Sonachalam and Ranjit Babu (2015) focus on the optimization of composite pressure vessels, looking at factors such as the layering and orientation of fibers to achieve maximum strength and resistance to failure under different loading conditions.

The optimization of such vessels is critical to improving their overall performance. Several parameters, including material type, fiber orientation, and manufacturing methods, significantly affect the vessel's ability to handle high-pressure environments. This research is crucial in understanding the underlying mechanics of GFRP tanks and how to maximize their efficiency for different applications.

1.4. Mechanical Properties and Reinforcement Techniques

The mechanical properties of GFRP materials are of particular importance when considering the design of tanks. Puttegowda (Year) explores how the reinforcement of GFRP with materials such as sisal fibers, epoxy resins, and graphite fillers can enhance its wear resistance and mechanical properties. The combination of glass fibers and other reinforcements not only improves the strength but also increases the tank's resistance to environmental degradation, thereby extending its service life.

In a similar vein, Garg et al. (2023) focus on the enhancement of mechanical performance in E-glass fiber epoxy composites by incorporating coal-derived graphene oxide. This research indicates that such reinforcement strategies can significantly increase the tensile and flexural strength of GFRP, which is critical for the structural reliability of tanks subjected to varying loads and environmental conditions.

1.5. Residual Strength and Long-Term Durability

Long-term performance and the residual strength of GFRP tanks are vital considerations when designing for prolonged use. Russo et al. (2015) conducted residual strength testing on pultruded GFRP material under various temperature cycles, evaluating the material’s response to environmental changes. The study concludes that GFRP materials maintain their integrity over time, even under varying thermal conditions, making them suitable for applications where temperature fluctuations are a concern.

Furthermore, Erdemli Günaslan et al. (2014) discuss the properties of GFRP materials used in strengthening applications. Their findings underscore the versatility and reliability of GFRP in structural applications, emphasizing that these materials can effectively reinforce existing structures while maintaining high performance.

1.6. Application in Specialized Storage Systems

The application of GFRP materials in the storage of specific substances, such as liquefied gases, is another area of interest. Tripathi et al. (2017) investigate the design and analysis of composite cylinders for storing liquefied gases, emphasizing the need for specialized designs that ensure the safety and integrity of the storage system. The study highlights the role of GFRP in offering a lightweight and durable alternative to traditional materials, especially in the context of high-pressure applications.

Additionally, Bhavya et al. (2012) conduct a failure analysis of composite cylinders, identifying potential failure modes and proposing solutions to mitigate risks associated with composite pressure vessels. Their research is instrumental in understanding the limits of GFRP materials and how design modifications can improve the overall safety and performance of GFRP tanks.

The literature reviewed demonstrates the critical role of GFRP materials in the design and construction of tanks and vessels, with particular emphasis on the structural integrity, durability, and efficiency of these systems. The combination of glass fibers with epoxy resins and other reinforcing materials offers significant advantages in terms of mechanical properties, wear resistance, and resistance to environmental degradation. Advances in the understanding of GFRP materials continue to enhance their application in a wide range of industries, from water storage to chemical processing and gas storage. Future research should focus on optimizing the design parameters, improving manufacturing processes, and further exploring the long-term performance of GFRP tanks to ensure their reliability and sustainability in various demanding applications

2. Structure

2.1. Research Methodology

Determining the data of chromium- iron Capacity tank.

In this research, the design specifications of chromium- iron capacity tank are defined in table 1

Table 1: Format for Capacity steel container.

TYPE	**Hull cylindrical, Top cone 15°, Flat bottom**
Design Temperature	Less than 90°C
Design Pressure	Hydrostatic pressure
Specific Gravity	1.839
Tank Dimension	3000mm x 4000mm
Tank breadth	15.85 mm

2.2. Investigation of chromium- iron capacity tank agreeing to the identification.

In this investigate, modeling of the chromium- iron tank having over determinations is done utilizing analysis software. Figure 2 specify of the demonstrate is done utilizing ANSYS software computer program for deciding the distinctive stretch actuated within the container.

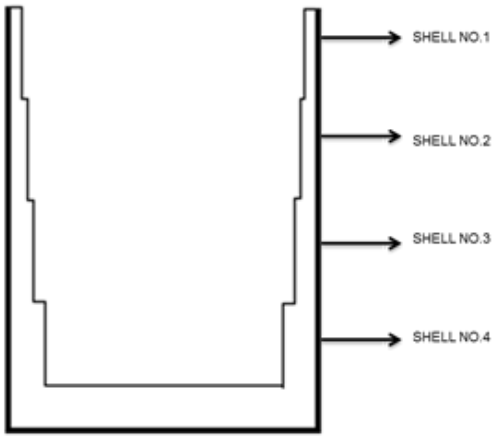

Fig. 2 Variable breadth of hull

2.3. Plan of all around and hollow glass fortified plastic capacity container.

Step 1: To begin with, I Preferred that the container is made up of 4 courses each of external breadth 300 cm and the breadth changing from top to bottom. Stature of all direction is 100cm.

Step 2: Estimation of breadth of hull for different direction.

Breadth of hull =∑ [Number of stacks (n) x Mass of support / singal range (m) x Breadth of fiber (t)]

Overlay Plan: [ONE]

UZCSM * mCSM * nCSM + UZWR * mWR x nWR ≥ Constraining stackCapacity (Q)

UZ = Plan stacking (N/ per kg/m2 of Fiber)

The stack constrained admissible unit stacking UL = u/k, k = plan figure. About scene, the esteem of k is treat as 11.98 (i.e.) 12.

Stretching is εd= 0.118%

The stretching restricted admissible singal stacking US = XZ xεd

Here, XZ = singal factor (N/mm per kg/$m$of fiber)

Now vl is more than vs at that specified space vZ is goes up tthen this equction will be opposite.

Mat 1. v = 2.0 N/cm every kg/m2 of fibre

Mat 2.v = 2.5 N/cm per every/ m2 of fibre

Breadth of fiber (t) is taken as:

For 450 CSM = 2.5 mm every kg/m2 of fibre

For 610 WR = 1.6 mm every kg/m2 of fibre

All around every singal Stack estimation (E):

Static fluid weight at container foot, rho = rho gh/104 N/ cm2 where rho = breadth of fluid put away, g = speeding up by the earth force, h= stature of fluid bracket.

For not stable stature, E = pr N/cm where, r = distance across of hull.

Consider cover development, as one of the two options:

For Cover No. 1,

n= number of stacks of 450 mat 1

n= number of stacks of 610 mat 1

$19.11n \geq Q$ (Eq. 1)

For Cover No. 2,

n = number of stacks of 450 mat 1

n - 1 = number of stacks of 610 mat 2

$19.11n \geq Q + 11.61$ (Eq. 2)

Table 2 Breadth of hulls founded

Portion	BREADTH (MM)	No. of FGM Stacking	No. of Mandering stacking
HULL NO.1	9.077	3	2
HULL NO.2	11.178	4	3
HULL NO.3	13.279	5	4
HULL NO.4	17.481	7	6

The Two stack are laid then again in such a way that the surrounding stack is of 450.2 CSM. In expansion to this, a add up to of 1.50 KG/M2 of CSM is conveyed on Two sides.

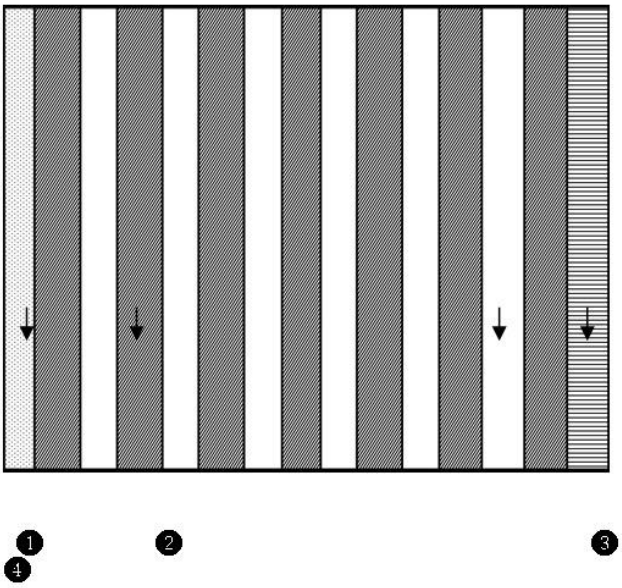

Fig. 3 Cover stacking

1. Reactive Property stopper.
2. fiberglass mat
3. Meandering piece
4. Outside stacking onsurface with authoritative particles.

Step 3: Calculating the value of bottom and top breadth.

Bottom breadth is break even with of most extreme breadth of the hull at foot =1.74802 cm
Consider knuckle support at the base corner. This breadth is half of the base breadth = 0.9001 cm
Therefore, add up to breadth at base = 1.74802+0.9001 =2.64803 cm.

Up breadth ought to be capable to require stack all faculty andl less auxiliary stack.
taken cover breadth as 1.4cm.

Examination of glass fortified material capacity container concurring to the over comes out selected.

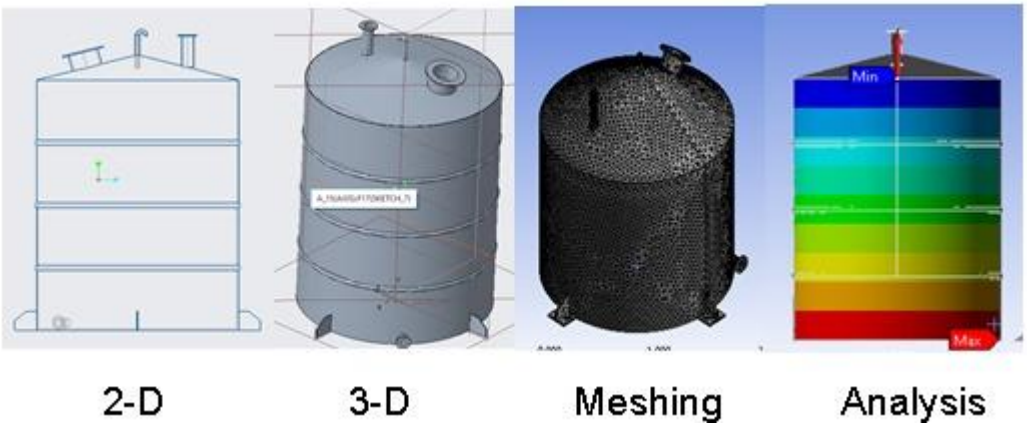

Fig. 4 General Process

By investigate, form of the fiber strengthened material capacity container known over determinations is find utilizing design analysis Program.

Checked the demonstrate is find utilizing design program deciding the diverse stretching actuated within container.

3. Result

All Miss-happening in glass strengthened material capacity container:-

Greatest distortion gotten within the GFRP capacity tank is rise to 0.096389 cm.

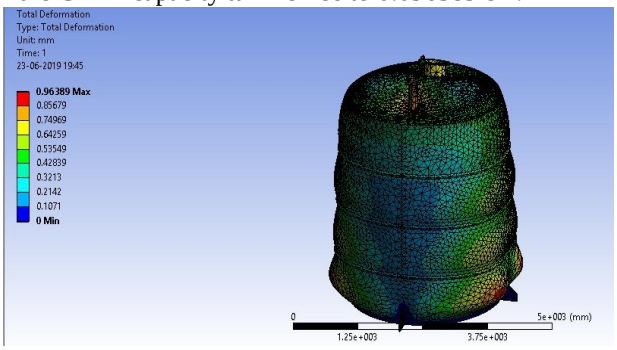

Fig. 5 Add up to deformation

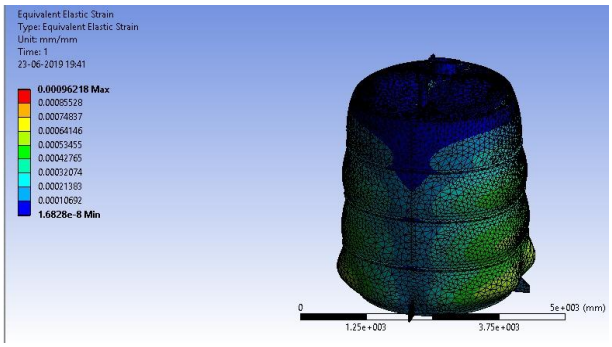

Fig. 6 Proportionate Versatile stretch for GFRP container

- Same as Flexible Stretch in Fiber strengthened material capacity
- Maximum Foremost Versatile Strain in Fiber strengthened material capacity container

- Identical versatile stretch within the GFRP capacity container is rise to to 0.00096218

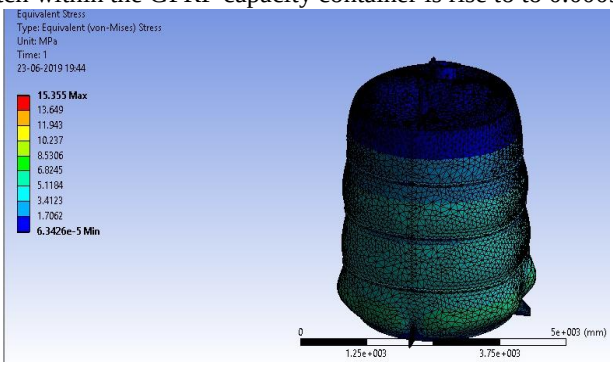

Fig. 7 Most extreme Vital Flexible strain for GFRP tank

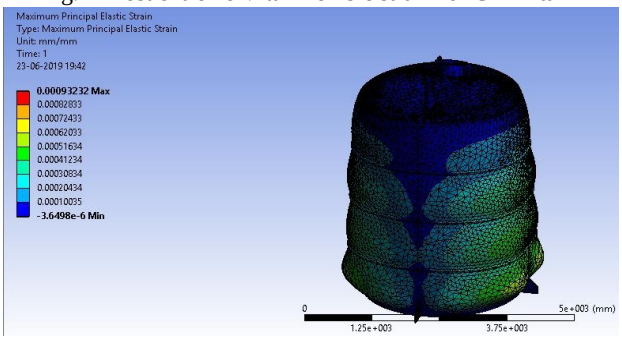

Fig. 8 Most extreme Shear Versatile stretch for GFRP tank

- Highest Shear Versatile Stretch in GFRP strengthened
- Identical Push in GFRP capacity container:
- Material capacity container:

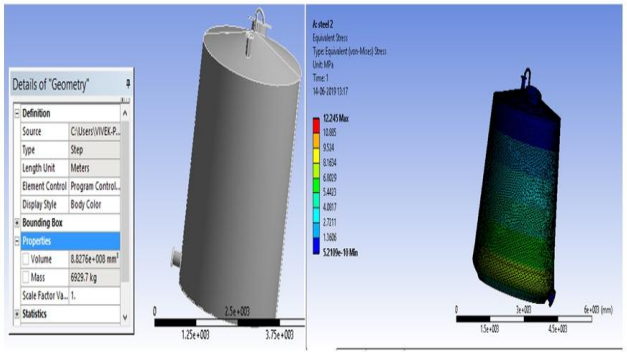

Fig 9 Proportionate stretch GFRP tank

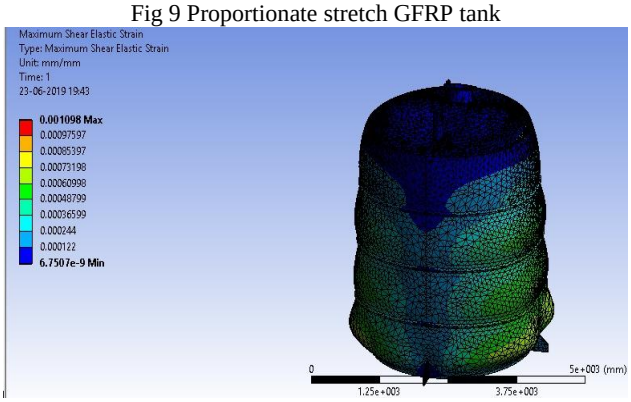

Fig 10 Mass and stresses for GFRP tank

- Strength in stainless steel capacity tank:

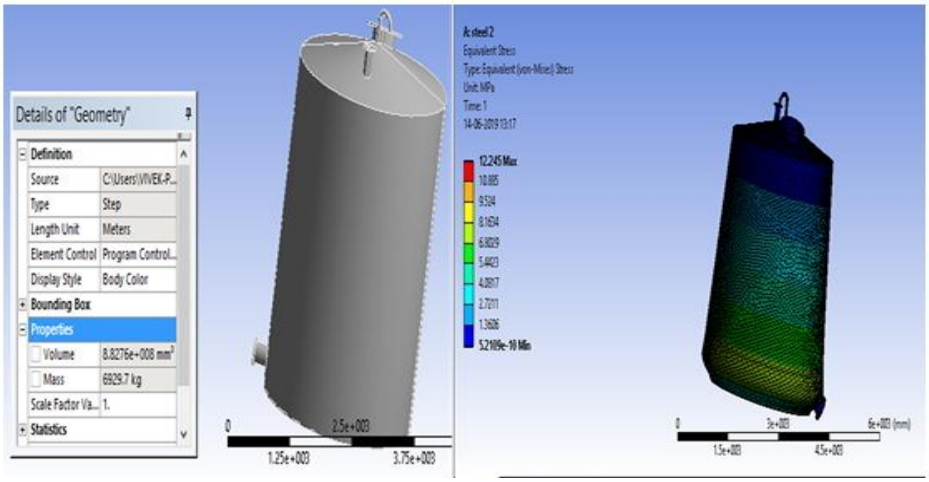

Fig. 11 weight and stretch on chromium- iron capacity tank

4. Conclusion

In this Information Book indicates that the laminate's greatest admissible strain is 1.3εd. The investigation demonstrates a most extreme strain of 0.001098 mm/mm, which is lower than the admissible edge. In this manner, the proposed plan is considered substantial.

Comparative analysis reveals that FRP capacity tanks boast an impressive strength-to-weight ratio of 673.961 Pa/N, significantly outperforming chromium- iron tanks at 180.125 Pa/N. This notable difference highlights the enhanced durability and lightweight benefits of FRP tanks, making them an attractive option for construction projects.

The installation costs of FRP capacity tanks are significantly lower than those of chromium- iron tanks. Furthermore, FRP tanks boast minimal maintenance needs and straightforward inspection procedures. Their relatively low weight also streamlines transportation, providing an advantage over traditional chromium- iron tanks

References

[1]. British Standards Institution. (1987). *Design and construction of vessels and tanks in reinforced plastics* (BS 4994:1987).

[2]. Kar, S., & Gupta, R. (2023). Efficiency of a glass fiber-reinforced polymer (GFRP) tank in pursuit of reliable water resources through rainwater harvesting. *Environmental Engineering & Management Journal (EEMJ)*, 22(1), 85.

[3]. Nair, L., Arasu, Y., & V. S., I. (2015). Design of laminated pressure vessel. *International Journal of Science and Research (IJSR)*, 4(8).

[4]. Puttegowda, M. (Year). Enhancing wear resistance, mechanical properties of composite materials through sisal and glass fiber reinforcement with epoxy resin and graphite filler. *Journal of the Indian Chemical Society*, 101(10).

[5]. Paul Ayyampilli, S., & Suresh, R. (2024). Study on mechanical and flammability properties of natural fibre polymer composites. *CE Publishing collections, Emerald Publishing*.

[6]. Sonachalam, M., & Ranjit Babu, B. G. (2015). Optimization of composite pressure vessel. *International Journal of Science and Research (IJSR)*, 4(3).

[7]. Priyashagadevan, M., & Kalaiarasi, K. A. (2017). Experimental investigation on strength behaviour between GGFRP & steel bars reinforced in columns. *International Journal of Science and Research (IJSR)*, 7(6).

[8]. Garg, A., Basu, S., & Mehta, R. (2023). Enhancing the mechanical performance of E-glass fiber epoxy composites using coal-derived graphene oxide. *Journal of Polymer Composites*, 10.

[9]. Namala, K. K. (2023). *Materials Today: Proceedings*, 43(1).

[10]. Erdemli Günaslan, S., Karaşin, A., & Öncü, M. E. (2014). Properties of GFRP materials for strengthening. *IJISET - International Journal of Innovative Science, Engineering & Technology*, 1(9).

[11]. Russo, S., Ghadimi, B., Lawania, K., & Rosano, M. (2015). Residual strength testing in pultruded GFRP material under a variety of temperature cycles and values. *Composite Structures*.

[12]. Schneider, G., & Woerth, O. (2017). The use of GFRP (fiberglass-reinforced plastic) in phosphate fertilizer and sulphuric acid processes. *NIGIS, CORCON*, Paper No. CCFI12.

[13]. Schneider, G., & Woerth, O. (2017). The use of GFRP (fiberglass-reinforced plastic) in phosphate fertilizer and sulphuric acid processes. *NIGIS, CORCON, Paper No. CCFI12*.

[14]. Tripathi, A., Kumar, A., & Chandrakar, M. K. (2017). Design and analysis of a composite cylinder for the storage of liquefied gases. *IJSRD - International Journal for Scientific Research & Development*, 5(3).

[15]. Bhavya, S., Kumar, P. R., & Abdul Kalam, S. (2012). Failure analysis of a composite cylinder. *IOSR Journal of Mechanical and Civil Engineering (IOSR-JMCE)*, 3(3).

International conference on Smart Material, Manufacturing and Characterization Techniques – 2024

Paper ID: ICSMMCT-01063

Consequence of Sliding Distance and Load on Wear Behaviour of Epoxy Composite Filled by Spherical Alumina Nanoparticles

Arvinda Kumar Pandit[1], Vijay Verma[2], Vijay Kumar Dwivedi[3]

[1]*FIT Engineering College, Meerut, India - 250001*
[2]*Bundelkhand Institute of Engineering and Technology, Jhansi, India – 284128*
[3]*GLA University, Mathura, India – 2814062*

Abstract

Epoxy alumina composite containing a low (0.5 wt.%) weight fraction of alumina reinforcement was fabricated by solid solution method. Ultra-sonication process is used to disperse for uniform mixing of alumina nanoparticles in the epoxy. The spherical-shaped alumina oxide with varying dia. from 27-43 nm was used in the study. Friction and sliding wear behavior were evaluated by tribometer according to ASTM standard G-99. Two sliding distances were taken in the present investigation as 2000 m and 4000 m. Applied load and sliding velocity were kept constant during study at 20 N and 1.26 m/sec respectively.

Keywords: *Coefficient of Friction, Adhesive Wear, Alumina Oxide, Nanocomposite.*

1. Introduction

Two-particle wear is defined as the deprivation of a material by the removal of tiny particulates from the work surface. Limitation of crafting properties in metals, the polymer becomes the modern choice of designers for structural purposes. High specific strength and specific modulus relative to metals and alloys attracts giants of sector such as automotive, aerospace, military, and etc. for using polymer composites. High specific surface area of nano size fillers will impart ultimate properties and its variation in polymer nanocomposites. At same level of filler content, the number and specific surface area of nano filler is exponentially high will have higher interfacial region relative to micro-composite and unblended polymer. This will also lead to higher improvement in mechanical and other physical properties. Several types of fillers can be blended in the polymer matrix to improve the performance of the polymer composite [1-7]. The engineering structure often has some relative movement between mating parts. Asperities or roughness on the matting surface results in friction. Friction leads to wear or degradation of counter components and finally failure results in these components.

In a compressive study, Osterle et al. suggest wear debris is a vital part of attaining the preferred friction coefficient. The author further suggested that course wear particles eject from the matting surface more easily compared to fine wear debris particles. Course wear particles result in high wear loss compared to fine wear debris. Fine wear debris may result in three-particle wear in place of two-particle wear, thus accelerating wear further [8]. Verma and Tiwari in their investigation come out with the suggestion that rod shape filler is inferior compared to spherical filler and leads to reduce wear of composite with spherical filler. The decreased wear rate is reported due to the rolling of the spherical particles and behaving as nano balls between matting surfaces resulting in reduced plowing of material from the counter [9]. Carbon filters also decrease the sp. wear rate and the COF of epoxy composites. Decrease of more than 30% in specific wear rate and the coefficient of friction was recently reported by Sharma et al. in their study, with the addition of 1 wt.% graphite nanoparticles (GNP) in glass fiber-filled epoxy composite. Increase of resistance to wear was accounted to formation of an interlayer of graphite between the counter surface. The GNP also reduces the fiber pullout and matrix fracture as the reasons for improved wear resistance of the epoxy composite [6].

Brown concluded that tensile stiffness and strength improve with by nanofiber alumina particles filler. He also found that the nanofibers exhibit better-reinforcing efficiency than mono-dispersed sphere-shaped silica and other nano scale composite filler by CNF or sphere-shaped alumina particulates [10]. Chang et al. investigation reported that the sp. wear of PEI reduces by addition of SCF and graphite flakes. The addition of fibers exhibited better wear resistance. Also, the frictional coefficient and contact temperature reduce on adding TiO2 [11]. Jakab et al. in their investigation report that the self-lubricating property of the fillers will decrease sp. wear of polymer composes. The size of reinforced filler particles influences the wear rate as courser reinforced particles decrease the metal removal on account of the higher interfacial bond between filler and matrix. Whereas fine lesser size filler particles may enhance the wear rate due to plowing and forming bigger discontinuities of the work surface [7]. Generally, the filler content i.e. wt.% concentration of filler in

Published online on: ***February 01, 2025***
Corresponding Author's E-mail ID: vijay020180@gmail.com

polymer composite will improve the wear resistance and coefficient of friction of the polymer composite. [12]. The sp. wear of polymer composites can be governed by the load applied, sliding velocity, and sliding distance. The reinforcement of ceramic particles in the binary and hybrid composite will improve the tribological property of the polymer composite. The wear resistance will improve with increasing wt.% reinforcement of filler with homogeneous dispersion. If the concentration of filler increases beyond an optimum limit the agglomeration of filler will adversely affect the wear behavior of polymer composite [13–15]. Erosion resistance increase linearly for both the cylindrical and spherical fillers of Al2O3 and resistance to erosion increases with addition of cylindrical compared to spherical [16].

Based on the available literature we can say that the behavior of polymer composite will be affected not only by the wt.% concentration of reinforcement. The sliding distance, load, and rubbing velocity will also govern wear resistance of polymer composite. Present paper investigates the effect of sliding distance, the load applied, and the sliding velocity of wear behavior of epoxy filled by low wt.% of alumina nanofiller..

2. Experimental

2.1. Material:

In the present study, mixture of epoxy LY 556 and hardener HY 951 is used as matrix which were supplied by Singhal Chemicals, Meerut. Specific density of Epoxy LY 556 and Hardener HY 951 is 1.10 gm/cm3 and 0.98 gm/cm3 at 25°C respectively. The mixing ratio is constant at 10:1. The filler material used is Alumina Oxide (Al2O3) which was supplied Nanoamor Inc. USA. The average size of filler particles is 27-43 nm

2.2. Method:

The epoxy composite was prepared by mixing epoxy with nano Al2O3 powder by solid solution method. Homogeneous dispersion of filler is achieved by an ultra-sonication process for 60 minutes. The hardener is then mixed into the solution and then the mixture is poured in an acrylic mold. The mold is left for 24 hrs. for curing after that heated at 100°C for 4 hours to complete curing. The samples were prepared from the composite as per the ASTM G-99 for the pin-on-disk test. Two sliding distances were taken in the present investigation as 2000 m and 4000 m. The applied load and sliding velocity are kept constant at 20 N and 1.26 m/sec respectively. The weight for weight loss was measured to determine the specific wear rate.

3. Results and Discussions:

Table 1 shows the summary of the test parameters and compiled values of the results achieved after testing. Wear rate and specific wear were calculated from the data by using the standard equation [6-7,9]. From the table 1, it is clear that on increasing the rubbing distance the sp. wear also decreases. Coefficient of friction for unfilled epoxy enhances a little bit but for composite, it will decrease with an increase in sliding distance.

Table 1 shows summary of wear test parameters and results for 2000 m and 4000 m sliding distances.

Sample Name	Sliding Distance	Intital Mass	Final Mass	Mass Loss	Specific Wear	Mean COF
Unfilled Epoxy	2000	5.7255	5.7218	0.0037	1.19E-07	0.500
	4000	5.7167	5.7114	0.0053	8.49E-08	0.58
0.50 wt% Spheical composite	2000	5.7017	5.7006	0.0011	3.53E-08	0.57
	4000	5.6941	5.6867	0.0074	1.19E-08	0.33

Figure 1 illustrates graphical deviation of sp. wear with rubbing distance for unblended epoxy and 0.5 wt.% composite. Decrease in sp. wear might a result of formation of a stable transfer layer between the test specimens and the counter material. The decrease in wear is more with composite might be due to the reinforcement of ceramic material in the epoxy matrix.

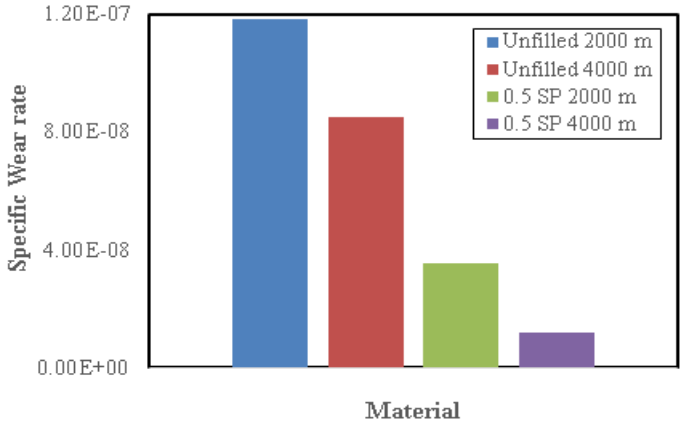

Fig. 1 Illustrates the behavior of Sp. wear by various material and rubbing distance

Figure 2, shows variation of COF with sliding distance and material. From the graph, it is clear that as the sliding distance of unfilled epoxy increases, the coefficient of friction (COF) decreases. This may be due to the change in the shear rate. With the increase in sliding distance, the layer materialization is extra constant, with reduced quantity of craters were visualized. In the same way, as the sliding distance of 0.50wt% spherical reinforced alumina oxide increases, the coefficient of friction (COF) decreases. This is due to the reason that due to the increase in the sliding distance, smoothening of the surface is caused due to the detachment of the spherical-filled alumina oxide. The unattached material will now roll between the two mating surfaces thereby reducing the contact surface area.

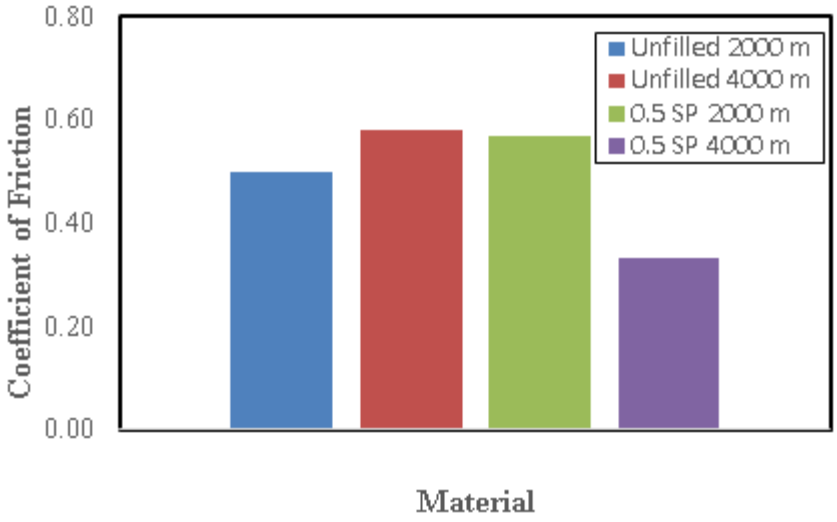

Fig. 2 illustrates the behavior of COF with material and rubbing distance

4. Conclusions

Epoxy composite is fabricated with the addition of 0.5 wt,% of Al2O3 filler. Based on the study following are the main conclusions.

- Increasing the sliding distance will decrease the Sp. wear rate of unblended and Al2O3 blended epoxy composite.
- Coefficient of friction decreases with increase in sliding distance for composite.
- In the case of unfilled epoxy, the COF increases with sliding distance due to increased roughness.

Acknowledgements

The author acknowledges the support and cooperation of Prof. (Dr.) Quasim Murtaza, DTU for allowing to perform experiment in the Manufacturing Lab.

References

[1]. Shukla, D. K., Sonia, P., & Verma, V. (2013). Applied mechanics and materials, 390, 557-561.
[2]. Verma, V., Shukla, D. K., & Kumar, V. (2014). Procedia materials science, 5, 669-678.
[3]. Verma, V., Sayyed, A. H. M., Sharma, C., & Shukla, D. K. (2020). Journal of polymer research, *27*(388). https://doi.org/10.1007/s10965-020-02359-z
[4]. Verma, V., & Sharma, C. (2020). Theoretical and applied fracture mechanics, *110*, 102807. https://doi.org/10.1016/j.tafmec.2020.102807
[5]. Shivhare, Y., Narwariya, M., Sharma, C., Verma, V., & Pandey, A. K. (2022). IJERMCE, *9*(6), 37-41.
[6]. Sharma, N., Kumar, S., & Singh, K. K. (2022). Tribology international, *172*, 107580. https://doi.org/10.1016/j.triboint.2022.107580
[7]. Jakab, B., Panaitescu, I., & Gamsjager, N. (2021). Polymer testing, *100*, 107243. https://doi.org/10.1016/j.polymertesting.2021.107243
[8]. Österle, W., Dörfel, I., Prietzel, C., Rooch, H., Cristol-Bulthé, A.-L., Degallaix, G., & Desplanques, Y. (2009). Wear, *267*, 781–788. https://doi.org/10.1016/j.wear.2008.11.023
[9]. Verma, V., & Tiwari, H. (2020). Proc. IMechE Part J: Journal of engineering tribology, 1–13. https://doi.org/10.1177/1350650120970433
[10]. Brown, G. M., & Ellyin, F. (2011). Journal of applied polymer science, *119*, 1459–1468. https://doi.org/10.1002/app.32662
[11]. Chang, L., Zhang, Z., Zhang, H., & Friedrich, K. (2005). Tribology international, *38*, 966–973. https://doi.org/10.1016/j.triboint.2005.07.026
[12]. Krishnudu, D. M., Reddy, P. V., Sreeramulu, D., & Reddy, R. V. S. (2023). Hybrid advances, *3*, 100040. https://doi.org/10.1016/j.hybadv.2023.100040
[13]. Shubham, J., Jena, A., Balaboina, A. R., Prusty, R. K., & Ray, B. C. (2022). Materialia, *26*, 101589. https://doi.org/10.1016/j.mtla.2022.101589
[14]. Sharma, R., & Sharma, D. (2022). Materials today: Proceedings. https://doi.org/10.1016/j.matpr.2023.02.136
[15]. Jayaraman, R., Karthikeyan, T., & Arunkumar, S. (2023). Materials today: Proceedings. https://doi.org/10.1016/j.matpr.2023.08.233
[16]. Pandit, A. K., Verma, V., & Dwivedi, V. K. (2023). Journal of the Institution of Engineers (India): Series D. https://doi.org/10.1007/s40033-023-00515-5

International conference on Smart Material, Manufacturing and Characterization Techniques – 2024

Paper ID: ICSMMCT-01065

A Comprehensive Review on Porous FGM Structure Supported on Elastic Foundation

Vineet Kumar[1], M. Singh[2]

[1]*M. E. Deptt., Engg. College Bikaner, Rajasthan, India*
[2]*B.L.I. College, Dankaur, Greater Noida, U.P., India*

Abstract

Functionally graded materials (FGMs) are the enhanced category of materials that are extensively used in rectangular and circular plates. It was developed to improve the material quality based on the required properties for applications. These materials are tailored in such a way that the composition of constituents materials is varying in thickness as well as in other two directions. The advantage of grading the material properties is that to reduce the smooth transition from one material to other materials without any sharp gradient interface. FGMs have been utilized in numerous engineering purposes, for example nuclear power, aerospace industries, optoelectronics and civil engineering. Further, important trends are the expansion of FGMs porous structures, where inside pores progressions present within materials have substantial capability to advance improve the increased performances. A similar fashion, elastic foundation is also important to support the FGMs plates in various engineering applications. A systematic review is presented in the present article on forms of FGMs, effect of porosity and potential uses of elastic foundations.

Keywords: *FGMs; Gradation rule; Structural materials; Porosity; Elastic foundation.*

1. Introduction

Materials have acted in a needed function in the development of our society and culture. In this phase of development, a group of scientists and engineers built high technology material i.e. FGMs in the decade of 1980's in Japan. These are made up of two or added integral phases which have permanent and have smoothly varying composition, see in Figure 1& 2. In regards of FGMs applications, it enables a wide role in the field of biomedical science, space industries, and mechanical- civil engineering

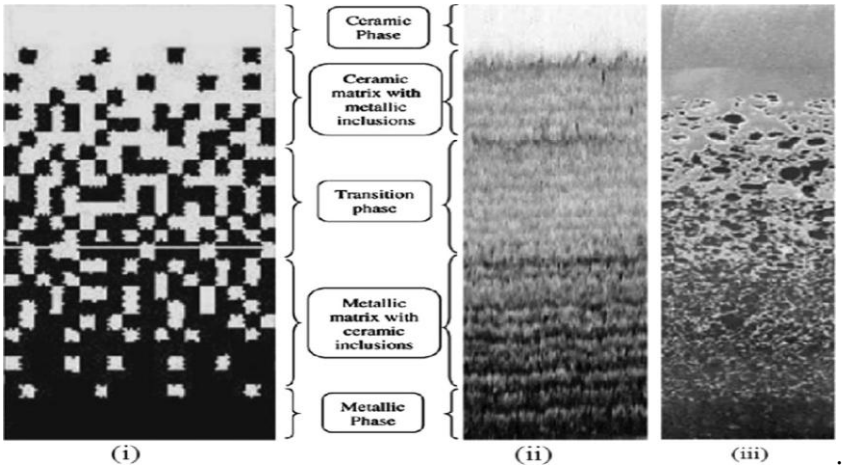

Fig.1 Cross section of material gradation of structure. [1].

Published online on: ***February 01, 2025***
Corresponding Author's E-mail ID: vineetrana81@gmail.com

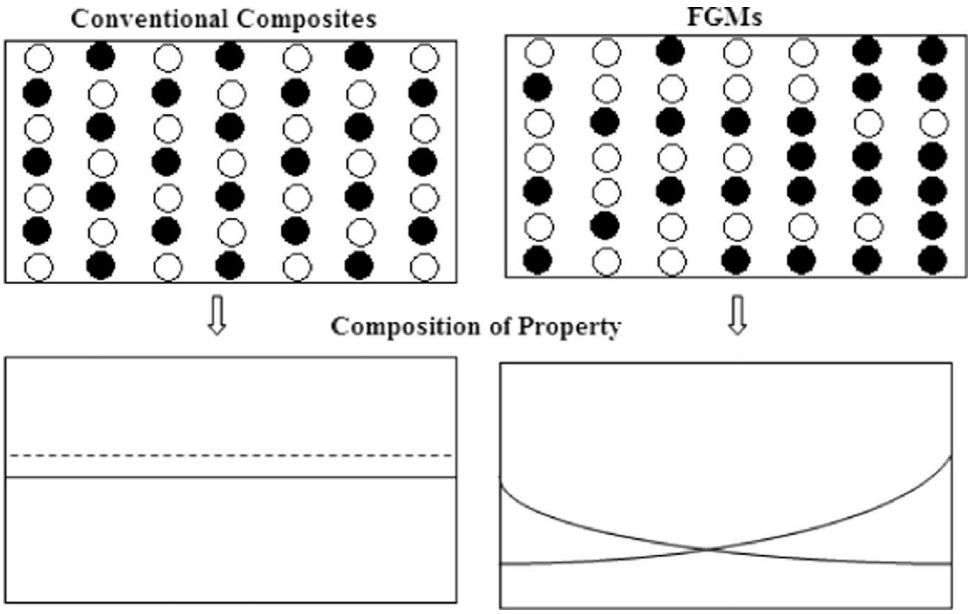

Figure 2. Property **v**ariation.[2].

2. Applications of FGMs

FGMs are preferred over other traditional composite materials as they can be graded according to the requirement. Initially, it was used in the field of nuclear power plants but in recent research has shown its application in various grounds comparable aerospace industries, optoelectronics, and biomaterials etc. FG materials have many applications over the conventional materials due to its excellent feature that can tolerate critical operating conditions as depicted in Figure 3.

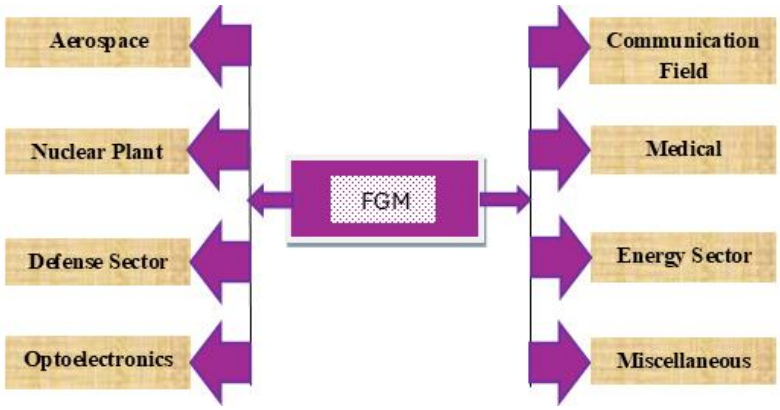

Figure 3. Applications of functionally graded materials.

3. Homogenization of FGMs

There are two common schemes to homogenize functionally graded materials by mixing the two different constituents of materials. Normally, the material properties depend on the volume segment on each ingredient's materials. During material modelling of functionally graded materials, finite element technique and analytical method is applied to calculate the stress-strain, deformation, plastic yielding and crack propagation etc. These two methods of modelling require the micromechanics of the cross-section of the materials. For this purpose, two micromechanics models are commonly used i.e Mori Tanaka scheme and Voigt Model.

3.1. Mori-Tanaka Method

This approach efforts aimed at composite materials with sections of the tailored microstructure with distinctly specified unremitting matrix and a broken particulate phase [3]. The Bulk modulus ($\aleph$) and Shear modulus (ψ) are estimated as follows:

$$\frac{\aleph_e-\aleph_m}{\aleph_c-\aleph_m}=\frac{V_c}{1+V_m\frac{\aleph_c-\aleph_m}{\aleph_m+4/3\psi_m}},\qquad \frac{\psi_e-\psi_m}{\psi_c-\psi_m}=\frac{V_c}{1+V_m\frac{\psi_c-\psi_m}{\psi_m+f_1}}\qquad \text{where, } f_1=\frac{\psi_m\left(9\aleph_m+8\psi_m\right)}{6\left(\aleph_m+2\psi_m\right)},$$

$$E=\frac{9\aleph_e\vartheta_e}{3\aleph_e+\vartheta_e},\ \vartheta=\frac{3\aleph_e-2\vartheta_e}{2\left(3\aleph_e+\vartheta_e\right)}$$

3.2. Voigt Model

The material properties can be tailored/ graded in one and all three direction relating to the volume fraction of the integral materials. The Voigt model is widely utilized for homogenization techniques to determine the effective properties (Young's modulus, Density and Poisson ratio) and considered as follows:

3.2.1 Power Law

The mainly worked micro-mechanics model for the FGM is the Voigt model based on the simple power law[4–8]. The volume fraction of the two different ingredients materials is expected to obey the power law function.

3.2.2 Exponential Law

The effective properties in z-diection can be estimated by using the exponential gradation law. Commonly, two types of exponential law [9–11] are applied in the present work. Where, S denoted the effective properties of the FG materials while S_C & S_m represents the mechanical properties of ceramic and metals respectively.

$$S(z)=(S_C-S_m)V_C+S_m,$$

Power Law $V_C=\left(\frac{z}{h}+\frac{1}{2}\right)^p$, Exponential Law $S(z)=S_Ce^{-\delta(1-2Z/h)}$, $\delta=1/2\ln\left(S_C/S_m\right)$

3.2.3 Sigmoidal Law

Another way of pridicting the effective properties of FGMs is assuming by using two simple power law. Sigmoidal law[12] has one possitive advantage that it act for the continous variation of the effective properties of materials among others homozination methods.

$$S(z)=S_C+\frac{(S_C-S_m)}{2}\left(\frac{2z}{h(x,y)}+1\right)^p \qquad for\ -h(x,y)/2\le z\le 0$$

$$S(z)=S_m+(S_C-S_m)\left(1-\frac{1}{2}\left(1-\frac{2z}{h(x,y)}\right)^p\right) \qquad for\quad 0\le z\le h(x,y)/2$$

4. Effect of porosity

In recent years, development of computational methods has been more interesting with porous FG materials. It is difficult to manufacture the materials without pores. So, important trends are the enhancement of FG porous structures, where interior pore progressions present substantial capability to further improve the occurrences. Rezaei and Saidi [13–15] uses the porosity functions for different types of analysis like as free vibration and buckling loading. Gupta and Talha [16]

investigated the flexural and free vibration responses of porous FGM plate under thermal environment. Singh and Harsha [17, 18] carried out the solution of sandwich plate using the various types of porosity. Dhuria et al. [19] investigated the static and buckling response of porous FG materials plate. Li et al. [20] carried out the iso-geometric analysis of bi-directional FGM plates with influence of porosity. Various types of porosity are applied in conjunction with the power law given in different literatures.

Type-I, Even porosity distribution

$$S(z) = S_{\mathrm{m}} + (S_C - S_{\mathrm{m}})V_C - \frac{e}{2}(S_C + S_{\mathrm{m}})$$

Type -II, Uneven porosity distribution

$$S(z) = S_{\mathrm{m}} + (S_C - S_{\mathrm{m}})V_C - \frac{e}{2}(S_C + S_{\mathrm{m}})\left\{1 - 2\frac{|z|}{h}\right\}$$

Type – III, Symmetric Enhanced distribution

$$S(z) = \left\{S_{\mathrm{m}} + (S_C - S_{\mathrm{m}})V_C\right\}\left\{1 - e\cos(\pi z / h)\right\}$$

Type- IV, Bottom Enhanced distribution

$$S(z) = \left\{S_{\mathrm{m}} + (S_C - S_{\mathrm{m}})V_C\right\}\left[1 - e\cos\left\{\pi / 2(z / h + 0.5)\right\}\right]$$

Type- V, Top Enhanced distribution

$$S(z) = \left[S_{\mathrm{m}} + (S_C - S_{\mathrm{m}})V_C\right]\left[1 - e\cos\left\{\pi / 2(z / h - 0.5)\right\}\right]$$

Type- VI, Logarithmic distribution

$$S(z) = S_m + (S_C - S_m)V_C - \log(1 + 0.5e)(S_C + S_m)\left[1 - \frac{|2z|}{h}\right]$$

5. Elastic Foundations

This segment deals with analysis of structural FGMs plate supported on elastic foundations. This part of analysis has significant impact on the structural analysis, as it is motivated by structures such as resting on railroad tracks, navigation locks and highway pavement. These all are important part of mechanical and civil engineering. In order to this, mathematical analysis are complex due to the complexity of modeling of the elastic foundations. To get rid of this problem it is needed to idealized the actions of elastic foundations. In this direction, the basic mechanical model was offered by the Winker's [21]. The Winkler model is named the one parameter with one direction foundation which is devised by linearly spread out verticle spring. The relation for the surface of plate and load interaction.

(i) Basic foundation named Winkler parameter [21]

$$f(Winkler) = K_w w_0$$

However, Pasternak foundation model included the extra shear layer over the spring, which have additional advantage to accommodate the stability effect in a transverse direction in conjunction with vertical direction.

(ii) Two parameter foundation Pasternak foundation [21]

$$f(Pasternak) = K_w w_0 - K_P \nabla^2 w_0$$

Where $\nabla^2 = \partial^2 / \partial x^2 + \partial^2 / \partial y^2$ symbolized the Laplace operator.

(iii) Three parameter Kerr foundation [22]

Further, a new model was deveoped via placing the shear layer bonding the two verticle upward and downward springs layers.

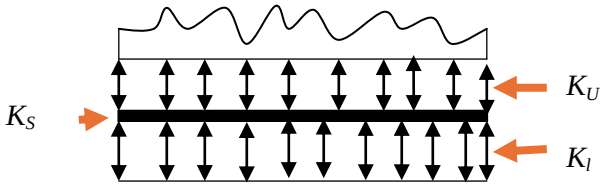

$$f\left(Kerr\right)=\frac{K_l K_u}{K_l+K_u}w_0-\frac{K_s K_u}{K_l+K_u}\nabla^2 w_0$$

Figure 4. Schematic diagramme for Kerr model

K_l, K_u & K_s denoted the strength for down spring, upper spring &, shear spring layer compress linking two verticle spring tiers, correspondingly as depicted in Figure 4. This model can be can be transformed into Pasternak foundation after placing the K_u equal to infinity.

6. Conclusion

This paper reviews the developments in the field of porous FG material structures. The basic concepts linkage the evaluation approaches, types of FG gradation laws, types of porosity and elastic foundations. On reviewed, porous FG structures have significantly offer addition in their properties for the application of bending, mechanical buckling and vibrations. The different types of elastic foundation are used for various applications based on the real engineering structures.

References

[1] Jha, D. K., Kant, T., & Singh, R. K. (2013). A critical review of recent research on functionally graded plates. *Composite Structures, 96*, 833–849.

[2] Gupta, A., & Talha, M. (2015). Recent development in modeling and analysis of functionally graded materials and structures. *Progress in Aerospace Sciences, 79*, 1–14.

[3] Benveniste, Y. (1987). A new approach to the application of Mori-Tanaka's theory in composite materials. *Mechanics of Materials*, 147–157.

[4] Reddy, J. N. (2000). Analysis of functionally graded plates. *International Journal of Numerical Methods in Engineering, 47*, 663–684.

[5] Kumar, V., Singh, S. J., Saran, V. H., & Harsha, S. P. (2020). Exact solution for free vibration analysis of linearly varying thickness FGM plate using Galerkin-Vlasov's method. *Proceedings of the Institution of Mechanical Engineers, Part L: Journal of Materials: Design and Applications*, 1–18.

[6] Kumar, V., Singh, S. J., & Harsha, S. P. (2023). Temperature-dependent vibration characteristics of porous FG material plates utilizing FSDT. *International Journal of Structural Stability and Dynamics, 24*, 1–35.

[7] Kumar, V., Singh, S. J., Saran, V. H., & Harsha, S. P. (2023). Effect of elastic foundation and porosity on buckling response of linearly varying functionally graded material plate. *Structures, 55*, 1186–1203.

[8] Kumar, V., Singh, S. J., Saran, V. H., & Harsha, S. P. (2021). Vibration characteristics of porous FGM plate with variable thickness resting on Pasternak's foundation. *European Journal of Mechanics - A/Solids, 85*, 104124.

[9] Chakraverty, S., & Pradhan, K. K. (2014). Free vibration of exponential functionally graded rectangular plates in thermal environment with general boundary conditions. *Aerospace Science and Technology, 36*, 132–156.

[10] Mantari, J. L., & Guedes Soares, C. (2012). Bending analysis of thick exponentially graded plates using a new trigonometric higher-order shear deformation theory. *Composite Structures, 94*, 1991–2000.

[11] Kumar, P., & Harsha, S. P. (2022). Static, buckling and vibration response analysis of three-layered functionally graded piezoelectric plate under thermo-electric mechanical environment. *Springer Singapore*, 1561–1598.

[12] Kumar, V., Singh, S. J., Saran, V. H., & Harsha, S. P. (2020). An analytical framework for rectangular FGM tapered plate resting on the elastic foundation. *Materials Today: Proceedings, 28*, 1719–1726.

[13] Rezaei, A. S., & Saidi, A. R. (2016). Application of Carrera unified formulation to study the effect of porosity on natural frequencies of thick porous-cellular plates. *Composites Part B: Engineering*, 361–370.

[14] Rezaei, A. S., & Saidi, A. R. (2015). Exact solution for free vibration of thick rectangular plates made of porous materials. *Composite Structures, 134*, 1051–1060.

[15] Rezaei, A. S., & Saidi, A. R. (2017). Buckling response of moderately thick fluid-infiltrated porous annular sector plates. *Acta Mechanica, 228*, 3929–3945.

[16] Gupta, A., & Talha, M. (2018). Influence of porosity on the flexural and free vibration responses of functionally graded plates in thermal environment. *International Journal of Structural Stability and Dynamics*, 1–31.

[17] Singh, S. J., & Harsha, S. P. (2020). Thermal buckling of porous symmetric and non-symmetric sandwich plate with homogeneous core and S-FGM face sheets resting on Pasternak foundation. *International Journal of Mechanics and Materials in Design, 16*, 707–731.

[18] Singh, S. J., & Harsha, S. P. (2020). Analysis of porosity effect on free vibration and buckling responses for sandwich sigmoid function-based functionally graded material plate resting on Pasternak foundation using Galerkin Vlasov's method. *Journal of Sandwich Structures and Materials*, 1–44.

[19] Dhuria, M., Grover, N., & Goyal, K. (2021). Influence of porosity distribution on static and buckling responses of porous functionally graded plates. *Structures*, *34*, 1458–1474.

[20] Li, S., Zheng, S., & Chen, D. (2020). Porosity-dependent isogeometric analysis of bi-directional functionally graded plates. *Thin-Walled Structures*, *156*, 106999.

[21] Wang, Y. H., Tham, L. G., & Cheung, Y. K. (2005). Beams and plates on elastic foundations: A review. *Progress in Structural Engineering and Materials*, *7*, 174–182.

[22] Kneifati, M. C. (1985). Analysis of plates on a Kerr foundation model. *Journal of Engineering Mechanics*, *111*, 1325–1342.

Material Science Education Using Social AR

N.Manglani[1], M. Kacha[2], U. Jain[3], G. Sahoo[4] and A. Chouhan[5]

[1,2,3,4,5]*Shah & Anchor Kutchhi Engineering College, Mumbai, India 400088*

Abstract

This study investigates the integration of Augmented Reality (AR) within social media to enhance material science education, focusing on its impact on student engagement and comprehension. Traditional educational methods often fall short of effectively conveying complex material science concepts. By embedding AR into social media, this initiative seeks to leverage the engaging, interactive nature of these platforms to facilitate a more dynamic learning environment. The research explores how AR-enhanced interactions on platforms like Instagram can boost motivation, foster collaboration, and improve knowledge retention among students, particularly those in Generation Z. It also examines the scalability and pedagogical effectiveness of AR applications in diverse educational settings. However, challenges such as maintaining academic rigor, managing distractions, and ensuring equitable access to technology are addressed to optimize the educational benefits of this innovative approach.

Keywords: *Augmented Reality, Social media, Social AR, Material science education, Technology-enhanced learning.*

1. Introduction

In the realm of education, the fusion of technology and pedagogy has continually redefined the landscape, offering innovative means to engage learners and enhance comprehension. Material science education, with its intricate concepts and practical applications, stands as a vital domain where such advancements can significantly impact learning outcomes. However, traditional instructional methods often struggle to convey the intricacies of material science effectively, limiting students' ability to grasp complex phenomena. Against this backdrop, the emergence of augmented reality (AR) heralds a new era in educational methodology, promising immersive, interactive, and collaborative learning experiences.

In contrast to traditional AR applications that offer immersive and interactive simulations within dedicated platforms or devices, AR on social media leverages existing social networking platforms to deliver AR content to a broader audience. The integration of AR within social media environments not only expands accessibility but also fosters collaboration and knowledge sharing among students and educators. By seamlessly embedding AR content into familiar social media interfaces, learners can engage with material science concepts in real-world contexts while benefiting from the interactive and community-driven nature of social media platforms. This convergence of AR and social media has the potential to revolutionize material science education by providing students with dynamic, personalized learning experiences that bridge the gap between theory and practice while cultivating essential 21st-century skills.

The study aims to assess the efficacy of integrating augmented reality (AR) technology within social media platforms to enhance student engagement and comprehension in material science education. It seeks to investigate how AR-enhanced social media platforms impact student motivation and participation in material science learning activities. Additionally, the research aims to explore the feasibility and scalability of implementing AR-driven educational interventions via social media across diverse educational contexts. Furthermore, the study aims to identify pedagogical strategies and best practices for designing and implementing AR-based learning experiences within social media environments to optimize material science learning outcomes. Through these objectives, the research endeavors to shed light on the potential of AR-enabled social media platforms to revolutionize material science education

2. Literature Review

2.1. Evolution of Material Science Education

Material science education has evolved from traditional classroom instruction, which relied heavily on textbooks and static visuals, to embrace more dynamic and interactive technologies. The early methods, while foundational, often limited students' understanding of complex material behaviors and applications. This educational landscape began to change with the introduction of computer-based simulations and virtual labs, which provided safer, more scalable, and cost-effective ways for students to explore and interact with material properties, significantly enhancing both accessibility and engagement.

The transformative integration of Augmented Reality (AR) marked a further evolution in teaching material science. AR

Published online on: ***February 01, 2025***

Corresponding Author's E-mail ID: namrata.manglani@sakec.ac.in

has made learning experiences profoundly immersive and interactive, allowing students to interact with three-dimensional models and real-time simulations that bridge the gap between theoretical learning and practical application. Additionally, merging AR with social media platforms has not only broadened its educational reach but also democratized access to advanced learning tools, fostering global collaboration among students and educators. As AR technology continues to advance, its role in material science education is set to grow, cementing its place as an indispensable educational tool that prepares students for the future challenges of the industry[1][2].

2.2 Augmented Reality Applications in Education

Augmented Reality (AR) has rapidly emerged as a transformative technology within the educational sector. AR's ability to superimpose digital information into the real world has revolutionized the learning experience by making it more immersive and interactive. In material science education, AR's applications are particularly potent. It enables the visualization of intricate structures like atomic arrangements and chemical bonds, thereby providing students with a tangible and intuitive understanding of concepts that are often difficult to grasp through traditional instructional methods [3].

Research demonstrates that AR enhances student interaction with learning materials through its capability to create 3D simulations and interactive environments. This not only aids in deeper comprehension of the subject matter but also significantly boosts student engagement and motivation. By engaging with dynamic models and participating in simulated experiments, students gain a more nuanced understanding of material science, which can inspire a greater interest and curiosity in the field. Furthermore, AR's flexibility allows for its application across different educational levels and settings, adapting to the specific learning needs of students and enhancing the overall educational experience by making it more accessible and adaptable [4][5].

The effectiveness of technology-enhanced learning tools such as AR and Virtual Reality (VR) has been well-documented, particularly in the context of material science education. These technologies facilitate hands-on experiences and detailed explorations of material behaviors within safe, cost-effective virtual environments. This is especially advantageous in material science, where conducting experiments can often involve expensive materials, potentially hazardous conditions, or complex setups [8]. The scalability and adaptability of digital tools cater to diverse educational needs, allowing for personalized learning experiences that can engage large numbers of students with varying learning preferences. Constructivist learning theories serve as a solid basis for comprehending how individuals actively shape knowledge through interactions with their surroundings. Rooted in the works of Piaget, Vygotsky, and Dewey [10], constructivism suggests that learning is a dynamic process influenced by learners' prior experiences, knowledge, and social engagements. At the core of constructivist ideals is the idea that learners derive meaning through active engagement with content, rather than merely receiving information passively. The ability to customize the presentation and complexity of material science concepts to suit individual needs ensures that students remain engaged and receive instruction that is best suited to their learning styles. Moreover, empirical studies suggest that early exposure to such interactive and technologically advanced learning tools can significantly influence students' interest in pursuing further education and careers in STEM fields, particularly in areas as demanding and dynamic as material science [9]..

2.2. Role of Social Media in Educational Contexts

The integration of Learning Management Systems (LMS) with social media represents a significant shift in educational technology, emphasizing enhanced student engagement and collaboration. By adopting interactive social media features like forums and shared content spaces, LMS platforms are evolving from simple content delivery channels to vibrant educational environments that promote active learning and community involvement. However, this integration also presents challenges such as balancing social engagement with academic rigor and managing both formal and informal learning settings effectively. Continuous adaptation, informed by user feedback and pedagogical impact, is crucial to maintaining educational integrity while leveraging the benefits of social media. As these technologies evolve, ongoing research is essential to refine strategies that ensure these tools effectively complement traditional learning methods and meet the diverse needs of modern learners [6][7].

2.3. Previous Studies on Technology-Enhanced Learning in Material Science Education

The Integration of E-learning platforms within material science education highlights the transition from traditional teaching methods to innovative e-learning approaches. E-learning platforms support virtual laboratories and other interactive tools that enhance the educational experience by simulating real-world material science applications. These technologies enable students to explore complex concepts through an interactive, digital format that improves accessibility and caters to

diverse learning styles. The effectiveness of these e-learning methods is assessed through their integration into the material science curriculum, combining them with conventional hands-on laboratory experiences. The findings indicate that e-learning tools do not compromise educational quality but rather enhance understanding and engagement. Specifically, the use of virtual laboratories allows students who lack physical access to traditional lab facilities to gain practical experience and knowledge, thereby democratizing education and extending learning opportunities to a broader audience [8]. Learning of material science is fused with advanced computational tools, such as Material Studio, Atomistix Toolkit, and Virtual NanoLab. A new era in learning may be opened with this kind of fusion, which is realized through strong simulation capabilities for in-depth analyses and visualization at atomic and molecular levels

3. Methodology

The methodology for designing effective Social AR for material science education consist of following stages.

3.1. Identification of Target Audience

First step refers to identification of specific groups of individuals who will be the primary recipients and beneficiaries of the social AR (augmented reality experience) developed for material science education.

- Students / GenZ's (specify level: high school, university)
- Educators in material science
- General public with a potential interest

In addition to grouping the audience in above three categories we have to categorize them based on their prior knowledge and social Media Usage

3.2. Development of augmented reality content

Creating a successful social augmented reality (AR) experience involves five essential steps and is an organized, iterative process. This methodical approach guarantees that the augmented reality application is both technically sound and entertaining and instructive for the target user base. The process begins with identifying the project's original goals and target audience and continues with ideation, prototyping, thorough development, and refinement before the AR experience is deployed. Because each step builds on the one before it, it is possible to make constant changes based on user feedback and testing. The steps in the AR planning process are outlined in the sections that follow, along with an explanation of how each one affects the creation of a strong educational tool designed to improve material science learning.

1. **Planning:** Define project goals, target audience, and initial concept directions.
2. **Ideation:** Brainstorm creative ideas and features for the AR experience.
3. **Prototyping:** Create a basic, functional version of the AR experience for initial testing.
4. **Development & Refinement:** After developing the AR prototype, it undergoes internal testing to identify and fix technical issues. User feedback is then collected and used to iteratively refine the AR experience, enhancing its usability and effectiveness.
5. **Deployment:** Launch the finalized AR experience and make it accessible to your target audience

3.3. Selection of social media platforms

The target audience, such as Generation Z students, is highly active on certain social media platforms, so it's important to take that into account when choosing one for augmented reality (AR) in education. Table 1 assists the developer for choosing relevant platforms based on the content type and target audience.

3.4. Data collection and analysis

In the realm of social media, understanding and optimizing user engagement is key for content creators. Instagram, a leading platform in this landscape, provides vital insights through its analytics tools. Here we explore these methodologies, focusing on Instagram Analytics in Figure 1.

Table 1. Few of the most popular platforms for social AR

Platform	Target Audience	AR Creation Tools	Unique Features
Instagram	Gen Z	Meta Spark Studio	Powerful analytics, cutting-edge AR
Snapchat	Gen Z, young adults	Lens Studio	Immersive experiences, pioneering AR work
Facebook	Broad demographic	Meta Spark Studio	Wide reach for diverse audiences
TikTok	Younger audiences	Effect House	Short video format, growing AR integration

Fig.1. Statistical Analysis Sample of Instagram Effect

Overall Performance: The number of times our effect was viewed on Instagram is 14.9K with a 2% increase. Users have used our effect to capture a photo or video 3.7K times, showing a 49% increase. The creations made with our effect have been shared on Instagram 568 times, with a 43% increase. The total estimated impressions of our effect is 16.5K, showing a 52% increase.

Engagement: The conversion funnel shows that 25% of users who opened the effect captured something, 15% shared their creations, and a smaller percentage continued further.

User Demographics: Among the users who interacted with our effect, 68% were female, 30% were male, and 2% did not specify. Different age groups also interacted with our effect, but further details were not provided.

4. Results: Material Science via Social AR

Augmented reality (AR) integration with social media platforms presents a promising avenue for enhancing user engagement and interaction. Several existing platforms offer tools and features to facilitate the development and deployment of AR models within social media environments. One prominent platform is Meta Spark Studio (v180), which provides a user-friendly interface and robust capabilities for creating AR effects tailored to various social media platforms, including Instagram and Facebook.

The integration of AR models into social media interfaces showcased the seamless convergence of cutting-edge technology and social media engagement, offering users an immersive journey into the microscopic world of atoms and molecules. Through Meta Spark Studio's intuitive interface, our team meticulously crafted visually stunning atomic models as shown in Figure 2, seamlessly integrated into users' Instagram feeds. Real-time previews facilitated iterative refinement, ensuring the optimal balance between aesthetic appeal and educational utility.

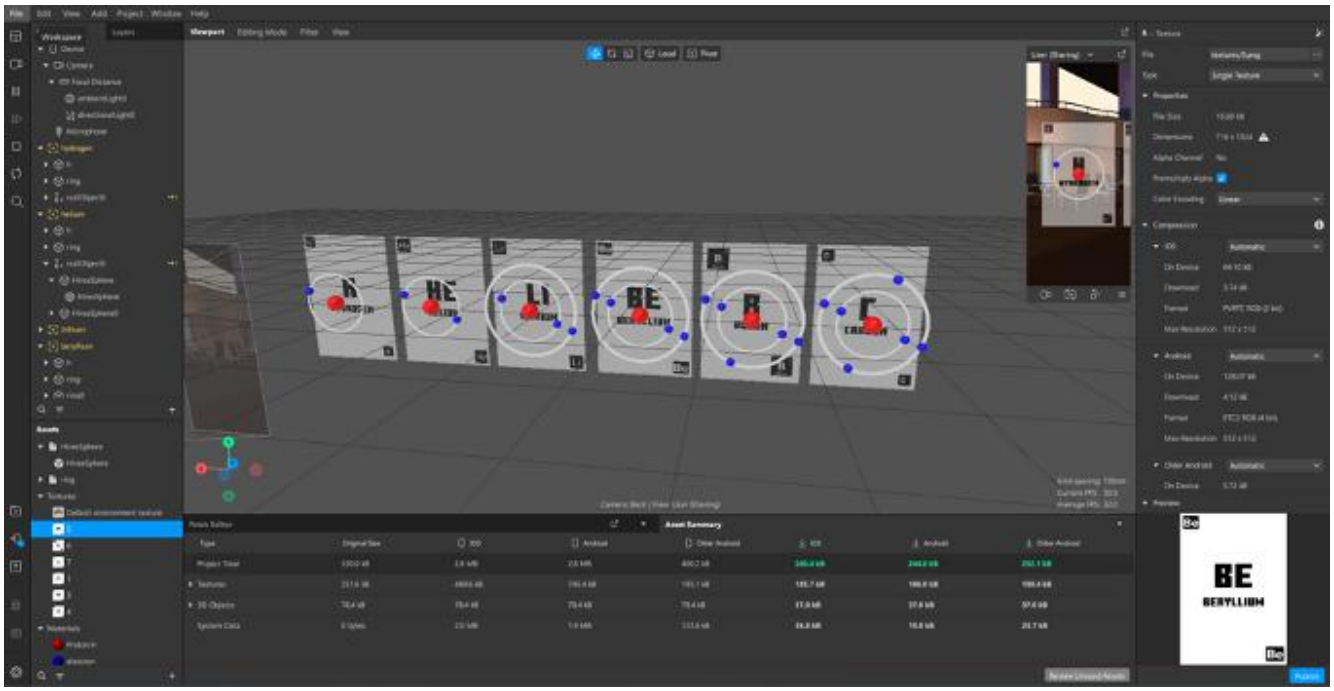

Fig. 2. Atomic Models on Meta Spark Studio

The integration of AR models into Instagram's interface showcased the seamless convergence of cutting-edge technology and social media engagement, offering users an immersive journey into the microscopic world of atoms and molecules. Through Meta Spark Studio's intuitive interface, our team meticulously crafted visually stunning atomic models, which can be seamlessly integrated into users' Instagram feeds.

Fig. 3. Tracker based atomic models on Instagram

The above figure 3 showcases the innovative integration of tracker-based atomic models developed on Spark AR Studio and their implementation on Instagram. The image illustrates a user engaging with the model: one phone functions as the tracker, while another utilizes the model through Instagram's Effect (filter) feature.

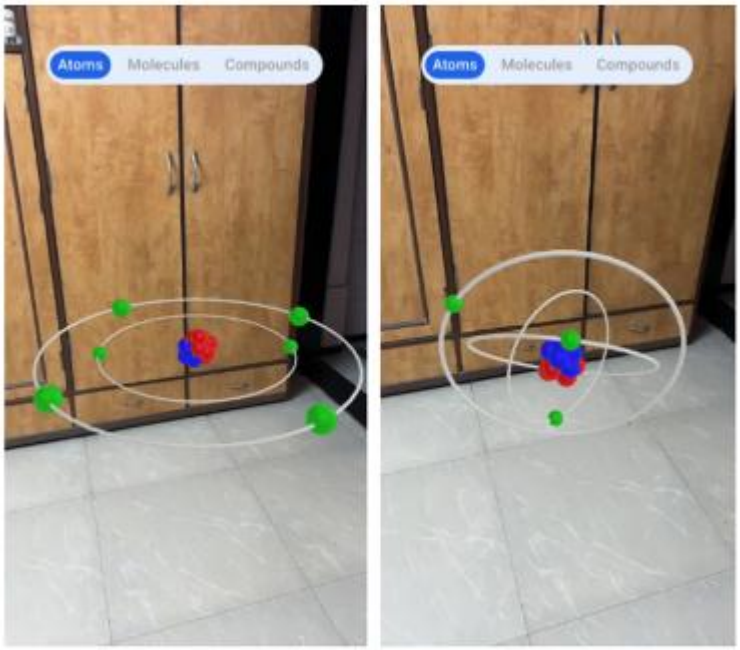

Fig. 4. Plane tracker based atomic models on Instagram

Figure 4 illustrates a groundbreaking utilization of plane tracking technology for displaying atomic, molecular and compound models within the Instagram interface. Developed by Varun Raikar, 1M1B Foundation; this plane tracker enables seamless exploration of atomic structures. Furthermore, it offers users additional features such as molecular and compound views, enriching their interaction. By selecting elements from the periodic table, like carbon and lithium, users can delve into their respective properties. For instance, tapping on carbon unveils its atomic structure, with further options available to explore molecular structures and associated compounds. This implementation underscores the potential of plane tracking technology in delivering dynamic and educational content to Instagram users.

5. Conclusion and Future Scope:

Conclusion: The teaching of material science could be entirely transformed by integrating Social Augmented Reality (AR) into classroom environments. Through immersive and interactive learning experiences via social media platforms, this promising technology can improve student engagement and comprehension. Social AR can support a better understanding and recall of material science by bringing complicated ideas to life, appealing to a generation that is accustomed to digital interactions. It will not only improve the accessibility and interest of educational information but also revolutionize the way material science is taught and acquired in a variety of settings. With its ability to combine theory with real-world applications in a visually exciting fashion, this technology has the potential to transform material science teaching as it develops significantly. Social AR has enormous transformational potential in material science teaching, despite certain obstacles including possible diversions and technical difficulties. It portends a time when theory and practical applications are smoothly merged in digital learning settings, empowering students and improving academic results.

Future Scope: The current study focuses on using augmented reality (AR) in social media for material science education primarily targeted at students. However, the future potential of this technology is vast. We envision developing a

platform that allows educators to easily create and customize AR educational materials. This platform would also make these resources widely accessible to the general public, democratizing learning opportunities beyond traditional classroom settings. Such advancements could transform educational practices across various disciplines, enhancing global access to interactive and engaging learning experiences.

Acknowledgments

N.M, M.K, U.J, A.C & G.S would like to thank An AR Creator Mr. Varun Raikar, and 1M1B Foundation for allowing us to showcase their work and Principal Dr. Bhavesh Patel and the Management of Shah & Anchor Kutchhi Engineering college for support during the preparation of this manuscript

References

[1] Abbaschian, R. (1990). Materials education—A challenge. *MRS Bulletin, 15*(8), 18-22. https://doi.org/10.1557/S0883769400058887

[2] Akuma, F. V., & Callaghan, R. (2016). Framework for reducing teaching challenges relating to improvisation of science education equipment and materials in schools. *EURASIA Journal of Mathematics, Science and Technology Education, 12*(10), 2697-2717.

[3] Alzahrani, N. (2020). Augmented reality: A systematic review of its benefits and challenges in e-learning contexts. *Applied Sciences, 10*(5660). https://doi.org/10.3390/app10165660

[4] Pengcheng, F., Mingquan, Z., & Xuesong, W. (2011). The significance and effectiveness of augmented reality in experimental education. *2011 International Conference on E-Business and E-Government (ICEE)*, Shanghai, China, 1-4. https://doi.org/10.1109/ICEBEG.2011.5881654

[5] Vuta, D. (2021). Augmented reality technologies in education - A literature review. *Bulletin of the Transilvania University of Braşov, 13*(62), 35. https://doi.org/10.31926/but.es.2020.13.62.2.4

[6] Hidayat, R., & Wardat, Y. (2023). A systematic review of augmented reality in science, technology, engineering, and mathematics education. *Education and Information Technologies.* https://doi.org/10.1007/s10639-023-12157-x

[7] Li, N., Chang, L., Gu, Y., & Duh, H. (2011). Sociality of mobile collaborative AR: Augmenting a dual-problem space for social interaction in collaborative social learning. *International Conference on Advanced Learning Technologies (ICALT)*, 467-469. https://doi.org/10.1109/ICALT.2011.145

[8] Molinari, A. (2017). Learning management systems and the integration with social media services: A case study. *2017 IEEE/ACM International Conference on Advances in Social Networks Analysis and Mining (ASONAM)*, Sydney, NSW, Australia, 775-781.

[9] Dobrzanski, L., Brom, F., & Brytan, Z. (2007). The teaching of material science matters using e-learning techniques. *Archives of Materials Science and Engineering, 28*.

[10] Pardjono, P. (2016). Active learning: The Dewey, Piaget, Vygotsky, and constructivist theory perspectives. *Jurnal Ilmu Pendidikan Universitas Negeri Malang, 9*(3), 105376.

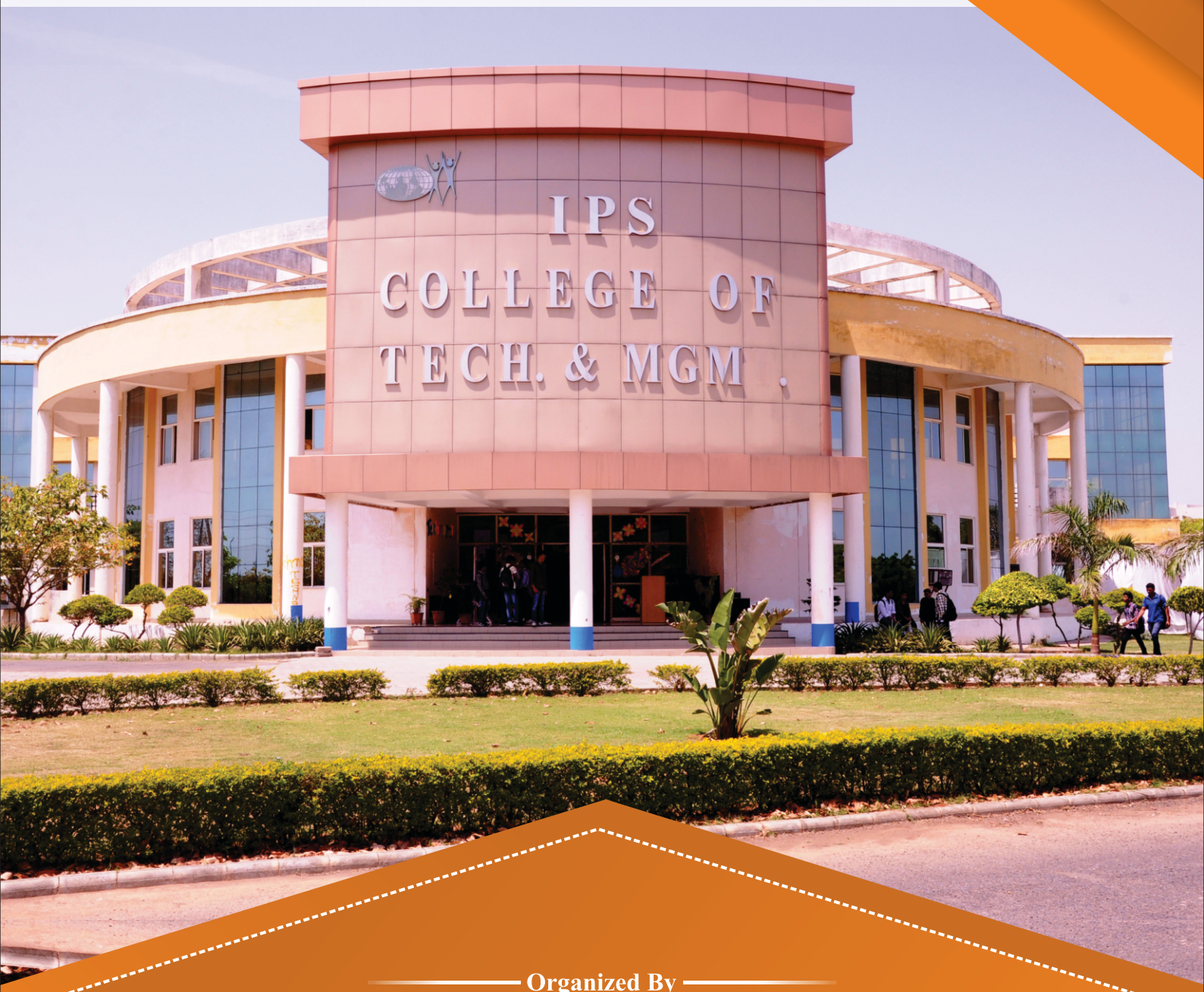

Organized By

IPS COLLEGE OF TECHNOLOGY & MANAGEMENT, GWALIOR, INDIA

Shivpuri Link Road, Gwalior, Madhya Pradesh (India)-474001

Email: info@ipsgwalior.org, icsmmct2024@gmail.com

Ph: +91-9826900722, +91-7987274927, +91-9450135681, +91-9754728428

Website: http://ipsgwalior.org/icsmmct2024, ipsgwalior.org

ISBN NO : 978-81-983356-6-1